

# Nontrivial topological structures of spacetime and implications for particle propagation

Zur Erlangung des akademischen Grades eines  
DOKTORS DER NATURWISSENSCHAFTEN  
von der Fakultät für Physik des  
Karlsruher Instituts für Technologie (KIT)

genehmigte

**DISSERTATION**

von

M. Sc. Fabrizio Sorba  
aus Villar San Costanzo, Italien

Tag der mündlichen Prüfung: 20. Juni 2014

Referent: Prof. Dr. F.R. Klinkhamer (KIT)  
Korreferent: Prof. Dr. Hanno Sahlmann (University of  
Erlangen-Nürnberg)

## Abstract

Spacetime foam, which describes the quantum fluctuations of spacetime, is one of the possible characteristics of a quantum theory of gravity. It is important to understand how it can affect particle propagation, in order to be able to attain information from experimental data and shed light on the nature of the gravitational interaction at the very smallest scales (see part I for more details).

One of the many approaches to spacetime foam consists in equipping spacetime with a distribution of microscopic structures with nontrivial topology, known as “topological defects” or “spacetime defects.” In this thesis, we follow this approach by considering various scenarios where different types of defects are embedded in spacetime, in order to investigate different aspects of spacetime foam.

In particular, we are interested in understanding the effects of a Lorentz-invariant distribution of time-dependent defects on the propagation of particles. This is accomplished in part II for point-like defects, where we find that no modification to the photon dispersion relation is introduced (at most, in a certain extension of the model, the photon can acquire mass). However, this model is very simple and does not take into account the structure and extension of the defects.

In part III, we consider the case in which the defects have an extension, and we compare different types of defects. We determine that the dispersion relation of electromagnetic waves is modified in this case and depends not only on the topological structure of the defects but also on their differential structure.

To study the effects of a distribution of extended time-dependent defects, we develop in part IV a lattice model of spacetime foam and analyze numerically the propagation of a scalar field. The results are in agreement with those in the previous parts.

It has been observed that one of the defect types introduced in part III, being a vacuum solution of general relativity, may serve to regularize the Schwarzschild black hole. In part V, we study the behavior of geodesics for such a solution. We observe that this regularized solution allows for the appearance of closed time-like curves, though these disappear in a non-eternal model of a black hole.

In part VI, we present the results of our studies.

# Contents

<b>I</b>	<b>Introduction</b>	<b>5</b>
<b>1</b>	<b>General overview of spacetime foam and Lorentz violation</b>	<b>7</b>
1.1	Spacetime foam . . . . .	7
1.1.1	Topological defects . . . . .	12
1.2	Lorentz violation . . . . .	13
1.2.1	Experimental tests . . . . .	15
<b>II</b>	<b>Spacetime foam from time-dependent, point-like defects</b>	<b>17</b>
<b>2</b>	<b>Basic features</b>	<b>17</b>
2.1	CPT anomaly . . . . .	18
2.2	Sprinkling and Lorentz invariance . . . . .	20
<b>3</b>	<b>Effective theory</b>	<b>22</b>
3.1	Scalar field . . . . .	24
3.2	Vector field . . . . .	28
<b>4</b>	<b>Explicit model</b>	<b>30</b>
4.1	Scalar propagator . . . . .	32
4.1.1	Quantum propagator . . . . .	33
4.1.2	Classical propagator . . . . .	34
4.2	Vector propagator . . . . .	35
4.2.1	$\Pi_q(k)$ . . . . .	39
4.2.1.1	Dimensional regularization . . . . .	40
4.2.2	$\Pi_{cl}(k)$ . . . . .	43
4.3	Renormalization . . . . .	43
4.4	Dispersion relation . . . . .	45
4.5	Extensions of the model . . . . .	46
4.5.1	PT-symmetric extension . . . . .	47
<b>III</b>	<b>Spacetime foam from static extended defects</b>	<b>51</b>
<b>5</b>	<b>Defects in Minkowski space</b>	<b>51</b>
5.1	Defect structure (review) . . . . .	51
5.2	Massless case (review) . . . . .	55
5.2.1	Plane wave in spherical coordinates . . . . .	56
5.2.2	Boundary conditions . . . . .	57
5.2.3	Dispersion relation . . . . .	58
5.3	Massive case . . . . .	58
5.3.1	Maxwell equations in curved spacetime . . . . .	59
5.3.2	Plane wave in the Schwarzschild metric . . . . .	61
5.3.3	Boundary conditions . . . . .	63
5.3.4	Dispersion relation . . . . .	64
5.3.5	Radial equation . . . . .	65
<b>6</b>	<b>Defect metric</b>	<b>69</b>
6.1	Metric (review) . . . . .	69
6.2	Scalar waves . . . . .	72

6.2.1	Radial equation around $y = 0$ . . . . .	76
6.2.2	Plane waves . . . . .	80
6.2.3	Dispersion relation . . . . .	84
6.3	Electromagnetic waves . . . . .	86
6.3.1	Derivation of electromagnetic solutions . . . . .	88
6.3.1.1	From Debye potential . . . . .	88
6.3.1.2	From a change of coordinates . . . . .	90
6.3.2	Study of Maxwell equations around $y = 0$ . . . . .	91
6.3.3	Plane waves . . . . .	93
6.3.4	Dispersion relation . . . . .	95
<b>IV Numerical calculations of a lattice spacetime foam model</b>		<b>97</b>
<b>7</b>	<b>Lattice action</b>	<b>97</b>
7.1	The algorithm . . . . .	99
7.2	Percolation . . . . .	101
<b>8</b>	<b>Results</b>	<b>103</b>
8.1	Time-dependent defects . . . . .	103
8.1.1	Continuum limit . . . . .	107
8.1.2	Results in 3 and 4 dimensions . . . . .	112
8.2	Static defects . . . . .	113
<b>V Regularized black hole from extended defect metric</b>		<b>117</b>
<b>9</b>	<b>Geodesics</b>	<b>117</b>
9.1	Metric and geodesic equations . . . . .	117
9.2	Massless case . . . . .	119
9.3	Massive case . . . . .	120
9.3.1	Null-like geodesics . . . . .	121
9.3.2	Painlevé-Gullstrand extension . . . . .	122
9.3.3	Kruskal extension . . . . .	124
9.3.3.1	Kruskal topology . . . . .	126
9.3.4	Penrose diagram . . . . .	127
9.3.5	Time-like geodesics . . . . .	128
9.3.6	$E > 1$ . . . . .	128
9.3.7	$E = 1$ . . . . .	129
9.3.8	$E < 1$ . . . . .	130
9.3.9	Closed time-like curves in a Skyrme exact solution . . . . .	132
<b>10</b>	<b>Star collapse</b>	<b>136</b>
<b>VI Conclusions</b>		<b>140</b>
<b>11</b>	<b>Summary of the results</b>	<b>140</b>
<b>12</b>	<b>Discussion</b>	<b>142</b>
	<b>References</b>	<b>144</b>

## Part I

# Introduction

The main goal that physics is trying to achieve nowadays is the unification of all fundamental interactions—electromagnetic, weak, strong, and gravitational—into a single fundamental theory. The first three interactions are already described by a very successful and unified model, the standard model of particle physics, which is a quantum field theory with local gauge invariance with respect to the group  $SU(3) \times SU(2) \times U(1)$ . This model has produced some of the most accurate predictions in the history of physics, which have always been confirmed experimentally. As an example, theoretical estimations of the notorious anomalous magnetic moment of the electron  $g - 2$  agree with the experimental results at order  $10^{-11}$  [1, 2]. The standard model has also predicted the existence of a number of particles that have always been found experimentally, the last example being the Higgs boson responsible for the spontaneous symmetry breaking of the electroweak symmetry  $SU(2) \times U(1)$ , which has recently been observed at the Large Hadron Collider.

Gravitational interaction is instead described by the classical field theory of general relativity, in which gravitational attraction is described as the effect of the curvature of spacetime caused by the presence of energy. Even in this case, the theory has always been very successfully confirmed by experiments [3]. However, due to the classical nature of this theory, it cannot be reconciled with the other interactions described instead by quantum models. So one would expect general relativity to be just the classical limit of a more fundamental quantum theory of gravity. Unfortunately, standard quantization techniques do not work with this theory, so many alternative approaches are under investigation, the most famous examples of which are represented by string theory and loop quantum gravity.

The main difficulty in constructing a quantum theory of gravity is the lack of experimental data to constrain the theoretical models. As already mentioned, in fact, current experimental results are in very good agreement with both the standard model of particles than with general relativity, and there is no direct evidence of physics beyond these models. In fact, the two theories apply to very different scales, namely the standard model applying to (quantum) microscopic scales and general relativity dealing with (classical) macroscopic scales, and it is therefore a challenging task to test the overlapping region where gravity becomes important at microscopic scales. This is due to the weakness of gravity in particle interactions, which, compared to other forces, makes it completely negligible even at the highest achievable energy scales. The scale at which gravity is expected to become important in particle interactions is the Planck scale, which is 8 orders of magnitude above the energy scale of the highest energy particles ever observed [4].

It is nevertheless of crucial importance to find a way to measure experimentally the effects of gravity at these scales, if one is ever to arrive at building a theory of quantum gravity. One of the more widely accepted features of such a theory is that, due to the uncertainty principle, it should describe quantum fluctuations in spacetime, to which one usually refers using the label ‘spacetime foam’. These fluctuations are, in general, expected to affect the propagation of

particles, for example by introducing modifications to particle dispersion relations. These modifications are also expected to become relevant at energy scales comparable to the Planck energy, and there is little hope of directly measuring them at ordinary scales. However, it has been pointed out that these microscopic effects could possibly be magnified in certain circumstances, for example when particles travel through cosmological distances, and become detectable at much lower energy scales. Hence, it is important to investigate how these spacetime fluctuations modify the propagation of particles, since these modifications can be constrained with experimental data, and knowledge on the microscopic structure of spacetime can possibly be obtained.

In this thesis, therefore, we consider different approaches to the study of spacetime foam to understand how different characteristics of the spacetime fluctuations modify the propagation of particles. We take into account very simplified models in which spacetime fluctuations are described classically by nontrivial topological small-scale structures (defects) distributed in spacetime.

In particular, in part II we try to construct a Lorentz-invariant spacetime foam model based on point-like topological defects. In fact, many spacetime foam models cause particles to have Lorentz-violating dispersion relations, but this is usually due to the fact that these models explicitly break Lorentz invariance from the outset. However, this non-invariance is not required *a priori*, and it is interesting to see what happens when Lorentz invariance is maintained. Moreover, some arguments indicate that Lorentz-violating models may be ruled out on the basis that even tiny modifications in this respect, through radiative corrections, could become excessively large at small energy scales.

In part III, instead, we compare the effects of different static spacetime foam models, which are based on static extended topological defects that are homeomorphic to each other (they have the same topology) but are not diffeomorphic. In particular, we start by reviewing an old result concerning the propagation of electromagnetic waves in a spacetime foam model based on a defect that is obtained by removing a ball from the spatial hypersurface of Minkowski spacetime and identifying antipodal points on its surface. We generalize this result to the case in which the defect is massive. Then, we consider another type of defect that has been obtained recently, and that, unlike the previous one, is a vacuum solution of general relativity. We compare the scalar and electromagnetic wave solutions in the manifold describing this new defect with the solutions obtained for the previous type of defect. Finally, we derive the dispersion relation for electromagnetic waves propagating in a spacetime foam model based on this new type defect.

In part IV, we approach the study of particle propagation in spacetime foam in a different way, i.e. with the aid of numerical calculations. We introduce the discretized action of a scalar field that propagates in a lattice filled with a distribution of extended defects, and we consider both cases discussed in the previous sections, i.e. time-dependent and static defects. This model serves on one hand to investigate the effects of a distribution of extended time-dependent defects, on the other hand to test the analytic results obtained in the previous parts and to explore values of parameters not covered by the analytic models.

In part V, we explore a slightly different topic. It has been observed that the second type of defect discussed in part III (which is a vacuum solution of general relativity) can be interpreted as a regularization of the standard Schwarzschild black hole solution. Away from the defect surface, the two solutions are in-

deed diffeomorphic. Moreover, the defect solution is regular everywhere, so it cures the Schwarzschild singularity albeit at the price of introducing a nontrivial topology. Here, we investigate the behaviors of the geodesics in this defect metric and compare them with standard Schwarzschild results.

Finally, in part VI, we present the conclusions of our studies.

## 1 General overview of spacetime foam and Lorentz violation

Before introducing the specific spacetime foam models studied in this work, we want to provide in this section a more detailed introduction to the concepts of spacetime foam and Lorentz violation.

### 1.1 Spacetime foam

Spacetime foam (or quantum foam) is a concept introduced by Wheeler [5, 6] to indicate the quantum fluctuations of spacetime. This is a widely accepted feature of gravitational interaction despite the fact that, until now, there is no experimental evidence to support it. Nevertheless, if gravitational interaction were to be described ultimately by a quantum theory, then it must definitely display quantum fluctuations. It is an intrinsic property of quantum mechanics that the result of any measurement of an observable  $A$  in a general state  $\psi$  is afflicted by uncertainty

$$\delta A = \sqrt{\langle \hat{A}^2 \rangle_\psi - \langle \hat{A} \rangle_\psi^2}, \quad (1.1)$$

where  $\langle \hat{A} \rangle_\psi$  is the expectation value of the operator  $\hat{A}$  in the state  $\psi$ . Moreover, an uncertainty relation holds between the fluctuations of two non-commuting observables  $A$  and  $B$

$$\delta A \delta B \geq \left| \frac{1}{2i} [\hat{A}, \hat{B}] \right|. \quad (1.2)$$

Considering, for example, the position and momentum operator with standard commutation relation  $[\hat{x}_i, \hat{p}_j] = i\hbar\delta_{ij}$ , this equation provides the uncertainty relation  $\delta x_i \delta p_i \geq \hbar/2$ .

Experimental evidence of quantum fluctuations has been observed in a wide range of phenomena, both in quantum mechanics and in quantum field theories. Consider, for example, the vacuum state of the standard model of particles. Due to quantum fluctuations, this state is not really empty but can be depicted as a continuous bubbling of virtual particles that appear and vanish everywhere in spacetime for a very short time (in fact, the uncertainty relation between time and energy,  $\delta E \simeq \hbar/(2\delta t)$ , tells us that the shorter the temporal scale of the fluctuations, the higher their energy). The effects of these virtual particles have been observed experimentally. In quantum electrodynamics (QED), the appearance of virtual electron-positron pairs affects the propagation of photons—the so-called vacuum polarization—so that the electric charge is effectively screened. Such a screening effect depends on the distance away from the electric charge, so that, in an atom, electrons closer to the nucleus perceive a larger charge than distant electrons (Lamb Shift) [7]. Another example is the Casimir effect, which also can be explained in terms of quantum vacuum fluctuations [8].

In the same way that fields in a quantum field theory (e.g. the electron field in QED) display quantum fluctuations, we would expect the metric describing the geometry of spacetime to display fluctuations in a quantum theory of gravity. As discussed by Wheeler, such fluctuations should affect both the geometry and the topology of spacetime, and they are expected to become important at the Planck scale. Indeed, at the Planck scale, the strength of the gravitational field becomes comparable to that of the other forces, and the (quantum) gravitational interaction between fundamental particles cannot be neglected, as it is, instead, in the present formulation of quantum field theory. We can use a simple argument [9] to arrive at this result. Consider a photon of wavelength  $\lambda = c/\nu$ . From quantum mechanics, we know that the energy carried by this photon is  $E = 2\pi\hbar c/\lambda$ . On the other hand, special relativity tells us that this energy is equivalent to the mass  $m = E/c^2$  which, due to general relativity, curves the geometry of spacetime. To quantify this effect, we can calculate the Schwarzschild radius  $r_S$  associated with the mass  $m$  and compare it with the wavelength of the photon, in which case we obtain

$$r_S = \frac{2Gm}{c^2} = 4\pi \frac{\hbar G}{c^3} \frac{1}{\lambda} = 4\pi \frac{\ell_P^2}{\lambda}, \quad (1.3)$$

where  $\ell_P \simeq 1.6 \times 10^{-35} m$  is the Planck length. We observe that the Schwarzschild radius associated with photons with wavelengths much larger than the Planck length is negligible with respect to the wavelength itself,  $r_S \ll \lambda$ . This means that spacetime around the photon is almost exactly flat and we can therefore ignore its gravitational field. However, this is not the case when the photon wavelength approaches the Planck length. In this case, the Schwarzschild radius becomes comparable to the wavelength and we cannot avoid taking into account the photon's gravitational field. In particular, for  $\lambda < 2\sqrt{\pi}\ell_P$ , we have  $r_S > \lambda$  and the photon seems to have no option but to collapse into a microscopic black hole, at least according to classical general relativity. Nonetheless, the classical formulation of general relativity is expected to break down at this scale in favor of a quantum theory of gravity. One can infer this conclusion not only from analogy with the other interactions (which are described, at the microscopic level, by quantum theories), but also from the observation that it seems impossible to couple a classical metric field to quantum matter fields without running into inconsistencies [10]. Unfortunately, standard quantization approaches do not work for general relativity and, up till now, there is no definitive answer on to how quantize gravity.

To derive an estimate of the magnitude of the metric fluctuations, we can initially proceed simply on the basis of dimensional considerations. Consider the Einstein field equations

$$G_{\mu\nu} = \frac{8\pi G}{c^4} T_{\mu\nu}. \quad (1.4)$$

Since the Einstein tensor  $G_{\mu\nu}$  is given by second-order derivatives of the metric, we can express it as  $G_{\mu\nu} \sim g_{\mu\nu}/L^2$ , where  $L$  is some length scale. In the same way, the stress-energy tensor  $T_{\mu\nu}$  has dimensions of energy density  $T_{\mu\nu} \sim E/L^3$ . If, as before, we consider a photon with energy  $E = 2\pi\hbar c/\lambda$ , from the uncertainty principle we obtain a fluctuation in its energy at the scale  $L = \lambda$ , given by  $\delta E \sim \hbar c/L$ . Inserting these expressions into the Einstein equations we

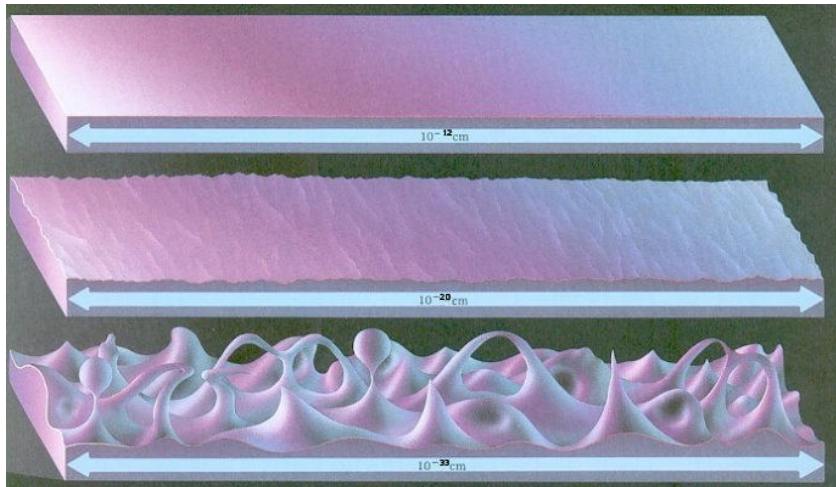


Figure 1: Pictorial representation of spacetime foam. The structure of space-time, which appears smooth and flat at large scales, becomes very complicated and topologically nontrivial at the Planck scale. Image from Ref. [11]

obtain

$$\frac{\delta g_{\mu\nu}}{L^2} \sim \frac{8\pi G}{c^4} \frac{\delta E}{L^3} \implies \delta g_{\mu\nu} \sim \frac{\ell_P^2}{L^2}, \quad (1.5)$$

from which we see that, indeed, the fluctuations become important at scales comparable with the Planck scale.

A more reliable estimation [12] of the fluctuations' magnitude can be obtained in the context of linearized gravity which, as it is not afflicted by the nonlinear nature of general relativity, can be quantized by employing standard quantization techniques. Linearized gravity is obtained by assuming the metric field is described by a background static metric, and for simplicity we consider this to be the Minkowski metric  $\eta_{\mu\nu}$ , plus a perturbation  $h_{\mu\nu}$  which must be determined from the Einstein equations, explicitly

$$g_{\mu\nu} = \eta_{\mu\nu} + h_{\mu\nu}. \quad (1.6)$$

Given this assumption, the Ricci scalar turns out to be

$$R = \partial_\mu \partial_\nu h^{\mu\nu} - \partial^2 h, \quad (1.7)$$

where  $h = h^\mu{}_\mu = \eta^{\mu\nu} h_{\mu\nu}$ . Inserting this expression into the Einstein-Hilbert action

$$S = \int d^4x \sqrt{-g} \left( \frac{c^4}{16\pi G} R + \mathcal{L}_{\text{matter}} \right), \quad (1.8)$$

expanded at the second order in  $h_{\mu\nu}$  gives

$$S = -\frac{\hbar}{32\pi\ell_P^2} \int d^4x h^{\mu\nu} \partial^2 h_{\mu\nu} + c \int d^4x h^{\mu\nu} \left( T_{\mu\nu} - \frac{1}{2} T \eta_{\mu\nu} \right) + \mathcal{O}(h^3). \quad (1.9)$$

Observing that this expression in vacuum,  $T_{\mu\nu} = 0$ , is analogous to the action of a free massless scalar field, quantization can be performed in a straightforward

manner. One finds that the correlator of field  $h_{\mu\nu}$  can be expressed in terms of the correlator of a quantum scalar field  $\phi$

$$\langle h(t, \vec{x})h(t, \vec{y}) \rangle = \frac{16\pi\ell_P^2}{\hbar} \langle \phi(t, \vec{x})\phi(t, \vec{y}) \rangle = \frac{8\ell_P^2}{\pi(\vec{x} - \vec{y})^2}, \quad (1.10)$$

where we consider the special case of an equal time propagator. Observing that the quantum propagator is a measure of the fluctuations of the field, by setting  $L = |\vec{x} - \vec{y}|$  we obtain

$$\delta h \sim \sqrt{\langle h(t, \vec{x})h(t, \vec{y}) \rangle} \implies \delta g_{\mu\nu} \sim \frac{\ell_P}{L}. \quad (1.11)$$

This expression differs from that derived previously, but again it shows that vacuum fluctuations of the metric become important at the Planck scale (see Fig. 1).

We stated briefly that not only the geometry but also the topology of spacetime should be afflicted by these fluctuations—this is a widely accepted conclusion, and there are actually a couple of arguments in its favor [12]. The first is simply that, since vacuum fluctuations of the metric below the Planck scale become much more larger than the metric itself ( $\delta g \gg g \sim 1$ ), they can be better described by a change in topology than by a change in geometry. The second is based on the Feynman path integral approach to quantization. Observing that in standard quantum field theory one has to sum over all possible configurations of a field, independently of the fact that they are well-behaved, in the same way in quantum gravity one should sum over all possible geometries independently of their topology.

We have tried to provide some simple arguments in favor of the concept of spacetime foam; however, lacking a definitive theory of quantum gravity, we must be careful when dealing with these arguments and bear in mind that they could turn out to be false in the end. In fact, they are based on the assumption that the description of spacetime in terms of manifold, metric, and Einstein field equations is still possible (in some quantized form) at the Planck scale. Nevertheless, it could also be that these notions are emerging classical manifestations at large scales of a completely different quantum theory at the Planck scale [13, 14].

Given the fact that there is no definitive theory on quantum gravity, many different approaches to the treatment of spacetime foam have been explored. Just to list a few examples, we can cite Refs. [15, 16, 17], where a path integral approach to spacetime foam is considered, Ref. [18], where an algebraic approach is proposed, Refs. [19, 20, 21], where spacetime foam is discussed in the context of string theory, Ref. [22], where spacetime foam is discussed in the context of loop quantum gravity, Refs. [23, 24], where spacetime foam is modeled as a gas of wormholes, Ref. [25], where an approach based on random walks is introduced, Ref. [26, 27], where a holographic model of spacetime foam is discussed, and so on.

Interest in these models resides principally in understanding how the quantum fluctuations of spacetime affect the propagation of particles. In fact, if they produce any kind of modifications, these should be, in principle, experimentally observable, thereby providing some experimental ground on which to construct a suitable theory of quantum gravity. The main difficulty in this direction is indeed the lack of any experimental data, due to the smallness of the Planck scale,

which is far below the experimental capability of current technology. As an example, consider the Large Hadron Collider (LHC), which at present is the most powerful particle accelerator in the world and is supposed to be able to reach energy in the center of the mass of proton-proton collisions of  $E_{CM} \sim 10^{13} eV$  [28]. This is, however, 15 orders of magnitude below the Planck energy  $E_P \sim 10^{28} eV$  at which quantum gravity fluctuations are expected to become important, and Eq. (1.11) tell us that the effects of these fluctuations at energy scale  $E_{CM}$  should be suppressed as  $\delta g_{\mu\nu} \sim E_{CM}/E_P \sim 10^{-15}$ . At the same time, ultra-high energy cosmic rays (UHECRs) reach energies of  $E_{cr} \sim 10^{21} eV$  [4], which are also way below Planck energy. One might even wonder if there will ever be any chance of measuring these quantum gravitational effects.

The hope is that, even if it is not possible to probe the Planck scale directly, it is nevertheless possible to measure some of its consequences at lower energies. A strong argument in favor of this idea has been proposed in Ref. [29], where it is argued that the tiny effects of spacetime fluctuations on the propagation of cosmic rays can sum up over the huge distances traveled by these particles and eventually become measurable. Another argument is discussed in Ref. [31], where it is shown that, even if spacetime fluctuations are negligible at the energy scale of ordinary particles, they are not for virtual particles that enter loop diagrams (since these are integrated over all possible values of energy), in which case these effects can show up as radiative corrections, even for low-energy particles.

From these considerations, it seems worthwhile investigating how spacetime foam affects the propagation of particles. The principal effect expected in the majority of the approaches to spacetime foam is a modification of particle dispersion relations, as if foamy spacetime could be represented by a dispersive medium with a nontrivial refractive index. This is usually associated with a violation of Lorentz symmetry, due to the presence in these models of terms that explicitly or spontaneously break this symmetry. Given the importance of this phenomenon we will discuss it more in detail in subsection 1.2. The modifications introduced by spacetime foam can lead to phenomena which do not occur in Minkowski space such as the appearance of an energy-dependent velocity of propagation for photons, vacuum birefringence, vacuum Cherenkov radiation, decoherence, blurring images of distant sources, and so on. See Ref. [30] for more details.

Before discussing Lorentz violation, we wish to provide some information on the particular spacetime foam models investigated in this work. We consider a very simplified situation in which spacetime foam is described at the classical level, i.e. we introduce a classical manifold endowed with a given distribution of nontrivial microscopic structures (representing the spacetime fluctuations) in which the particles propagate. To arrive at a quantum model, in the path integral formalism, we should sum over all possible distributions. Another simplification is that we build our foam model out of one particular microscopic structure, i.e. a specific type of topological defect, while, according to the idea of quantum fluctuation, any kind of microscopic structure should be taken into account.

To be more specific, in part II we try to build a Lorentz-invariant spacetime foam model made up of point-like topological defects; in reality, there is no reason *a priori* why spacetime foam must break Lorentz symmetry. Moreover, it has been pointed out in Ref. [31], and further discussed in Refs. [32, 33],

that even microscopic Lorentz-violating contributions at the Planck scale should affect low-energy particles (through radiative effects) with very large contributions that are not experimentally observed. On this basis, it is interesting to investigate spacetime foam models that preserve Lorentz invariance.

In part III, instead, we consider static but extended topological defects. In this case, we investigate how defects with the same topological structure but with different differential structures influence the propagation of particles. In fact, the model of part II, dealing with point-like defects, does not take into account the internal structure of the defects. But the defects are expected to have an extension and therefore can be endowed with different topological and differential structures. It is interesting to investigate how these structures affect the propagation of particles.

### 1.1.1 Topological defects

Here, we want to sketch in a bit more detail the concept of topological defect, as introduced above. Topological defects [34] are usually discussed in cosmology and condensed matter theory, and in these contexts they are defined as topological solitons, i.e. non-perturbative solutions of the field equations that are topologically distinct from the vacuum solution. In the context of cosmology, they are expected to originate during symmetry-breaking phase transitions in the early universe, such as the electroweak symmetry-breaking described by the Higgs mechanism. Depending on which particular symmetry is broken, different types of defect can originate. In cosmology, one finds four possible type of defects, namely domain walls, cosmic strings, magnetic monopoles, and textures. It is usually to these particular structures that one refers by using the term “topological defect”.

In the context of spacetime fluctuations, we class as a topological defect any microscopic structure of spacetime with non-trivial topology. The most notorious example of these defects is represented by the wormhole, which, firstly introduced in Ref. [5], can be obtained by removing two regions of spacetime and identifying their boundary. This is usually schematically depicted as in Fig. 2, where the two removed regions, the “mouths”, are connected by a tunnel. In this work, however, we will not deal with Wheeler wormholes but

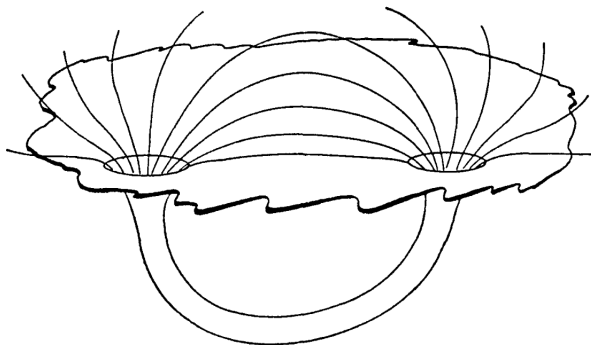


Figure 2: Pictorial representation of a Wheeler wormhole. Image from Ref. [5]

with simpler types of defect. In particular, in part III, we consider a (static)

defect obtained by removing a single region of space and identifying antipodal points on its boundary, as illustrated in Fig. 3. Observe that, as it happens for

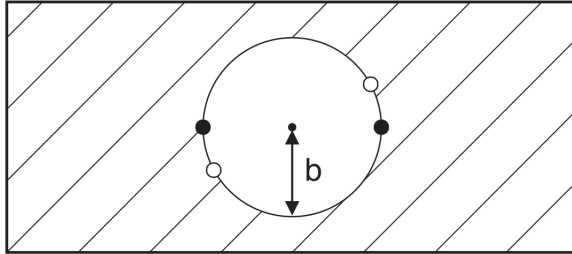


Figure 3: Schematic representation of a defect with antipodal points on the boundary identified. Image from Ref. [67]

the wormhole, the first homotopy group of this defect is nontrivial. Moreover, it can be shown that the topology of the defect embedded in Minkowski spacetime is  $\mathbb{R} \times (\mathbb{R}P^3 - \{0\})$ , where  $\mathbb{R}P^3$  is the 3-dimensional projective space.

In part II, instead, we consider a defect represented by a single point removed from Minkowski spacetime ( $M = \mathbb{R}^4 - \{0\}$ ). We observe that the first (and second) homotopy group in this case is trivial but higher homotopy groups are not, and so we can conclude that  $M$  and Minkowski spacetime are really topologically inequivalent manifolds.

## 1.2 Lorentz violation

We can now give a brief introduction to the topic of Lorentz violation. Lorentz invariance is a well-established result of standard physics. In particular, the standard model of particles is formulated to be Lorentz-invariant, which means that its action is constructed to be invariant under the special orthogonal group in Minkowski spacetime  $SO(1, 3)$ , defined as the group of transformations that preserve the Minkowski metric  $\eta_{\mu\nu} = \text{diag}(-1, 1, 1, 1)$ , explicitly

$$\Lambda^\nu{}_\mu \in SO(1, 3) \iff \Lambda^\rho{}_\mu \Lambda^\sigma{}_\nu \eta_{\rho\sigma} = \eta_{\mu\nu}. \quad (1.12)$$

From this relation, one can immediately see that scalar products (obtained by contracting two vectors with the metric) are Lorentz-invariant

$$p' \cdot k' = \eta_{\mu\nu} p'^\mu k'^\nu = \eta_{\mu\nu} \Lambda^\mu{}_\rho p^\rho \Lambda^\nu{}_\sigma k^\sigma = \eta_{\rho\sigma} p^\rho k^\sigma = p \cdot k. \quad (1.13)$$

It is also well-established, both theoretically and experimentally, that any result obtained in the context of the standard model is Lorentz-invariant, and that no spontaneous Lorentz symmetry breaking can occur in this theory. This is an extremely useful result because, if a violation of Lorentz symmetry were ever to be detected, one would know immediately that it is due to physics beyond the standard model. On the other hand, it is a common feature of quantum gravity models to display violations of Lorentz invariance, both by introducing terms that explicitly break the symmetry or by allowing for mechanisms that break it spontaneously (as discussed, for example, in Ref. [35] in the context of string theory).

A violation of Lorentz symmetry, in general, will result in a modification of the dispersion relation of particles, such as

$$E^2 = p^2 + m^2 + f(E, p, \alpha), \quad (1.14)$$

where the parameter  $\alpha$  is related to the scale at which the new physics appear (the Planck scale in the case of quantum gravity). This result can be used to constrain or falsify the particular spacetime foam or quantum gravity model one is investigating.

As a simple toy example, we can consider the case in which Lorentz invariance is explicitly broken by the introduction of a preferred direction  $n_\mu = \{1, 0, 0, 0\}$  (this can be achieved, for example, by considering a static spacetime foam model). We assume also that this preferred direction modifies the equation of motion of a massless scalar field in two different ways corresponding to two different models, for example with the term  $\alpha n_\mu \partial^\mu \phi$  in one case and  $\alpha' n_\mu \partial^\mu \partial^2 \phi$  in the other (observe that  $\alpha$  and  $\alpha'$  have different dimensionality). For the two cases, we obtain the modified dispersion relations

$$E^2 = \alpha p + p^2, \quad E^2 = p^2 + \alpha' p^3, \quad (1.15)$$

and, calculating the group velocity ( $v_g = \partial E / \partial p$ ), we see that in both cases the velocity of the particle depends on its frequency. However, in the first case the velocity increases at small frequencies, while in the second case it increases at large frequencies. Since experimentally we do not observe anomalous variations in the velocity of particles at small energies, we can reject the first model, while measuring the behavior of high-energy particles can constrain the parameter  $\alpha'$  in the second model.

A useful framework for dealing with Lorentz violation is the standard model extension [36], which provides an extension of the standard model of particles in which all possible Lorentz-violating terms that can arise from a more fundamental theory as the effect of spontaneous symmetry breaking are taken into account. The importance of this model resides in its generality and the fact that it is independent of the underlying theory. From an experimental point of view, one can simply deal with the parameters of the model, while from the theoretical standpoint, one simply has to use these parameters to constrain the particular model at hand. For example, the extended quantum electrodynamics Lagrangian is given by

$$\mathcal{L}_{SME} = \mathcal{L}_{SM} + \mathcal{L}_{LV}, \quad (1.16)$$

where  $\mathcal{L}_{LV}$  is the Lorentz-violating Lagrangian and  $\mathcal{L}_{SM}$  is the standard QED Lagrangian

$$\mathcal{L}_{SM} = \frac{i}{2} \bar{\psi}_n \gamma^\mu \overleftrightarrow{D}_\mu \psi_n - m_n \bar{\psi}_n \psi_n - \frac{1}{4} F_{\mu\nu} F^{\mu\nu}, \quad (1.17)$$

where  $n = 1, 2, 3$  indicates the lepton family, the covariant derivative is given by  $D_\mu = \partial_\mu + iqA_\mu$ , and the field strength is  $F_{\mu\nu} = \partial_\mu A_\nu - \partial_\nu A_\mu$ . The Lorentz-violating terms in  $\mathcal{L}_{LV}$  can be grouped accordingly to their behavior under CPT

transformation and are given by

$$\begin{aligned}
\mathcal{L}_{\text{lepton}}^{(+)} &= -\frac{1}{2}(H_l)_{\mu\nu nm}\bar{\psi}_n\sigma^{\mu\nu}\psi_m + \frac{i}{2}(c_l)_{\mu\nu nm}\bar{\psi}_n\gamma^\mu\overleftrightarrow{D}^\nu\psi_m + \\
&\quad + \frac{i}{2}(d_l)_{\mu\nu nm}\bar{\psi}_n\gamma_5\gamma^\mu\overleftrightarrow{D}^\nu\psi_m, \\
\mathcal{L}_{\text{lepton}}^{(-)} &= -(a_l)_{\mu nm}\bar{\psi}_n\gamma^\mu\psi_m - (b_l)_{\mu nm}\bar{\psi}_n\gamma_5\gamma^\mu\psi_m, \\
\mathcal{L}_{\text{photon}}^{(+)} &= -\frac{1}{4}(k_F)_{\mu\nu\rho\sigma}F^{\mu\nu}F^{\rho\sigma}, \\
\mathcal{L}_{\text{photon}}^{(-)} &= \frac{1}{2}(k_{AF})^\mu\epsilon_{\mu\nu\rho\sigma}A^\nu F^{\rho\sigma},
\end{aligned} \tag{1.18}$$

where (+) indicates a CPT even term, while (−) is a CPT odd term. Note that these terms preserve gauge invariance and power counting renormalizability. From this extended Lagrangian, it is possible to derive the dispersion relations for the leptons and photons given in the high energy limit ( $M_{Pl} \gg E \gg m$ ) by [37]

$$\begin{aligned}
E_e^2 &= m_e^2 + p^2 + f_e^{(1)}p + f_e^{(2)}p^2, & \text{electron,} \\
E_\gamma^2 &= (1 + f_\gamma^2)p^2, & \text{photon,}
\end{aligned} \tag{1.19}$$

where the coefficients  $f_A^{(i)}$  are obtained from the coupling parameters in  $\mathcal{L}_{LV}$ . Note that, since the standard model can be interpreted very well as an effective theory, the requirement for power counting renormalizability is often dropped and other terms are allowed to enter into the dispersion relations. Hence, the dispersion relations for electrons and photons can be expressed more generally as

$$\begin{aligned}
E_e^2 &= m_e^2 + p^2 + \eta_e^{(n)}\frac{p^n}{M_{Pl}^{n-2}}, & \text{electron,} \\
E_\gamma^2 &= p^2 + \eta_\gamma^{(n)}\frac{p^n}{M_{Pl}^{n-2}}, & \text{photon.}
\end{aligned} \tag{1.20}$$

### 1.2.1 Experimental tests

Ultra high-energy cosmic/gamma rays (UHECR/UHEGR) are the best experimental candidates for measuring the tiny effects (corresponding to Lorentz-violating modified dispersion relations for particles) of spacetime fluctuations. As mentioned previously, in fact, these phenomena possess two important features that add up to and increase the chances of probing very small scales (possibly even the Planck scale at which quantum gravity effects are expected to appear). The first characteristic is the energy of these particles,  $E \sim 10^{20}eV$ , which is much higher than the energies obtainable with current technology. The second is the cosmological distance traveled by these particles, which can magnify microscopic effects. Note that, on the other hand, lack of knowledge on the precise composition of cosmic rays and their emission mechanisms, as well as the lack of a large experimental sample, is a significant source of error.

The idea that the cosmological distance traveled by high-energy particles is a crucial characteristic is based on considerations about the time of flight of photons [25]. As we have observed, a Lorentz-violating modified dispersion relation implies an energy-dependent velocity of propagation, in which case two particles with different energies will take different times to travel the same

distance  $d$ . According to Eq. (1.20), the time difference for two photons of momenta  $p_1$  and  $p_2$  is

$$\Delta t^{(n)} = \frac{n-1}{2} \frac{p_2^{n-2} - p_1^{n-2}}{M_{Pl}^{n-2}} \eta_\gamma^{(n)} d, \quad (1.21)$$

and increases linearly with the distance  $d$ . Consequently, the greater the distance traveled by the particles, the greater the time difference  $\Delta t$ . This formula is based on the assumption that the photons are emitted at the same time, but the aforementioned incomplete understanding of how high-energy gamma rays are produced (for example, in gamma ray bursts) introduces a large systematic error into this type of measurement.

Other methods used to constrain the parameters of the modified dispersion relations (1.20) include, for example, vacuum birefringence, based on the fact that in principle different helicity states can be described by different dispersion relations, threshold reactions, based on the fact that modified dispersion relations can allow for otherwise forbidden processes such as photon decay or vacuum Cherenkov radiation, UHECR interactions with the cosmic microwave backgrounds, based on the fact that the GZK limit on the energy of cosmic rays could be altered by Lorentz-violating modifications, and so on. See Ref. [37] for more details on these kinds of measurement.

## Part II

# Spacetime foam from time-dependent, point-like defects

In this part, we present a Lorentz-invariant spacetime foam model and study how it affects the propagation of particles. As mentioned in the introduction, spacetime foam describes the quantum fluctuations of spacetime that originate from applying the uncertainty principle to gravity in an eventual quantization of this interaction. As pointed out in Ref. [6], these fluctuations may, in principle, affect both the geometry and the topology of the spacetime manifold. In this part (as well as in the rest of this thesis), we are mostly interested in the study of the second type of fluctuation, namely topological fluctuations.

From the uncertainty principle, these fluctuations are expected to be larger at smaller scales. We can therefore assume that nontrivial topological structures will show up only at very small scales (comparable to the Planck scale). Since ordinary particles have energies (and consequently resolving power) far below the Planck scale, we can safely avoid describing the structure of the fluctuations and just consider them to be simply point-like defects.

Also, since these defects originate from quantum fluctuations, they should be properly described by a quantum model. However, in this work, we consider the simpler case in which they are described by classical objects. As a result, spacetime foam can be represented by a classical background field which, through its interaction with elementary particles, affects their propagation dynamics.

In the following, we start by introducing the basic features that characterize the defects and their distribution in spacetime. Then, we show how the classical background field describing the spacetime foam can be obtained in general and how it affects the propagation of particles. Finally, we introduce a specific model to describe, more accurately, the propagation of photons in such a spacetime foam. We observe that, as long as the properties of the model remain Lorentz-invariant, the dispersion relation of the photon remains unchanged. We observe also that a possible modification of the photon dispersion relation can be obtained in a certain extension of the model (which maintains Lorentz invariance), and this modification is the appearance of a photon mass.

## 2 Basic features

In this section, we introduce the fundamental characteristics upon which the spacetime foam model that we want to study is constructed, namely the CPT anomaly and sprinkling. The CPT anomaly is an anomalous contribution to the field action that originates from the non-trivial topology of the defects (i.e. the fundamental constituents of the spacetime foam). Sprinkling, instead, is a procedure that allow us to distribute the defects into spacetime in a Lorentz-invariant manner.

## 2.1 CPT anomaly

It has been shown [38, 39] that, in certain chiral gauge theories defined over a manifold with nontrivial topology (e.g. with a compact spatial dimension), a CPT anomaly can appear. Observe that, due to the theorem proved in Ref. [41], such a violation of the CPT symmetry necessarily implies a violation of the Lorentz symmetry. In Ref. [40], the appearance of the CPT anomaly has been derived in case the nontrivial topology is realized at small scales (due to the presence of a static topological defect). A spacetime foam model obtained by averaging the effects of many defects distributed in spacetime has been introduced, and modified dispersion relations for scalar and photons derived accordingly. It should be noted, however, that due to the static nature of the defects, the spacetime foam model obtained in this way is intrinsically Lorentz-violating. Here, we want to generalize this result to the case of time-dependent defects so that we can construct a Lorentz-invariant spacetime foam model.

We start by briefly summarizing the framework of Ref. [40]. The manifold considered in this work is  $M = \mathbb{R} \times M_3$ , where  $M_3 = \mathbb{R} \times (\mathbb{R}^2 - \{0\})$ , and  $M$  is equipped with the Minkowski metric  $\eta_{\mu\nu} = \text{diag}(1, -1, -1, -1)$ . The gauge group considered is  $SO(10)$  (which, we recall, contains the standard model as a subgroup) with gauge fields  $B_\mu(x)$  and Weyl fermions  $\psi_\alpha(x)$  ( $\alpha = 1, 2$  is a spinor index) in the **16** representation. The fermionic action is given by

$$S(\psi, \bar{\psi}, B) = i \int_M d^4x \bar{\psi} \bar{\sigma}^\mu (\partial_\mu + B_\mu) \psi, \quad (2.1)$$

where  $\bar{\sigma} = (\mathbf{1}, \sigma^1, \sigma^2, \sigma^3)$ , and  $\sigma^i$  are the Pauli matrices. One is interested in the effective action  $\Gamma(B)$  for the gauge fields obtained by integrating out the chiral fermions

$$e^{i\Gamma(B)} = \int \mathcal{D}\psi \mathcal{D}\bar{\psi} e^{iS(\psi, \bar{\psi}, B)}. \quad (2.2)$$

By introducing cylindrical coordinates around the linear defect, and then choosing a special class of gauge fields,  $B'$ , which are  $\phi$ -independent and with vanishing components along  $\phi$  ( $\phi$  being the angular variable), one is able to integrate over the  $\phi$  variable in the fermionic action (2.1). The result is a new 3-dimensional action that contains an infinite sum over Dirac fermions  $\eta_n(x)$  ( $n \in (-\infty, \infty)$ ). From this action, one can finally determine the contribution to the effective gauge field action  $\Gamma(B')$  corresponding to the sector  $n = 0$  (that describes a massless fermion). Such a contribution contains the CPT anomaly and is given by

$$\Gamma_{CPT}(B') = \int_M d^4x \frac{x^1 \omega_{CS}(B'_0, B'_1, B'_3) + x^2 \omega_{CS}(B'_0, B'_2, B'_3)}{2\sqrt{(x^1)^2 + (x^2)^2}}, \quad (2.3)$$

in which  $\omega_{CS}$  is the Chern-Simons density [42, 43]

$$\omega_{CS}(B_0, B_1, B_2) = \frac{\epsilon^{\mu\nu\rho}}{16\pi^2} \text{tr} \left( B_{\mu\nu} B_\rho - \frac{2}{3} B_\mu B_\nu B_\rho \right) \quad (2.4)$$

where  $\epsilon^{\mu\nu\rho}$  is the 3-dimensional Levi-Civita symbol and  $B_{\mu\nu}$  is the Yang-Mills field strength tensor,  $B_{\mu\nu} = \partial_\mu B_\nu - \partial_\nu B_\mu + [B_\mu, B_\nu]$ . Restricting this result to the Abelian subgroup  $U(1) \subset SO(10)$  corresponding to electromagnetism

(whose gauge field has been renamed  $A_\mu$ ), one obtains the anomalous contribution to the effective electromagnetic action

$$\Gamma_{CPT}(A) = \frac{1}{32\pi} \int_{\mathbb{R}^4} d^4x f_M(x; A) \epsilon^{\mu\nu\rho\sigma} F_{\mu\nu}(x) F_{\rho\sigma}(x), \quad (2.5)$$

where  $F_{\mu\nu} = \partial_\mu A_\nu - \partial_\nu A_\mu$  and  $f_M(x; A)$  is a functional that carries the imprint of the topological structure of the defect.

A static spacetime foam model is obtained by considering a random uniform distribution of defects in space. Since it is not possible to calculate directly the CPT anomalous term for many defects, one assumes that the contributions from the individual defects add up incoherently, resulting in a static background field  $g(\vec{x})$ . Hence, the photon action in this spacetime foam model takes the form

$$S_{photon} = -\frac{1}{4} \int_{\mathbb{R}^4} d^4x \{F_{\mu\nu}(x) F^{\mu\nu}(x) + g(\vec{x}) \epsilon^{\mu\nu\rho\sigma} F_{\mu\nu}(x) F_{\rho\sigma}(x)\}. \quad (2.6)$$

The background field is assumed to vanish on average and to vary over length scales much smaller than the photon wavelength ( $a \ll \lambda$ , where  $a^3 = 1/\rho$  and  $\rho$  is the 3-dimensional number density of defects  $\rho = \langle N(V_3)/V_3 \rangle$ ). This is explicitly given by

$$g(\vec{x}) = \lambda \sum_n \epsilon_n h(\vec{x} - \vec{x}_n), \quad (2.7)$$

where  $h(\vec{x}_n)$  is the contribution of the defect placed at the random position  $\vec{x}_n \in \mathbb{R}^3$  and the numbers  $\epsilon_n = \pm 1$  are assigned randomly to each defect (so that the total contribution vanishes on average). From Eq. (2.6), it is possible to obtain the modified dispersion relation

$$\omega^2 = (1 - a_0) c^2 \vec{k}^2 - a_1 c^2 \vec{k}^4 + \dots, \quad (2.8)$$

where the positive coefficients  $a_i$  can be calculated once the specific form of  $h(\vec{x})$  is given.

Here, we want to generalize this approach to the case where the defects are time-dependent. Explicitly, we consider a topological defect described by the manifold  $M = \mathbb{R}^4 - \{0\}$  equipped with the standard Minkowski metric  $\eta_{\mu\nu} = \text{diag}(1, -1, -1, -1)$  (that is, Minkowski spacetime with a single point removed). We then make the assumption that such a spacetime causes an anomalous contribution to the electromagnetic action analogous to that derived for a static defect (Eq. (2.5)). We can obtain a (non-static) spacetime foam model by randomly distributing the defects in spacetime according to a uniform distribution with (4-dimensional) number density  $\rho = \langle N(V_4)/V_4 \rangle$ , where again the contributions from individual defects add up incoherently into a (non-static) background field  $g(x)$ . The photon action in this spacetime foam model is

$$S_{photon} = -\frac{1}{4} \int_{\mathbb{R}^4} d^4x \{F_{\mu\nu}(x) F^{\mu\nu}(x) + g(x) \epsilon^{\mu\nu\rho\sigma} F_{\mu\nu}(x) F_{\rho\sigma}(x)\}, \quad (2.9)$$

where the background field is given by

$$g(x) = \lambda \sum_n \epsilon_n h(x - x_n). \quad (2.10)$$

Note that the defect shape  $h(x)$  now also depends on the time ( $x \in \mathbb{R}^4$ ), and the random defect positions  $x_n \in \mathbb{R}^4$  are also chosen in the entire Minkowski spacetime.

Since we are interested in building a spacetime foam model that is not only time-dependent but also does not explicitly break Lorentz invariance, we want the distribution of defects to be Lorentz-invariant. Therefore before proceeding to study the model, in the next subsection we show how to obtain such a Lorentz-invariant distribution.

## 2.2 Sprinkling and Lorentz invariance

In order to obtain a distribution of defects  $\{x_n\}$  that is Lorentz-invariant, we borrow a method introduced in causal set theory [44, 45, 46, 47], i.e sprinkling. This method is used in causal set theory to discretize a Lorentzian manifold maintaining local Lorentz invariance. Once the sprinkled points are obtained, the rest of the manifold is removed and the points endowed with a causal structure form a causal set, namely a discrete realization of spacetime. Observe that what we want to do to construct our spacetime foam model is somehow complementary to what happens in causal set theory. In fact, in this instance, once we have identified the Lorentz-invariant set of sprinkled points, we remove them from Minkowski spacetime and use the continuum remnant of the manifold as a description of spacetime.

Sprinkling is nothing more than a Poisson process realized over the manifold at hand, in our case Minkowski spacetime, the result of which is a Poisson distribution. This means that the probability of finding  $n$  defects in a spacetime region of volume

$$V = \int_{\text{region}} d^4x \sqrt{-\eta}, \quad (2.11)$$

is given by

$$P_n(V) = \frac{(\rho V)^n e^{-\rho V}}{n!}, \quad (2.12)$$

where  $\rho$  is a parameter of the distribution. Note that, according to Eq. (2.12), when we consider an infinitesimal volume  $\delta V$ , the probability of finding a single defect in that region is proportional to the volume

$$P_{n=1}(\delta V) = \rho \delta V + \mathcal{O}(\delta V^2). \quad (2.13)$$

Instead, the probability of finding more than one defect is negligible when  $\delta V \rightarrow 0$

$$P_{n>1}(\delta V) = \mathcal{O}(\delta V^n). \quad (2.14)$$

An explicit realization of a Poisson process is given by the following prescription [46]: given a region of spacetime of volume  $V$

- divide  $V$  into small boxes of volume  $\delta V$ ,
- place a defect into each box with probability  $P = \rho \delta V$ ,
- the Poisson process is obtained in the limit  $\delta V \rightarrow 0$ .

Since the Poisson process described by the previous steps only depends on the spacetime volume, it must be invariant under any volume-preserving linear transformation. The class of volume-preserving linear transformations contains, of course, the Lorentz group. This can be seen simply by calculating the Jacobian determinant, which, for a Lorentz transformation, is  $\det \mathcal{J} = 1$ . Since this is in unity, the volume form  $d^4x$  is preserved,  $d^4x \rightarrow d^4x' = \det \mathcal{J} d^4x = d^4x$  (this implies that if in a Lorentz transformation the time coordinate is dilated by a factor  $\gamma$ , one of the spatial coordinates undergoes contraction by the same factor).

We have seen that the Poisson process is Lorentz-invariant, and the same is true for the resulting Poisson distribution (2.12) (which also depends only on the spacetime volume), but it could still be argued that, since it is a random process, some of its realizations  $\{x_n\}$  may exhibit some degree of asymmetry and not be Lorentz-invariant. However, it has been proved in Ref. [47] that each realization of a Poisson process is individually Lorentz-invariant.

Lorentz invariance in this context has the following meaning [46]:

*“The discrete set of sprinkled points must not, in and of itself, serve to pick out a preferred reference frame.”*

This means that the statistical properties of the distribution of defects (e.g. the mean density of defects) do not depend on the reference frame in which we choose to measure them. In fact, we want to stress that the number of defects contained in different regions of equal volume  $V$  is not constant but fluctuates from region to region

$$N(V) = \langle N(V) \rangle \pm \delta N(V). \quad (2.15)$$

The mean value  $\langle N(V) \rangle$  and the standard deviation  $\delta N(V)$  can be calculated from the Poisson distribution (2.12) and are given by

$$\begin{aligned} \langle N(V) \rangle &= \sum_{n=0}^{\infty} n P_n(V) = \rho V, \\ \delta N(V) &= \sqrt{\sum_{n=0}^{\infty} (n - \langle N(V) \rangle)^2 P_n(V)} = \sqrt{\rho V}. \end{aligned} \quad (2.16)$$

From these equations, we can also deduce the expected value of the number density of defects  $\rho_{obs}$  in a region of spacetime volume  $V$ , which is given by

$$\rho_{obs} = \langle \rho_{obs} \rangle \pm \delta \rho_{obs} = \frac{\langle N(V) \rangle}{V} \pm \frac{\delta N(V)}{V} = \rho \pm \sqrt{\frac{\rho}{V}}, \quad (2.17)$$

from which we can finally identify the parameter  $\rho$  in Eq. (2.12) with the mean value of the density of defects  $\rho_{obs}$ . Note also that, even if the density of defects is not constant from region to region, the fluctuations in its value become negligible when the mean volume available to a single defect,  $V_d = 1/\rho$ , is much smaller than volume  $V$  of the region considered

$$V_d = \frac{1}{\rho} \ll V \Rightarrow \frac{\delta \rho_{obs}}{\rho_{obs}} = \frac{1}{\sqrt{\rho V}} \sim 0. \quad (2.18)$$

This means that we can treat the density as a constant quantity in spacetime,  $\rho_{obs}(x) = \rho$ , as long as we are dealing with scales much larger than volume  $V_d$  available to the defects.

In Figs. 4 and 5, we compare the behavior under Lorentz boost of a sprinkled set of points and of a regular distribution.

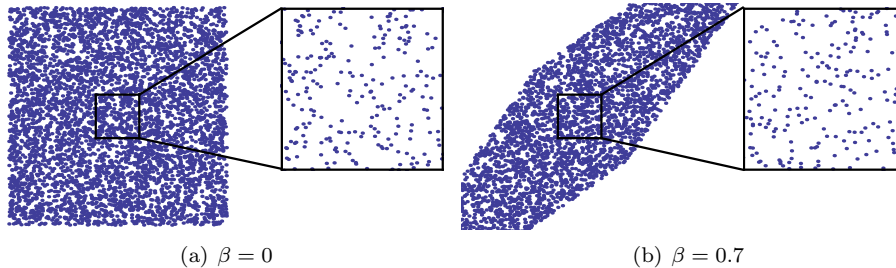


Figure 4: Example of sprinkling in a finite region of 2-dimensional Minkowski spacetime as it looks in two different inertial frames. The second frame (b) is boosted by a Lorentz boost factor  $\beta = 0.7$  along the positive spatial axis with respect to the first frame (a). Observe that, while the shape of the region changes from (a) to (b), it is not possible to find any difference in the distribution of defects in the two cases.

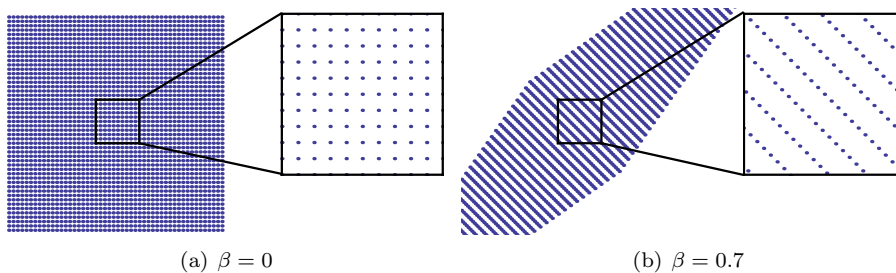


Figure 5: Same as in the previous figure, where the sprinkling has been substituted by a regular distribution. Note that in this case both the shape of the region and the characteristics of the distribution change from (a) to (b): in (a) the density of defects is uniform, in (b) it is not. This distribution is not Lorentz-invariant. In fact, in accordance with the definition given above, it identifies a preferred reference frame ( $\beta = 0$ ), in which the density of defects is uniform.

### 3 Effective theory

Now that we have established a method to obtain a Lorentz-invariant distribution of defects, we can proceed to study the effective theory introduced in Sec. 2.1, given for a vector field by the action (2.9). We recall that this action describes the effective theory of a photon propagating in a flat spacetime filled with a Lorentz-invariant distribution (i.e. a sprinkling) of point-like defects, where the effect of each defect, given by the anomalous contribution (2.5), is averaged into a background field  $g(x)$  (Eq. (2.10)).

We begin by considering precisely the background field  $g(x)$ , which, we recall,

is defined as

$$g(x) = \lambda \sum_n \epsilon_n h(x - x_n), \quad (3.1)$$

where the numbers  $\epsilon_n = \pm 1$  are assigned randomly to each defect with uniform probability and the distribution of defects  $\{x_n\}$  has been obtained through a sprinkling process over Minkowski spacetime with density parameter  $\rho$  so that

$$\rho_{obs} = \frac{N(V)}{V} = \rho \pm \sqrt{\frac{\rho}{V}}. \quad (3.2)$$

We assume that the volume available to each defect  $V_d$  is much smaller than the scale of the process considered (determined, for example, by the wavelength of the photon,  $V_d \ll \lambda^4$ ), in this way we can consider the density of defects to be constant ( $\rho_{obs}(x) = \rho$ ). We assume also that the shape function  $h(x)$ , which describes the contribution of a single defect to the background field, is a Lorentz-invariant quantity

$$h(x) \equiv h(x^2). \quad (3.3)$$

Since later in the calculation we will need to manipulate expressions involving the Fourier transform of the field  $g(x)$ , we want to derive here some simplified formulas. We start by introducing the Fourier transform of  $g(x)$

$$g(q) = \int d^4x g(x) e^{iq \cdot x} = \lambda \sum_n \epsilon_n \int d^4x h(x - x_n) e^{iq \cdot x} = \lambda h(q) \sum_n \epsilon_n e^{iq \cdot x_n}, \quad (3.4)$$

where, in the last step, we changed coordinates  $x'^\mu = x^\mu - x_n^\mu$  to obtain the Fourier transform  $h(q)$  of the shape function  $h(x)$ . To calculate the sum over  $n$  we observe that, as long as we are concerned with scales much larger than  $V_d = 1/\rho$ , we can approximate the sum with an integral over a continuous variable  $dn$ . Moreover, since the sprinkling process ensures proportionality between the number of defects and the volume in which they are distributed ( $\langle N(V) \rangle = \rho V$ ), we can rewrite the integral over the number variable  $dn$  as an integral in spacetime  $d^4x$ . Consider now the simpler case in which  $\epsilon_n = 1$ , the sum in Eq. (3.4) becomes

$$\sum_n e^{iq \cdot x_n} = \int_0^\infty dn e^{iq \cdot x(n)} = \rho \int_{\mathbb{R}^4} d^4x e^{iq \cdot x} = (2\pi)^4 \rho \delta^4(q). \quad (3.5)$$

However, when the random number  $\epsilon_n = \pm 1$  is reintroduced, the sum vanishes on average. To show this explicitly, one can simply rewrite the distribution of defects  $\{x_n\}$  as a sum of two subsets, collecting in one subset,  $\{x_n^{(+)}\}$ , those defects with  $\epsilon_n = +1$  and in the other,  $\{x_n^{(-)}\}$ , the defects with  $\epsilon_n = -1$ . Since the numbers  $\epsilon_n$  are associated randomly with each defect with uniform probability, the two subsets  $\{x_n^{(\pm)}\}$  still describe Poisson distributions with equal densities  $\rho/2$ . Now, the sum in Eq. (3.4) can be carried on separately on the two subsets as in Eq. (3.5), and since the result in the two cases differ only for a minus sign, their contributions cancel out each other.

We can consider now the case in which we have to calculate the product of two Fourier transforms of the background field

$$g(q)g(p) = \lambda^2 h(q)h(p) \sum_{n,m} \epsilon_n \epsilon_m e^{iq \cdot x_n} e^{ip \cdot x_m}, \quad (3.6)$$

where we need to compute a double sum over  $n$  and  $m$ . This time, it is useful to split the sum into a term where  $n = m$  and a term where  $n \neq m$

$$\sum_{n,m}^{\infty} \epsilon_n \epsilon_m e^{iq \cdot x_n} e^{ip \cdot x_m} = \sum_n^{\infty} (\epsilon_n)^2 e^{i(q+p) \cdot x_n} + \sum_{n \neq m}^{\infty} \epsilon_n \epsilon_m e^{iq \cdot x_n} e^{ip \cdot x_m}. \quad (3.7)$$

In this way, the first term can be immediately calculated as in Eq. (3.5), while the second term vanishes on average. In fact, again, one can subdivide the sum in the second term into two parts, one where  $\epsilon_n \epsilon_m = +1$  and one where  $\epsilon_n \epsilon_m = -1$ , the contributions of which are equal on average—apart for a minus sign—and therefore their sum vanishes. Finally, the product (3.6) provides the result

$$g(q)g(p) = (2\pi)^4 \lambda^2 \rho h(q)h(p) \delta^4(q+p). \quad (3.8)$$

### 3.1 Scalar field

We can now move on to study the effects of the spacetime foam model described by the background field  $g(x)$  on the propagation of particles. We start by considering the simpler case of a scalar field  $\phi(x)$  whose effective action (analogous to Eq. (2.9) for a vector field) is given by [40]

$$S_\phi = \int d^4x e^{g(x)} (\partial_\mu \phi(x) \partial^\mu \phi(x) - m^2 \phi(x)^2). \quad (3.9)$$

From this action one derives the equation of motion

$$(\partial^2 + m^2)\phi(x) = -\partial_\mu g(x) \partial^\mu \phi(x). \quad (3.10)$$

Moving to momentum space, it is better to consider for the moment the system confined to a box of 4-volume  $V$  (in order to have a non-vanishing Fourier transform of the field  $g(x)$ ), in which case we obtain

$$(k^2 - m^2)\phi(k) = -\frac{1}{(2\pi)^4} \int_V d^4q q \cdot (k - q) g_V(q) \phi(k - q). \quad (3.11)$$

We note that at this stage, with the system inside a box, the Fourier integral over  $q$  is actually a discrete Fourier sum. Since we will later take the limit  $V \rightarrow \infty$ , we use for simplicity the symbol of integration, even for the intermediate steps.

We are interested in obtaining a modified dispersion relation from this equation in the form

$$(k^2 - m^2)\phi(k) = A(k)\phi(k). \quad (3.12)$$

Assuming we have a small coupling constant,  $\lambda \ll 1$ , we can expand the solution  $\phi(k)$  perturbatively in powers of  $\lambda$

$$\phi(k) = \phi^{(0)}(k) + \lambda \phi^{(1)}(k) + \lambda^2 \phi^{(2)}(k) + \dots \quad (3.13)$$

Inserting this expression into Eq. (3.11) gives

$$\begin{aligned} & (k^2 - m^2) \left( \phi^{(0)}(k) + \lambda \phi^{(1)}(k) + \lambda^2 \phi^{(2)}(k) + \dots \right) = \\ & = \lambda \int_V \frac{d^4q}{(2\pi)^4} q \cdot (q - k) g_V(q) \left( \phi^{(0)}(k - q) + \lambda \phi^{(1)}(k - q) + \lambda^2 \phi^{(2)}(k - q) + \dots \right), \end{aligned} \quad (3.14)$$

and equating the terms with the same number of powers of  $\lambda$ , we obtain

$$\begin{aligned}
\lambda^0 & (k^2 - m^2)\phi^{(0)}(k) = 0, \\
\lambda^1 & (k^2 - m^2)\phi^{(1)}(k) = -\frac{1}{(2\pi)^4} \int_V d^4q \, q \cdot (k - q) g_V(q) \phi^{(0)}(k - q), \\
\lambda^2 & (k^2 - m^2)\phi^{(2)}(k) = -\frac{1}{(2\pi)^4} \int_V d^4q \, q \cdot (k - q) g_V(q) \phi^{(1)}(k - q), \\
& \dots
\end{aligned} \tag{3.15}$$

from which we can calculate the terms of the expansion (3.13). Explicitly, taking the limit  $V \rightarrow \infty$  and making use of the result (3.8), the first elements of Eq. (3.13), in terms of the free solution  $\phi^{(0)}(q)$ , are given by

$$\begin{aligned}
\phi^{(1)}(k) &= \int \frac{d^4q}{(2\pi)^4} g(q) \frac{q \cdot (q - k)}{k^2 - m^2} \phi^{(0)}(k - q), \\
\phi^{(2)}(k) &= \int \frac{d^4q}{(2\pi)^4} \frac{\rho h^2(q)}{k^2 - m^2} \frac{q \cdot (q - k) q \cdot k}{(k - q)^2 - m^2} \phi^{(0)}(k), \\
\phi^{(3)}(k) &= \int \frac{d^4q d^4p}{(2\pi)^8} \frac{\rho g(q) h^2(q) q \cdot (q - k) p \cdot (p + q - k) p \cdot (k - q)}{(k^2 - m^2)[(k - q)^2 - m^2][(k - q - p)^2 - m^2]} \phi^{(0)}(k - q), \\
\phi^{(4)}(k) &= \int \frac{d^4q d^4p}{(2\pi)^8} \frac{\rho^2 h^2(q) h^2(p) q \cdot (q - k) (q \cdot k) p \cdot (p - k) (p \cdot k)}{(k^2 - m^2)^2 [(k - q)^2 - m^2][(k - p)^2 - m^2]} \phi^{(0)}(k), \\
& \dots
\end{aligned} \tag{3.16}$$

where we have suppressed, for simplicity, the factors  $+i\epsilon$  in the denominators. We observe that all the odd terms of the expansion ( $\phi^{(1)}$ ,  $\phi^{(3)}$ , ...) contain a factor  $g(q)$  which, as we have seen, vanishes in the limit  $V \rightarrow \infty$ ; consequently, they do not contribute to the expansion of  $\phi(k)$ .

If we now introduce the functions

$$F(k) = \frac{\rho}{(2\pi)^4} \int d^4q \frac{h^2(q)}{k^2 - m^2 + i\epsilon} \frac{q \cdot (q - k) q \cdot k}{(k - q)^2 - m^2 + i\epsilon}, \tag{3.17a}$$

$$F_1(k) = \frac{\rho}{(2\pi)^4} \int d^4q h^2(q) \frac{q \cdot (q - k) q \cdot k}{(k - q)^2 - m^2 + i\epsilon}, \tag{3.17b}$$

the expansion (3.13) for the field  $\phi(k)$  can be rewritten as

$$\phi(k) = (1 + \lambda^2 F(k) + \lambda^4 F(k)^2 + \lambda^6 F(k)^3 + \dots) \phi^{(0)}(k), \tag{3.18}$$

while the set of equations (3.15) becomes

$$\begin{aligned}
\lambda^0 & (k^2 - m^2)\phi^{(0)}(k) = 0, \\
\lambda^2 & (k^2 - m^2)\phi^{(2)}(k) = F_1(k)\phi^{(0)}(k), \\
\lambda^4 & (k^2 - m^2)\phi^{(4)}(k) = F_1(k)F(k)\phi^{(0)}(k), \\
\lambda^6 & (k^2 - m^2)\phi^{(6)}(k) = F_1(k)F(k)^2\phi^{(0)}(k), \\
\lambda^8 & (k^2 - m^2)\phi^{(8)}(k) = F_1(k)F(k)^3\phi^{(0)}(k), \\
& \dots
\end{aligned} \tag{3.19}$$

Using these expressions we can rewrite Eq. (3.14) as

$$\begin{aligned} (k^2 - m^2) \left( \phi^{(0)}(k) + \lambda^2 \phi^{(2)}(k) + \lambda^4 \phi^{(4)}(k) + \dots \right) = \\ = (0 + \lambda^2 F_1(k) + \lambda^4 F_1(k)F(k) + \lambda^6 F_1(k)F(k)^2 + \lambda^8 F_1(k)F(k)^3 + \dots) \phi^{(0)}(k). \end{aligned} \quad (3.20)$$

This can be further manipulated to obtain

$$\begin{aligned} (k^2 - m^2) (1 + \lambda^2 F(k) + \lambda^4 F(k)^2 + \lambda^6 F(k)^3 + \dots) \phi^{(0)}(k) = \\ = \lambda^2 F_1(k) (1 + \lambda^2 F(k) + \lambda^4 F(k)^2 + \lambda^6 F(k)^3 + \dots) \phi^{(0)}(k), \end{aligned} \quad (3.21)$$

and, given Eq. (3.18), we finally get

$$(k^2 - m^2)\phi(k) = \lambda^2 F_1(k)\phi(k), \quad (3.22)$$

where we have re-summed all of the terms of the perturbative expansion of  $\phi(k)$ . Observe that this equation has exactly the same form as Eq. (3.12) with  $A(k) = \lambda^2 F_1(k)$ . The modified dispersion relation of the scalar field turns out to be

$$k^2 - m^2 = \lambda^2 F_1(k). \quad (3.23)$$

What remains to be done is to calculate the integral  $F_1(k)$  (Eq. (3.17b)). We note that, since in Eq. (3.19),  $F_1(k)$  always acts on the zero order  $\phi^{(0)}$  of the expansion of the scalar field, for which the standard dispersion relation holds, we can make use of relation  $k^2 - m^2 = 0$  in the integral (the Fourier transform of  $\phi^{(0)}(x)$  contains a Dirac delta function  $\delta(k^2 - m^2)$  see Refs. [40, 48]). Thus, the modification  $A(k)$  that we want to calculate becomes

$$A(k) = \frac{\lambda^2 \rho}{(2\pi)^4} \int d^4 q h^2(q^2) \frac{q \cdot (q - k) q \cdot k}{q^2 - 2q \cdot k + i\epsilon}. \quad (3.24)$$

In order to simplify this expression we use the Wick rotation [49] to move to Euclidean space

$$\begin{aligned} q_0 \rightarrow q_\tau = -i q_0, \\ k_0 \rightarrow k_\tau = -i k_0. \end{aligned} \quad (3.25)$$

In this way, we can introduce spherical coordinates (in 4 dimensions) and integrate over the angular variables. Equation (3.24) becomes

$$A(k_E) = \frac{\lambda^2 \rho}{(2\pi)^4} 2\pi^2 i \int_0^\infty dq_E q_E^3 h(-q_E^2)^2 \frac{q_E^2}{8k_E^2} \left( 2k_E^2 - q_E^2 + q_E^2 \sqrt{1 - \frac{4k_E^2}{q_E^2}} \right). \quad (3.26)$$

Now, we can rewrite this integral as a 4-dimensional integral independent of the angular variables, and then we can rotate it back to Minkowski spacetime and obtain

$$A(k) = \frac{\lambda^2 \rho}{(2\pi)^4} \int d^4 q h^2(q^2) \frac{q^2}{8k^2} \left( q^2 - 2k^2 - q^2 \sqrt{1 - \frac{4k^2}{q^2}} \right). \quad (3.27)$$

The problem with this expression is that it is valid only for  $4k^2 < q^2$ , but we have to integrate over all values of  $q$ . For a static background field  $g(\vec{q})$  [40],

a similar condition appears but it only concerns the spatial coordinates. In that case, it is possible to produce a meaningful result by assuming the shape function  $h(\vec{q})$  is different from zero only for momenta  $\vec{q}^2$  larger than a certain threshold  $\vec{q}_{low}^2$ . In the present case, we can make an analogous assumption

$$h(q^2) = 0 \quad \text{for } q^2 < q_{low}^2; \quad (3.28)$$

however, there is no reasonable explanation which guarantees its validity. To circumvent this problem, we will introduce in Sec. 4 an explicit model in which the expression of the shape function  $h(q)$  is known, and that allows us to evaluate completely the integral in the modification  $A(k)$ .

For the moment, we simply assume that the shape function  $h(q)$  is such as to ensure that the condition (3.28) is satisfied. Now we can proceed to expand the square root in powers of  $k^2$  (provided  $k^2 < q_{low}^2/4$ )

$$A(k) = \frac{\lambda^2 \rho}{(2\pi)^4} \int d^4 q h^2(q^2) \frac{1}{4} \left( k^2 + 2 \frac{k^4}{q^2} + 5 \frac{k^6}{q^4} + O(k^8) \right). \quad (3.29)$$

The modified dispersion relation turns out to be

$$k^2 - m^2 = ak^2 + bk^4 + ck^6 + O(k^8), \quad (3.30)$$

where

$$\begin{aligned} a &= \frac{\lambda^2 \rho}{4(2\pi)^4} \int d^4 q h^2(q^2), & b &= \frac{\lambda^2 \rho}{4(2\pi)^4} \int d^4 q h^2(q^2) \frac{2}{q^2}, \\ c &= \frac{\lambda^2 \rho}{4(2\pi)^4} \int d^4 q h^2(q^2) \frac{5}{q^4}. \end{aligned} \quad (3.31)$$

In order to obtain a well-formed dispersion relation we can solve Eq. (3.30) as an algebraic equation in  $k^2$ . Neglecting for simplicity the terms  $O(k^6)$ , we end up with two possible solutions

$$\begin{aligned} k_1^2 &= \frac{m^2}{1-a} + \frac{b m^4}{(1-a)^3} + O(m^6), \\ k_2^2 &= \frac{1-a}{2b} - \frac{m^2}{1-a} - \frac{b m^4}{(1-a)^3} + O(m^6). \end{aligned} \quad (3.32)$$

To choose the physical one, we require that when the perturbation weakens (i.e. when  $\lambda \rightarrow 0$ ), the modified dispersion relation approaches the dispersion relation for the free theory. We see immediately that this requirement is satisfied only by the first relation. We therefore have to discard the second option (which diverges for  $\lambda \rightarrow 0$ ) and we are left with the solution:

$$k^2 = \frac{m^2}{1-a} + \frac{b m^4}{(1-a)^3} + O(m^6), \quad (3.33)$$

where the coefficients  $a$  and  $b$  are Lorentz-invariant quantities. These coefficients are defined in equation (3.31) and depend on the microscopic features of the model (such as the form of the function  $h(q)$  and the density of defects  $\rho$ ). We started with a Lorentz-invariant spacetime foam model and we arrived at a

modified dispersion relation which is still completely Lorentz-invariant, the only effect being a rescaling of the mass of the scalar field.

We wish to remark, however, that this result, Eq. (3.33), has been derived on the basis of an assumption, namely Eq. (3.28), which is not physically justified and consequently its validity is questionable. As we said, in order to circumvent this problem, we will introduce in Sec. 4 an explicit model that allows us to perform calculations without relying on this assumption. Moreover, in this section, all the results have been obtained within the framework of classical field theory. In Sec. 4 we will work instead within the framework of quantum field theory.

### 3.2 Vector field

Before introducing the explicit model we mentioned above, we would like to discuss briefly the propagation of a photon field within the framework of the previous subsection.

We start by considering the photon effective action (2.9), which for convenience we re-propose here:

$$S_{A_\mu} = -\frac{1}{4} \int d^4x (F_{\mu\nu} F^{\mu\nu} + g(x) \epsilon^{\mu\nu\rho\sigma} F_{\mu\nu} F_{\rho\sigma}), \quad (3.34)$$

where the field strength tensor  $F_{\mu\nu}$  is given by  $F_{\mu\nu} = \partial_\mu A_\nu(x) - \partial_\nu A_\mu(x)$ , and the background field  $g(x)$  is defined in equation (2.10). Imposing the Lorentz gauge condition

$$\partial_\mu A^\mu(x) = 0, \quad (3.35)$$

the equations of motion turn out to be

$$\partial^2 A^\nu(x) = -\partial_\mu g(x) \epsilon^{\mu\nu\rho\sigma} \partial_\rho A_\sigma. \quad (3.36)$$

Taking the truncated Fourier transform of these equations (which we restrict to a box of volume  $V$  for the moment), we obtain

$$k^2 A^\nu(k) = -\frac{1}{(2\pi)^4} \int_V d^4q \epsilon^{\mu\nu\rho\sigma} q_\mu(k_\rho - q_\rho) g_V(q) A_\sigma(k - q). \quad (3.37)$$

We would like to obtain an expression analogous to Eq. (3.24), from which we can easily extract the dispersion relation of the photon, i.e.

$$k^2 A^\nu(k) = B^{\mu\nu}(k) A_\mu(k). \quad (3.38)$$

Following the procedure used for the scalar field, we can expand the solution  $A^\nu(k)$  in powers of the coupling constant  $\lambda$

$$A^\nu(k) = A^{(0)\nu}(k) + \lambda A^{(1)\nu}(k) + \lambda^2 A^{(2)\nu}(k) + \dots, \quad (3.39)$$

and substitute this expansion in Eq. (3.37). Taking the limit  $V \rightarrow \infty$ , and after some manipulations, we arrive at the result

$$k^2 A^\nu(k) = -\frac{6\lambda^2 \rho}{(2\pi)^4} \int d^4q \delta_{[\lambda}^\mu \delta_{\beta}^\nu \delta_{\gamma]}^\rho \frac{q_\mu(k_\rho - q_\rho) q^\lambda k^\beta}{(k - q)^2 + i\epsilon} h^2(q) A^\gamma(k), \quad (3.40)$$

where the square brackets mean anti-symmetrization ( $\delta_{[\lambda}^{\mu} \delta_{\beta]}^{\nu} = \delta_{\lambda}^{\mu} \delta_{\beta}^{\nu} - \delta_{\beta}^{\mu} \delta_{\lambda}^{\nu}$ ). Again, we can rely on the fact that  $A^{(0)\gamma}(k)$  is the solution of the free theory for which the condition  $k^2 = 0$  holds. Moreover, we can insert the Lorentz gauge condition  $k \cdot A(k) = 0$  into the integral, in order to simplify its expression and obtain

$$k^2 A^{\nu}(k) = -\frac{6\lambda^2 \rho}{(2\pi)^4} \int d^4 q \left( \frac{(q \cdot k)^2 \delta_{\gamma}^{\nu}}{q^2 - 2q \cdot k + i\epsilon} - \frac{(q \cdot k) q_{\gamma} k^{\nu}}{q^2 - 2q \cdot k + i\epsilon} \right) h^2(q) A^{\gamma}(k). \quad (3.41)$$

We want to compare this solution with the modified equation (3.38). Using the Passarino-Veltman reduction formula [50], to manipulate the second term in the round brackets of Eq. (3.41), we obtain

$$k^2 A^{\nu}(k) = \left( \frac{k^{\mu} k^{\nu}}{k^2} - g^{\mu\nu} \right) \frac{6\lambda^2 \rho}{(2\pi)^4} \int d^4 q h^2(q) \frac{(q \cdot k)^2}{q^2 - 2q \cdot k + i\epsilon} A_{\mu}(k). \quad (3.42)$$

Applying the Wick rotation, in order to simplify the angular integrals (and then rotating back to Minkowski space), we get

$$B^{\mu\nu}(k) = \left( \frac{k^{\mu} k^{\nu}}{k^2} - g^{\mu\nu} \right) B(k), \quad (3.43)$$

where

$$B(k) = \frac{3\lambda^2 \rho}{4(2\pi)^4} \int d^4 q h^2(q) \frac{q^2}{k^2} \left( q^2 - 2k^2 - q^2 \sqrt{1 - \frac{4k^2}{q^2}} \right). \quad (3.44)$$

As for the scalar field, this expression is valid only for  $4k^2 < q^2$ , while we have to integrate over all values of  $q$ . Assuming, then, that the shape function  $h(q)$  satisfies the assumption (3.28), and that  $k^2 < q_{low}^2/4$ , we can now expand the square root in powers of  $k^2$ , thereby obtaining

$$B(k) = \frac{3\lambda^2 \rho}{4(2\pi)^4} \int d^4 q h^2(q) \left( 2k^2 + 4\frac{k^4}{q^2} + 10\frac{k^6}{q^4} + O(k^6) \right). \quad (3.45)$$

Equation (3.42) can be written as

$$k^2 A^{\nu}(k) = \left( \frac{k^{\mu} k^{\nu}}{k^2} - g^{\mu\nu} \right) B(k) A_{\mu}(k). \quad (3.46)$$

Taking into account that we are working in the Lorentz gauge, for which condition (3.35) holds, we see that (3.46) simplifies further and we remain with

$$k^2 A^{\nu}(k) = -B(k) A^{\nu}(k), \quad (3.47)$$

from which we obtain the modified dispersion relation

$$k^2 = -ak^2 - bk^4 - ck^6 + O(k^8), \quad (3.48)$$

where the coefficients  $a$ ,  $b$ , and  $c$  are given by

$$\begin{aligned} a &= \frac{3\lambda^2 \rho}{2(2\pi)^4} \int d^4 q h^2(q^2), & b &= \frac{3\lambda^2 \rho}{2(2\pi)^4} \int d^4 q h^2(q^2) \frac{2}{q^2}, \\ c &= \frac{3\lambda^2 \rho}{2(2\pi)^4} \int d^4 q h^2(q^2) \frac{5}{q^4}. \end{aligned} \quad (3.49)$$

Solving equation (3.48) with respect to  $k^2$ , we obtain three different solutions (at order  $O(k^6)$ )

$$\begin{aligned} k_1^2 &= 0, \\ k_2^2 &= -\frac{1+a}{b} - \frac{(1+a)^2 c}{b^3} + \dots, \\ k_3^2 &= -\frac{b}{c} + \frac{1+a}{b} + \frac{(1+a)^2 c}{b^3} + \dots. \end{aligned} \tag{3.50}$$

We have to choose the physical solution from amongst these three. In order to do so, we require, as for the scalar field, that as the perturbation fades the modified dispersion relation approaches the standard dispersion relation. We see that the second and third relations diverge when the coupling constant  $\lambda$  goes to zero. Hence, we are left with the standard dispersion relation

$$k^2 = 0. \tag{3.51}$$

We can conclude that the dispersion relation for a massless vector field remains completely unchanged in this model of spacetime foam.

## 4 Explicit model

We introduce in this section a specific model that allows us to calculate more in detail the effects of Lorentz-invariant spacetime foam on the propagation of photons. In this model, defects are represented simply by Dirac delta functions, and they do not couple directly to the photon field as in the action (2.9). Instead, the interaction between the defects and the photon is mediated by a scalar field. The effective action of this model is given by [51]

$$\begin{aligned} S = \int d^4x \left\{ -\frac{1}{4} F_{\mu\nu} F^{\mu\nu} - \frac{1}{2} (\partial_\mu A^\mu)^2 + \frac{m_0^2}{2} (\partial_\mu \phi \partial^\mu \phi - m_1^2 \phi^2) + \right. \\ \left. + \alpha \phi \sum_{n=1}^{\infty} \epsilon_n \delta^4(x - x_n) - \frac{\lambda}{4} \phi \epsilon^{\mu\nu\rho\sigma} F_{\mu\nu} F_{\rho\sigma} \right\}. \end{aligned} \tag{4.1}$$

The first term in the action is the standard kinetic term of the photon field  $A_\mu(x)$ , while the second is a gauge-fixing term (we use the Feynman gauge in this case). The third term is the free action of the mediator scalar field, which has been multiplied by a mass parameter  $m_0^2$  so that the field  $\phi(x)$  has zero mass dimension. The fourth term describes the interaction between the scalar field and the defects, represented, as mentioned above, by Dirac delta functions. The distribution of defects in Minkowski spacetime  $\{x_n\}$  is still obtained through a sprinkling process of density parameter  $\rho$ , to ensure Lorentz invariance, and the numbers  $\epsilon_n = \pm 1$  are still assigned randomly to the defects with uniform probability. The last term describes the interaction between the scalar field and the photon. The particular form of this term is such as to resemble the anomalous contribution due to the nontrivial topology of the defects (2.5).  $\alpha$  and  $\lambda$  are two dimensionless coupling constants.

We want to show how this model can be traced back to the effective action introduced in the previous section, Eq. (2.9). Consider then the case of  $\lambda = 0$ , in

which the interaction between the scalar field and the photon field is suppressed. The equation of motion for the scalar field in this case is

$$(\partial^2 + m_1^2) \phi(x) = \frac{\alpha}{m_0^2} \sum_n \epsilon_n \delta^4(x - x_n), \quad (4.2)$$

which has the solution

$$\phi(x) = \int \frac{d^4 k}{(2\pi)^4} \phi(k) e^{ikx}, \quad \phi(k) = \frac{-\alpha}{m_0^2(k^2 - m_1^2 + i\epsilon)} \sum_n \epsilon_n e^{ikx_n}. \quad (4.3)$$

If we reactivate the interaction with the photon, assuming that  $\lambda \ll 1$ , we can substitute, in first approximation, this solution directly into the last term of the action (4.1), in which case we obtain

$$S_{A_\mu} = -\frac{1}{4} \int d^4 x \left\{ F_{\mu\nu} F^{\mu\nu} + g(x) F_{\mu\nu} \hat{F}^{\mu\nu} \right\}, \quad (4.4)$$

which is exactly the action (2.9) that we considered previously. The advantage of the model presented here is that the background field  $g(x)$  is not arbitrary but is proportional to the solution of the scalar field equation (4.2):

$$\begin{aligned} g(x) &= \lambda \phi(x) = \int \frac{d^4 k}{(2\pi)^4} \left( \lambda h(k) \sum_n \epsilon_n e^{ikx_n} \right) e^{-ikx} = \\ &= \int \frac{d^4 k}{(2\pi)^4} \left( \frac{-\alpha \lambda}{m_0^2(k^2 - m_1^2 + i\epsilon)} \sum_n \epsilon_n e^{ikx_n} \right) e^{-ikx}. \end{aligned} \quad (4.5)$$

In this way, we can compute the modified dispersion relation in the framework of quantum field theory, by taking advantage of renormalization techniques. This leads us to a finite result that is more reliable than the approximate expansions obtained in the previous section.

We start by pointing out that the possible dispersion relations of a field coincide with the poles of its propagator [52]. Therefore, we will calculate the photon propagator

$$\langle \Omega | A_\mu(a) A_\nu(b) | \Omega \rangle, \quad (4.6)$$

where  $|\Omega\rangle$  represents the vacuum state in the spacetime foam model under consideration. We need to expand perturbatively this vacuum state in order to recover the more tractable Minkowski vacuum  $|0\rangle$  (in which the expressions of free particle propagators are known). In this work, we approach the calculation within the canonical perturbative framework of quantum field theory and we refer to Ref. [53] for an equivalent treatment based on Feynman diagrams.

Explicitly, the photon propagator can be expanded as

$$\begin{aligned} \langle \Omega | A_\mu(a) A_\nu(b) | \Omega \rangle &= \langle 0 | A_\mu(a) A_\nu(b) e^{-i \int d^4 x \mathcal{H}_{int}(x)} | 0 \rangle = \\ &= \langle 0 | A_\mu(a) A_\nu(b) | 0 \rangle - i \int d^4 x \langle 0 | A_\mu(a) A_\nu(b) \mathcal{H}_{int}(x) | 0 \rangle - \\ &- \int d^4 x d^4 y \langle 0 | A_\mu(a) A_\nu(b) \mathcal{H}_{int}(x) \mathcal{H}_{int}(y) | 0 \rangle + \dots, \end{aligned} \quad (4.7)$$

where the interaction Hamiltonian is given by

$$\mathcal{H}_{int}(x) = -\mathcal{L}_{int}(x) = \frac{1}{2}g(x)\varepsilon^{\alpha\beta\rho\sigma}\partial_\alpha A_\beta(x)\partial_\rho A_\sigma(x). \quad (4.8)$$

In terms of Feynman diagrams, the expansion (4.7) is described by

$$\text{Diagram} = \text{Diagram} + \text{Diagram} + \text{Diagram} + \dots \quad (4.9)$$

where the double wavy line represents the full photon propagator, the single wavy line denotes the photon propagator in Minkowski spacetime, the plain line corresponds to the scalar propagator, and a cross represents the interaction between the scalar field and the defects.

Due to the properties of the background field  $g(x)$ , the first-order perturbation vanishes (as we observed in the previous section). The first nontrivial contribution comes from the second-order perturbation, which we indicate as

$$C_{\mu\nu}(a-b) = - \int d^4x d^4y \langle 0|A_\mu(a)A_\nu(b)\mathcal{H}_{int}(x)\mathcal{H}_{int}(y)|0\rangle. \quad (4.10)$$

## 4.1 Scalar propagator

Since the interaction between the defects and the photon field is mediated by a scalar field in the action (4.1), we need the expression of the scalar propagator, in order to compute the modified photon propagator. Observe that, in this model, the scalar field does not perceive the topological structure of the defects. In fact, while in the photon sector there is an anomalous term reminiscent of the anomaly (2.5), the scalar sector is not in the form of (3.9), introduced in Sec. 3.1 to describe the anomalous contribution of the defect topology to the scalar action.

We can obtain two different expressions for the scalar propagator, by using two different approaches. One considers the interaction between the scalar and the defects as a small perturbation ( $\alpha \ll 1$ ) of the free scalar field in Minkowski spacetime, while the second constructs the propagator starting directly from the classical solution (4.3) of the scalar field equation (4.2). We will refer to the first option as the “quantum propagator” and to the second as the “classical propagator”. We note also that both propagators are derived in the case of  $\lambda = 0$ , where the interaction between the scalar and the photon is turned off. Hence, in principle, we should also consider the perturbative contribution caused by this interaction when writing down the scalar propagator. However, this correction contributes to the photon propagator only at order  $\lambda^4$ , while the quantity  $C_{\mu\nu}(a-b)$  (Eq. (4.10)) that we want to calculate is of order  $\lambda^2$ . In conclusion, we can safely ignore this correction to the scalar propagator.

We start by studying the quantum propagator.

### 4.1.1 Quantum propagator

Consider the scalar sector of the action (4.1) with  $\lambda = 0$ . For small  $\alpha$ , we can use perturbation theory to calculate the scalar field propagator in terms of the standard free propagator in Minkowski space

$$\begin{aligned} \langle \Omega | \phi(x) \phi(y) | \Omega \rangle &= \langle 0 | \phi(x) \phi(y) e^{-i \int d^4 z \mathcal{H}_{int}(z)} | 0 \rangle = \\ &= \langle 0 | \phi(x) \phi(y) | 0 \rangle - i \int d^4 z \langle 0 | \phi(x) \phi(y) \mathcal{H}_{int}(z) | 0 \rangle - \\ &\quad - \int d^4 z d^4 w \langle 0 | \phi(x) \phi(y) \mathcal{H}_{int}(z) \mathcal{H}_{int}(w) | 0 \rangle + \dots, \end{aligned} \quad (4.11)$$

where  $\mathcal{H}_{int}(z)$  is given by

$$\mathcal{H}_{int}(z) = -\alpha \phi(z) \sum_{n=1}^{\infty} \epsilon_n \delta^4(z - z_n), \quad (4.12)$$

and the free scalar propagator is given by [48]

$$\langle 0 | \phi(x) \phi(y) | 0 \rangle = \int \frac{d^4 q}{(2\pi)^4} D_0(q) e^{-iq(x-y)}, \quad D_0(q) = \frac{i}{m_0^2(q^2 - m_1^2 + i\epsilon)}. \quad (4.13)$$

As usual, the first-order perturbation vanishes, while at the second order, we have

$$C(x-y) = -\alpha^2 \int d^4 z d^4 w \langle 0 | \phi(x) \phi(y) \phi(z) \phi(w) \sum_{n,m} \epsilon_n \epsilon_m \delta^4(z - z_n) \delta^4(w - w_m) | 0 \rangle. \quad (4.14)$$

We can make some manipulations in the last factor:

$$\begin{aligned} \sum_{n,m} \epsilon_n \epsilon_m \delta^4(z - z_n) \delta^4(w - w_m) &= \sum_n \delta^4(z - z_n) \delta^4(w - w_n) + \\ &\quad + \sum_{n \neq m} \epsilon_n \epsilon_m \delta^4(z - z_n) \delta^4(w - w_m), \end{aligned} \quad (4.15)$$

where the second sum in the right-hand side vanishes. Introducing the Fourier transform of the delta function, and substituting the sum by an integral, one gets

$$\begin{aligned} \sum_n \delta^4(z - z_n) \delta^4(w - w_n) &= \sum_n \int \frac{d^4 q}{(2\pi)^4} \frac{d^4 p}{(2\pi)^4} e^{-iq \cdot z} e^{-ip \cdot w} e^{i(q+p) \cdot z_n} = \\ &= \rho \int d^4 s \frac{d^4 q d^4 p}{(2\pi)^8} e^{-iq \cdot z} e^{-ip \cdot w} e^{i(q+p) \cdot s} = \rho \int \frac{d^4 q d^4 p}{(2\pi)^4} e^{-iq \cdot z} e^{-ip \cdot w} \delta^4(q + p) = \\ &= \rho \int \frac{d^4 q}{(2\pi)^4} e^{-iq \cdot (z-w)} = \rho \delta^4(z - w). \end{aligned} \quad (4.16)$$

Replacing this result in equation (4.14) and using the Wick's theorem [48], we obtain

$$\begin{aligned}
C(x-y) &= -\alpha^2 \int d^4z d^4w \langle 0 | \phi(x) \phi(y) \phi(z) \phi(w) \rho \delta^4(z-w) | 0 \rangle = \\
&= -\alpha^2 \rho \int d^4z \langle 0 | \overbrace{\phi(x) \phi(y) \phi(z) \phi(z)}^{\text{Wick}} | 0 \rangle = \\
&= -\alpha^2 \rho \int d^4z \langle 0 | \phi(x) \phi(z) | 0 \rangle \langle 0 | \phi(z) \phi(y) | 0 \rangle,
\end{aligned} \tag{4.17}$$

which, after inserting the free propagator (4.13), becomes

$$\begin{aligned}
C(x-y) &= -\alpha^2 \rho \int d^4z \frac{d^4q}{(2\pi)^4} \frac{d^4p}{(2\pi)^4} D_0(q) D_0(p) e^{-iq(x-z)} e^{-ip(z-y)} = \\
&= -\alpha^2 \rho \int d^4z \frac{d^4q}{(2\pi)^4} \frac{d^4p}{(2\pi)^4} D_0(q) D_0(p) e^{-iqx} e^{ipy} e^{iz(q-p)} = \\
&= -\alpha^2 \rho \int \frac{d^4q}{(2\pi)^4} \frac{d^4p}{(2\pi)^4} D_0(q) D_0(p) e^{-iqx} e^{ipy} (2\pi)^4 \delta^4(q-p) = \\
&= -\alpha^2 \rho \int \frac{d^4q}{(2\pi)^4} D_0(q) D_0(q) e^{-iq(x-y)}.
\end{aligned} \tag{4.18}$$

Finally, substituting this expression in the expansion (4.11), we get

$$\langle \Omega | \phi(x) \phi(y) | \Omega \rangle = \int \frac{d^4q}{(2\pi)^4} \{ D_0(q) - \alpha^2 \rho D_0(q)^2 + \dots \} e^{-iq(x-y)}, \tag{4.19}$$

where we observe that higher powers of the factor  $(-\alpha^2 \rho D_0(q))$  appear in higher terms of the expansion. Taking them into account we obtain the re-summed propagator:

$$\begin{aligned}
D_q(q) &= \overline{D(q)} = D_0(q) \{ 1 - \alpha^2 \rho D_0(q) + (-\alpha^2 \rho D_0(q))^2 + \dots \} = \\
&= D_0(q) \sum_{n=0}^{\infty} (-\alpha^2 \rho D_0(q))^n = D_0(q) \frac{1}{1 + \alpha^2 \rho D_0(q)}.
\end{aligned} \tag{4.20}$$

Explicitly, inserting the expression for  $D_0(q)$ , the quantum propagator turns out to be

$$\begin{aligned}
D_q(q) &= \frac{i}{m_0^2(q^2 - m_1^2)} \cdot \frac{1}{1 + \alpha^2 \rho \frac{i}{m_0^2(q^2 - m_1^2)}} = \\
&= \frac{i}{m_0^2(q^2 - m_1^2) + i\alpha^2 \rho \frac{m_0^2(q^2 - m_1^2)}{m_0^2(q^2 - m_1^2)}} = \frac{i}{m_0^2(q^2 - m_1^2 + i\alpha^2 \frac{\rho}{m_0^2})}.
\end{aligned} \tag{4.21}$$

#### 4.1.2 Classical propagator

The equation of motion for the scalar field derived from the action (4.1), in the case of  $\lambda = 0$ , is

$$(\partial^2 + m_1^2)\phi(x) = \frac{\alpha}{m_0^2} \sum_n \epsilon_n \delta^4(x - x_n), \tag{4.22}$$

which has the classical solution

$$\phi_{cl}(x) = \int \frac{d^4 q}{(2\pi)^4} \left( \frac{-\alpha}{m_0^2(q^2 - m_1^2 + i\epsilon)} \sum_n \epsilon_n e^{iq \cdot x_n} \right) e^{-iq \cdot x}. \quad (4.23)$$

Using this expression, the classical propagator is given by

$$\begin{aligned} D_{cl}(x-y) &= \langle 0 | \phi_{cl}(x) \phi_{cl}(y) | 0 \rangle = \\ &= \int \frac{d^4 q d^4 p}{(2\pi)^8} \left( \frac{\alpha^2 \sum_{n,m} \epsilon_n \epsilon_m e^{iq \cdot x_n} e^{ip \cdot x_m}}{m_0^4(q^2 - m_1^2 + i\epsilon)(p^2 - m_1^2 + i\epsilon)} \right) e^{-iq \cdot x} e^{-ip \cdot y}. \end{aligned} \quad (4.24)$$

As usual, we can replace the double sum with an integral, which gives us

$$\sum_{n,m} \epsilon_n \epsilon_m e^{iq \cdot x_n} e^{ip \cdot x_m} = \rho \int d^4 x e^{i(q+p) \cdot x} = (2\pi)^4 \rho \delta^4(q+p), \quad (4.25)$$

from which the classical propagator turns out to be

$$D_{cl}(x-y) = \alpha^2 \rho \int \frac{d^4 q}{(2\pi)^4} \frac{1}{m_0^4(q^2 - m_1^2 + i\epsilon)^2} e^{-iq \cdot (x-y)}. \quad (4.26)$$

## 4.2 Vector propagator

We now turn to the study of the photon propagator  $\langle \Omega | A_\mu(a) A_\nu(b) | \Omega \rangle$  which, for  $\lambda \ll 1$ , can be expanded perturbatively as in Eq. (4.7)

$$\begin{aligned} \langle \Omega | A_\mu(a) A_\nu(b) | \Omega \rangle &= \langle 0 | A_\mu(a) A_\nu(b) e^{-i \int d^4 x \mathcal{H}_{int}(x)} | 0 \rangle = \\ &= \langle 0 | A_\mu(a) A_\nu(b) | 0 \rangle - i \int d^4 x \langle 0 | A_\mu(a) A_\nu(b) \mathcal{H}_{int}(x) | 0 \rangle - \\ &\quad - \int d^4 x d^4 y \langle 0 | A_\mu(a) A_\nu(b) \mathcal{H}_{int}(x) \mathcal{H}_{int}(y) | 0 \rangle + \dots, \end{aligned} \quad (4.27)$$

where we remember

$$\mathcal{H}_{int}(x) = -\mathcal{L}_{int}(x) = \frac{\lambda}{2} \phi(x) \epsilon^{\alpha\beta\rho\sigma} \partial_\alpha A_\beta(x) \partial_\rho A_\sigma(x). \quad (4.28)$$

The free photon propagator is given by [48]

$$\begin{aligned} \langle 0 | A_\mu(a) A_\nu(b) | 0 \rangle &= D_{\mu\nu}(a-b) = \int \frac{d^4 k}{(2\pi)^4} D_{\mu\nu}(k) e^{-ik(a-b)}, \\ D_{\mu\nu}(k) &= g_{\mu\nu} \Delta_F(k), \quad \Delta_F(k) = \frac{-i}{k^2 + i\epsilon}, \end{aligned} \quad (4.29)$$

and the scalar propagator is

$$\langle 0 | \phi(x) \phi(y) | 0 \rangle = D(x-y) = \int \frac{d^4 q}{(2\pi)^4} D(q) e^{-iq(x-y)}, \quad (4.30)$$

where we have to choose the appropriate expression for  $D(q)$  from amongst those derived in the previous subsection. As pointed out previously, the first-order perturbation vanishes and we renamed the second-order perturbation

$$C_{\mu\nu}(a-b) = - \int d^4x d^4y \langle 0|A_\mu(a)A_\nu(b)\mathcal{H}_{int}(x)\mathcal{H}_{int}(y)|0\rangle. \quad (4.31)$$

This term gives us the first nontrivial modification to the photon propagator. From this expression, we want to obtain the second-order re-summed propagator of the photon,  $\overline{D_{\mu\nu}(k)}$ , which can be represented diagrammatically as

$$\overline{D_{\mu\nu}(k)} = \text{---} + \text{---} + \text{---} + \dots, \quad (4.32)$$

where the crossed plain line represents one of the two possible scalar propagators derived above ( $D_q(q)$  or  $D_{cl}(q)$ ). We want to stress that this expression is not equivalent to the perturbative expansion (4.27); in fact, it only contains higher powers of the second-order contribution  $C_{\mu\nu}(a-b)$ , but in Eq. (4.27) other contributions also appear at higher orders. For example, the fourth-order diagram

$$\text{---} \quad (4.33)$$

is not accounted for in the re-summation (4.32).

Inserting the explicit expression of  $\mathcal{H}_{int}$  (Eq. (4.28)) into  $C_{\mu\nu}(a-b)$  (Eq. (4.31)), we obtain

$$C_{\mu\nu}(a-b) = - \frac{\lambda^2}{4} \int d^4x d^4y \epsilon^{\alpha\beta\rho\sigma} \epsilon_{\gamma\delta\eta\tau} \times \langle 0|A_\mu(a)A_\nu(b)\phi(x)\partial_\alpha A_\beta(x)\partial_\rho A_\sigma(x)\phi(y)\partial^\gamma A^\delta(y)\partial^\eta A^\tau(y)|0\rangle. \quad (4.34)$$

Using the Wick theorem, we can rewrite the above vacuum expectation value in terms of propagators

$$\langle 0|A_\mu(a)A_\nu(b)\overbrace{\phi(x)\partial_\alpha A_\beta(x)\partial_\rho A_\sigma(x)\phi(y)\partial^\gamma A^\delta(y)\partial^\eta A^\tau(y)}|0\rangle = \langle 0|\phi(x)\phi(y)|0\rangle \times \left(\frac{\partial}{\partial x^\alpha}\langle 0|A_\mu(a)A_\beta(x)|0\rangle\right) \left(\frac{\partial}{\partial x^\rho}\frac{\partial}{\partial y_\gamma}\langle 0|A_\sigma(x)A^\delta(y)|0\rangle\right) \frac{\partial}{\partial y_\eta}\langle 0|A^\tau(y)A_\nu(b)|0\rangle. \quad (4.35)$$

We can now use the expressions (4.29) and (4.30) for the photon and scalar propagators. Recalling furthermore that

$$\epsilon^{\alpha\beta\rho\sigma} \epsilon_{\gamma\delta\eta\tau} = 4! \delta_{[\gamma}^\alpha \delta_\delta^\beta \delta_\eta^\rho \delta_{\tau]}^\sigma, \quad (4.36)$$

we get

$$\begin{aligned}
C_{\mu\nu}(a-b) &= -3!\lambda^2 \delta_{[\gamma}^{\alpha} \delta_{\delta}^{\beta} \delta_{\eta}^{\rho} \delta_{\tau]}^{\sigma} \int d^4x d^4y \frac{d^4q d^4k d^4p_1 d^4p_2}{(2\pi)^{16}} D(q) e^{-iq(x-y)} \times \\
&g_{\mu\beta} \Delta_F(k) \delta_{\sigma}^{\delta} \Delta_F(p_1) \delta_{\nu}^{\tau} \Delta_F(p_2) \frac{\partial}{\partial x^{\alpha}} e^{-ik(a-x)} \frac{\partial}{\partial x^{\rho}} \frac{\partial}{\partial y_{\gamma}} e^{-ip_1(x-y)} \frac{\partial}{\partial y_{\eta}} e^{-ip_2(y-b)} = \\
&= -3!\lambda^2 \delta_{[\gamma}^{\alpha} \delta_{\delta}^{\beta} \delta_{\eta}^{\rho} \delta_{\tau]}^{\sigma} g_{\mu\beta} \delta_{\sigma}^{\delta} \delta_{\nu}^{\tau} \int d^4x d^4y \frac{d^4q d^4k d^4p_1 d^4p_2}{(2\pi)^{16}} (ik_{\alpha})(-ip_{1\rho}) \times \\
&(ip_1^{\gamma})(-ip_2^{\eta}) D(q) \Delta_F(k) \Delta_F(p_1) \Delta_F(p_2) e^{-ix(q-k+p_1)} e^{-iy(p_2-p_1-q)} e^{-ika} e^{ip_2b}.
\end{aligned} \tag{4.37}$$

The product of Kronecker deltas in the above expression can be simplified as follows:

$$\delta_{[\gamma}^{\alpha} \delta_{\delta}^{\beta} \delta_{\eta}^{\rho} \delta_{\tau]}^{\sigma} g_{\mu\beta} \delta_{\sigma}^{\delta} \delta_{\nu}^{\tau} = \delta_{[\gamma}^{\alpha} \delta_{\sigma}^{\beta} \delta_{\eta}^{\rho} \delta_{\nu]}^{\tau} g_{\mu\beta} = (3-d) \delta_{[\gamma}^{\alpha} \delta_{\eta}^{\rho} \delta_{\nu]}^{\beta} g_{\mu\beta}, \tag{4.38}$$

and the integrals in  $x$  and  $y$  can be computed, resulting in two delta functions that cancel out the integrals in  $p_1$  and  $p_2$ . The result is

$$C_{\mu\nu}(a-b) = \int \frac{d^4k}{(2\pi)^4} C_{\mu\nu}(k) e^{-ik(a-b)}, \tag{4.39}$$

where

$$C_{\mu\nu}(k) = 3!\lambda^2 \delta_{[\gamma}^{\alpha} \delta_{\eta}^{\rho} \delta_{\nu]}^{\beta} g_{\mu\beta} \Delta_F(k)^2 \int \frac{d^4q}{(2\pi)^4} k_{\alpha} k^{\eta} (k_{\rho} - q_{\rho}) (k^{\gamma} - q^{\gamma}) D(q) \Delta_F(k-q). \tag{4.40}$$

We still have to do some manipulations with the Kronecker deltas

$$\begin{aligned}
&\delta_{[\gamma}^{\alpha} \delta_{\eta}^{\rho} \delta_{\nu]}^{\beta} g_{\mu\beta} k_{\alpha} k^{\eta} (k_{\rho} - q_{\rho}) (k^{\gamma} - q^{\gamma}) = (\delta_{\gamma}^{\alpha} \delta_{\eta}^{\rho} \delta_{\nu}^{\beta} - \delta_{\gamma}^{\alpha} \delta_{\nu}^{\rho} \delta_{\eta}^{\beta} + \\
&\quad + \delta_{\nu}^{\alpha} \delta_{\gamma}^{\rho} \delta_{\eta}^{\beta} - \delta_{\nu}^{\alpha} \delta_{\eta}^{\rho} \delta_{\gamma}^{\beta} + \delta_{\eta}^{\alpha} \delta_{\nu}^{\rho} \delta_{\gamma}^{\beta} - \delta_{\eta}^{\alpha} \delta_{\gamma}^{\rho} \delta_{\nu}^{\beta}) g_{\mu\beta} k_{\alpha} k^{\eta} (k_{\rho} - q_{\rho}) (k^{\gamma} - q^{\gamma}) = \\
&= g_{\mu\nu} k \cdot (k-q) k \cdot (k-q) - k_{\mu} (k_{\nu} - q_{\nu}) k \cdot (k-q) + k_{\mu} k_{\nu} (k-q)^2 - \\
&\quad - (k_{\mu} - q_{\mu}) k_{\nu} k \cdot (k-q) + (k_{\mu} - q_{\mu}) (k_{\nu} - q_{\nu}) k^2 - g_{\mu\nu} k^2 (k-q)^2 = \\
&= g_{\mu\nu} (k^4 - 2k^2 k \cdot q + (k \cdot q)^2 - k^4 - k^2 q^2 + 2k^2 k \cdot q) + \\
&\quad + k_{\mu} k_{\nu} (k^2 + k \cdot q - k^2 + q^2 - 2k \cdot q - k^2 + k \cdot q + k^2) + \\
&\quad + k_{\mu} q_{\nu} (k^2 - k \cdot q - k^2) + q_{\mu} k_{\nu} (k^2 - k \cdot q - k^2) + q_{\mu} q_{\nu} k^2 = \\
&= g_{\mu\nu} ((k \cdot q)^2 - k^2 q^2) + k_{\mu} k_{\nu} q^2 - k_{\mu} q_{\nu} k \cdot q - q_{\mu} k_{\nu} k \cdot q + q_{\mu} q_{\nu} k^2 = \\
&= q_{\alpha} q_{\beta} \{ g_{\mu\nu} (k^{\alpha} k^{\beta} - k^2 g^{\alpha\beta}) + k_{\mu} k_{\nu} g^{\alpha\beta} - k_{\mu} \delta_{\nu}^{\alpha} k^{\beta} - \delta_{\mu}^{\alpha} k_{\nu} k^{\beta} + \delta_{\mu}^{\alpha} \delta_{\nu}^{\beta} k^2 \}.
\end{aligned} \tag{4.41}$$

Inserting this result into Eq. (4.40), we obtain

$$\begin{aligned}
C_{\mu\nu}(k) &= 3!\lambda^2 \Delta_F(k)^2 \int \frac{d^4q}{(2\pi)^4} D(q) \Delta_F(k-q) q_{\alpha} q_{\beta} \times \\
&\{ g_{\mu\nu} (k^{\alpha} k^{\beta} - k^2 g^{\alpha\beta}) + k_{\mu} k_{\nu} g^{\alpha\beta} - k_{\mu} \delta_{\nu}^{\alpha} k^{\beta} - \delta_{\mu}^{\alpha} k_{\nu} k^{\beta} + \delta_{\mu}^{\alpha} \delta_{\nu}^{\beta} k^2 \}.
\end{aligned} \tag{4.42}$$

Using the Passarino-Veltman reduction procedure, we can further simplify this expression. It can be shown easily that the following equality holds

$$\int \frac{d^4q}{(2\pi)^4} D(q) \Delta_F(k-q) q_{\alpha} q_{\beta} = \left\{ \frac{(k^2 I_0 - I_1)}{k^2 (d-1)} g^{\alpha\beta} - \frac{(k^2 I_0 - d I_1)}{k^2 (d-1)} \frac{k_{\alpha} k_{\beta}}{k^2} \right\}, \tag{4.43}$$

where  $I_0$  and  $I_1$  are given by

$$\begin{aligned} I_0 &= \int \frac{d^4 q}{(2\pi)^4} D(q) \Delta_F(k-q) q^2, \\ I_1 &= \int \frac{d^4 q}{(2\pi)^4} D(q) \Delta_F(k-q) (q \cdot k)^2. \end{aligned} \quad (4.44)$$

Substituting the result (4.43) into Eq. (4.42), we obtain

$$\begin{aligned} C_{\mu\nu}(k) &= 3! \lambda^2 \Delta_F(k)^2 \left\{ \frac{(k^2 I_0 - I_1)}{k^2(d-1)} g_{\alpha\beta} - \frac{(k^2 I_0 - d I_1)}{k^2(d-1)} \frac{k_\alpha k_\beta}{k^2} \right\} \times \\ &\quad \{ g_{\mu\nu} (k^\alpha k^\beta - k^2 g^{\alpha\beta}) + k_\mu k_\nu g^{\alpha\beta} - k_\mu \delta_\nu^\alpha k^\beta - \delta_\mu^\alpha k_\nu k^\beta + \delta_\mu^\alpha \delta_\nu^\beta k^2 \} = \\ &= 3! \lambda^2 \Delta_F(k)^2 \left\{ \frac{(k^2 I_0 - I_1)}{k^2(d-1)} [g_{\mu\nu} k^2 (1-d) + k_\mu k_\nu (d-2) + g_{\mu\nu} k^2] - \right. \\ &\quad \left. - \frac{(k^2 I_0 - d I_1)}{k^2(d-1)} \frac{k_\alpha k_\beta}{k^2} [g_{\mu\nu} (k^4 - k^4) + k_\mu k_\nu (k^2 - 2k^2 + k^2)] \right\} = \\ &= -3! \lambda^2 \Delta_F(k)^2 \frac{(d-2)}{(d-1)} (k^2 I_0 - I_1) \left\{ g_{\mu\nu} - \frac{k_\mu k_\nu}{k^2} \right\}. \end{aligned} \quad (4.45)$$

So, finally, we arrive at

$$C_{\mu\nu}(k) = - \left\{ g_{\mu\nu} - \frac{k_\mu k_\nu}{k^2} \right\} \Delta_F(k)^2 a(k), \quad (4.46)$$

where  $a(k)$  is given by

$$a(k) = 3! \lambda^2 \frac{(d-2)}{(d-1)} \int \frac{d^4 q}{(2\pi)^4} D(q) \Delta_F(k-q) (k^2 q^2 - (q \cdot k)^2). \quad (4.47)$$

The perturbation expansion (4.27) turns out to be

$$\langle \Omega | A_\mu(a) A_\nu(b) | \Omega \rangle = g_{\mu\nu} \Delta_F(k) - \left\{ g_{\mu\nu} - \frac{k_\mu k_\nu}{k^2} \right\} a(k) \Delta_F(k)^2 + \dots, \quad (4.48)$$

and we observe that higher powers of  $a(k) \Delta_F(k)$  appear in higher terms of the expansion. We need to take them into account in order to calculate the re-summed propagator (4.32)

$$\overline{D}_{\mu\nu}(k) = \left\{ g_{\mu\nu} - \frac{k_\mu k_\nu}{k^2} \right\} \Delta_F(k) \sum_n (-a(k) \Delta_F(k))^n + \frac{k_\mu k_\nu}{k^2} \Delta_F(k). \quad (4.49)$$

Since, as discussed in Ref. [48] regarding the vacuum polarization of the photon in quantum electrodynamics, the last term does not contribute to any calculation, we can drop it and then obtain

$$\overline{D}_{\mu\nu}(k) = \left\{ g_{\mu\nu} - \frac{k_\mu k_\nu}{k^2} \right\} \Delta_F(k) \frac{1}{1 + \Pi(k)}, \quad (4.50)$$

where, in analogy with the result in QED, we call

$$\Pi(k) = a(k) \Delta_F(k) = 4 \lambda^2 \Delta_F(k) \int \frac{d^4 q}{(2\pi)^4} D(q) \Delta_F(k-q) \{ k^2 q^2 - (q \cdot k)^2 \}. \quad (4.51)$$

In order to compute this integral, we need the explicit expression of the scalar field propagator. We found in Sec. 4.1 that there are two possible expressions for the scalar propagator, in which case we arrive at two different results,  $\Pi_q(k)$  and  $\Pi_{cl}(k)$ , inserting, respectively,  $D_q(q)$  (Eq. (4.21)) and  $D_{cl}(q)$  (Eq. (4.26)) into Eq. (4.51). Specifically, these are

$$\Pi_q(k) = \frac{-4\lambda^2 i}{k^2 + i\epsilon} \int \frac{d^4 q}{(2\pi)^4} \frac{i}{m_0^2(q^2 - m_1^2 + i\frac{\alpha^2 \rho}{m_0^2})} \frac{-i}{(k-q)^2 + i\epsilon} \{k^2 q^2 - (q \cdot k)^2\}, \quad (4.52a)$$

$$\Pi_{cl}(k) = \frac{-4\lambda^2 i}{k^2 + i\epsilon} \int \frac{d^4 q}{(2\pi)^4} \frac{\alpha^2 \rho}{m_0^4(q^2 - m_1^2 + i\epsilon)^2} \frac{-i}{(k-q)^2 + i\epsilon} \{k^2 q^2 - (q \cdot k)^2\}. \quad (4.52b)$$

#### 4.2.1 $\Pi_q(k)$

In order to integrate  $\Pi_q(k)$ , we use the identity

$$(q \cdot k)^2 = \frac{1}{4}(k^2 + q^2 - (k-q)^2)^2 = \frac{1}{4}(k^4 + q^4 + 2q^2 k^2 + (k-q)^4 - 2(k^2 + q^2)(k-q)^2). \quad (4.53)$$

Inserting this expression into the curly brackets in Eq. (4.52a), we then obtain

$$\{k^2 q^2 - (q \cdot k)^2\} = \frac{1}{4} \{2k^2 q^2 - k^4 - q^4 - (k-q)^4 + 2(k^2 + q^2)(k-q)^2\}, \quad (4.54)$$

and  $\Pi_q(k)$  becomes

$$\Pi_q(k) = \frac{\lambda^2}{m_0^2} \frac{i}{k^2 + i\epsilon} \int \frac{d^4 q}{(2\pi)^4} \frac{k^4 + q^4 - 2k^2 q^2 + (k-q)^4 - 2(k^2 + q^2)(k-q)^2}{(q^2 - m_1^2 + i\frac{\alpha^2 \rho}{m_0^2})((k-q)^2 + i\epsilon)}. \quad (4.55)$$

Renaming for simplicity  $M^2 = m_1^2 - i\frac{\alpha^2 \rho}{m_0^2}$ , and dropping out temporarily the factors  $i\epsilon$ , we have

$$\Pi_q(k) = \frac{\lambda^2}{m_0^2} \frac{i}{k^2 + i\epsilon} \int \frac{d^4 q}{(2\pi)^4} \left\{ \frac{k^4}{(q^2 - M^2)(k-q)^2} + \frac{q^4}{(q^2 - M^2)(k-q)^2} - \frac{2k^2 q^2}{(q^2 - M^2)(k-q)^2} + \frac{(k-q)^2}{(q^2 - M^2)} - \frac{2(k^2 + q^2)}{(q^2 - M^2)} \right\}. \quad (4.56)$$

Using the substitution  $q^2 = (q^2 - M^2) + M^2$ , the expression between the curly brackets becomes

$$\begin{aligned} \{\dots\} &= \left\{ \frac{k^4}{(q^2 - M^2)(k-q)^2} + \frac{((q^2 - M^2) + M^2)^2}{(q^2 - M^2)(k-q)^2} - \frac{2k^2((q^2 - M^2) + M^2)}{(q^2 - M^2)(k-q)^2} - \right. \\ &\quad \left. - \frac{2q \cdot k}{(q^2 - M^2)} - \frac{k^2}{(q^2 - M^2)} - \frac{((q^2 - M^2) + M^2)}{(q^2 - M^2)} \right\} = \\ &= \left\{ \frac{k^4 - 2k^2 M^2 + M^4}{(q^2 - M^2)(k-q)^2} + \frac{q^2}{(k-q)^2} - \frac{M^2}{(k-q)^2} - \frac{2(k^2 - M^2)}{(k-q)^2} - \right. \\ &\quad \left. - \frac{2q \cdot k}{(q^2 - M^2)} - \frac{k^2 + M^2}{(q^2 - M^2)} - 1 \right\}. \end{aligned} \quad (4.57)$$

Because of the invariance of the integral with respect to translation, we can make the substitution  $q \rightarrow q' = (k - q)$  in the second, third, and fourth terms of the above expression. In particular, the second term becomes

$$\frac{q^2}{(k - q)^2} = \frac{(k - q')^2}{q'^2} = \frac{k^2}{q'^2} + \frac{q'^2}{q'^2} - \frac{2q' \cdot k}{q'^2}, \quad (4.58)$$

and we obtain

$$\begin{aligned} \{\dots\} &= \left\{ \frac{(k^2 - M^2)^2}{(q^2 - M^2)(k - q)^2} + \frac{k^2 - M^2}{q^2} + 1 - \frac{2q \cdot k}{q^2} - \frac{2(k^2 - M^2)}{q^2} \right. \\ &\quad \left. - \frac{2q \cdot k}{(q^2 - M^2)} - \frac{k^2 + M^2}{(q^2 - M^2)} - 1 \right\} = \\ &= \left\{ \frac{(k^2 - M^2)^2}{(q^2 - M^2)(k - q)^2} - \frac{k^2 - M^2}{q^2} - \frac{2q \cdot k}{q^2} - \frac{2q \cdot k}{(q^2 - M^2)} - \frac{k^2 + M^2}{(q^2 - M^2)} \right\}. \end{aligned} \quad (4.59)$$

Now using the Wick rotation

$$q = (q_0, \vec{q}) \longrightarrow q_E = (q_\tau, \vec{q}) = (-iq_0, \vec{q}), \quad (4.60)$$

and introducing spherical coordinates, we see that the two terms containing the scalar product  $q \cdot k$  vanish. The integral  $\Pi_q(k)$  now becomes

$$\Pi_q(k) = -\frac{\lambda^2}{m_0^2 k^2} \int \frac{d^4 q_E}{(2\pi)^4} \left\{ \frac{(k^2 - M^2)^2}{(q_E^2 + M^2)(k_E - q_E)^2} + \frac{k^2 - M^2}{q_E^2} + \frac{k^2 + M^2}{(q_E^2 + M^2)} \right\}. \quad (4.61)$$

#### 4.2.1.1 Dimensional regularization

The above integral is divergent, so we use dimensional regularization to calculate it. First of all, we rewrite the 4-dimensional integral in  $d$  dimensions

$$\int \frac{d^4 q_E}{(2\pi)^4} \Rightarrow \int \frac{d^d q}{(2\pi)^d} = \mu^{4-d} \int \frac{d\Omega_d}{(2\pi)^d} \int_0^\infty dq q^{d-1}, \quad (4.62)$$

where  $\mu$  is a mass parameter introduced for dimensional reasons. Moreover, we observe that

$$\int \frac{d\Omega_d}{(2\pi)^d} = \frac{1}{(2\pi)^d} \frac{2\pi^{\frac{d}{2}}}{\Gamma(\frac{d}{2})}. \quad (4.63)$$

Then, we set  $d = 4 - \epsilon$  so that the original four-dimensional integral is recovered in the limit  $\epsilon \rightarrow 0$ .

In this framework, we have to calculate three integrals:

$$\begin{aligned} A_0(k) &= \int \frac{d^4 q_E}{(2\pi)^4} \frac{1}{(q_E^2 + M^2)}, \\ A_{00}(k) &= \int \frac{d^4 q_E}{(2\pi)^4} \frac{1}{q_E^2}, \\ B_1(k) &= \int \frac{d^4 q_E}{(2\pi)^4} \frac{1}{(q_E^2 + M^2)(k_E - q_E)^2}. \end{aligned} \quad (4.64)$$

Consider first  $A_0(k)$ , which becomes

$$A_0(k) = \mu^{4-d} \int \frac{d\Omega_d}{(2\pi)^d} \int_0^\infty \frac{dq q^{d-1}}{(q^2 + M^2)} = \frac{\mu^\epsilon}{(2\pi)^{4-\epsilon}} \frac{2\pi^{2-\epsilon/2}}{\Gamma(2-\frac{\epsilon}{2})} \int_0^\infty \frac{dq q^{3-\epsilon}}{(q^2 + M^2)}. \quad (4.65)$$

In the radial integral, we can apply the consecutive changes of variables  $q' = q^2$  and  $x = M^2/(q' + M^2)$  from which we obtain

$$\int_0^\infty \frac{dq q^{3-\epsilon}}{(q^2 + M^2)} = \frac{1}{2} \int_0^\infty \frac{dq' q'^{1-\epsilon/2}}{(q' + M^2)} = \frac{1}{2} (M^2)^{1-\epsilon/2} \int_0^1 dx x^{-2+\epsilon/2} (1-x)^{1-\epsilon/2}. \quad (4.66)$$

Recalling that

$$\int_0^1 dx x^\alpha (1-x)^\beta = \frac{\Gamma(1+\alpha)\Gamma(1+\beta)}{\Gamma(2+\alpha+\beta)}, \quad (4.67)$$

$A_0(k)$  becomes

$$A_0(k) = \frac{\mu^\epsilon}{(2\pi)^{4-\epsilon}} \frac{2\pi^{2-\epsilon/2}}{\Gamma(2-\frac{\epsilon}{2})} \frac{1}{2} (M^2)^{1-\epsilon/2} \Gamma(2-\frac{\epsilon}{2}) \Gamma(\frac{\epsilon}{2}-1). \quad (4.68)$$

Expanding this result in powers of  $\epsilon$ , we can isolate the divergent terms and get

$$A_0(k) = \frac{M^2}{8\pi^2} \left( -\frac{1}{\epsilon} - \frac{1}{2} + \frac{\gamma}{2} + \frac{1}{2} \log(M^2) - \frac{1}{2} \log(\mu^2) - \frac{1}{2} \log(4\pi) \right) + O(\epsilon), \quad (4.69)$$

where  $\gamma$  is the Euler-Mascheroni constant. Renaming for simplicity

$$\frac{1}{\epsilon} - \frac{\gamma}{2} + \frac{1}{2} \log(4\pi) = \frac{1}{2\hat{\epsilon}}, \quad (4.70)$$

we finally obtain

$$A_0(k) = -\frac{M^2}{16\pi^2} \left( \frac{1}{\hat{\epsilon}} - \log\left(\frac{M^2}{\mu^2}\right) + 1 \right) + O(\epsilon). \quad (4.71)$$

Moving to the next integral  $A_{00}(k)$ , we see that it is a special case ( $M^2 = 0$ ) of the integral  $A_0(k)$  that we have just computed. We can therefore conclude that

$$A_{00}(k) = \lim_{M^2 \rightarrow 0} A_0(k) = 0. \quad (4.72)$$

The last integral we need to compute is

$$\begin{aligned} B_1(k) &= \int \frac{d^4 q_E}{(2\pi)^4} \frac{1}{(q_E^2 + M^2)(k_E - q_E)^2} = \\ &= \frac{\mu^\epsilon}{(2\pi)^{4-\epsilon}} \frac{2\pi^{2-\epsilon/2}}{\Gamma(2-\frac{\epsilon}{2})} \int_0^\infty \frac{dq q^{3-\epsilon}}{(q^2 + M^2)(k_E - q)^2}. \end{aligned} \quad (4.73)$$

In this case, we need to introduce the Feynman parametrization

$$\frac{1}{AB} = \int_0^1 dx \frac{1}{(xA + (1-x)B)^2}, \quad (4.74)$$

which gives us

$$\begin{aligned}
\int \frac{d^d q}{(q^2 + M^2)(k_E - q)^2} &= \int_0^1 dx \int \frac{d^d q}{(x(k_E - q)^2 + (1-x)(q^2 + M^2))^2} = \\
&= \int_0^1 dx \int \frac{d^d q}{(q^2 - 2xq \cdot k_E + xk_E^2 + M^2(1-x))^2} = \\
&= \int_0^1 dx \int \frac{d^d q}{((q - xk_E)^2 + (1-x)(M^2 + xk_E^2))^2} = \int_0^1 dx \int \frac{d^d l}{(l^2 + \Delta)^2}, \tag{4.75}
\end{aligned}$$

where we have renamed  $\Delta = (1-x)(M^2 + xk_E^2) = (1-x)(M^2 - xk^2)$  and  $l = (q - xk_E)$ . Applying the changes to variables  $l' = l^2$  and  $y = \frac{\Delta^2}{l' + \Delta^2}$  to the radial component of the integral, we get

$$\int_0^\infty dl \frac{l^{3-\epsilon}}{(l^2 + \Delta)^2} = \frac{1}{2} \int_0^\infty dl' \frac{l'^{1-\epsilon/2}}{(l' + \Delta)^2} = \frac{1}{2} \Delta^{-\epsilon/2} \int_0^1 dy y^{\epsilon/2-1} (1-y)^{1-\epsilon/2}. \tag{4.76}$$

Moreover, recalling that

$$\int_0^1 dy y^\alpha (1-y)^\beta = \frac{\Gamma(1+\alpha)\Gamma(1+\beta)}{\Gamma(2+\alpha+\beta)}, \tag{4.77}$$

we obtain

$$B_1(k) = \frac{\mu^\epsilon}{(2\pi)^{4-\epsilon}} \frac{2\pi^{2-\epsilon/2}}{\Gamma(2-\frac{\epsilon}{2})} \frac{1}{2} \int_0^1 dx \Delta^{-\epsilon/2} \frac{\Gamma(\frac{\epsilon}{2})\Gamma(2-\frac{\epsilon}{2})}{\Gamma(2)}. \tag{4.78}$$

Expanding in powers of  $\epsilon$  the above expression

$$B_1(k) = \frac{1}{16\pi^2} \left( \frac{1}{\hat{\epsilon}} - \int_0^1 dx \log\left(\frac{\Delta(x)}{\mu^2}\right) \right) + O(\epsilon), \tag{4.79}$$

where the integral over  $x$  gives

$$\begin{aligned}
\int_0^1 dx \log\left(\frac{\Delta(x)}{\mu^2}\right) &= \int_0^1 dx \log\left(\frac{(1-x)(M^2 - xk^2)}{\mu^2}\right) = \\
&= -2 + \log\left(\frac{M^2}{\mu^2}\right) + \left(1 - \frac{M^2}{k^2}\right) \log\left(1 - \frac{k^2}{M^2}\right), \tag{4.80}
\end{aligned}$$

$B_1(k)$  turns out to be

$$B_1(k) = \frac{1}{16\pi^2} \left( \frac{1}{\hat{\epsilon}} + 2 - \log\left(\frac{M^2}{\mu^2}\right) - \left(1 - \frac{M^2}{k^2}\right) \log\left(1 - \frac{k^2}{M^2}\right) \right) + O(\epsilon). \tag{4.81}$$

We now have all of the quantities that we need to write the  $\Pi_q(k)$  expression:

$$\begin{aligned}
\Pi_q(k) &= \frac{\lambda^2 M^2}{16\pi^2 m_0^2} \left\{ \left( \frac{1}{\hat{\epsilon}} - \log\left(\frac{M^2}{\mu^2}\right) \right) \left( 3 - \frac{k^2}{M^2} \right) + \right. \\
&\quad \left. + \left( 5 - \frac{M^2}{k^2} - 2\frac{k^2}{M^2} \right) + \frac{(k^2 - M^2)^3}{k^4 M^2} \log\left(1 - \frac{k^2}{M^2}\right) \right\}, \tag{4.82}
\end{aligned}$$

where, we recall,  $M^2 = m_1^2 - i\frac{\alpha^2 \rho}{m_0^2}$ .

### 4.2.2 $\Pi_{cl}(k)$

The calculation of  $\Pi_{cl}(k)$  is similar to the computation of  $\Pi_q(k)$  in the previous section, in that we have

$$\Pi_{cl}(k) = \frac{-4\lambda^2 i}{k^2 + i\epsilon} \int \frac{d^4 q}{(2\pi)^4} \frac{\alpha^2 \rho}{m_0^4 (q^2 - m_1^2 + i\epsilon)^2} \frac{-i}{(k-q)^2 + i\epsilon} \{k^2 q^2 - (q \cdot k)^2\}, \quad (4.83)$$

which, using equation (4.53), becomes

$$\begin{aligned} \Pi_{cl}(k) = & \frac{\lambda^2 \alpha^2 \rho}{m_0^4 k^2} \{A_0(k) + (k^2 + m_1^2)B_0(k) + 2(k^2 - m_1^2)B_1(k) - \\ & -(k^2 - m_1^2)^2 C_0(k)\}, \end{aligned} \quad (4.84)$$

where the integrals  $A_0(k)$ ,  $B_0(k)$ ,  $B_1(k)$  and  $C_0(k)$  are analogous to those obtained in the previous section and can be computed in the same way (via dimensional regularization). Explicitly, they are given by

$$\begin{aligned} A_0(k) &= \int \frac{d^4 q}{(2\pi)^4} \frac{1}{q^2 - m_1^2 + i\epsilon} = \frac{1}{16\pi^2} m_1^2 \left( \frac{1}{\hat{\epsilon}} - \log \left( \frac{m_1^2}{\mu^2} \right) + 1 \right), \\ B_0(k) &= \int \frac{d^4 q}{(2\pi)^4} \frac{1}{(q^2 - m_1^2 + i\epsilon)^2} = \frac{1}{16\pi^2} \left( \frac{1}{\hat{\epsilon}} - \log \left( \frac{m_1^2}{\mu^2} \right) \right), \\ B_1(k) &= \int \frac{d^4 q}{(2\pi)^4} \frac{1}{(q^2 - m_1^2 + i\epsilon)((k-q)^2 + i\epsilon)} = \\ &= \frac{1}{16\pi^2} \left( \frac{1}{\hat{\epsilon}} - \log \left( \frac{m_1^2}{\mu^2} \right) + 2 - \left( 1 - \frac{m_1^2}{k^2} \right) \log \left( 1 - \frac{k^2}{m_1^2} - i\epsilon \right) \right), \\ C_0(k) &= \int \frac{d^4 q}{(2\pi)^4} \frac{1}{(q^2 - m_1^2 + i\epsilon)^2 ((k-q)^2 + i\epsilon)} = \frac{1}{16\pi^2} \frac{1}{k^2} \log \left( 1 - \frac{k^2}{m_1^2} - i\epsilon \right). \end{aligned} \quad (4.85)$$

Inserting these expressions into Eq. (4.84),  $\Pi_{cl}(k)$  turns out to be:

$$\Pi_{cl}(k) = \frac{3\lambda^2 \alpha^2 \rho}{16\pi^2 m_0^4} \left\{ \frac{1}{\hat{\epsilon}} + \frac{4}{3} - \frac{m_1^2}{k^2} - \log \frac{m_1^2}{\mu^2} - \left( 1 - \frac{m_1^2}{k^2} \right)^2 \log \left( 1 - \frac{k^2}{m_1^2} - i\epsilon \right) \right\}. \quad (4.86)$$

## 4.3 Renormalization

Since both of the regularized expressions we have obtained, Eqs. (4.82) and (4.86), are divergent in the limit  $\hat{\epsilon} \rightarrow 0$  (i.e. when we try to restore the physical 4 dimensions of spacetime), we still need to renormalize them in order to obtain finite and subsequently useful results. In order to achieve this aim, we need to absorb the divergent term  $1/\hat{\epsilon}$  into a renormalized coupling constant  $\lambda_{ren}$ .

Consider a generic process involving an internal photon propagator carrying a certain momentum  $k^2 = s$ , the amplitude for which can be expressed as

$$\lambda^2 D_{\mu\nu}(s) \frac{1}{1 + \lambda^2 \Pi_0(s)} S^{\mu\nu} = \lambda_{ren}^2 D_{\mu\nu}(s) S^{\mu\nu}, \quad (4.87)$$

where we have defined  $\Pi_0(s) = \Pi(s)/\lambda^2$  and  $S^{\mu\nu}$  contains the details of the process. The relationship between the renormalized coupling constant  $\lambda_{ren}$  at the scale  $s$  and the bare coupling constant  $\lambda$  is given by

$$\lambda_{ren}^2 = \frac{\lambda^2}{1 + \lambda^2 \Pi_0(s)}, \quad \lambda^2 = \frac{\lambda_{ren}^2}{1 - \lambda_{ren}^2 \Pi_0(s)}. \quad (4.88)$$

Rewriting the same process at a different scale  $k^2$ , in terms of the renormalized coupling constant, we get

$$\begin{aligned} D_{\mu\nu}(k) \frac{\lambda^2}{1 + \lambda^2 \Pi_0(k)} S^{\mu\nu} &= D_{\mu\nu}(s) \frac{\lambda_{ren}^2}{(1 - \lambda_{ren}^2 \Pi_0(s))(1 + \lambda_{ren}^2 \Pi_0(k))} S^{\mu\nu} = \\ &= D_{\mu\nu}(k) \frac{\lambda_{ren}^2}{1 + \lambda_{ren}^2 (\Pi_0(k) - \Pi_0(s))} S^{\mu\nu} = D_{\mu\nu}(k) \frac{\lambda_{ren}^2}{1 + \lambda_{ren}^2 \Pi_{ren}(k)} S^{\mu\nu}. \end{aligned} \quad (4.89)$$

From this equation, we identify the renormalized quantity  $\Pi_{ren}(k)$  as

$$\Pi_{ren}(k) = \Pi_0(k) - \Pi_0(s). \quad (4.90)$$

This quantity, if the process considered is renormalizable, is finite<sup>1</sup>, as the divergent part is absorbed into the new coupling constant  $\lambda_{ren}$ . Since the scale  $s$  at which we perform the renormalization is, in principle, arbitrary, we can choose it in such a way as to simplify our expression. This happens at the pole of the scalar propagator, specifically at  $s = M^2$ , if we consider the quantum propagator  $D_q$  (Eq. (4.21)), or at  $s = m_1^2$ , if we consider the classical propagator  $D_{cl}$  (Eq. (4.26)).

If we try to apply this renormalization procedure to the quantity  $\Pi_q(k)$  (Eq. (4.82)), obtained from the quantum scalar propagator  $D_q$ , we obtain

$$\begin{aligned} \Pi_{qren}(k) &= \frac{1}{\lambda^2} (\Pi_q(k) - \Pi_q(M)) = \frac{M^2}{16\pi^2 m_0^2} \left\{ \left( \frac{1}{\hat{\varepsilon}} - \log \left( \frac{M^2}{\mu^2} \right) \right) \left( 1 - \frac{k^2}{M^2} \right) + \right. \\ &\quad \left. + \left( 3 - \frac{M^2}{k^2} - 2 \frac{k^2}{M^2} \right) + \frac{(k^2 - M^2)^3}{k^4 M^2} \log \left( 1 - \frac{k^2}{M^2} \right) \right\}, \end{aligned} \quad (4.91)$$

where we see that the divergence  $1/\hat{\varepsilon}$  has not been removed, because the divergent term's coefficient depends on the momentum  $k^2$  (which in turn is attributable to the presence of derivatives of the fields in the interaction Hamiltonian  $\mathcal{H}_{int}$  (4.28)). We can try to absorb the residual divergence into other parameters of the model, such as the photon field's normalization. Introducing the renormalized photon field as

$$A_{ren}^\mu(k) = \frac{1}{\sqrt{Z}} A^\mu(k), \quad (4.92)$$

with  $Z = 1 + \lambda_{ren}^2 \delta$ , the amplitude (4.89) can be rewritten as

$$D_{\mu\nu}^{ren}(k) \frac{\lambda_{ren}^2}{1 + \lambda_{ren}^2 \Pi_{ren}(k)} S^{\mu\nu} = \frac{-i \lambda_{ren}^2 g_{\mu\nu} S^{\mu\nu}}{k^2 + \lambda_{ren}^2 (k^2 \delta + \Pi_{qren}(k) k^2)}; \quad (4.93)$$

<sup>1</sup>In certain cases, some residual divergence may be left. However, if the theory can be renormalized, this residual divergence can be absorbed into other parameters of the theory.

however, we see immediately that, even in this case, it is not possible to cancel the divergence. We conclude that the loop integral  $\Pi_q(k)$  is not renormalizable, and we therefore discard the quantum propagator (4.21) as a suitable scalar propagator for the present model.

Luckily, when we apply the renormalization procedure to the other possible integral  $\Pi_{cl}(k)$  (Eq. (4.86)) obtained from the classical scalar propagator  $D_{cl}$ , we obtain

$$\begin{aligned}\Pi_{cl\ ren}(k) &= \frac{1}{\lambda^2} (\Pi_{cl}(k) - \Pi_{cl}(m_1^2)) = \\ &= \frac{3\alpha^2\rho}{16\pi^2 m_0^4} \left\{ \frac{m_1^2}{k^2} + \left(1 - \frac{m_1^2}{k^2}\right)^2 \log\left(1 - \frac{k^2}{m_1^2} - i\epsilon\right) - 1 \right\},\end{aligned}\quad (4.94)$$

where the divergence, in this case, cancels out. Therefore, we will use only this expression in the following discussion and we will drop the subscript  $cl$ , thus referring to Eq. (4.94) simply as  $\Pi_{ren}(k)$ .

Finally, we can state that the renormalized re-summed propagator for the photon field at the second order in  $\lambda$  in the effective theory (4.1) is given by

$$\overline{D}_{\mu\nu}^{ren}(k) = \frac{-ig_{\mu\nu}}{k^2(1 + \lambda_{ren}^2 \Pi_{ren}(k))}, \quad (4.95)$$

with  $\Pi_{ren}(k)$  given by Eq. (4.94).

#### 4.4 Dispersion relation

As stated at the beginning of this section, the possible dispersion relations of a field are determined by the poles of its propagator, i.e., they are the solutions of the dispersion equation:

$$k^2(1 + \lambda_{ren}^2 \Pi_{ren}(k)) = 0. \quad (4.96)$$

Assuming for the moment that  $\Pi_{ren}(k)$  is regular at  $k^2 = 0$ , we find immediately that one possible solution is the standard dispersion relation

$$k^2 = 0. \quad (4.97)$$

The other possible dispersion relation is the solution of the equation

$$(1 + \lambda_{ren}^2 \Pi_{ren}(k)) = 0, \quad (4.98)$$

which, in this case, is

$$1 + \frac{3\alpha^2\lambda_{ren}^2\rho}{16\pi^2 m_0^4} \left\{ \frac{m_1^2}{k^2} + \left(1 - \frac{m_1^2}{k^2}\right)^2 \log\left(1 - \frac{k^2}{m_1^2} - i\epsilon\right) - 1 \right\} = 0. \quad (4.99)$$

In order to avoid tachyonic solutions we impose  $k^2 \geq 0$ . Moreover, introducing for simplicity the two parameters

$$\gamma = \frac{3\alpha^2\lambda_{ren}^2\rho}{16\pi^2 m_0^4}, \quad x = \frac{k^2}{m_1^2}, \quad (4.100)$$

and assuming  $0 \leq x < 1$ , Eq. (4.99) can be rewritten as

$$f_\gamma(x) = \left(\frac{x}{x-1}\right)^2 \left(\frac{1}{\gamma} + \frac{1}{x} - 1\right) + \log(1-x) = 0. \quad (4.101)$$

Unfortunately, this equation cannot be solved analytically, and so the simplest way to obtain some information on its solutions is to use a graphical method. By plotting  $f_\gamma(x)$  for various (real) values of  $\gamma$ , we find that the only possible solution of this equation is given by  $x = 0$ , see Fig. 6.

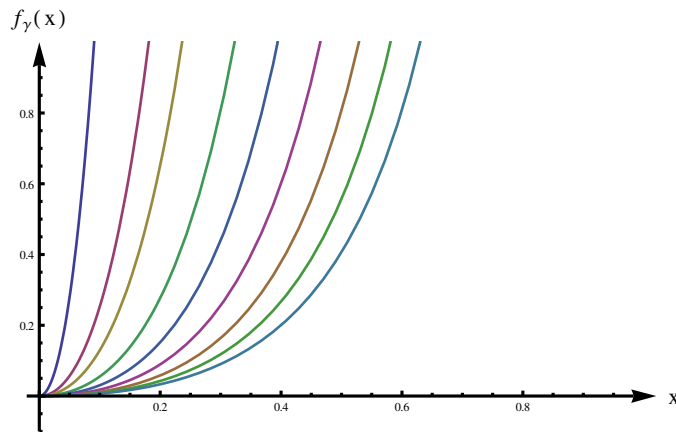


Figure 6:  $f_\gamma(x)$  from Eq. (4.101) evaluated for different values of  $\gamma$  in the range  $(0.01, 10)$ . The intersections of the curves with the  $x$  axis correspond to the solutions of the dispersion equation. We observe that the only possible solution is  $x = 0$  independently of the value of  $\gamma$ .

We conclude that, in the Lorentz-invariant spacetime foam model defined by the effective action (4.1), the photon dispersion relation is unaffected by the presence of the topological defects and remains unchanged, i.e.

$$k^2 = 0. \quad (4.102)$$

## 4.5 Extensions of the model

In this subsection, we wish to discuss briefly how the dispersion relation (4.102) changes when we introduce modifications to the spacetime foam model considered herein.

The previous results were obtained in line with the hypothesis that the wavelength of the photon is much larger than the mean separation between the defects, so that we could ignore the fluctuations of the density of defects and simply consider  $\rho_{obs} = \rho = \text{const}$ , see Eq. (2.18). It is interesting to investigate what happens when we discard this assumption and allow the photon to perceive the density fluctuations. Unfortunately, the model becomes much more complicated in this case, and we are not able to derive general results. For simplicity, we consider a 2-dimensional spacetime and parametrize the fluctuations with trigonometric functions (i.e. using periodic fluctuations instead of random fluctuations). This allows us to perform some explicit calculations but

nonetheless introduces a periodic structure that is not present in the original model and which breaks Lorentz invariance as shown in Fig. 5.

We assume that the density of defects is given by

$$\rho(x) = \rho(1 + A^2 \cos(\omega_0 x_0) \cos(\omega_1 x_1)). \quad (4.103)$$

By setting  $\omega_0 = \omega_1 = 2\pi/\sqrt{V}$  and  $A = (4/(\rho V))^{1/4}$ , where  $V \simeq \lambda_{\text{photon}}^2$ ,  $\lambda_{\text{photon}}$  being the wavelength of the photon, we determine that the mean value  $\langle \rho \rangle$  and standard deviation  $\delta\rho$  are given by

$$\begin{aligned} \langle \rho \rangle &= \frac{1}{V} \int_V d^2x \rho(x) = \rho, \\ \delta\rho &= \sqrt{\frac{1}{V} \int_V d^2x (\rho(x) - \langle \rho \rangle)^2} = \sqrt{\frac{\rho}{V}}, \end{aligned} \quad (4.104)$$

as expected from Eq. (2.17). Inserting Eq. (4.103) into Eq. (3.8), which gives the product of two Fourier transforms of the background field  $g(x)$ , we obtain

$$\begin{aligned} g(q)g(p) &= (2\pi)^2 \lambda^2 \rho h(q)h(p) \left\{ \delta^{(2)}(k+p) + \frac{A^2}{4} \left[ \delta^{(2)}(k+p+\omega) + \right. \right. \\ &\quad \left. \left. + \delta^{(2)}(k+p-\omega) + \delta(k_0+p_0+\omega_0)\delta(k_1+p_1+\omega_1) + \right. \right. \\ &\quad \left. \left. + \delta(k_0+p_0-\omega_0)\delta(k_1+p_1-\omega_1) \right] \right\}, \end{aligned} \quad (4.105)$$

where  $\omega$  is the vector with components  $\omega_0$  and  $\omega_1$ . From this equation it follows, by assuming  $\omega_0 = \omega_1 = \omega_* \simeq 1/\lambda_{\text{photon}} \ll 1$  so that we can perform a power expansion in  $\omega_*$  around zero, that the one-loop correction to the photon field is

$$\Pi(k) = -\frac{4}{k^2} \left\{ I_2(k^2) - \frac{4\rho A^2 \omega_*^2}{k^4 m_0^4} (k^2 I_0(k^2) - 2I_1(k^2)) (k_0^2 + k_1^2) \right\}, \quad (4.106)$$

where  $I_0$ ,  $I_1$ , and  $I_2$  are one-loop integrals (which, unfortunately, are not renormalizable). We observe that this result contains a Lorentz-violating term proportional to  $(k_0^2 + k_1^2)$ . As mentioned, such a violation originates from the periodic structure of the fluctuations, which explicitly breaks the Lorentz invariance of the Poisson distribution of defects. A more appropriate description of the density fluctuations can be obtained by dividing spacetime into boxes of volume  $V \simeq \lambda_{\text{photon}}^4$ , and then assigning to each box a constant density that varies from box to box according to the Poisson distribution. However, we are unable to obtain explicit results in this model, and what one can observe numerically is that Eq. (3.8) is modified also in this case, but by some random function instead of simple delta functions as in Eq. (4.105). As a result, we may infer that the density fluctuations do not break Lorentz invariance in this case, but they may possibly introduce some other modifications to the one-loop correction (4.94) that may reflect on the photon dispersion relation as well.

#### 4.5.1 PT-symmetric extension

Here, we want to describe an interesting extension of the spacetime foam model introduced in Sec. 4. This is obtained simply by replacing the real coupling constant  $\lambda$  in the action (4.1) with an imaginary one:

$$\lambda \rightarrow \lambda' = i\lambda. \quad (4.107)$$

Such a substitution makes the interaction Hamiltonian (4.28) non-Hermitian; however, this is not necessarily a problem as long as the theory remains symmetric under the combination of parity transformation  $P$  and time reversal  $T$

$$PT : \mathcal{L}(x) \rightarrow \mathcal{L}(x). \quad (4.108)$$

In fact, it has been shown [54, 55] that non-Hermitians but  $PT$  symmetric quantum mechanics can still describe physically acceptable models. In particular, the spectrum of the Hamiltonian operator remains real and positive under certain circumstances (see also Refs. [56, 57, 58] for applications of  $PT$  symmetric models to the study of real physical systems). The extension to  $PT$  symmetric quantum field theory has also been investigated in Refs. [59, 60].

We observe that the effective action (4.1) with the imaginary coupling constant  $i\lambda$  is indeed symmetric under  $PT$  transformation, if we replace the scalar field  $\phi$  with a pseudoscalar  $\tilde{\phi}$  which transforms as

$$PT : \tilde{\phi}(x) \rightarrow -\tilde{\phi}(-x). \quad (4.109)$$

Consider, in particular, the fourth and fifth terms in Eq. (4.1). The fourth term transforms under  $PT$  as

$$PT : \alpha \tilde{\phi}(x) \sum_{n=1}^{\infty} \epsilon_n \delta^4(x - x_n) \rightarrow -\alpha \tilde{\phi}(-x) \sum_{n=1}^{\infty} \epsilon_n \delta^4(-x - x_n), \quad (4.110)$$

and seems not to be invariant under  $PT$  transformation. Nevertheless, we observe that the minus sign coming from the pseudoscalar field can be absorbed into the random numbers  $\epsilon_n$ , without any observable consequences. From this finding we can conclude that this term is indeed  $PT$  symmetric. The fifth term also turns out to be  $PT$  symmetric

$$PT : -\frac{i\lambda}{4} \tilde{\phi}(x) F_{\mu\nu}(x) \tilde{F}^{\mu\nu}(x) \rightarrow -\frac{i\lambda}{4} \tilde{\phi}(-x) F_{\mu\nu}(-x) \tilde{F}^{\mu\nu}(-x), \quad (4.111)$$

given that

$$PT : F_{\mu\nu}(x) \rightarrow -F_{\mu\nu}(-x), \quad PT : \tilde{F}^{\mu\nu}(x) \rightarrow -\tilde{F}^{\mu\nu}(-x), \quad PT : i \rightarrow -i, \quad (4.112)$$

where we have introduced the dual field strength tensor  $\tilde{F}^{\mu\nu}(x) = \epsilon^{\mu\nu\rho\sigma} F_{\rho\sigma}(x)$ .

Given these considerations, we can assume that the  $PT$  symmetric extension of the effective action (4.1) still provides a physically acceptable description of a photon propagating in the Lorentz-invariant spacetime foam model considered herein. In this case, the photon re-summed propagator (4.95) is given by

$$\overline{D_{\mu\nu}^{ren}}(k) = \frac{-ig_{\mu\nu}}{k^2(1 - \lambda_{ren}^2 \Pi_{ren}(k))}, \quad (4.113)$$

with  $\Pi_{ren}(k)$  still given by Eq. (4.94). As a result, the second dispersion equation ( $1 - \lambda_{ren}^2 \Pi_{ren}(k) = 0$ ), in terms of the variables  $x$  and  $\gamma$  (Eq. (4.100)), becomes

$$f_{\gamma}(x) = \left(\frac{x}{x-1}\right)^2 \left(\frac{1}{\gamma} - \frac{1}{x} + 1\right) - \log(1-x) = 0, \quad (4.114)$$

which is plotted in Fig. 7 (again, it is not possible to find an analytic solution, and we must therefore rely on graphical methods).

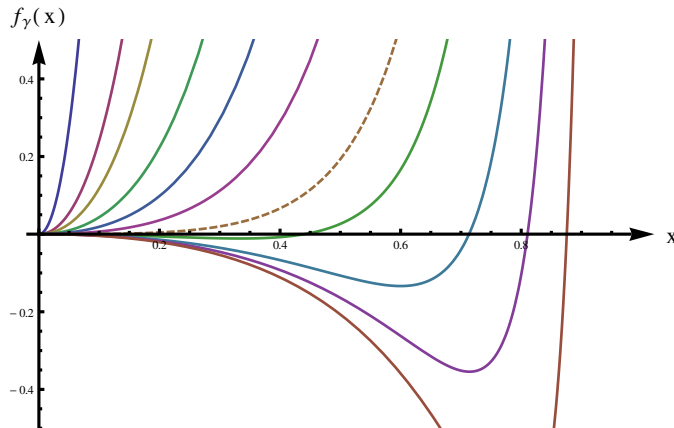


Figure 7:  $f_\gamma(x)$  from Eq. (4.114) (obtained in the  $PT$  symmetric extension of the model) evaluated for different values of  $\gamma$  in the range  $(0.01, 10)$ . Intersections of the curves with the  $x$  axis correspond to the solutions of the dispersion equation. We observe that a second non-standard solution appears for  $\gamma > \gamma_c$ . The curve corresponding to  $\gamma = \gamma_c$  is represented by a dashed line.

From Fig. 7, we see that, in this case, a second solution appears for large  $\gamma$ , which provides the modified dispersion relation

$$k^2 = \beta(\gamma) m_1^2, \quad (4.115)$$

which describes the appearance of a photon mass. We observe that  $\beta(\gamma)$  varies in the range  $[0, 1]$  and that it grows as  $\gamma$  grows (as we would have expected for a physical solution, since  $\gamma \propto \lambda^2 \alpha^2 \rho$ ). Studying the behavior of  $\beta(\gamma)$  for  $\gamma$  which goes to zero, we find that it reaches zero at a critical value  $\gamma_c$  ( $\gamma_c = 2$  at the renormalization scale we used, though it changes at different renormalization scales). Below this value, the second solution disappears and we are left with the standard dispersion relation as the only possible solution. Then, a modified dispersion relation, where the photon acquires mass, can appear only for

$$\gamma > \gamma_c \implies \lambda_{ren}^2 > \frac{16\pi^2 m_0^4 \gamma_c}{3\alpha^2 \rho}. \quad (4.116)$$

The presence of the critical point  $\gamma_c$  seems to indicate the presence of a phase transition. We speculate, given the proportionality between  $\gamma$  and  $\rho$ , that this transition could be related to the percolation of defects. Percolation theory [61], as illustrated in Sec. 7.2, describes the formation and properties of clusters of objects randomly distributed in a lattice with probability  $P$ , or in a continuum space with density  $\rho$ . This model undergoes a second-order phase transition at a certain critical probability (or critical density) where there appear infinitely large clusters.

In support of this idea, we observe that the behavior of the parameter  $\beta(\gamma)$  is well-described by the critical exponent  $\beta$  of percolation in 4 dimensions, see

Fig. 8. In fact, from the general theory of second-order phase transition [62, 63], we know that the behaviors of physical quantities (such as order parameter, correlation length, etc.) near a critical point are described by power laws. The exponents of these power laws are called “critical exponents” and are independent of most of the particular characteristics of the model considered, instead depending only on very general features (such as dimensionality and symmetries). As a result, it happens that very different models can be described by the same set of critical exponents (it is said that they belong to the same universality class). Consequently, if the phase transition that we have observed in our model is related to the percolation phase transition, we expect that the order parameter  $\beta(\gamma)$  should be described by the same critical exponent  $\beta$  of the continuous percolation model in four dimensions

$$\beta(\gamma) \propto \left(1 - \frac{\gamma_c}{\gamma}\right)^\beta. \quad (4.117)$$

The exponent  $\beta$  in the lattice percolation in four dimensions is  $\beta = 0.64$  [61], and lattice percolation and continuous percolation belong to the same universality class (at least in  $\mathbb{R}^2$  and  $\mathbb{R}^3$  [64], and we assume that the same is true in 4 dimensions).

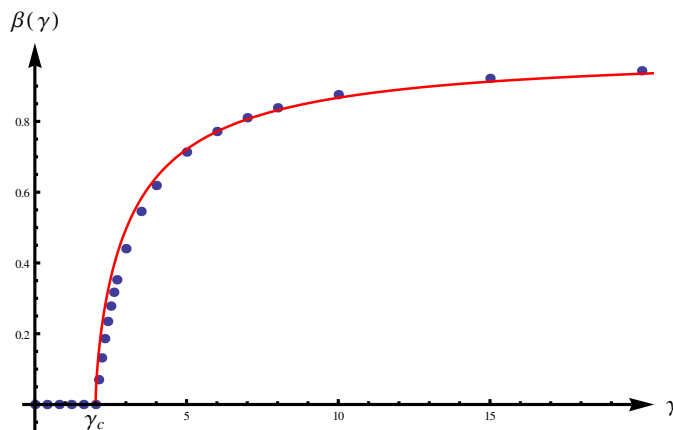


Figure 8:  $\beta(\gamma)$  from Eq. 4.115 (blue dots) compared with the expected behavior of the order parameter (Eq. (4.117)) described by the exponent  $\beta = 0.64$  obtained in four-dimensional lattice percolation (red solid line).

In Fig. 8, we indeed observe that the function  $\beta(\gamma)$  is well-interpolated by Eq. (4.117) with  $\beta = 0.64$ .

The appearance of a photon mass from the interaction of the photon field with spacetime defects has also been discussed in Refs. [65, 66]. These works also consider the case in which defects are embedded in spacetime in a Lorentz invariant way. However, they consider a different type of interaction between photons and defects characterized by momentum violation.

## Part III

# Spacetime foam from static extended defects

In this part, we move to the study of topological defects that are extended and time-independent. This means that a distribution of defects of this kind explicitly breaks Lorentz invariance. In fact, such a distribution selects a particular reference frame in which the defects are static, but any Lorentz boost will break this feature.

We start by describing a type of defect obtained from Minkowski spacetime by surgery that has already been studied in the literature, see Refs. [67, 68]. We review the propagation of electromagnetic waves in a spacetime foam model obtained from this kind of defect and how it modifies the dispersion relation. We then generalize these results to the case where the defect becomes massive.

In the next section 6, we proceed to study another, more interesting, type of defect that has been obtained in Ref. [69]. This defect has the same topology of the previous one, but the two are not diffeomorphic. Unlike the first one, this new type of defect is a vacuum solution of general relativity. We start by studying how a scalar field behaves in the metric describing this type of defect, and then we show how the propagation of waves changes in this metric with respect to the first type of defect. We continue by deriving the electromagnetic solutions and calculating the electromagnetic dispersion relation in a spacetime foam model based on this type of defect.

## 5 Defects in Minkowski space

### 5.1 Defect structure (review)

Consider Minkowski spacetime  $\mathbb{R} \times \mathbb{R}^3$  with metric  $\eta_{\mu\nu} = \text{diag}(-1, 1, 1, 1)$  and Cartesian coordinates  $x^\mu = (x^0, x^i) = (x^0, \vec{x})$ . The topological defect is obtained by removing a ball of radius  $b$  from the spatial hypersurface  $\mathbb{R}^3$  and identifying antipodal points on the boundary [67]. After this operation, Minkowski spacetime must be substituted by the manifold  $\mathbb{R} \times M_b$ , where  $M_b$  is given by

$$M_b = \{ \vec{x} \in \mathbb{R}^3 \mid \vec{x}^2 \geq b^2 \wedge (\vec{x} \equiv -\vec{x} \text{ for } \vec{x}^2 = b^2) \}, \quad (5.1)$$

and where we have chosen the origin of the coordinates  $x^i$  to coincide with the center of the defect and ‘ $\equiv$ ’ stands for point-wise identification. The structure of the submanifold  $M_b$  is illustrated in Fig. 9.

In spherical coordinates

$$(x^1, x^2, x^3) = (r \sin \theta \cos \phi, r \sin \theta \sin \phi, r \cos \theta), \quad (5.2)$$

the defect is described by the standard Minkowski metric

$$ds^2 = -dt^2 + dr^2 + r^2 (d\theta^2 + \sin^2 \theta d\phi^2), \quad (5.3)$$

with the conditions

$$r \geq b, \quad (t, b, \theta, \phi) \equiv (t, b, \pi - \theta, \phi + \pi). \quad (5.4)$$

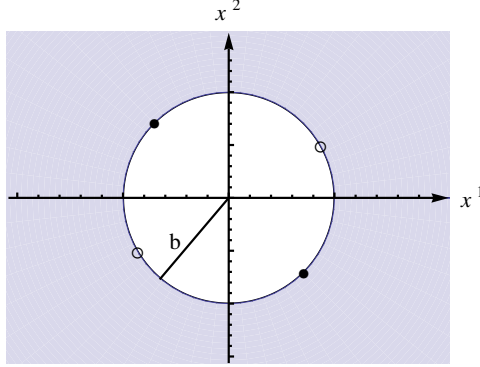


Figure 9: Section ( $x^3 = 0$ ) of the submanifold  $M_b$ . The interior of the sphere of radius  $b$ , centered on the origin, is removed and antipodal points on the boundary identified.

Observe that by using the diffeomorphism

$$r \rightarrow \rho = \frac{b}{r}, \quad (5.5)$$

it is possible to map the entire manifold  $M_b$  to the closed unit ball with antipodal points on the boundary identified (minus the origin corresponding to  $r = \infty$  in  $M_b$ ) [68]. Since the closed ball with antipodal points on the boundary identified has the topology of the 3-dimensional real projective space  $\mathbb{R}P^3$ , we can conclude that the topology of the defect manifold is

$$\mathbb{R} \times M_b \simeq \mathbb{R} \times (\mathbb{R}P^3 - \{0\}), \quad (5.6)$$

where “ $\simeq$ ” stands for “homeomorphism”.

In Ref. [68], a new system of coordinates  $\{\tilde{y}, z, x\}$  has been introduced that is more suitable for describing the manifold  $M_b$  than standard spherical coordinates. In this coordinate system, three charts  $U_i$  are needed to completely cover  $M_b$ , each one surrounding one of the Cartesian axes  $x^i$  but not intersecting the others. We introduce a subscript to indicate to which particular chart the new coordinates refer (the system of coordinates  $\{\tilde{y}_i, z_i, x_i\}$  is associated with the chart  $U_i$ , which surrounds the Cartesian axis  $x^i$ ). This new system of coordinates and the standard spherical coordinates are related in the three charts by the following transformations:

- Chart  $U_1$  surrounding  $x^1$

$$\begin{cases} \tilde{y}_1 = r - b, \\ z_1 = \theta, \\ x_1 = \phi, \end{cases} \quad |\phi| < \frac{\pi}{2}, \quad \begin{cases} \tilde{y}_1 = b - r, \\ z_1 = \pi - \theta, \\ x_1 = \phi - \pi, \end{cases} \quad |\phi| > \frac{\pi}{2}. \quad (5.7)$$

$$\begin{cases} r = \tilde{y}_1 + b, \\ \theta = z_1, \\ \phi = x_1, \end{cases} \quad \tilde{y}_1 > 0, \quad \begin{cases} r = b - \tilde{y}_1, \\ \theta = \pi - z_1, \\ \phi = x_1 + \pi, \end{cases} \quad \tilde{y}_1 < 0. \quad (5.8)$$

- Chart  $U_2$  surrounding  $x^2$

$$\begin{cases} \tilde{y}_2 = r - b, \\ z_2 = \theta, \\ x_2 = \phi - \frac{\pi}{2}, \end{cases} \quad 0 < \phi < \pi, \quad \begin{cases} \tilde{y}_2 = b - r, \\ z_2 = \pi - \theta, \\ x_2 = \phi - \frac{3\pi}{2}, \end{cases} \quad \pi < \phi < 2\pi. \quad (5.9)$$

$$\begin{cases} r = \tilde{y}_2 + b, \\ \theta = z_2, \\ \phi = x_2 + \frac{\pi}{2}, \end{cases} \quad \tilde{y}_2 > 0, \quad \begin{cases} r = b - \tilde{y}_2, \\ \theta = \pi - z_2, \\ \phi = x_2 + \frac{3\pi}{2}, \end{cases} \quad \tilde{y}_2 < 0. \quad (5.10)$$

- Chart  $U_3$  surrounding  $x^3$

$$\begin{aligned} |\phi| < \frac{\pi}{2} : & \quad |\phi| > \frac{\pi}{2} : \\ \begin{cases} \begin{cases} \tilde{y}_3 = r - b, \\ z_3 = \frac{\pi}{2} - \theta, \\ x_3 = \phi, \end{cases} & 0 < \theta < \frac{\pi}{2}, \\ \begin{cases} \tilde{y}_3 = b - r, \\ z_3 = \theta, \\ x_3 = \phi, \end{cases} & \frac{\pi}{2} < \theta < \pi, \end{cases} & \begin{cases} \begin{cases} \tilde{y}_3 = r - b, \\ z_3 = \frac{\pi}{2} + \theta, \\ x_3 = \phi - \pi, \end{cases} & 0 < \theta < \frac{\pi}{2}, \\ \begin{cases} \tilde{y}_3 = b - r, \\ z_3 = \pi - \theta, \\ x_3 = \phi - \pi, \end{cases} & \frac{\pi}{2} < \theta < \pi. \end{cases} \end{aligned} \quad (5.11)$$

$$\begin{aligned} \tilde{y}_3 > 0 : & \quad \tilde{y}_3 < 0 : \\ \begin{cases} \begin{cases} r = b + \tilde{y}_3, \\ \theta = \frac{\pi}{2} - z_3, \\ \phi = x_3, \end{cases} & 0 < z_3 < \frac{\pi}{2}, \\ \begin{cases} r = b + \tilde{y}_3, \\ \theta = z_3 - \frac{\pi}{2}, \\ \phi = x_3 + \pi, \end{cases} & \frac{\pi}{2} < z_3 < \pi, \end{cases} & \begin{cases} \begin{cases} r = b - \tilde{y}_3, \\ \theta = \pi - z_3, \\ \phi = x_3 + \pi, \end{cases} & 0 < z_3 < \frac{\pi}{2}, \\ \begin{cases} r = b - \tilde{y}_3, \\ \theta = z_3, \\ \phi = x_3, \end{cases} & \frac{\pi}{2} < z_3 < \pi. \end{cases} \end{aligned} \quad (5.12)$$

Note that the standard spherical coordinates are ill-defined on the  $x^3$  axis. A better approach is to introduce a new set of spherical coordinates to describe the chart  $U_3$

$$(x^1, x^2, x^3) = (r \sin \hat{\theta} \sin \hat{\phi}, r \cos \hat{\theta}, r \sin \hat{\theta} \cos \hat{\phi}). \quad (5.13)$$

With this choice, the transformation rules between  $\{\tilde{y}_3, z_3, x_3\}$  and  $\{r, \hat{\theta}, \hat{\phi}\}$  are obtained by substituting  $\theta$  and  $\phi$  with  $\hat{\theta}$  and  $\hat{\phi}$  and changing the index to  $i = 3$  in Eqs. (5.7) and (5.8). One therefore obtains

- Chart  $U_3$  surrounding  $x^3$  (regular coordinates)

$$\begin{cases} \tilde{y}_3 = r - b, \\ z_3 = \hat{\theta}, \\ x_3 = \hat{\phi}, \end{cases} \quad |\hat{\phi}| < \frac{\pi}{2}, \quad \begin{cases} \tilde{y}_3 = b - r, \\ z_3 = \pi - \hat{\theta}, \\ x_3 = \hat{\phi} - \pi, \end{cases} \quad |\hat{\phi}| > \frac{\pi}{2}. \quad (5.14)$$

$$\begin{cases} r = \tilde{y}_3 + b, \\ \hat{\theta} = z_3, \\ \hat{\phi} = x_3, \end{cases} \quad \tilde{y}_3 > 0, \quad \begin{cases} r = b - \tilde{y}_3, \\ \hat{\theta} = \pi - z_3, \\ \hat{\phi} = x_3 + \pi, \end{cases} \quad \tilde{y}_3 < 0. \quad (5.15)$$

Standard spherical coordinates range in

$$r \in [0, +\infty), \quad \theta \in [0, \pi], \quad \phi \in [0, 2\pi), \quad (5.16)$$

while the new set of coordinates  $\{\tilde{y}, z, x\}$  has ranges

$$\tilde{y} \in (-\infty, +\infty), \quad z \in (0, \pi), \quad x \in \left(-\frac{\pi}{2}, \frac{\pi}{2}\right). \quad (5.17)$$

We note that the standard angular coordinates  $\theta$  and  $\phi$  cover the entire solid angle  $\Omega = 4\pi$ . Instead, the new angular coordinates  $z$  and  $x$  cover only half of it, namely  $\Omega' = \Omega/2 = 2\pi$ . Conversely, the standard radial coordinate  $r$  is restricted to the positive real numbers  $\mathbb{R}^+$ , while the new “radial coordinate”  $\tilde{y}$  takes value on the whole real line  $\mathbb{R}$ . This is somewhat reminiscent of the procedure adopted to describe the Einstein-Rosen bridge [70]. For such a solution, a new radial coordinate  $u^2 = r - 2m$  is also introduced whose range is  $u \in (-\infty, +\infty)$  (see also Ref. [12]). However, in that case, the angular coordinates are not modified.

The metric of the manifold  $\mathbb{R} \times M_b$  in these new coordinates becomes

$$ds^2 = -dt^2 + d\tilde{y}^2 + (b + |\tilde{y}|)^2 (dz^2 + \sin^2 z dx^2). \quad (5.18)$$

Note that, since in each chart the metric turns out to be the same, we have dropped the subscript  $i$ . One important feature of these coordinates is that one does not need to implement additional boundary conditions to describe the structure of the defect—as happens with spherical coordinates. Moreover, the defect manifold in the new coordinate system is a well-defined differentiable manifold, while in spherical coordinates this is not the case (spherical coordinates are ill-defined at the defect surface). It follows that the new manifold, described by the metric (5.18), is not globally diffeomorphic to the defect described in standard spherical coordinates (Eqs. (5.3) and (5.4)). See Sec. 6 for more details.

One can calculate the scalar curvature  $R$  and the Kretschmann scalar  $K$  obtaining [68]

$$R = g^{\mu\nu} R_{\mu\nu} = -8 \frac{\delta(\tilde{y})}{b + |\tilde{y}|}, \quad K = R_{\mu\nu\rho\sigma} R^{\mu\nu\rho\sigma} = \frac{1}{2} R^2, \quad (5.19)$$

where  $R_{\mu\nu}$  is the Ricci curvature tensor and  $R_{\mu\nu\rho\sigma}$  is the Riemann tensor. From these quantities we see that the metric (5.18) is flat everywhere apart from on the defect surface, where it has a delta function singularity.

## 5.2 Massless case (review)

In this section, we briefly review the work done in Ref. [67], in which three different types of defects were introduced. Here, we consider only the first one ( $\tau = 1$  in Ref. [67]), which is described in standard spherical coordinates by the metric

$$ds^2 = -dt^2 + dr^2 + r^2(d\theta^2 + \sin^2\theta d\phi^2), \quad (5.20)$$

with the restriction  $r \geq b$  and the identification of antipodal points on the surface of the defect

$$\vec{x}_b \equiv -\vec{x}_b \iff (b, \theta, \phi) \equiv (b, \pi - \theta, \phi + \pi). \quad (5.21)$$

From such a condition, it is possible to derive the behavior of vector and pseudo-vector fields on the defect surface [68]. One finds, in fact, that given a smooth map  $I$  from a manifold  $M$  into itself [71]

$$I : p \in M \rightarrow p' = I(p) \in M, \quad (5.22)$$

the differential map  $I_*$  describes the induced transformation on the tangent space

$$I_* : \vec{v} \in T_p M \rightarrow \vec{v}' = I_*(\vec{v}) \in T_{I(p)} M. \quad (5.23)$$

Using the decomposition of a vector in its tangent and normal components (and the fact that the normal versor can be obtained by the cross-product of orthogonal tangent versors), one finds that the differential map  $I_*$  completely defines the behavior of vector fields with respect to the transformation  $I$ . For the present case, the map  $I$  is

$$\vec{x} \rightarrow \vec{x}' = I(\vec{x}) = -\vec{x}. \quad (5.24)$$

The differential map  $I_*$  is given by the Jacobian of the transformation  $I$ . For Eq. (5.24), it gives simply  $I_* = -1$ . It follows that, on the defect surface, the electric field  $\vec{E}$  must satisfy the conditions

$$\vec{E}(x_b) \cdot \vec{n}(x_b) = -\vec{E}(-x_b) \cdot \vec{n}(-x_b), \quad \vec{E}(x_b) \wedge \vec{n}(x_b) = \vec{E}(-x_b) \wedge \vec{n}(-x_b). \quad (5.25)$$

The magnetic field  $\vec{B}$ , being a pseudovector, must transform according to

$$\vec{B}(x_b) \cdot \vec{n}(x_b) = \vec{B}(-x_b) \cdot \vec{n}(-x_b), \quad \vec{B}(x_b) \wedge \vec{n}(x_b) = -\vec{B}(-x_b) \wedge \vec{n}(-x_b), \quad (5.26)$$

where  $\vec{n}(x)$  is the versor normal to the defect surface at the point  $\vec{x}$ .

The idea behind this calculation is to study how an incident plane electromagnetic wave scatters with the defect. Since the incident electric and magnetic fields do not satisfy the boundary conditions (5.25) and (5.26), a scattered field must be introduced so that the total fields (given by the sum of the incident and scattered fields) satisfy them accordingly. A spacetime foam model can be obtained by randomly distributing the defects into  $\mathbb{R}^3$  with number density  $\rho$ . From the form of the scattered field, and from the characteristics of the distribution, one can finally obtain the electric and magnetic permittivities  $\epsilon$  and  $\mu$  of spacetime, which provide the electromagnetic dispersion relation throughout the formula

$$\omega^2 = \frac{c^2 k^2}{\epsilon \mu}. \quad (5.27)$$

### 5.2.1 Plane wave in spherical coordinates

We consider the plane electromagnetic wave propagating along the Cartesian axis  $Z$

$$\begin{aligned}\vec{E} &= E_0 \operatorname{Re}(e^{ikr \cos \theta}) \hat{X}, \\ \vec{B} &= E_0 \operatorname{Re}(e^{ikr \cos \theta}) \hat{Y}.\end{aligned}\quad (5.28)$$

Rewriting the Cartesian basis vectors  $\{\hat{X}, \hat{Y}, \hat{Z}\}$  in spherical coordinates

$$\begin{aligned}\hat{X} &= \sin \theta \cos \phi \hat{r} + \cos \theta \cos \phi \hat{\theta} - \sin \phi \hat{\phi}, \\ \hat{Y} &= \sin \theta \sin \phi \hat{r} + \cos \theta \sin \phi \hat{\theta} + \cos \phi \hat{\phi}, \\ \hat{Z} &= \cos \theta \hat{r} - \sin \theta \hat{\theta},\end{aligned}\quad (5.29)$$

and expressing the trigonometric functions in terms of spherical harmonics, the components of the electric field in spherical coordinates become

$$\begin{aligned}E_r &= -\sqrt{\frac{2\pi}{3}} E_0 \operatorname{Re}(e^{ikr \cos \theta})(Y_1^1 - Y_1^{-1}), \\ E_\theta &= -\frac{1}{\tan \theta} \sqrt{\frac{2\pi}{3}} E_0 \operatorname{Re}(e^{ikr \cos \theta})(Y_1^1 - Y_1^{-1}) = \frac{E_r}{\tan \theta}, \\ E_\phi &= -\frac{i}{\sin \theta} \sqrt{\frac{2\pi}{3}} E_0 \operatorname{Re}(e^{ikr \cos \theta})(Y_1^1 + Y_1^{-1}) = -E_r \frac{\tan \phi}{\sin \theta}.\end{aligned}\quad (5.30)$$

We can now introduce the plane wave expansion [72]

$$e^{ikr \cos \theta} = 4\pi \sum_{l,m} i^l j_l(kr) Y_l^{*m}(\theta_k, \phi_k) Y_l^m(\theta, \phi), \quad (5.31)$$

where  $\theta_k = 0$  for a wave propagating along the  $Z$  axis. Rewriting the products of spherical harmonics as an expansion in terms of single spherical harmonics [73]

$$Y_{l_1}^{m_1} Y_{l_2}^{m_2} = \sum_{l,m} \sqrt{\frac{(2l_1+1)(2l_2+1)}{4\pi(2l+1)}} c(l_1, m_1; l_2, m_2; l, m) c(l_1, 0; l_2, 0; l, 0) Y_l^m, \quad (5.32)$$

where  $c(l_1, m_1; l_2, m_2; l, m)$  are the Clebsch-Gordan coefficients, we finally obtain

$$\begin{aligned}E_r &= \sqrt{\pi} E_0 \sum_{l=\text{odd}} i^{l-1} (j_{l-1}(kr) + j_{l+1}(kr)) \sqrt{\frac{l(l+1)}{2l+1}} (Y_l^1 - Y_l^{-1}), \\ E_\theta &= E_r \tan \theta, \\ E_\phi &= E_r \frac{\tan \phi}{\sin \theta} = \frac{\sqrt{\pi}}{\sin \theta} E_0 \sum_{l=\text{odd}} i^{l-2} (j_{l-1}(kr) + j_{l+1}(kr)) \sqrt{\frac{l(l+1)}{2l+1}} (Y_l^1 + Y_l^{-1}).\end{aligned}\quad (5.33)$$

We recall here some useful formulas:

$$\begin{aligned}
\frac{2l+1}{kr} j_l(kr) &= (j_{l-1}(kr) + j_{l+1}(kr)), \\
P_l^1(\cos\theta) \cos\phi &= \sqrt{\pi} \sqrt{\frac{l(l+1)}{2l+1}} (Y_l^1 - Y_l^{-1}), \\
P_l^1(\cos\theta) \sin\phi &= -i\sqrt{\pi} \sqrt{\frac{l(l+1)}{2l+1}} (Y_l^1 + Y_l^{-1}),
\end{aligned} \tag{5.34}$$

which allow us to make a connection with the results of Ref. [74] and which we will need in the study of massive defects. Using these formulas, we can rewrite  $E_r$  as

$$E_r = E_0 \sum_{l=\text{odd}} i^{l-1} \frac{2l+1}{kr} j_l(kr) P_l^1(\cos\theta) \cos\phi, \tag{5.35}$$

and similarly for  $E_\theta$  and  $E_\phi$ .

### 5.2.2 Boundary conditions

We have written the expression for a plane wave propagating along the  $Z$  axis in spherical coordinates. We wish to verify if this incident wave satisfies the boundary conditions of the defect placed at the origin. The boundary conditions for the electric and magnetic fields, Eqs. (5.25) and (5.26), expressed in components in spherical coordinates are given by

$$\begin{aligned}
E_r(-x_b) &= -E_r(x_b), & E_\theta(-x_b) &= E_\theta(x_b), & E_\phi(-x_b) &= E_\phi(x_b), \\
B_r(-x_b) &= B_r(x_b), & B_\theta(-x_b) &= -B_\theta(x_b), & B_\phi(-x_b) &= -B_\phi(x_b),
\end{aligned} \tag{5.36}$$

where  $x_b$  represents a point on the boundary of the defect

$$x_b = (b, \theta, \phi), \quad -x_b = (b, \pi - \theta, \phi + \pi). \tag{5.37}$$

We observe that the behavior of the fields under parity transformation is completely determined by their angular dependence. Considering first the electric field, we can easily verify that these conditions are automatically satisfied by  $E_r$  and  $E_\theta$  but not by  $E_\phi$ , which means that the incident plane wave  $E^{in}$  reaching the defect surface must produce a scattered field  $E^s$  so that the total field  $E^T = E^{in} + E^s$  satisfies the boundary conditions. The scattered field, in general, can be expressed in terms of a multipole expansion. In order to simplify the problem, we consider the case of an incident wave with a wavelength much greater than the defect size ( $kb \ll 1$ ) so that, in first approximation, we can work with static fields. In this way, we can write the scattered field as the gradient of an electrostatic potential ( $E^s = -\vec{\nabla}\Phi$ ). In terms of a multipole expansion, the potential is

$$\Phi(r, \theta, \phi) = \sum_{l,m} A_l^m \frac{1}{r^{l+1}} Y_l^m(\theta, \phi), \tag{5.38}$$

where the coefficients  $A_l^m$  are determined by the boundary condition

$$E_\phi^T(-x_b) = E_\phi^T(x_b) \iff E_\phi^{in}(-x_b) + E_\phi^s(-x_b) = E_\phi^{in}(x_b) + E_\phi^s(x_b). \tag{5.39}$$

From this equation, one obtains

$$A_l^{\pm 1} = \mp i^{l-1} \sqrt{\pi} b^{l+2} (j_{l-1}(kb) + j_{l+1}(kb)) \sqrt{\frac{l(l+1)}{2l+1}} E_0. \quad (5.40)$$

### 5.2.3 Dispersion relation

Since the size of the defect is assumed to be small with respect to the wavelength, the leading contribution to the multipole expansion of  $\Phi$  comes from the first term in the expansion. This term corresponds to a dipole oriented along the  $X$  axis (parallel to the incident electric field) and with a dipole moment:

$$\vec{p} = p \hat{X}, \quad p = b^3 (j_0(kb) + j_2(kb)) E_0. \quad (5.41)$$

Now, we can build a spacetime foam model based on this type of defect. We replace standard Minkowski spacetime  $\mathbb{R} \times \mathbb{R}^3$  with a new manifold  $\mathbb{R} \times M_1$ , where  $M_1$  is obtained by filling  $\mathbb{R}^3$  with a random distribution of defects with number density  $\rho$  ( $\langle N(V) \rangle = \rho V$ ). The polarization of such a space is

$$\vec{P} = \frac{1}{V} \sum_i \vec{p}_i = \rho \vec{p}. \quad (5.42)$$

From the relations<sup>2</sup>  $\vec{P} = \chi_e \vec{E}$  and  $\varepsilon = 1 + 4\pi\chi_e$ , we can finally derive the electric permittivity:

$$\varepsilon \simeq 1 + 4\pi\rho b^3 (j_0(kb) + j_2(kb)). \quad (5.43)$$

An analogous derivation for the magnetic field leads to the magnetic permeability

$$\mu \simeq 1 - 2\pi\rho b^3 (j_0(kb) + j_2(kb)). \quad (5.44)$$

Finally, the dispersion relation turns out to be

$$\omega^2 = \frac{c^2 k^2}{\varepsilon(k)\mu(k)} \simeq \frac{c^2 k^2}{[1 + 4\pi\rho b^3 (j_0(kb) + j_2(kb))][1 - 2\pi\rho b^3 (j_0(kb) + j_2(kb))]}, \quad (5.45)$$

which, expanded in powers of  $kb$ , becomes

$$\omega^2 \simeq (1 - 2\rho\pi b^3) c^2 k^2 + \frac{\rho\pi b^5}{5} c^2 k^4 + \dots \quad (5.46)$$

### 5.3 Massive case

We want to generalize the previous calculation to the case in which the defect acquires a mass  $m = \ell/2$ . In such a case, the defect is no longer described by the flat Minkowski metric (5.20), but it must be described by the Schwarzschild metric

$$ds^2 = - \left(1 - \frac{\ell}{r}\right) dt^2 + \frac{1}{\left(1 - \frac{\ell}{r}\right)} dr^2 + r^2 (d\theta^2 + \sin^2 \theta d\phi^2). \quad (5.47)$$

Instead, the boundary conditions do not change:

$$r \geq b, \quad (b, \theta, \phi) \equiv (b, \pi - \theta, \phi + \pi). \quad (5.48)$$

<sup>2</sup>Following Ref. [67], we use Gaussian units [74].

Given the spherical symmetry of the Schwarzschild metric, we find that all modifications with respect to the massless case involve only the radial component of the results, while the angular dependence remains the same. This is a great simplification—as we can see from the fact that the boundary conditions involve only the angular coordinates.

### 5.3.1 Maxwell equations in curved spacetime

Since the space around the defect is not flat in this case, we must find the solutions of the Maxwell equations in the Schwarzschild metric. In order to study a situation analogous to the one discussed for the massless defect, we can require that these solutions approach the plane wave solution in flat spacetime at spatial infinity (since the Schwarzschild metric is asymptotically flat).

Vacuum Maxwell equations in flat spacetime can be written as [75]

$$\begin{aligned}\partial_\mu F^{\mu\nu} &= 0, \\ \partial_{[\mu} F_{\nu\lambda]} &= 0,\end{aligned}\tag{5.49}$$

where  $F_{\mu\nu}$  is the Maxwell field strength tensor related to the vector potential  $A_\mu$  through the relation

$$F_{\mu\nu} = \partial_\mu A_\nu - \partial_\nu A_\mu.\tag{5.50}$$

The principle of minimal coupling [76] gives us a simple recipe to rewrite these equations in a general metric. We need to replace the Minkowski metric with the metric at hand and replace any partial derivative with a covariant derivative. Maxwell equations in the general metric  $g_{\mu\nu}$  become

$$\begin{aligned}\nabla_\mu F^{\mu\nu} &= \partial_\mu (g^{1/2} F^{\mu\nu}) = 0, \\ \nabla_{[\mu} F_{\nu\lambda]} &= \partial_{[\mu} F_{\nu\lambda]} = 0,\end{aligned}\tag{5.51}$$

where  $F^{\mu\nu} = g^{\mu\rho} g^{\nu\sigma} F_{\rho\sigma}$ , and  $g$  is minus the determinant of the metric ( $g^{1/2} = \sqrt{-\det(g_{\mu\nu})}$ ), so that the argument of the square root is positive. The covariant derivative of a 2-tensor is given by

$$\begin{aligned}\nabla_\mu T^{\rho\sigma} &= \partial_\mu T^{\rho\sigma} + \Gamma_{\mu\nu}^\rho T^{\nu\sigma} + \Gamma_{\mu\nu}^\sigma T^{\rho\nu}, \\ \nabla_\mu T_{\rho\sigma} &= \partial_\mu T_{\rho\sigma} - \Gamma_{\mu\rho}^\nu T_{\nu\sigma} - \Gamma_{\mu\sigma}^\nu T_{\rho\nu},\end{aligned}\tag{5.52}$$

where the Christoffel symbols  $\Gamma_{\mu\nu}^\lambda$  are obtained from the metric

$$\Gamma_{\mu\nu}^\lambda = \frac{1}{2} g^{\lambda\rho} (\partial_\nu g_{\rho\mu} + \partial_\mu g_{\rho\nu} - \partial_\rho g_{\mu\nu}).\tag{5.53}$$

Observe that, if the covariant derivative is contracted with the tensor and this is completely antisymmetric ( $T^{\mu\nu} = -T^{\nu\mu}$ ), the expression of the Christoffel symbols simplifies and one gets

$$\nabla_\mu T^{\mu\nu} = g^{-1/2} \partial_\mu (g^{1/2} T^{\mu\nu}).\tag{5.54}$$

Note also that following the minimal coupling prescription, one is led to rewrite the Maxwell field strength tensor as

$$F_{\mu\nu} = \nabla_\mu A_\nu - \nabla_\nu A_\mu = \partial_\mu A_\nu - \partial_\nu A_\mu.\tag{5.55}$$

However, even if the final result is correct, inserting the covariant derivative is not appropriate in this case. In fact,  $F_{\mu\nu}$  is by definition the exterior derivative of the connection  $A_\mu$ , and as such it always takes the form (5.50) independently of the metric [77].

When one tries to write these equations explicitly, for example for the Schwarzschild metric, one finds a system of coupled linear differential equations that is hard to solve. In flat spacetime, in spherical coordinates, the same problem arises, but it can be circumvented by the introduction of Debye potentials. That is, electromagnetic solutions can be obtained from the solutions of the scalar wave equation (see Ref. [74]). In short, given a solution  $\Pi(t, r, \theta, \phi)$  of the scalar wave equation  $\partial^2\Pi = 0$ , one can verify that the vector quantities

$$\begin{cases} \vec{E}_E = \nabla \wedge \nabla \wedge \vec{r} \Pi, & \begin{cases} \vec{E}_M = -\vec{B}_E, \\ \vec{B}_M = \vec{E}_E, \end{cases} \end{cases} \quad (5.56)$$

are two sets of independent solutions of the vacuum Maxwell equations. Fortunately, such a formalism has been generalized to curved spacetimes. In fact, the study of electromagnetic waves in Schwarzschild geometry was quite popular in the 1970s, see for example Refs. [78], [79], [80], [81], [82], [83]. Here, we want to summarize briefly the work of Ref. [78], where it is described how the formalism of Debye potentials can be extended to certain classes of curved geometries.

In this work, it was shown that the four potential  $A_\mu$  can indeed be expressed in terms of two Debye scalar potentials,  $\pi$  and  $\phi$ :

$$A_\mu = \partial_\nu \pi (u^\nu v_\mu - v^\nu u_\mu) + \epsilon_\mu^{\nu\rho\sigma} \partial_\nu \phi v_\rho u_\sigma, \quad (5.57)$$

where  $u^\mu$  and  $v^\mu$  are two vectors satisfying  $u_\mu v^\mu = 0$ . If it is possible to write the metric in the form<sup>3</sup>

$$ds^2 = H^2(x, y, u, v) (dx^2 + \epsilon_1 F^2(x, y) dy^2) + \epsilon_2 dv^2 + \epsilon_3 du^2, \quad (5.58)$$

with the conditions

$$\begin{aligned} \epsilon_1 \epsilon_2 \epsilon_3 &= -1; \\ v_\mu &= \partial_\mu v, \quad v_\mu v^\mu = \epsilon_2 = \pm 1, \quad \nabla_\mu v_\nu = \frac{1}{2} \Theta h_{\mu\nu}; \\ u_\mu &= \partial_\mu u, \quad u_\mu u^\mu = \epsilon_3 = \pm 1, \quad \nabla_\mu u_\nu = \frac{1}{2} V h_{\mu\nu}; \\ h_{\mu\nu} &= g_{\mu\nu} - \epsilon_2 v_\mu v_\nu - \epsilon_3 u_\mu u_\nu; \end{aligned} \quad (5.59)$$

the four-potential  $A_\mu$  (Eq. (5.57)) is then a solution of the Maxwell equations (Eq. (5.51)), if the Debye potentials  $\pi$  and  $\phi$  satisfy the Debye equation

$$D(\pi) = \nabla_\mu \partial^\mu \pi - \epsilon_2 \Theta \partial_\mu \pi v^\mu - \epsilon_3 V \partial_\mu \pi u^\mu = 0. \quad (5.60)$$

In a subsequent work [79], it was shown how the method can be applied to the Schwarzschild spacetime. Rescaling the radial and time variables in the Schwarzschild metric (5.47) to  $r' = r/\ell$  and  $t' = t/\ell$ , and introducing the Regge-Wheeler coordinate  $v = r' + \ln(r' - 1)$ , the Schwarzschild metric can be cast in the form

$$ds^2 = \frac{r'^3}{r' - 1} (d\theta^2 + \sin^2 \theta d\phi^2) + dv^2 - dt'^2, \quad (5.61)$$

<sup>3</sup>This is not the only possibility, as there is another suitable form for the metric, but it is not relevant to our discussion.

which is equivalent to Eq. (5.58) with the identifications

$$\begin{aligned} \theta = x, \quad \phi = y, \quad v = v, \quad t' = u; \\ \varepsilon_1 = 1, \quad \varepsilon_2 = 1, \quad \varepsilon_3 = -1, \quad H^2(x^\mu) = \frac{r'^3(v)}{r'(v) - 1}, \quad F^2(\theta, \phi) = \sin^2 \theta; \\ v_\mu = \partial_\mu v = (0, 0, 1, 0), \quad u_\mu = \partial_\mu u = (0, 0, 0, 1). \end{aligned} \quad (5.62)$$

The Debye equation is now

$$D(\pi) = g^{-\frac{1}{2}} \partial_\mu g^{\frac{1}{2}} g^{\mu\nu} \partial_\nu \pi - \Theta \partial_v \pi = 0, \quad (5.63)$$

where  $\Theta = (2r' - 3)/r'^2$ . Expanding the first term, it becomes

$$D(\pi) = \left[ \frac{r' - 1}{r'^3 \sin \theta} \left( \partial_\theta (\sin \theta \partial_\theta) + \frac{1}{\sin \theta} \partial_\phi^2 \right) + \partial_v^2 - \partial_{t'}^2 \right] \pi = 0. \quad (5.64)$$

Given the spherical symmetry of this metric, we can use for the Debye potentials the expressions

$$\pi = P(r', \theta) \cos \phi e^{-i\omega t'}, \quad \phi = -P(r', \theta) \sin \phi e^{-i\omega t'}, \quad (5.65)$$

where  $\omega = \ell k$  is a dimensionless separation constant proportional to the wave number  $k$ . The expression  $P(r', \theta)$  is given by

$$P(r', \theta) = \sum_{n=1}^{\infty} D_n R_n(r') P_n^1(\cos \theta), \quad (5.66)$$

where  $R_n(r')$  is a solution of the radial equation

$$\partial_v^2 R_n + \omega^2 \left( 1 - \frac{n(n+1)}{\omega^2} \frac{(r' - 1)}{r'^3} \right) R_n = 0. \quad (5.67)$$

The constants  $D_n$  are found by requiring the solution  $P(r', \theta)$  to represent an incident plane wave at  $\theta = \pi$ ,  $r' \rightarrow \infty$ .

### 5.3.2 Plane wave in the Schwarzschild metric

Before studying the radial equation (5.67), we want to describe the electromagnetic plane wave in the Schwarzschild metric (following the approach of Ref. [83]) and derive the dispersion relation for electromagnetic plane waves in a spacetime filled with massive defects.

As in the previous subsection, we introduce dimensionless coordinates  $x = r/\ell$ ,  $\alpha = \ell k$  and the Regge-Wheeler (tortoise) coordinate  $y = x + \log(x - 1)$ . As the Schwarzschild metric (5.47) is asymptotically flat, we can write an incoming plane wave propagating along the  $Z$  axis as

$$\begin{aligned} \vec{E} \stackrel{x \rightarrow \infty}{\simeq} E_0 e^{i\alpha y \cos \theta} \hat{X}, \\ \vec{B} \stackrel{x \rightarrow \infty}{\simeq} E_0 e^{i\alpha y \cos \theta} \hat{Y}, \end{aligned} \quad (5.68)$$

where  $\{X, Y, Z\}$  are Cartesian coordinates. Note that these expressions differ from the standard plane wave solution in flat spacetime by a logarithmic factor,

which reflects the long-range nature of gravity. We can then introduce the plane wave expansion

$$e^{i\alpha y \cos \theta} = \sum_l i^l (2l+1) P_l(\cos \theta) \frac{R_{l\alpha}^{(plane)}(x)}{\alpha x}, \quad (5.69)$$

with the requirement that this expression approaches that of a plane wave in flat spacetime at infinity:

$$\frac{R_{l\alpha}^{(plane)}(x)}{\alpha x} \underset{x \rightarrow \infty}{\simeq} j_l(\alpha y) \simeq \frac{\sin(\alpha y - \frac{\pi}{2}l)}{\alpha x}, \quad (5.70)$$

where  $R_{l\alpha}$  is a solution of the radial wave equation (5.67). The radial wave equation can be expressed equally in terms of the variable  $x$  instead of the tortoise coordinate  $y$ , and one gets

$$x^2(x-1)^2 \partial_x^2 R_{l\alpha} + x(x-1) \partial_x R_{l\alpha} + (\alpha^2 x^4 - l(l+1)x(x-1)) R_{l\alpha} = 0. \quad (5.71)$$

Introducing an orthonormal frame  $\{\widehat{\omega}_r, \widehat{\omega}_\theta, \widehat{\omega}_\phi\}$  (where  $\widehat{\omega}_r = \sqrt{1 - \ell/r} \hat{r}$ ,  $\widehat{\omega}_\theta = \hat{\theta}$ ,  $\widehat{\omega}_\phi = \hat{\phi}$ ) we can expand the plane wave as

$$\begin{aligned} \vec{E} &\underset{x \rightarrow \infty}{\simeq} E_0 e^{i\alpha y \cos \theta} (\sin \theta \cos \phi \widehat{\omega}_r + \cos \theta \cos \phi \widehat{\omega}_\theta - \sin \phi \widehat{\omega}_\phi) = \\ &= E_r \widehat{\omega}_r + E_\theta \widehat{\omega}_\theta + E_\phi \widehat{\omega}_\phi. \end{aligned} \quad (5.72)$$

In Ref. [83], the authors follow closely the derivation of Ref. [74]. They write the general solution of the wave equation in the Schwarzschild metric in terms of Debye potentials as a multipole expansion and use the previous asymptotic relations to identify the coefficients. They find, for the radial component of the electric field, the expression

$$E_r = E_0 \sum_{l=1}^{\infty} i^{l-1} \frac{2l+1}{\alpha^2 x^2} R_{l\alpha}^{(plane)}(x) P_l^1(\cos \theta) \cos \phi. \quad (5.73)$$

Here, we proceed following the approach of Ref. [67], described in Sec. 5.2.1, and we obtain

$$E_r = \sqrt{\pi} E_0 \sum_{l=1}^{\infty} i^{l-1} \frac{2l+1}{\alpha^2 x^2} R_{l\alpha}^{(plane)}(x) \sqrt{\frac{l(l+1)}{2l+1}} (Y_l^1 - Y_l^{-1}). \quad (5.74)$$

Note that this expression coincides with Eq. (5.73), making use of the equivalences (5.34). The other components follow from the identifications

$$E_\theta = E_r \frac{\tan \theta}{\sqrt{1 - \ell/r}}, \quad E_\phi = -E_r \frac{\tan \phi}{\sin \theta \sqrt{1 - \ell/r}}. \quad (5.75)$$

In particular

$$E_\phi = \frac{\sqrt{\pi} E_0}{\sin \theta \sqrt{1 - \ell/r}} \sum_{l=1}^{\infty} i^{l-2} \frac{2l+1}{\alpha^2 x^2} R_{l\alpha}^{(plane)}(x) \sqrt{\frac{l(l+1)}{2l+1}} (Y_l^1 + Y_l^{-1}). \quad (5.76)$$

The radial function  $R_{l\alpha}^{(plane)}(x)$  can be rewritten as

$$R_{l\alpha}^{(plane)}(x) = \frac{1}{2i} \left( e^{-i\frac{\pi}{2}l} R_{l\alpha}^{(+)}(x) - e^{+i\frac{\pi}{2}l} R_{l\alpha}^{(-)}(x) \right), \quad (5.77)$$

where  $R_{l\alpha}^{(\pm)}(x)$  are two independent solutions of the radial equation (5.71). In Ref. [83], these solutions are obtained in the form of an asymptotic expansion

$$R_{l\alpha}^{(+)}(x) = e^{i\alpha y} \sum_{n=0}^{\infty} \mu_n(l, \alpha) \frac{1}{x^n}, \quad R_{l\alpha}^{(-)}(x) = (R_{l\alpha}^{(+)}(x))^*, \quad (5.78)$$

where the coefficients  $\mu_n(l, \alpha)$  are given by the recursion formula

$$\mu_{n+1}(l, \alpha) = \frac{(n(n+1) - l(l+1))\mu_n(l, \alpha) - (n^2 - 1)\mu_{n-1}(l, \alpha)}{2i\alpha(n+1)}, \quad (5.79)$$

with normalization  $\mu_0(l, \alpha) = 1$ . The solution expressed in this form has the asymptotic form

$$R_{l\alpha}^{(\pm)}(x) \stackrel{x \rightarrow \infty}{\simeq} e^{\pm i\alpha y}, \quad (5.80)$$

from which we see that  $R_{l\alpha}^{(plane)}(x)$  has the correct asymptotic behavior (5.70) to represent a plane wave. However, we will see that the solution in this form is not useful for our purposes, and we will therefore need to derive a more suitable expression.

### 5.3.3 Boundary conditions

The boundary conditions for the massive defects are the same as those described in Sec. 5.2.2 and the fields satisfy them in the same way (if we again restrict the sum in Eq. (5.69) over odd values of  $l$ ), since, as we mentioned, the angular dependence of the two solutions is the same. So, again, we assume  $kb \ll 1$  and need to introduce a static electric potential to correct the behavior of  $E_\phi$ . The multipole expansion of such a potential in the Schwarzschild metric is given by [84]

$$\Phi = \sum_{l,m} A_l^m f_l(r) Y_l^m(\theta, \phi). \quad (5.81)$$

This corresponds to a scattered electric field

$$\vec{E}_s = -\partial_r \Phi \hat{\omega}_r - \frac{1}{r\sqrt{1-\ell/r}} \partial_r \Phi \hat{\omega}_\theta - \frac{1}{r \sin \theta \sqrt{1-\ell/r}} \partial_r \Phi \hat{\omega}_\phi. \quad (5.82)$$

The function  $f_l(r)$  is given by

$$f_l(r) = -\frac{2(2l+1)!}{l!(l+1)!\ell^{l+1}} (r-\ell) \partial_r Q_l \left( \frac{2r}{\ell} - 1 \right), \quad (5.83)$$

where  $Q_l$  are the Legendre functions of the second kind. In particular, for  $l=1$ , we have

$$f_1(r) = 3 \frac{2r-\ell}{\ell^2 r} + 12 \frac{r-\ell}{\ell^3} \operatorname{arctanh} \left( 1 - \frac{2r}{\ell} \right). \quad (5.84)$$

The leading term of  $f_l(r)$  as  $r \rightarrow \infty$  is

$$f_l(r) \stackrel{r \rightarrow \infty}{\simeq} \frac{1}{r^{l+1}}. \quad (5.85)$$

The coefficients  $A_l^m$  are found from Eq. (5.39) to be

$$A_l^{\pm 1} = \mp \sqrt{\pi} E_0 i^{l-1} \left( \frac{2l+1}{k^2 b^2} R_{lk}^{(plane)}(b) \right) \sqrt{\frac{l(l+1)}{2l+1}} \frac{b}{f_l(b)} \equiv \mp A_l. \quad (5.86)$$

From the assumption  $kb \ll 1$ , it follows that the leading contribution to the scattered electric field comes from the dipole term. At large distances from the origin, we can compare this result with the one for a dipole of moment  $\vec{p} = p\hat{x}$  in flat spacetime

$$\Phi = A_1 f_1(r)(-Y_1^1 + Y_1^{-1}) \stackrel{r \rightarrow \infty}{\simeq} \Phi_{flat} = \frac{p}{r^2} \sin \theta \cos \phi, \quad (5.87)$$

from which we obtain the dipole moment

$$p = \left( \frac{3}{k^2 b^2} R_{1k}^{(plane)}(b) \right) \frac{b}{f_1(b)} E_0. \quad (5.88)$$

From Eqs. (5.34), (5.70), and (5.85), we observe that, for  $b \rightarrow \infty$  or  $\ell \rightarrow 0$  ( $x \rightarrow \infty$ ), this expression reduces to that obtained in flat spacetime.

A similar procedure applies to the magnetic field that gives the static magnetic potential

$$\Psi = \sum_l B_l f_l(r)(Y_l^1 + Y_l^{-1}), \quad (5.89)$$

where the coefficients  $B_l$  are

$$B_l = -\sqrt{\pi} E_0 i^{l-2} \left( \frac{2l+1}{k^2 b^2} R_{lk}^{(plane)}(b) \right) \sqrt{\frac{l(l+1)}{2l+1}} \frac{1}{\partial_r f_l(r)|_b}. \quad (5.90)$$

Again, the leading contribution comes from the dipole term. We compare the expression for  $\Psi$ , at large distances from the origin, with that obtained in flat spacetime for a magnetic dipole  $\vec{m} = m\hat{y}$

$$\Psi = B_1 f_1(r)(Y_1^1 + Y_1^{-1}) \stackrel{r \rightarrow \infty}{\simeq} \Psi_{flat} = \frac{m}{r^2} \sin \theta \sin \phi. \quad (5.91)$$

The magnetic moment of the defect turns out to be

$$m = E_0 \left( \frac{3}{k^2 b^2} R_{1k}^{(plane)}(b) \right) \frac{1}{\partial_r f_1(r)|_b}. \quad (5.92)$$

### 5.3.4 Dispersion relation

As for the case of massless defects, we now consider a space filled with a random distribution of massive defects with number density  $\rho$ . From the relations

$$\begin{aligned} \vec{P} &= \rho \vec{p} = \chi_e \vec{E}, & \varepsilon &= 1 + 4\pi \chi_e, \\ \vec{M} &= \rho \vec{m} = \chi_m \vec{B}, & \mu &= 1 + 4\pi \chi_m, \end{aligned} \quad (5.93)$$

we obtain the electric and magnetic permeabilities of such a spacetime foam model

$$\begin{aligned} \varepsilon &\simeq 1 + \frac{4\pi \rho b}{f_1(b)} \left( \frac{3}{k^2 b^2} R_{1k}^{(plane)}(b) \right), \\ \mu &\simeq 1 + \frac{4\pi \rho}{(\partial_r f_1(r))|_b} \left( \frac{3}{k^2 b^2} R_{1k}^{(plane)}(b) \right), \end{aligned} \quad (5.94)$$

from which follows the dispersion relation

$$\omega^2 \simeq \frac{c^2 k^2}{\left[1 + \frac{4\pi\rho b}{f_1(b)} \left(\frac{3}{k^2 b^2} R_{1k}^{(plane)}(b)\right)\right] \left[1 + \frac{4\pi\rho}{(\partial_r f_1(r))|_b} \left(\frac{3}{k^2 b^2} R_{1k}^{(plane)}(b)\right)\right]}. \quad (5.95)$$

We want to write this result as an expansion in powers of  $\ell$ . We start by observing that

$$\begin{aligned} \frac{b}{f_1(b)} &= b^3 - \frac{1}{2}b^2\ell - \frac{1}{20}b\ell^2 + O(\ell^3), \\ \frac{1}{(\partial_r f_1(b))|_b} &= -\frac{b^3}{2} + \frac{3}{8}b^2\ell - \frac{9}{32}b\ell^2 + O(\ell^3). \end{aligned} \quad (5.96)$$

We could introduce explicitly the first few terms of the expansion of  $R_{1k}^{(\pm)}(b)$  (5.78):

$$R_{1k}^{(\pm)}(b) = e^{\pm i k b} \left(\frac{b}{\ell} - 1\right)^{\pm i \ell k} \left(1 \pm \frac{i}{k b} - \frac{1}{2} \frac{\ell}{k^2 b^3} \pm \frac{5}{8} \frac{i \ell}{k^3 b^4} + O(b^{-5})\right). \quad (5.97)$$

However, the asymptotic expansion (5.78) is a good approximation to the solution  $R_{1k}^{(\pm)}(b)$  only for  $kb \gg 1$ , whereas we require  $kb \ll 1$ , in order to use the static field approximation. We need to find another form for the solution of the radial equation, in order to get a meaningful expansion for the dispersion relation.

### 5.3.5 Radial equation

The asymptotic expansion (5.78) is only a good approximation to the solution of the radial equation (5.71) for  $\alpha x = kr \gtrsim 5$ . In Ref. [83], the authors circumvent this problem by expressing the solution at small  $x$  as a linear combination of another set of (this time exact) solutions. These solutions are

$$S_{l\alpha}^{(+)}(x) = e^{i\alpha y} \sum_n \nu_n(l, \alpha) \left(1 - \frac{1}{x}\right)^n, \quad S_{l\alpha}^{(-)}(x) = (S_{l\alpha}^{(+)}(x))^*, \quad (5.98)$$

where the coefficients  $\nu_n(l, \alpha)$  are given by the recursion relation

$$\nu_{n+1}(l, \alpha) = \frac{(2n(n+1) + l(l+1))\nu_n(l, \alpha) - (n-1)(n+1)\nu_{n-1}(l, \alpha)}{(n+1)(n+1+2i\alpha)}, \quad (5.99)$$

with the normalization  $\nu_0(l, \alpha) = 1$ . This series converges quickly for small  $x$  but very slowly for large  $x$ . The asymptotic expansion (5.78) can be related to this solution, by using the equations

$$\begin{aligned} R_{l\alpha}^{(+)}(x) &= E_1(l, \alpha) S_{l\alpha}^{(+)}(x) + E_2(l, \alpha) S_{l\alpha}^{(-)}(x), \\ \partial_x R_{l\alpha}^{(+)}(x) &= E_1(l, \alpha) \partial_x S_{l\alpha}^{(+)}(x) + E_2(l, \alpha) \partial_x S_{l\alpha}^{(-)}(x), \end{aligned} \quad (5.100)$$

from which one obtains the coefficients

$$\begin{aligned}
E_1(l, \alpha) &= \left\{ \left( \frac{\partial_x S_{l\alpha}^{(-)}}{S_{l\alpha}^{(-)}} - \frac{\partial_x R_{l\alpha}^{(+)}}{R_{l\alpha}^{(+)}} \right) \left( \frac{\partial_x S_{l\alpha}^{(-)}}{S_{l\alpha}^{(-)}} - \frac{\partial_x S_{l\alpha}^{(+)}}{S_{l\alpha}^{(+)}} \right)^{-1} \frac{R_{l\alpha}^{(+)}}{S_{l\alpha}^{(+)}} \right\} \Bigg|_{x=x_m}, \\
E_2(l, \alpha) &= \left\{ \left( \frac{\partial_x R_{l\alpha}^{(+)}}{R_{l\alpha}^{(+)}} - \frac{\partial_x S_{l\alpha}^{(+)}}{S_{l\alpha}^{(+)}} \right) \left( \frac{\partial_x S_{l\alpha}^{(-)}}{S_{l\alpha}^{(-)}} - \frac{\partial_x S_{l\alpha}^{(+)}}{S_{l\alpha}^{(+)}} \right)^{-1} \frac{R_{l\alpha}^{(+)}}{S_{l\alpha}^{(-)}} \right\} \Bigg|_{x=x_m},
\end{aligned} \tag{5.101}$$

where the matching point  $x_m$  satisfies the relation  $x_m \gtrsim 5/\alpha$ . However, this method is not suitable in our case; in fact, we want to expand  $R_{l\alpha}^{(+)}(x)$  in powers of  $k$  ( $\alpha$ ) around zero, but the matching point  $x_m$  goes to infinity as  $\alpha$  goes to zero. Since the series expansion of  $S_{l\alpha}^{(\pm)}(x)$  converges very slowly for large  $x$ , we cannot truncate this series as  $\alpha \rightarrow 0$ , so we have to sum the whole series to obtain the coefficients.

Since this approach is not manageable, we resolve to investigate the solution with perturbative methods. As we are interested in the configuration of parameters

$$bk \ll 1, \quad \ell \ll b, \tag{5.102}$$

we can expand the radial equation in powers of  $\ell$ . In this way, it is possible to use perturbation theory to obtain the solution at order  $\ell$ . As we have observed, the radial wave equation (5.71) is equivalent to Eq. (5.67) when written in terms of the tortoise coordinate  $y$ :

$$\partial_y^2 R_{l\alpha}(y) + \left[ \alpha^2 - \frac{x(y) - 1}{x(y)^3} l(l+1) \right] R_{l\alpha}(y) = 0, \tag{5.103}$$

where  $x(y)$  is given by the Lambert  $W$  function

$$x(y) = 1 + W(e^{y-1}). \tag{5.104}$$

The radial equation in this form is analogous to the Schrodinger equation

$$\partial_y^2 R(y) + (\alpha^2 - V(y))R(y) = 0, \tag{5.105}$$

with the potential  $V(y)$  depicted in Fig. 10 for  $l = 1$ .

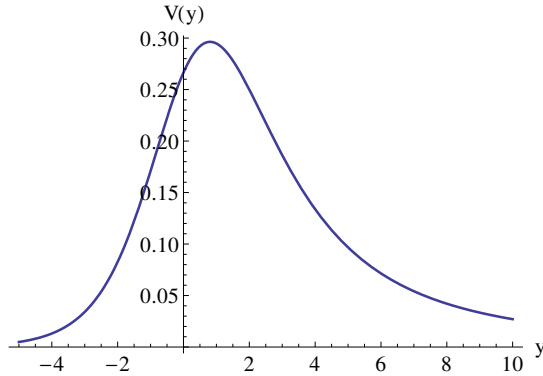


Figure 10: Potential  $V(y)$  in Eq. (5.105) for  $l = 1$ .

We observe that in the regions where the potential  $V(y)$  is much smaller than  $\alpha^2$ , we can ignore its contribution and the Schrodinger equation (5.105) reduces to the free equation with solutions  $R(y) = e^{\pm\alpha y}$ . This happens in the asymptotically flat region  $x \rightarrow \infty$  ( $r \rightarrow \infty$ ). However, this is not what we want to study—we are interested in the situation where  $\ell \rightarrow 0$  and  $k \ll 1/r$ . In this case,  $V(y)$  is always larger than  $\alpha^2$  (as  $\ell \rightarrow 0$ ,  $V(r) \simeq \ell^2/r^2 \gg \ell^2 k^2$  since  $rk \ll 1$ ), so we expect the deviation from the flat spacetime case to be larger at small values of  $k$ .

In order to apply perturbation theory, we rewrite the radial equation explicitly in terms of  $r$  and  $k$

$$\partial_r^2 R_{lk}(r) + \frac{\ell}{r^2(1-\ell/r)} \partial_r R_{lk}(r) + \left[ \frac{k^2}{(1-\ell/r)^2} - \frac{l(l+1)}{r^2(1-\ell/r)} \right] R_{lk}(r) = 0. \quad (5.106)$$

Expanding the solution  $R_{lk}(r)$  (and the coefficients of the equation) in powers of  $\ell$

$$R_{lk}(r) = R_{lk}^{(0)}(r) + \ell R_{lk}^{(1)}(r) + \ell^2 R_{lk}^{(2)}(r) + \dots, \quad (5.107)$$

and inserting these expansions into the radial equation, we obtain

$$\begin{aligned} \ell^0 \quad & \partial_r^2 R_{lk}^{(0)}(r) + \left[ k^2 - \frac{l(l+1)}{r^2} \right] R_{lk}^{(0)}(r) = 0, \\ \ell^1 \quad & \partial_r^2 R_{lk}^{(1)}(r) + \frac{1}{r^2} \partial_r R_{lk}^{(0)}(r) + \left[ k^2 - \frac{l(l+1)}{r^2} \right] R_{lk}^{(1)}(r) + \\ & + \left[ \frac{2k^2}{r} - \frac{l(l+1)}{r^3} \right] R_{lk}^{(0)}(r) = 0, \\ \ell^2 \quad & \partial_r^2 R_{lk}^{(2)}(r) + \frac{1}{r^2} \partial_r R_{lk}^{(1)}(r) + \frac{1}{r^3} \partial_r R_{lk}^{(0)}(r) + \left[ k^2 - \frac{l(l+1)}{r^2} \right] R_{lk}^{(2)}(r) + \\ & + \left[ \frac{2k^2}{r} - \frac{l(l+1)}{r^3} \right] R_{lk}^{(1)}(r) + \left[ \frac{3k^2}{r^2} - \frac{l(l+1)}{r^4} \right] R_{lk}^{(0)}(r) = 0, \\ & \dots \end{aligned} \quad (5.108)$$

We also have to implement the boundary condition given by Eq. (5.70) at each order

$$R_{lk}^{(plane)}(r) \stackrel{r \rightarrow \infty}{\simeq} kr j_l \left( kr + k\ell \log \left( \frac{r}{\ell} - 1 \right) \right). \quad (5.109)$$

By expanding both sides of the above expression in powers of  $\ell$ , we obtain

$$\begin{aligned} \ell^0 \quad & R_{lk}^{(0)}(r) \stackrel{r \rightarrow \infty}{\simeq} kr j_l(kr), \\ \ell^1 \quad & R_{lk}^{(1)}(r) \stackrel{r \rightarrow \infty}{\simeq} kr j_l'(kr) k \log \left( \frac{r}{\ell} \right), \\ \ell^2 \quad & R_{lk}^{(2)}(r) \stackrel{r \rightarrow \infty}{\simeq} kr \left( \frac{1}{2} k^2 \log \left( \frac{r}{\ell} \right)^2 j_l''(kr) - \frac{k}{r} j_l'(kr) \right), \\ & \dots \end{aligned} \quad (5.110)$$

We need the radial equation solution only for  $l = 1$ . At zero order, from Eqs. (5.108) and (5.110) it follows immediately that

$$R_{1k}^{(0)}(r) = kr j_1(kr) = \frac{\sin(kr)}{kr} - \cos(kr). \quad (5.111)$$

Inserting this result into Eq. (5.108) and making use of Eq. (5.110), we obtain at first order in  $\ell$

$$R_{1k}^{(1)}(r) = \left\{ \frac{\cos(kr)}{2kr} + \frac{3\sin(kr)}{4(kr)^2} + \left( \frac{\cos(kr)}{kr} + \sin(kr) \right) \left( \log\left(\frac{r}{\ell}\right) - \text{Ci}(2kr) \right) + \left( \cos(kr) - \frac{\sin(kr)}{kr} \right) \left( \text{Si}(2kr) - \frac{\pi}{2} \right) \right\} k, \quad (5.112)$$

where  $Ci(x)$  ( $Si(x)$ ) is the Cosine (Sine) integral. At second order, we can still find an approximate solution for  $kr \ll 1$ ; however, we are not able to find a solution at  $r \rightarrow \infty$ , and consequently we cannot implement the boundary condition.

We want to compare the approximate solution derived here with the numerical solution that one can obtain from the exact radial equation (5.106). In Fig. 11, we plot the function  $R(k) = \frac{3}{k^2 b^2} R_{1k}^{(plane)}(b)$  for a certain range of parameters.

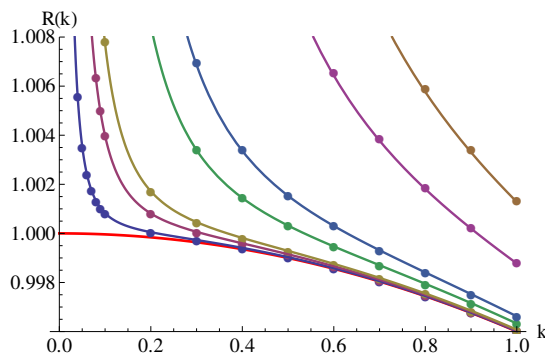


Figure 11: Numerical solutions of the radial wave equation,  $R(k) = \frac{3}{k^2 b^2} R_{1k}^{(plane)}(b)$ , are represented by dots, while the first-order analytic solutions are represented by solid lines. The lowest curve corresponds to the flat spacetime solution  $R(k) = (j_0(kb) + j_2(kb))$ , while upper curves correspond to increasing  $\ell$  in the range  $10^{-9} \leq \ell \leq 10^{-6}$ . The size of the defect has been set to  $b = 0.2$ .

We observe good agreement between the two sets of solutions (perturbative and numerical), and we notice also that, as expected, the solutions deviate from the  $\ell = 0$  case as  $k$  decreases.

Inserting the solution  $R_{1k}^{(plane)}(r) = R_{1k}^{(0)}(r) + \ell R_{1k}^{(1)}(r)$  into Eq. (5.94), which gives electric and magnetic permeabilities, we observe that, since  $R(k) = \frac{3}{k^2 b^2} R_{1k}^{(plane)}(b)$  grows indefinitely as  $k$  decreases, there exists a critical  $k = k_c$  below which the magnetic permeability  $\mu$  is negative. This means that the refractive index  $n = \sqrt{\epsilon\mu}$  becomes imaginary and the plane wave, instead of propagating through the space, is damped. We conclude that a spacetime filled with a distribution of massive defects appears to be opaque to low-frequency radiation. In Fig. 12 we show the behavior of the group velocity

$$v(k) = \frac{d}{dk} \omega(k) = \frac{d}{dk} \frac{ck}{\sqrt{\epsilon(k)\mu(k)}}, \quad (5.113)$$

that one obtains from this solution.

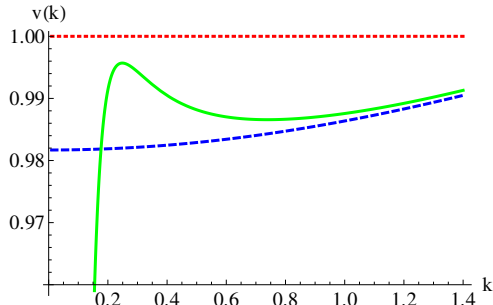


Figure 12: Group velocity for different dispersion relations: the red dotted line describes the standard dispersion relation in the absence of defects ( $\omega^2 = c^2 k^2$ ); the blue dashed line represents the dispersion relation obtained from defects with  $\ell = 0$  (Eq. (5.45)); and the green solid line corresponds to defects with  $\ell > 0$  (Eq. (5.95)). We used  $c = 1$ ,  $b = 1$ ,  $\rho = 0.006$ ,  $\ell = 0.005$ .

We note that indeed the velocity of propagation drops to zero at some  $k_c$  larger than zero. Moreover, for certain values of  $\rho$ , as  $k$  grows from  $k_c$  a maximum peak is reached before the curve approaches the flat spacetime result.

Finally, expanding Eq. (5.95) in powers of  $\ell$ ,  $\rho b^3$ , and  $kb$  we obtain

$$\begin{aligned} \omega^2 \simeq & (1 - 2\rho\pi b^3)c^2 k^2 + \frac{\rho\pi b^5}{5}c^2 k^4 + \rho\pi c^2 \ell \left\{ \frac{3}{2}(-5 + 4(\gamma + \log(2\ell k))) + \right. \\ & + \left. \left( -\frac{13}{4} + 3(\gamma + \log(2\ell k)) \right) b^2 k^2 - \pi b^3 k^3 + \right. \\ & + \left. \left( \frac{143}{20} - 3(\gamma + \log(2\ell k)) \right) \frac{b^4}{4} k^4 + \dots \right\} + \dots, \end{aligned} \quad (5.114)$$

where  $\gamma$  is the Euler–Mascheroni constant. An interesting feature of this dispersion relation, with respect to the flat spacetime case, is the appearance of a negative (at first order in  $\rho b^3$ ) mass term:

$$m^2 = -\frac{3}{2}\rho\pi c^2 \ell(5 - 4\gamma) + \dots \quad (5.115)$$

## 6 Defect metric

### 6.1 Metric (review)

We now introduce a different type of defect. As we mentioned at the beginning of this part, such a defect has the same topology as that described in the previous section, but the two are not diffeomorphic. An important feature of this new type of defect is that it is a vacuum solution of general relativity. The defect described in the previous section, instead, is not even a differentiable manifold in spherical coordinates, while, in the coordinate system  $\{t, \tilde{y}, z, x\}$ , it has a singular Ricci scalar (see Eq. (5.19)). The metric describing the new defect was obtained in Ref. [69] and further discussed in Refs. [85, 86, 87] in the context of black hole physics (see part V in this regard).

In a coordinate system  $\{t, y, z, x\}$  analogous to the one introduced in the previous section, the metric takes the form

$$ds^2 = - \left( 1 - \frac{\ell}{\sqrt{y^2 + b^2}} \right) dt^2 + \frac{\frac{y^2}{y^2 + b^2}}{1 - \frac{\ell}{\sqrt{y^2 + b^2}}} dy^2 + (y^2 + b^2)(dz^2 + \sin^2 z dx^2), \quad (6.1)$$

where  $b$  is the defect radius and  $\ell$  is related to the defect mass by  $m = \ell/2$ . In this section, however, we only consider the simplest case of a massless defect, for which the defect metric simplifies to

$$ds^2 = -dt^2 + \frac{y^2}{y^2 + b^2} dy^2 + (y^2 + b^2)(dz^2 + \sin^2 z dx^2). \quad (6.2)$$

The coordinates  $\{t, y, z, x\}$  have ranges

$$t \in (-\infty, +\infty), \quad y \in (-\infty, +\infty), \quad z \in (0, \pi), \quad x \in \left(-\frac{\pi}{2}, \frac{\pi}{2}\right). \quad (6.3)$$

A crucial difference with respect to the coordinates  $\{t, \tilde{y}, z, x\}$  introduced in the previous section is the relation between this new set of coordinates and standard spherical coordinates (given by Eqs. (5.7)-(5.15) for the previous type of defect). In this case, the radial coordinate  $r$  is related to  $y$  by the equation

$$r = \sqrt{y^2 + b^2}, \quad \forall y, \quad (6.4)$$

whose inverse is

$$\begin{cases} y = \sqrt{r^2 - b^2}, & |\phi| < \frac{\pi}{2}, \\ y = -\sqrt{r^2 - b^2}, & |\phi| > \frac{\pi}{2}. \end{cases} \quad (6.5)$$

The above transformations can be regarded as *a posteriori* conclusions. In fact, one does not need to know the relationship between the coordinate system  $\{t, y, z, x\}$  and standard spherical coordinates, in order to derive the metric (6.2). However, Eq. (6.4) must hold if we want the metric (6.2) to be equivalent to the Minkowski metric away from the defect surface.

Instead, the angular coordinates  $\theta$  and  $\phi$  are related to the coordinates  $z$  and  $x$ , as in the previous section. So, for example, the change of coordinates in the chart  $U_1$  surrounding the Cartesian axis  $x^1$  (given by Eqs. (5.7), (5.8) in the previous section) is given in this case by

$$\begin{cases} y_1 = \sqrt{r^2 - b^2}, \\ z_1 = \theta, \\ x_1 = \phi, \end{cases} \quad |\phi| < \frac{\pi}{2}, \quad \begin{cases} y_1 = -\sqrt{r^2 - b^2}, \\ z_1 = \pi - \theta, \\ x_1 = \phi - \pi, \end{cases} \quad |\phi| > \frac{\pi}{2}. \quad (6.6)$$

$$\begin{cases} r = \sqrt{y_1^2 + b^2}, \\ \theta = z_1, \\ \phi = x_1, \end{cases} \quad y_1 > 0, \quad \begin{cases} r = \sqrt{y_1^2 + b^2}, \\ \theta = \pi - z_1, \\ \phi = x_1 + \pi, \end{cases} \quad y_1 < 0. \quad (6.7)$$

The transformations for the charts  $U_2$  and  $U_3$  can be obtained similarly. In Fig. 13, the coordinate system  $\{y, z, x\}$  is compared to standard spherical coordinates.

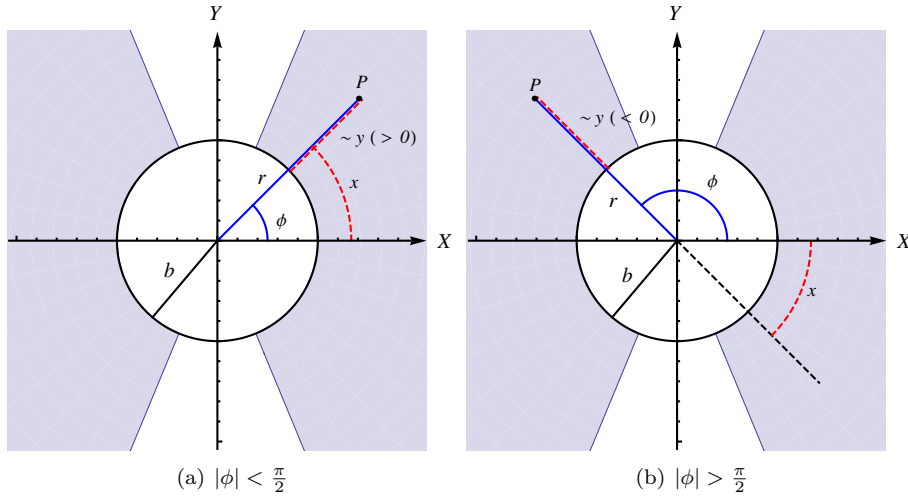


Figure 13: Equatorial section ( $\theta = z = \pi/2$ ) of the defect. Blue solid lines are used for spherical coordinates, red dashed lines are used for the coordinate system  $\{y, z, x\}$  (observe that, from Eq. (6.4), we have  $r - b \simeq |y| (1 - \frac{b}{r})$  for large  $r$ ). The shaded area represents the chart  $U_1$  in which the coordinate system  $\{y, z, x\}$  is valid.

As for the previous type of coordinates, this new system of coordinates automatically implements the point-wise identification on the boundary of the defect. Consequently, the defect manifold is completely determined by the metric (6.2), with no need to introduce additional boundary conditions. Moreover, the topology of the defect is the same as in the previous case ( $\mathbb{R} \times (\mathbb{R}P^3 - \{0\})$ , see Eq. (5.6)); in fact, the change of coordinates (6.6) defines a global homeomorphism between the defect manifold (6.2) and the defect defined in Minkowski spacetime (Eqs. (5.3) and (5.4)).

To show that the metric (6.1) is a vacuum solution of general relativity, we simply need to compute the Ricci tensor  $R_{\mu\nu}$ . We recall that in vacuum the Einstein field equations reduce to [88]

$$R_{\mu\nu} = 0. \quad (6.8)$$

The Ricci tensor is obtained by contracting the Riemann tensor  $R^\rho_{\mu\sigma\nu}$  and is given by

$$R_{\mu\nu} = R^\rho_{\mu\rho\nu} = \partial_\rho \Gamma^\rho_{\nu\mu} - \partial_\nu \Gamma^\rho_{\rho\mu} + \Gamma^\rho_{\rho\lambda} \Gamma^\lambda_{\nu\mu} - \Gamma^\rho_{\nu\lambda} \Gamma^\lambda_{\rho\mu}, \quad (6.9)$$

where the Christoffel symbols are defined in Eq. (5.53). Inserting the metric (6.1) into Eq. (6.9), one can readily verify that Eq. (6.8) is satisfied everywhere, in particular at the defect surface  $y = 0$ . From this result it follows that the Ricci scalar also vanishes everywhere, while the Kretschmann scalar does not vanish but is regular everywhere

$$R = g^{\mu\nu} R_{\mu\nu} = 0, \quad K = R_{\mu\nu\rho\sigma} R^{\mu\nu\rho\sigma} = \frac{12\ell^2}{(y^2 + b^2)^3}. \quad (6.10)$$

It is important to note that, also in this case, the change of coordinates (6.6) is not a global diffeomorphism from the defect manifold (6.2) to Minkowski

spacetime with a defect (Eqs. (5.3), (5.4)). This can be seen by considering the transformation rule for the radial coordinate (6.4). This transformation is continuous and differentiable everywhere, but it is not invertible around  $y = 0$ . In fact, from the inverse function theorem it follows that a continuous differentiable function is invertible around a point  $p$  only if its derivative does not vanish at  $p$ . From Eq. (6.4), we have

$$r'(y) = \frac{y}{\sqrt{y^2 + b^2}}, \quad (6.11)$$

which is indeed zero at  $y = 0$ . This implies that higher derivatives of the inverse function (6.5) are divergent and discontinuous at the defect surface. We observe that the transformation (6.6) is a local diffeomorphism in the two separate regions  $y > 0$  and  $y < 0$ .

Observe that, as we have already pointed out, the same is true for the change of coordinates introduced in the previous section (Eqs. (5.7)-(5.15)); in fact, it also does not define a global diffeomorphism from the defect manifold (5.18) to Minkowski spacetime with a defect (Eqs. (5.3), (5.4)). Take again the transformation rule for the radial coordinate, which is

$$r(y) = b + |\tilde{y}|. \quad (6.12)$$

This function is not even differentiable at  $\tilde{y} = 0$ , and it cannot represent a global diffeomorphism. Once again, though, the transformation rule defines a local diffeomorphism in the two separate regions  $\tilde{y} > 0$  and  $\tilde{y} < 0$ .

A last remark concerns the case  $b = 0$  (i.e. spacetime with no defect). In this case, the two changes of coordinates (6.4) and (6.12) are equivalent and reduce to

$$r(y) = |y|. \quad (6.13)$$

Consequently, the metrics (5.18) and (6.2) also reduce to the same expression. Equation (6.13) is again not differentiable at  $y = 0$ , but, as we shall see in the next subsection, the scalar wave solutions that one obtains in this system of coordinates are equivalent to those obtained in standard spherical coordinates (this is not the case when  $b \neq 0$ ). The point  $y = 0$  now coincides with the origin of the spherical coordinate system  $r = 0$ , which is itself ill-defined. Therefore, the two manifolds, Minkowski spacetime in spherical coordinates and the defect manifold in coordinates  $\{t, y, z, x\}$  with no defect ( $b = 0$ ), are globally diffeomorphic.

## 6.2 Scalar waves

In this subsection, we study the propagation of a scalar wave in the defect metric (6.2), where the parameter  $b$  (the radius of the defect) is assumed to be strictly larger than zero ( $b > 0$ ). We refer to this metric as the “defect metric,” in order to distinguish it from the Minkowski metric (which can be obtained, in coordinates  $\{t, y, z, x\}$ , from Eq. (6.2) by setting  $b = 0$ ).

The scalar wave equation (massless Klein-Gordon equation) in a general metric is [89]

$$\square\Phi = \nabla_\mu \nabla^\mu \Phi = g^{-\frac{1}{2}} \partial_\mu \left( g^{\frac{1}{2}} g^{\mu\nu} \partial_\nu \Phi \right) = 0, \quad (6.14)$$

which, for the metric (6.2), reads

$$-\partial_t^2 \Phi + \frac{y^2 + b^2}{y^2} \partial_y^2 \Phi + \frac{2y^2 - b^2}{y^3} \partial_y \Phi + \frac{\partial_z^2 \Phi}{y^2 + b^2} + \frac{\cot z \partial_z \Phi}{(y^2 + b^2)} + \frac{\partial_x^2 \Phi}{(y^2 + b^2) \sin^2 z} = 0. \quad (6.15)$$

Using the separation of variables  $\Phi(t, y, z, x) = T(t)R(y)Z(z)X(x)$ , one obtains the set of equations

$$\bullet \quad \partial_t^2 T + k^2 T = 0, \quad (6.16a)$$

$$\bullet \quad \frac{y^2 + b^2}{y^2} \partial_y^2 R + \frac{2y^2 - b^2}{y^3} \partial_y R + \left( k^2 - \frac{l(l+1)}{y^2 + b^2} \right) R = 0, \quad (6.16b)$$

$$\bullet \quad \partial_z^2 Z + \cot z \partial_z Z + \left( l(l+1) - \frac{m^2}{\sin^2 z} \right) Z = 0, \quad (6.16c)$$

$$\bullet \quad \partial_x^2 X + m^2 X = 0. \quad (6.16d)$$

Observe that these equations, apart from the radial component (6.16b), are locally equivalent to those obtained in spherical coordinates. Hence, we can write the general solution as

$$\Phi(t, y, z, x) = \int dk \sum_{l,m} a_{klm} e^{-ikt} \Phi_{klm}(y, z, x), \quad (6.17)$$

where

$$\Phi_{klm}(y, z, x) = R_{kl}(y) Y_l^m(z, x), \quad (6.18)$$

and  $R_{kl}(y)$  are the solutions of the radial equation, while  $Y_l^m(z, x)$  are spherical harmonics.

Solving the radial equation, we obtain for  $R_{kl}(y)$  the expression

$$R_{kl}(y) = c_1 j_l \left( k \sqrt{y^2 + b^2} \right) + c_2 y_l \left( k \sqrt{y^2 + b^2} \right), \quad (6.19)$$

where  $c_1$  and  $c_2$  are arbitrary constants and  $j_l(x)$  and  $y_l(x)$  are the spherical Bessel functions, respectively, of the first and second kind. The radial solution for the case  $b = 0$  is

$$R_{kl}^{(Min)}(y) = j_l(ky), \quad (6.20)$$

and is equivalent to the solution that one finds in Minkowski spacetime in standard spherical coordinates. To fix the value of the constants  $c_1$  and  $c_2$  in Eq. (6.19) we use the fact that, away from the origin  $y = 0$ , the change of variables (6.6) is a local diffeomorphism. Hence, we can use it to impose the boundary condition whereby, at spatial infinity

$$r = \sqrt{b^2 + y^2} \stackrel{y \rightarrow \infty}{\simeq} y, \quad (6.21)$$

the solution  $R_{kl}(y)$  must approach the solution  $R_{kl}^{(Min)}(y)$  that one obtains in Minkowski spacetime

$$R_{kl}(y) \stackrel{y \rightarrow \infty}{\simeq} j_l(ky). \quad (6.22)$$

In this way, the radial solution (6.19) reduces to

$$R_{kl}(y) = j_l(k \sqrt{y^2 + b^2}). \quad (6.23)$$

By substituting this result into the expression for  $\Phi_{klm}(y, z, x)$ , we find a scalar solution that behaves in a different way with respect to the result obtained in Minkowski spacetime. In Minkowski spacetime, the solution has parity eigenvalues  $(-1)^l$ , while in the defect metric the solution has parity eigenvalues  $(+1)$  for every  $l$ . The parity transformation in different systems of coordinates is

$$\vec{x} = \begin{cases} (y, z, x) \\ (r, \theta, \phi) \\ (X, Y, Z) \end{cases} \xrightarrow{P} -\vec{x} = \begin{cases} (-y, z, x) & \{t, y, z, x\}, \\ (r, \pi - \theta, \pi + \phi) & \text{Spherical}, \\ (-X, -Y, -Z) & \text{Cartesian}. \end{cases} \quad (6.24)$$

Explicitly, the scalar solutions in the Minkowski and the defect metric transform as

$$\begin{aligned} \Phi_{klm}^{(Min)} &= j_l(kr)Y_l^m(\theta, \phi) \xrightarrow{P} j_l(kr)Y_l^m(\pi - \theta, \phi + \pi) = (-1)^l \Phi_{klm}^{(Min)}, \\ \Phi_{klm}^{(def)} &= j_l(k\sqrt{y^2 + b^2})Y_l^m(z, x) \xrightarrow{P} j_l(k\sqrt{(-y)^2 + b^2})Y_l^m(z, x) = (+1)\Phi_{klm}^{(def)}. \end{aligned} \quad (6.25)$$

Since this is an important point, we wish to make it clear that the parity behaviors of the two solutions are really different. Let us consider first how the behavior under parity of the Minkowski solution in standard spherical coordinates translates in  $\{y, z, x\}$  coordinates. For simplicity, we consider the case  $|\phi| < \pi/2$ . The point  $\vec{x} = (r, \theta, \phi)$  is mapped via Eq. (6.6) to  $\vec{x}' = (\sqrt{y^2 + b^2}, z, x)$ . On the other hand, the parity transformation maps the point  $\vec{x}$  to  $-\vec{x} = (r, \theta', \phi') = (r, \pi - \theta, \pi + \phi)$ , where now  $|\phi'| > \pi/2$ . Then, under the change of coordinates (6.6), the point  $-\vec{x}$  is mapped to  $-\vec{x}' = (\sqrt{y^2 + b^2}, \pi - z', x' + \pi)$ , where  $z' = \pi - \theta' = z$  and  $x' = \phi' - \pi = x$ . Hence, we have  $-\vec{x}' = (\sqrt{y^2 + b^2}, \pi - z, x + \pi)$ . From these considerations, we obtain the scheme

$$\begin{array}{ccc} j_l(kr)Y_l^m(\theta, \phi) & \xleftrightarrow[\text{change}]{\text{coord}} & j_l(k\sqrt{y^2 + b^2})Y_l^m(z, x) \\ \updownarrow P & & \updownarrow P \\ j_l(kr)Y_l^m(\pi - \theta, \phi + \pi) & \xleftrightarrow[\text{change}]{\text{coord}} & j_l(-k\sqrt{y^2 + b^2})Y_l^m(z, x). \end{array} \quad (6.26)$$

The Minkowski solution expressed in  $\{y, z, x\}$  coordinates does not behave correctly under parity, i.e. it does not coincide with the solution obtained in the defect metric. We can reverse the reasoning and investigate how the behavior under parity of the defect solution  $\Phi^{(def)}$  is translated in spherical coordinates. Avoiding the details, we end up with the scheme

$$\begin{array}{ccc} j_l(k\sqrt{y^2 + b^2})Y_l^m(z, x) & \xleftrightarrow[\text{change}]{\text{coord}} & j_l(kr)Y_l^m(\theta, \phi) \\ \updownarrow P & & \updownarrow P \\ j_l(k\sqrt{y^2 + b^2})Y_l^m(z, x) & \xleftrightarrow[\text{change}]{\text{coord}} & j_l(kr)Y_l^m(\theta, \phi). \end{array} \quad (6.27)$$

Again, we see that the defect solution expressed in spherical coordinates is different from the Minkowski solution. Instead, the solution that one obtains in

Minkowski spacetime in coordinates  $\{t, y, z, x\}$  (i.e. setting  $b = 0$  in the metric (6.2))

$$\Phi^{(Min)}(t, y, z, x) = e^{-ikt} j_l(ky) Y_l^m(z, x), \quad (6.28)$$

exhibits the same behavior under parity of the solution that one obtains in Minkowski spacetime in spherical coordinates. The two solutions turn out to be completely equivalent when  $b = 0$ .

One can try to build, in the defect metric, a radial solution that behaves like the Minkowski solution, by imposing different boundary conditions at plus and minus infinity, thereby obtaining

$$R_{kl}(y) = j_l(kf(y)) = \begin{cases} j_l(k\sqrt{y^2 + b^2}), & y > 0, \\ j_l(-k\sqrt{y^2 + b^2}), & y < 0. \end{cases} \quad (6.29)$$

This expression is completely equivalent to the solution in Minkowski spacetime. The problem is that Eq. (6.29) is a solution of the radial equation (6.16b) only in the two separate regions  $y > 0$  and  $y < 0$ , but it is not a solution at  $y = 0$  where it is discontinuous (for odd  $l$ ). So, we have to reject this expression as a possible solution of the scalar radial wave equation in the metric (6.2).

When we represent the defect in Minkowski spacetime (removing a ball of radius  $b$  centered on the origin and identifying antipodal points on the boundary), the solution (6.29) has to be corrected by a scattered field, in order to satisfy the boundary condition at the defect surface. The boundary condition we use is that the field must be continuous through the defect

$$\Phi(t, b, \theta, \phi) = \Phi(t, b, \pi - \theta, \phi + \pi). \quad (6.30)$$

The total field is given by  $\Phi^{(tot)}(x) = \Phi^{(Min)}(x) + \Phi^{(scat)}(x)$ , and we must verify whether or not it can be an acceptable solution in the metric (6.2). The scattered field can be written as a multipole expansion

$$\Phi^{(scat)}(x) = \int dk \sum_{l,m} c_{klm} e^{-ikt} z_l(kr) Y_l^m(\theta, \phi), \quad (6.31)$$

where  $z_l(kr)$  is a generic spherical Bessel function. Imposing the boundary condition (6.30) at the defect surface, one can determine the constants  $c_{klm}$ , while the Sommerfeld radiation condition [90] allows us to identify  $z_l(kr)$  with the spherical Hankel function  $h_l^{(1)}(kr)$ . In conclusion, the total field  $\Phi^{(tot)}(x)$  can be expressed as

$$\Phi^{(tot)}(x) = \int dk \sum_{l,m} a_{klm} e^{-ikt} \left[ j_l(kr) - \frac{1 - (-1)^l}{2} \frac{j_l(kb) h_l^{(1)}(kr)}{h_l^{(1)}(kb)} \right] Y_l^m(\theta, \phi). \quad (6.32)$$

Rewriting the radial part of this solution in the coordinate system  $\{t, y, z, x\}$ , we obtain

$$R_{kl}^{(tot)}(y) = \begin{cases} j_l(k\sqrt{y^2 + b^2}) - \frac{1 - (-1)^l}{2} \frac{j_l(kb) h_l^{(1)}(k\sqrt{y^2 + b^2})}{h_l^{(1)}(kb)}, & y > 0, \\ j_l(-k\sqrt{y^2 + b^2}) - \frac{1 - (-1)^l}{2} \frac{j_l(-kb) h_l^{(1)}(-k\sqrt{y^2 + b^2})}{h_l^{(1)}(-kb)}, & y < 0. \end{cases} \quad (6.33)$$

Unlike Eq. (6.29), this last expression is continuous at the origin  $y = 0$ . Moreover, it satisfies the radial equation (6.16b) in the two separate regions  $y > 0$  and  $y < 0$ . However, at the origin, the second derivative is discontinuous, and therefore  $R^{(tot)}(y)$  is not a solution of the radial equation (6.16b) at  $y = 0$ . We conclude that the solution  $\Phi^{(tot)}(x)$  (Eq. (6.32)) that one obtains for a defect in Minkowski spacetime is not a solution of the wave equation in the defect metric (6.2). The solution of the wave equation in the metric (6.2) is given by Eqs. (6.17), (6.18), and (6.23), namely

$$\Phi(t, y, z, x) = \int dk \sum_{l,m} a_{klm} e^{-ikt} j_l(k\sqrt{y^2 + b^2}) Y_l^m(z, x). \quad (6.34)$$

In Fig. 14, we show the behavior of the two radial functions  $R_{kl}(y)$  and  $R_{kl}^{(tot)}(y)$  for  $l = 1$  and  $l = 3$ .

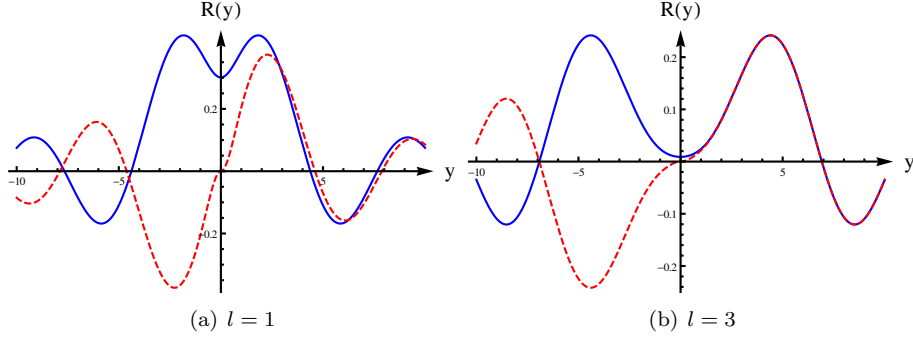


Figure 14: The behavior of the two radial functions obtained, respectively, in the defect metric and in the manifold describing a defect in Minkowski space, for  $l = 1$  and  $l = 3$  ( $k = 1$  and  $b = 1$ ). The blue solid line corresponds to  $R_{kl}(y)$  (Eq. (6.23)), while the red dashed line describes  $R_{kl}^{(tot)}(y)$  (Eq. (6.33)).

### 6.2.1 Radial equation around $y = 0$

We have observed that the solutions that one obtains in Minkowski spacetime and in the defect metric are equivalent in the two separate regions  $y > 0$  and  $y < 0$ , but they are not at the origin  $y = 0$ . We want to study in more detail, in a neighborhood of the origin, the radial wave equation in the defect metric (6.2) ( $b > 0$ ) and in the Minkowski metric ( $b = 0$ ), both expressed in the coordinate system  $\{t, y, z, x\}$ . The two radial equations are

$$\partial_y^2 R + \frac{2}{y} \partial_y R + \left( k^2 - \frac{l(l+1)}{y^2} \right) R = 0, \quad \text{Minkowski metric,} \quad (6.35a)$$

$$\frac{y^2 + b^2}{y^2} \partial_y^2 R + \frac{2y^2 - b^2}{y^3} \partial_y R + \left( k^2 - \frac{l(l+1)}{y^2 + b^2} \right) R = 0, \quad \text{defect metric.} \quad (6.35b)$$

Since for both equations the origin is a regular singular point, we can use the Frobenius method [91] to find the solutions around  $y = 0$ . With this method, we look for solutions of the form

$$R(y) = y^s \sum_{n=0}^{\infty} c_n y^n, \quad c_0 \neq 0, \quad (6.36)$$

where the exponent  $s$  is, in general, a real number. Before proceeding, it is useful to rewrite Eqs. (6.35) in the more suitable form

$$y^2 R'' + y p(y) R' + q(y) R = 0, \quad (6.37)$$

where the coefficients  $p(y)$  and  $q(y)$  are expanded in powers of  $y$ :  $p(y) = p_0 + p_1 y + p_2 y^2 + \dots$ ,  $q(y) = q_0 + q_1 y + q_2 y^2 + \dots$ . Substituting the expansion (6.36) into Eq. (6.37), one obtains

$$\sum_{n=0}^{\infty} [(n+s)(n+s-1) + p(y)(n+s) + q(y)] c_n y^{n+s} = 0, \quad (6.38)$$

and, in particular, for  $n = 0$ , one has

$$[s^2 + (p_0 - 1)s + q_0] c_0 y^s = 0, \quad (6.39)$$

Recalling that we assumed  $c_0 \neq 0$ , we arrive at the so-called ‘‘indicial’’ equation

$$s^2 + (p_0 - 1)s + q_0 = 0, \quad (6.40)$$

which has, in general, two roots,  $s_1$  and  $s_2$ , corresponding to two independent solutions. We assume that the roots are real and  $s_1 \geq s_2$ . The solution corresponding to the largest root can always be obtained from Eq. (6.36) with  $s = s_1$ , but if the difference between the two roots  $\Delta s = s_1 - s_2$  is an integer, the second solution is given by

$$R_2(y) = \alpha R_1(y) \log y + y^{s_2} \sum_{n=0}^{\infty} d_n y^n, \quad d_0 \neq 0. \quad (6.41)$$

We can now rewrite Eq. (6.38) as

$$y^s \sum_{n=0}^{\infty} \left\{ [(n+s)(n+s-1) + (n+s)p_0 + q_0] c_n + [(n+s-1)p_1 + q_1] c_{n-1} + [(n+s-2)p_2 + q_2] c_{n-2} + \dots \right\} y^n = 0, \quad (6.42)$$

from which the coefficients  $c_n$  of the first solution can be determined and turn out to be

$$c_n = - \frac{\sum_{i=1}^{\infty} [(n+s_1-i)p_i + q_i] c_{n-i}}{[(n+s_1)(n+s_1-1) + (n+s_1)p_0 + q_0]}. \quad (6.43)$$

When  $\Delta s$  is an integer, one has to insert the expression (6.41) into the differential equation (6.37), in order to find the coefficients of the second solution. After

some algebra, one obtains the recursion relation

$$d_n = \frac{-1}{[(n+s_2)(n+s_2-1) + (n+s_2)p_0 + q_0]} \left\{ \sum_{i=1}^{\infty} [(n+s_2-i)p_i + q_i] d_{n-i} + \alpha \left[ -c_{n-\Delta s} + 2(n+s_2-2)c_{n-\Delta s-2} + \sum_{i=0}^{\infty} p_i c_{n-\Delta s-i} \right] \right\}, \quad (6.44)$$

from which the value of  $\alpha$  is also determined.

For the specific equations in which we are interested (Eq. (6.35)), the functions  $p(y)$  and  $q(y)$ , and their expansions, are

$$\begin{cases} p(y) = 2, \\ q(y) = -l(l+1) + k^2 y^2, \end{cases} \quad \text{Minkowski metric,} \quad (6.45a)$$

$$\begin{cases} p(y) = \frac{2y^2 - b^2}{y^2 + b^2} = -1 + \frac{3}{b^2} y^2 - \frac{3}{b^4} y^4 + \dots, \\ q(y) = \frac{y^4}{y^2 + b^2} \left( k^2 - \frac{l(l+1)}{y^2 + b^2} \right) = \frac{b^2 k^2 - l(l+1)}{b^4} y^4 + \dots, \end{cases} \quad \text{defect metric,} \quad (6.45b)$$

from which we obtain the coefficients  $p_i$  and  $q_i$ . The solutions of the indicial equation are the roots  $s_1 = l$ ,  $s_2 = -(l+1)$  in the Minkowski metric, and  $s_1 = 2$ ,  $s_2 = 0$  in the defect metric, where, in both cases, the difference  $\Delta s$  is an integer. This is a crucial point. Observe, in fact, that while the roots in the Minkowski metric depend on  $l$ , those in the defect metric are independent of  $l$ . From this fact originates the different behavior of the solutions under parity transformation in the two metrics.

From Eq. (6.43), the coefficients  $c_n$  can be calculated for both metrics, and the first solutions (corresponding to the largest root) turn out to be (we can set  $c_0 = 1$  without any loss of generality)

$$R_1^{(\text{Min})}(y) = y^l \left\{ 1 - \frac{k^2}{4l+6} y^2 + \frac{k^4}{8(4l(l+4)+15)} y^4 + \dots \right\}, \quad (6.46a)$$

$$R_1^{(\text{def})}(y) = y^2 \left\{ 1 - \frac{3}{4b^2} y^2 + \frac{l(l+1) - b^2 k^2 + 15}{24b^4} y^4 + \dots \right\}, \quad (6.46b)$$

From Eq. (6.44), which gives the coefficients of the second solutions, we obtain (again, we set  $d_0 = 1$ )

$$R_2^{(\text{Min})}(y) = \alpha R_1^{(\text{Min})} \log y + y^{-l-1} \left\{ 1 + \frac{k^2}{4l-2} y^2 + \frac{\alpha c_{2-2l}}{6(l-1)} y^3 + \frac{k^4}{(8l-12)(4l-2)} y^4 + \dots \right\}, \quad (6.47a)$$

$$R_2^{(\text{def})}(y) = y^0 \left\{ 1 + d_2 y^2 + \frac{l(l+1) - b^2(k^2 + 6d_2)}{8b^4} y^4 + \dots \right\}. \quad (6.47b)$$

Note that the parameter  $\alpha$  in  $R_2^{(\text{Min})}(y)$  depends on the value of  $l$  (for example, for  $l = 1$  we obtain  $\alpha = 0$ ). In  $R_2^{(\text{def})}(y)$ , the coefficient  $d_2$  is undetermined and we can choose to set it to zero ( $d_2 = 0$ ).

Finally, the general solutions are given by

$$R^{(\text{Min})}(y) = a R_1^{(\text{Min})}(y) + b R_2^{(\text{Min})}(y), \quad (6.48a)$$

$$R^{(\text{def})}(y) = c R_1^{(\text{def})}(y) + d R_2^{(\text{def})}(y). \quad (6.48b)$$

In Minkowski spacetime, the first solution  $R_1^{(\text{Min})}(y)$  is proportional to  $j_l(ky)$  and has parity  $(-1)^l$ , while the second solution  $R_2^{(\text{Min})}(y)$  is proportional to  $y_l(ky)$  and has parity  $(-1)^{-l-1}$ . In the defect metric, instead, both solutions,  $R_1^{(\text{def})}(y)$  and  $R_2^{(\text{def})}(y)$ , have parity  $+1$ , and consequently there is no way to build a solution that is odd under parity.

In Fig. 15 we show the behavior of the solutions (6.48) (truncated at order  $y^{4+s}$ ) for  $l = 1$  compared to the exact solutions. To obtain the coefficients  $a$ ,  $b$ ,  $c$ , and  $d$  we impose that the solutions (6.48) and their derivatives coincide with the exact solutions in the proximity of the origin:

$$R^{(\text{Min})}(y) = j_l(ky) \quad y \sim 0, \quad (6.49a)$$

$$R^{(\text{def})}(y) = j_l(k\sqrt{y^2 + b^2}) \quad y \sim 0. \quad (6.49b)$$

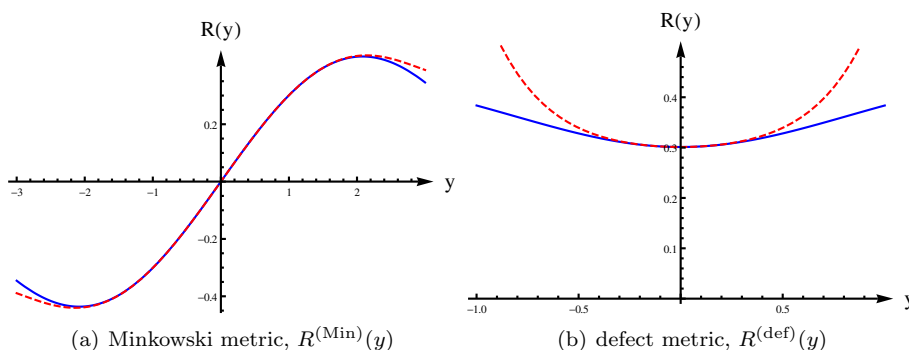


Figure 15: The behavior of the two radial solutions derived in this subsection and truncated at order  $y^{4+s}$  (red dashed lines) compared to the exact results presented in the previous subsection (blue solid lines). Fig. (a) depicts the result obtained in Minkowski spacetime, while Fig. (b) shows the results obtained in the defect metric (6.2) for  $l = 1$ ,  $k = 1$ , and  $b = 1$ .

Considering for a moment the defect manifold defined by Eq. (5.18), we observe that this metric is not differentiable at  $\tilde{y} = 0$ . This means that the Klein-Gordon equation is not defined around  $\tilde{y} = 0$ . If we write the scalar radial equation (analogous to Eq. (6.16b)) in this metric, we obtain

$$\partial_{\tilde{y}}^2 R + \frac{2\tilde{y}}{|\tilde{y}|(b + |\tilde{y}|)} \partial_{\tilde{y}} R + \left( k^2 - \frac{l(l+1)}{(b + |\tilde{y}|)^2} \right) R = 0, \quad (6.50)$$

whose coefficients are not continuous at  $\tilde{y} = 0$ . This equation is perfectly defined instead in the two separate regions  $\tilde{y} > 0$  and  $\tilde{y} < 0$ , in which the defect manifold with metric (5.18) is diffeomorphic to Minkowski spacetime and to the defect manifold with metric (6.2). Consequently, the scalar solutions obtained in these

last two manifolds, opportunely transformed, can serve also as solutions in the present case, since they are continuous at the defect surface. From the result in Minkowski spacetime Eq. (6.32), we obtain the radial solution

$$R_{kl}^A(\tilde{y}) = \begin{cases} \operatorname{Re} \left[ j_l(k(b + |\tilde{y}|)) - \frac{1 - (-1)^l j_l(kb) h_l^{(1)}(k(b + |\tilde{y}|))}{2 h_l^{(1)}(kb)} \right], & \tilde{y} > 0, \\ \operatorname{Re} \left[ j_l(-k(b + |\tilde{y}|)) - \frac{1 - (-1)^l j_l(-kb) h_l^{(1)}(-k(b + |\tilde{y}|))}{2 h_l^{(1)}(-kb)} \right], & \tilde{y} < 0. \end{cases} \quad (6.51)$$

From the result in the defect metric Eq. (6.34), we obtain the solution

$$R_{kl}^B(\tilde{y}) = j_l(k(b + |\tilde{y}|)), \quad \forall \tilde{y} \neq 0. \quad (6.52)$$

Observe that these solutions have different behaviors under parity— $R_{kl}^A(\tilde{y})$  has parity eigenvalues  $(-1)^l$ , while  $R_{kl}^B(\tilde{y})$  has parity eigenvalues  $(+1)$ . We conclude that in the non-smooth defect metric (5.18) the parity of the scalar solutions is not determined. We want to stress also that the two solutions  $R_{kl}^A(\tilde{y})$  and  $R_{kl}^B(\tilde{y})$ , even if they do define functions everywhere, are not differentiable at  $\tilde{y} = 0$  and therefore cannot be regarded as the solutions of any differential equation around  $\tilde{y} = 0$  [91]. On the other hand, the solution (6.23) obtained in the smooth defect metric (6.2) is perfectly defined and well-behaved (continuous and differentiable) as a solution of the radial equation (6.16b) around  $y = 0$ . See also Ref. [92] for a comparison of the different types of defects.

### 6.2.2 Plane waves

We wish to understand how a plane scalar wave propagating along the  $X$  Cartesian axis behaves in the defect metric (6.2) with  $b > 0$ , compared to the standard Minkowski case  $b = 0$ . For the moment, we do not consider the time dependence of the wave. Using the plane wave expansion, we obtain in the coordinate system  $\{y, z, x\}$

$$\Phi_{\text{even}}^{(\text{plane})}(y, z, x) = 4\pi\Phi_0 \sum_{l=\text{even}} \sum_{m=-l}^l i^l j_l(kr(y)) Y_l^m(z, x) Y_l^{*m}(z_k, x_k), \quad (6.53a)$$

$$\Phi_{\text{odd}}^{(\text{plane})}(y, z, x) = 4\pi\Phi_0 \sum_{l=\text{odd}} \sum_{m=-l}^l i^l j_l(kr(y)) Y_l^m(z, x) Y_l^{*m}(z_k, x_k), \quad (6.53b)$$

where  $r(y) = y$  in Minkowski spacetime and  $r(y) = \sqrt{y^2 + b^2}$  in the defect metric. Setting  $z_k = \pi/2$  and  $x_k = 0$ , corresponding to a wavevector  $\vec{k}$  aligned with the  $X$  axis, we can rewrite Eqs. (6.53) more compactly as

$$\Phi_{\text{even}}^{(\text{plane})}(y, z, x) = \Phi_0 \cos(kr(y) \sin z \cos x), \quad (6.54a)$$

$$\Phi_{\text{odd}}^{(\text{plane})}(y, z, x) = \Phi_0 \sin(kr(y) \sin z \cos x), \quad (6.54b)$$

the behavior of which is shown in Fig. 16.

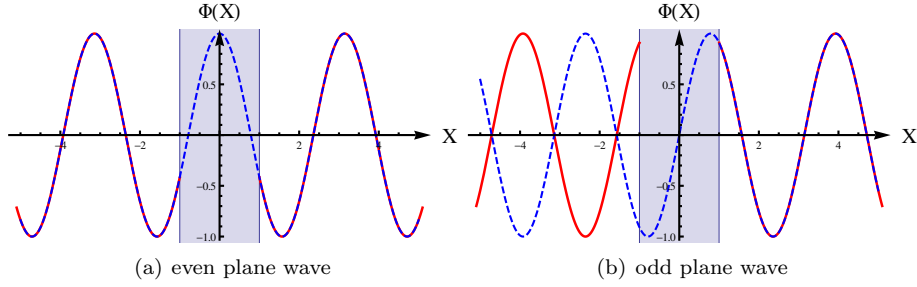


Figure 16: Behavior of the plane waves propagating along the Cartesian  $X$  axis in the defect metric (red solid line) and in Minkowski spacetime (blue dashed line). The shaded area around the origin represents the defect of radius  $b$ . We used  $z = \pi/2$ ,  $x = 0$ ,  $b = 1$ , and  $k = 2$ .

The plane wave on one side of the defect is equal to that on the other side shifted by a phase  $\delta$  (in Fig. 16, the phases are, respectively,  $\delta = 0$  (a) and  $\delta = \pi$  (b)). This phase shift can be expressed as a function of the distance between the defect position and the zeros of the plane wave. For example, consider a plane wave propagating along the  $X$  axis with initial phase  $\delta_0$

$$\Phi^{(plane)}(X) = \Phi_0 \sin(kX + \delta_0), \quad (6.55)$$

and a defect centered on the  $X$  axis at  $X_1$ . The phase of the wave on the other side of the defect is given by

$$\delta_1 = \pi - \delta_0 - 2kX_1. \quad (6.56)$$

We can use this formula iteratively to obtain the phase  $\delta_n$  of the plane wave after encountering  $n$  defects randomly distributed along the  $X$  axis at positions  $\{X_i\}$ :

$$\delta_n = \begin{cases} \delta_0 + 2k \sum_{i=1}^n (-1)^{i+1} X_i, & \text{n even,} \\ \pi - \delta_0 - 2k \sum_{i=1}^n (-1)^{i+1} X_i, & \text{n odd.} \end{cases} \quad (6.57)$$

Explicitly, the first few phases are

$$\begin{aligned} \delta_1 &= \pi - \delta_0 - 2kX_1, \\ \delta_2 &= \delta_0 + 2k(X_1 - X_2), \\ \delta_3 &= \pi - \delta_0 - 2k(X_1 - X_2 + X_3), \\ \delta_4 &= \delta_0 + 2k(X_1 - X_2 + X_3 - X_4). \end{aligned} \quad (6.58)$$

Examples are shown in Figs. 17 and 18.

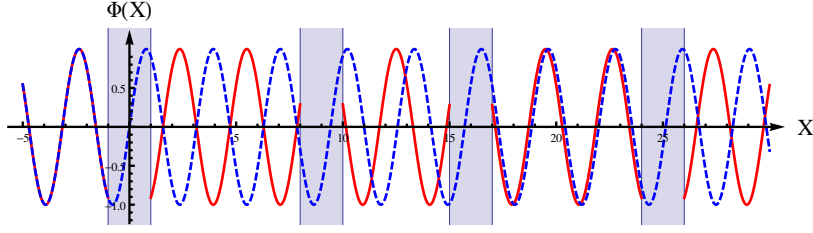


Figure 17: Plane wave propagating along the  $X$  axis encountering 4 defects (red solid line), compared to the same wave propagating in Minkowski spacetime (blue dashed line). The phase shifts are obtained from Eq. (6.57). We used  $z = \pi/2$ ,  $x = 0$ ,  $b = 1$ , and  $k = 2$ .

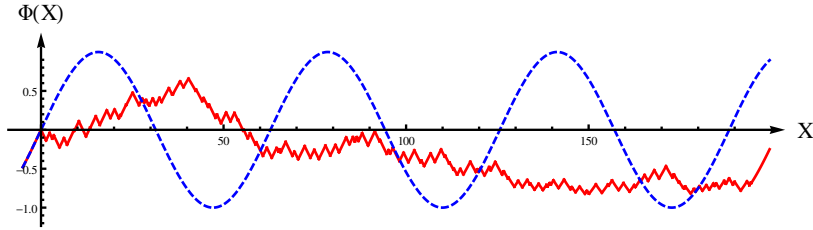


Figure 18: Same as in Fig. 17, but in the case of many defects with mean separation and sizes much smaller than the wavelength of the plane wave.

If the distribution of defects is dense, we can use an approximation to manipulate Eq. (6.57). We assume that  $n$  defects are randomly distributed in the interval  $\Delta X$  with linear density  $\rho_l = n/\Delta X$ . Then, each defect has at its disposal an average interval  $\delta X = \Delta X/n = 1/\rho_l$ . When  $\delta X \ll \Delta X$ , we can approximate the random distribution of defects with a regular distribution, where the defects are separated by the fixed distance  $\delta X$ . In this way, we can rewrite the sum in Eq. (6.57) as

$$\sum_{i=1}^n (-1)^{i+1} X_i \simeq \frac{\delta X}{2} + \sum_{i=2}^n (-1)^{i+1} \delta X \left( \frac{1}{2} + i - 1 \right) = (-1)^{n+1} \frac{\Delta X}{2}. \quad (6.59)$$

Substituting this result into Eq. (6.57), we arrive at

$$\delta_n \simeq \begin{cases} \delta_0 - k\Delta X, & n \text{ even,} \\ \pi - \delta_0 - k\Delta X, & n \text{ odd.} \end{cases} \quad (6.60)$$

Observe that this result does not depend on the density of defects  $\rho_l$  (but it is a good approximation only for  $\delta X \ll \Delta X$ ). By choosing the initial phase as  $\delta_0 = \pi/2$ , Eq. (6.60) provides the same result for  $n$  even and  $n$  odd.

We now consider the case in which the plane wave interacts with defects obtained from Minkowski spacetime by surgery (Eqs. (5.3) and (5.4)), and then we compare the results with those obtained above for defects described by the defect metric (6.2). The solution of the radial Klein-Gordon equation around a defect in Minkowski spacetime is given by Eq. (6.33). Note that this solution

differs from that in the defect metric (Eq. (6.23)) only for odd values of  $l$ . From the plane wave expansion, we obtain in this case

$$\Phi_{even}^{M(plane)}(y, z, x) = 4\pi\Phi_0 \sum_{l=even} \sum_{m=-l}^l i^l R_{kl}(y) Y_l^m(z, x) Y_l^{*m}(z_k, x_k), \quad (6.61a)$$

$$\Phi_{odd}^{M(plane)}(y, z, x) = 4\pi\Phi_0 \sum_{l=odd} \sum_{m=-l}^l i^l R_{kl}^{(tot)}(y) Y_l^m(z, x) Y_l^{*m}(z_k, x_k), \quad (6.61b)$$

where  $R_{kl}(y)$  and  $R_{kl}^{(tot)}(y)$  are given by, respectively, Eq. (6.23) and Eq. (6.33). A plane wave of the form of Eq. (6.55), propagating along the  $X$  axis with an initial phase  $\delta_0$ , can be written in the Minkowski and defect metrics as

$$\Phi^{(plane)}(y, z, x) = \Phi_0 \sin(kr(y) \sin z \cos x + \delta_0), \quad (6.62)$$

where  $r(y) = y$  in standard Minkowski spacetime and  $r(y) = \sqrt{y^2 + b^2}$  in the defect metric. For a defect in Minkowski spacetime, this plane wave can be expressed as

$$\Phi^{M(plane)}(y, z, x) = \sin \delta_0 \Phi_{even}^{M(plane)}(y, z, x) + \cos \delta_0 \Phi_{odd}^{M(plane)}(y, z, x). \quad (6.63)$$

In Fig. 19, we compare the behavior of Eq. (6.62) and Eq. (6.63) for  $\delta_0 = 0$  (a) and for  $\delta_0 = \pi/4$  (b).

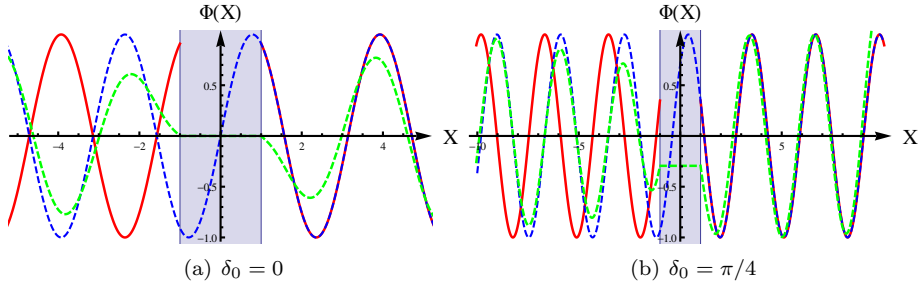


Figure 19: Behavior of plane waves propagating along the Cartesian  $X$  axis in the defect metric (6.2) (red solid line), in standard Minkowski spacetime (blue dashed line) and in Minkowski spacetime with a defect (green dashed line). Specifically, red solid lines describe Eq. (6.62) for  $r(y) = \sqrt{y^2 + b^2}$ , blue dashed lines describe Eq. (6.62) for  $r(y) = y$ , and green dashed lines describe Eq. (6.63). In Fig. (a) the initial phase is  $\delta_0 = 0$ , while in Fig. (b) we set  $\delta_0 = \pi/4$ . The shaded area around the origin represents the defect of radius  $b$ . We used  $z = z_k = \pi/2$ ,  $x = x_k = 0$ ,  $b = 1$  and  $k = 2$ .

Observe that, when  $\lambda \gg b$ , Eq. (6.61b) differs significantly from the solution in standard Minkowski spacetime only in a small neighborhood of the defect. We can conclude that, in this limit, the plane wave does not experience any phase shift when crossing a defect obtained from Minkowski spacetime by surgery.

### 6.2.3 Dispersion relation

We can use the phase shifts calculated in the previous section to derive the dispersion relation for scalar waves. Observe that Eq. (6.57) is obtained for a distribution of defects centered on the  $X$  axis and for a plane wave propagating along the same axis. This means, ultimately, that we are restricted to a two-dimensional spacetime  $(t, X)$ . We want to obtain the dispersion relation for such a spacetime (that is, a two-dimensional spacetime filled with a distribution of defects described by the defect metric (6.2)), and then compare it with the dispersion relation for a two-dimensional spacetime where the defects are obtained by surgery on Minkowski spacetime (Eqs. (5.3), (5.4)).

We follow the approach of Ref. [93] and consider a plane wave propagating initially in (two-dimensional) vacuum Minkowski spacetime (region I). At a certain point  $(t_0, X_0)$ , the plane wave enters a region II of length  $\Delta X$  filled with a distribution of defects with linear density  $\rho_l = n/\Delta X$ , and then continues to propagate in vacuum Minkowski spacetime (region III), as illustrated in Fig. 20. The incident plane wave is (in Cartesian coordinates  $(t, X)$ )

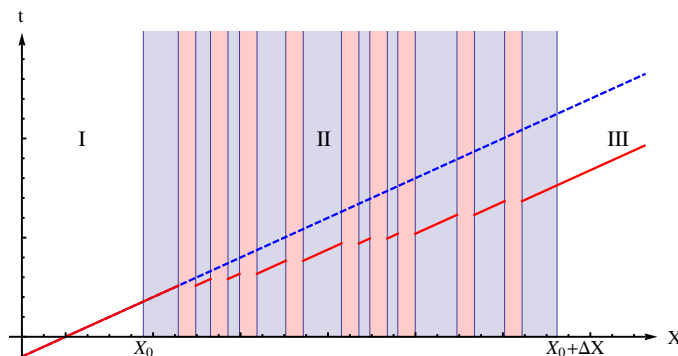


Figure 20: Regions I and III represent vacuum Minkowski spacetime, while region II, of length  $\Delta X$ , is filled with a random distribution of defects with density  $\rho_l$ . Also shown is the trajectory of a plane wave (red solid line) compared to the trajectory of a plane wave propagating in standard Minkowski space (with no defects) (blue dashed line).

$$\Phi^{(plane)}(t, X) = \Phi_0 \sin(kX - \omega t + \delta_0). \quad (6.64)$$

In a vacuum, the plane wave covers the distance  $\Delta X$  in the time  $\Delta t = \Delta X/c$ ; however, in the region filled with defects, the effective distance is  $\Delta X' = \Delta X - 2bn$ , and the crossing takes  $\Delta t' = (1 - 2\rho_l b)\Delta X/c$ .

In the third (vacuum) Minkowski region, we translate the coordinates  $(t, X)$  into a new set  $(t^*, X^*)$  whose origin is set at the point where the plane wave emerges in region III. We indicate with  $\Phi_{M0}^{(plane)}$  the plane wave that crosses region II with no defects ( $\rho_l = 0$ ), with  $\Phi_{M\rho_l}^{(plane)}$  the plane wave that crosses a region II filled with defects obtained from Minkowski spacetime by surgery and with  $\Phi_{d\rho_l}^{(plane)}$  the plane wave that crosses a region II filled with defects described

by the defect metric (6.2). Explicitly, we have

$$\begin{aligned}
\Phi_{M0}^{(plane)}(t^*, X^*) &= \Phi_0 \sin \left( k(X_0 + \Delta X) + kX^* - \omega \left( t_0 + \frac{\Delta X}{c} \right) - \omega t^* + \delta_0 \right), \\
\Phi_{M\rho_l}^{(plane)}(t^*, X^*) &= \Phi_0 \sin \left( k(X_0 + \Delta X) + kX^* - \omega \left( t_0 + \frac{\Delta X}{c} \right) - \omega t^* + \right. \\
&\quad \left. + \omega \frac{2\rho_l b}{c} \Delta X + \delta_0 \right), \\
\Phi_{d\rho_l}^{(plane)}(t^*, X^*) &= \Phi_0 \sin \left( k(X_0 + \Delta X) + kX^* - \omega \left( t_0 + \frac{\Delta X}{c} \right) - \omega t^* + \right. \\
&\quad \left. + \omega \frac{2\rho_l b}{c} \Delta X + \delta_n \right),
\end{aligned} \tag{6.65}$$

where  $\delta_n$  is given approximately by Eq. (6.60). Observe that, for a wave propagating in a vacuum ( $\Phi_{M0}^{(plane)}$ ), coordinates  $(t^*, X^*)$  are related to standard coordinates  $(t, X)$  by the transformations

$$\begin{aligned}
t &= t_0 + \frac{\Delta X}{c} + t^*, \\
X &= X_0 + \Delta X + X^*.
\end{aligned} \tag{6.66}$$

We can use these transformations to rewrite Eq. (6.65) in standard coordinates  $(t, X)$

$$\begin{aligned}
\Phi_{M0}^{(plane)}(t, X) &= \Phi_0 \sin(kX - \omega t + \delta_0), \\
\Phi_{M\rho_l}^{(plane)}(t, X) &= \Phi_0 \sin \left( kX - \omega t + \omega \frac{2\rho_l b}{c} \Delta X + \delta_0 \right), \\
\Phi_{d\rho_l}^{(plane)}(t, X) &= \Phi_0 \sin \left( kX - \omega t + \omega \frac{2\rho_l b}{c} \Delta X + \delta_n \right).
\end{aligned} \tag{6.67}$$

By choosing the initial phase shift as  $\delta_0 = \pi/2$ , the total phase shift experienced by the plane wave crossing region II is

$$\begin{aligned}
\delta_{M\rho_l} &= \omega \frac{2\rho_l b}{c} \Delta X, \\
\delta_{d\rho_l} &= \omega \frac{2\rho_l b}{c} \Delta X - k\Delta X.
\end{aligned} \tag{6.68}$$

We remember that these results are based on approximations that are valid in the limit  $\lambda \gg 1/\rho_l \gg b$ .

We can compare the above phase shifts with that obtained for a standard material with a refractive index  $n$

$$\delta_{mat} = \frac{\omega}{c} (1 - n) \Delta X. \tag{6.69}$$

The refractive index of the region of space filled with defects turns out to be

$$\begin{aligned}
n_{M\rho_l} &= 1 - 2\rho_l b, \\
n_{d\rho_l} &= 2 - 2\rho_l b,
\end{aligned} \tag{6.70}$$

where we have used the fact that  $\omega$  and  $k$ , in Eq. (6.65), are related by  $\omega = ck$ . From Eq. (6.70) we see that the modified dispersion relation ( $\omega = ck/n$ ) of the massless scalar field changes depending on which type of defect we consider. In particular, for a spacetime filled with defects obtained from Minkowski spacetime by surgery, the group velocity  $v_{M\rho_i}$  is larger than  $c$ , while, for a spacetime filled with defects described by the defect metric,  $v_{d\rho_i}$  is smaller than  $c$ .

### 6.3 Electromagnetic waves

We have derived the scalar wave solution in the defect metric (6.2). Now we can construct the corresponding electromagnetic solutions. Since we have seen that, in the two regions  $y > 0$  and  $y < 0$ , the coordinates  $\{y, z, x\}$  and spherical coordinates are related by diffeomorphism (see Eqs. (6.6), (6.7)), we can follow two different approaches. The first is to interpret the scalar solution  $\Phi(y, z, x)$  as the Debye potential for the electromagnetic solution. The two are related (in flat spacetime) by (see Sec. 6.3.1.1)

$$E^E = \nabla \wedge \nabla \wedge (\vec{r}\Phi), \quad E^M = -B^E, \quad (6.71)$$

$$B^E = -ik\nabla \wedge (\vec{r}\Phi), \quad B^M = E^E, \quad (6.72)$$

where ‘ $E$ ’ and ‘ $M$ ’ indicate two independent sets of solutions. The second method involves starting directly from the electromagnetic solutions in spherical coordinates and transforming them into the coordinate system  $\{y, z, x\}$  (see Sec. 6.3.1.2). In both cases, we arrive at the same two sets of solutions, depending on which transformation law we use:  $(\vec{E}^{(+)}, \vec{B}^{(+)})$  if we choose the change of coordinates defined for  $y > 0$ , and  $(\vec{E}^{(-)}, \vec{B}^{(-)})$  if we choose that defined for  $y < 0$ . Explicitly, these solutions are

$$\begin{cases} E_y^{(+)} = \frac{\sqrt{y^2 + b^2}}{y} E_r(\sqrt{y^2 + b^2}, z, x), \\ E_z^{(+)} = E_\theta(\sqrt{y^2 + b^2}, z, x), \\ E_x^{(+)} = E_\phi(\sqrt{y^2 + b^2}, z, x), \end{cases} \quad \begin{cases} E_y^{(-)} = E_y^{(+)}(y, \pi - z, x + \pi), \\ E_z^{(-)} = -E_z^{(+)}(y, \pi - z, x + \pi), \\ E_x^{(-)} = E_x^{(+)}(y, \pi - z, x + \pi), \end{cases} \quad (6.73)$$

and

$$\begin{cases} B_y^{(+)} = \frac{\sqrt{y^2 + b^2}}{y} B_r(\sqrt{y^2 + b^2}, z, x), \\ B_z^{(+)} = B_\theta(\sqrt{y^2 + b^2}, z, x), \\ B_x^{(+)} = B_\phi(\sqrt{y^2 + b^2}, z, x), \end{cases} \quad \begin{cases} B_y^{(-)} = -B_y^{(+)}(y, \pi - z, x + \pi), \\ B_z^{(-)} = B_z^{(+)}(y, \pi - z, x + \pi), \\ B_x^{(-)} = -B_x^{(+)}(y, \pi - z, x + \pi), \end{cases} \quad (6.74)$$

where the electric and magnetic fields in spherical coordinates are given in Eqs. (6.93), (6.94). The signs in the above expressions have been arranged so that the electromagnetic tensor has the same form in both regions  $y > 0$  and  $y < 0$ :

$$F^{\mu\nu} = \begin{pmatrix} 0 & -E_y & -E_z & -E_x \\ E_y & 0 & -B_x \frac{\sqrt{y^2 + b^2}}{y} \sin z & \frac{B_z \sqrt{y^2 + b^2}}{y \sin z} \\ E_z & B_x \frac{\sqrt{y^2 + b^2}}{y} \sin z & 0 & -\frac{B_x y}{(y^2 + b^2)^{3/2} \sin z} \\ E_x & \frac{B_z \sqrt{y^2 + b^2}}{y \sin z} & \frac{B_x y}{(y^2 + b^2)^{3/2} \sin z} & 0 \end{pmatrix}. \quad (6.75)$$

The solutions  $(\vec{E}^{(+)}, \vec{B}^{(+)})$  are explicitly given by Eqs. (6.88), (6.91). We have to verify if these expressions are indeed solutions of the Maxwell equations in the defect metric. Maxwell equations in a general metric are given by

$$\partial_\mu(g^{1/2}F^{\mu\nu}) = 0, \quad \partial_\lambda F_{\mu\nu} + \partial_\mu F_{\nu\lambda} + \partial_\nu F_{\lambda\mu} = 0. \quad (6.76)$$

By inserting Eq. (6.75) into (6.76), we observe that both sets,  $(\vec{E}^{(+)}, \vec{B}^{(+)})$  and  $(\vec{E}^{(-)}, \vec{B}^{(-)})$ , solve the equations. We want to stress that each of these sets is a valid solution in the whole coordinate domain  $-\infty < y < \infty$ , even if they have been obtained from a change of coordinates valid only in a restricted region  $y > 0$  or  $y < 0$  (see Sec. 6.3.2).

The spherical wave solutions  $(\vec{E}^{Min}, \vec{B}^{Min})$  that one obtains in standard Minkowski spacetime are given in the system of coordinates  $\{y, z, x\}$  (setting  $b = 0$  in Eqs. (6.73), (6.74)), by the combinations

$$\begin{cases} E_y^{Min} = \Theta(y)E_y^{(+)} - \Theta(-y)E_y^{(-)}, \\ E_z^{Min} = \Theta(y)E_z^{(+)} - \Theta(-y)E_z^{(-)}, \\ E_x^{Min} = \Theta(y)E_x^{(+)} + \Theta(-y)E_x^{(-)}, \end{cases} \quad \begin{cases} B_y^{Min} = \Theta(y)B_y^{(+)} + \Theta(-y)B_y^{(-)}, \\ B_z^{Min} = \Theta(y)B_z^{(+)} + \Theta(-y)B_z^{(-)}, \\ B_x^{Min} = \Theta(y)B_x^{(+)} - \Theta(-y)B_x^{(-)}, \end{cases} \quad (6.77)$$

where  $\Theta(y)$  is the Heaviside step function. We observe that, analogously to the scalar case, the solutions that one obtains in the defect metric when  $b = 0$  are equivalent to those in Minkowski spacetime in standard spherical coordinates.

From the study of the scalar field, we know that the nonstandard parity behavior of the solutions for the defect metric is the main difference with respect to the standard Minkowski solutions (see Sec. 6.2). In Table 1, we have summarized the behavior under parity of the electromagnetic solutions in standard Minkowski spacetime and in the defect metric.

Minkowski solution	P	defect solution	P
$E_r^E = B_r^M$	$(-1)^l$	$E_y^E = B_y^M$	-1
$E_\theta^E = B_\theta^M$	$(-1)^{l+1}$	$E_z^E = B_z^M$	+1
$E_\phi^E = B_\phi^M$	$(-1)^l$	$E_x^E = B_x^M$	+1
$B_r^E = -E_r^M$	+1*	$B_y^E = -E_y^M$	+1*
$B_\theta^E = -E_\theta^M$	$(-1)^l$	$B_z^E = -E_z^M$	+1
$B_\phi^E = -E_\phi^M$	$(-1)^{l+1}$	$B_x^E = -E_x^M$	+1

Table 1: Parity eigenvalues of the electromagnetic solutions of types  $E$  and  $M$  in Minkowski spacetime and in the defect metrics.

We observe that the basis vectors, in the  $\{y, z, x\}$  coordinates system, transform under parity as

$$P : (\hat{y}, \hat{z}, \hat{x}) \rightarrow (-\hat{y}, \hat{z}, \hat{x}). \quad (6.78)$$

\*The component vanishes identically.

Consequently, the electric and magnetic fields, in order to be a vector and a pseudovector, respectively, must transform as

$$\begin{aligned} P : (E_y, E_z, E_x) &\rightarrow (E_y, -E_z, -E_x), & \text{vector,} \\ P : (B_y, B_z, B_x) &\rightarrow (-B_y, B_z, B_x), & \text{pseudovector.} \end{aligned} \quad (6.79)$$

From Table 1 we see instead that both electric and magnetic field solutions in the defect metric behave like pseudovectors.

### 6.3.1 Derivation of electromagnetic solutions

In this section, we want to describe in more detail how the general electromagnetic solutions in the defect metric (6.2) can be obtained. As mentioned previously, we follow two different approaches that lead to the same results. The first approach is based on the formalism of Debye potential, which makes use of the scalar solution obtained in Sec. 6.2. The second approach consists in applying the change of coordinates (6.6) to the standard electromagnetic solutions in Minkowski spacetime.

#### 6.3.1.1 From Debye potential

We recall that the massless Klein-Gordon equation in the defect metric (6.2) gives

$$\Phi(y, z, x) = j_l(k\sqrt{y^2 + b^2})Y_l^m(z, x). \quad (6.80)$$

Due to the spherical symmetry of the metric, we can interpret this solution as the Debye potential for the electromagnetic solutions in the same metric. Following Ref. [74], in Minkowski spacetime, one has the relations

$$\begin{aligned} E^E &= \nabla \wedge \nabla \wedge (\vec{r}\Phi), & E^M &= -B^E, \\ B^E &= -ik\nabla \wedge (\vec{r}\Phi), & B^M &= E^E, \end{aligned} \quad (6.81)$$

where the superscripts ‘ $E$ ’ and ‘ $M$ ’ stand for “electric” and “magnetic” and denote two independent sets of solutions.

Since the defect metric is related to the Minkowski metric by a diffeomorphism in the two separate regions  $y > 0$  and  $y < 0$ , we can use the change of coordinates (6.7) in one of these regions to rewrite Eq. (6.81) in the defect metric. In a general metric, one has

$$(\nabla \wedge v)^i = g^{-1/2} \epsilon^{ijk} \partial_j v_k, \quad v_k = g_{kl} v^l. \quad (6.82)$$

The defect metric and its Jacobian determinant are

$$g_{ij} = \text{diag} \left( \frac{y^2}{y^2 + b^2}, y^2 + b^2, (y^2 + b^2) \sin^2 z \right), \quad g^{-1/2} = \frac{1}{y\sqrt{y^2 + b^2} \sin z}, \quad (6.83)$$

and consequently

$$v_y = \frac{y^2}{y^2 + b^2} v^y, \quad v_z = (y^2 + b^2) v^z, \quad v_x = (y^2 + b^2) \sin^2 z v^x. \quad (6.84)$$

From Eq. (6.81) we have, in Minkowski spacetime,  $v^i = r^i \Phi$ , and via a change of coordinates (observe that  $r = \sqrt{y^2 + b^2}$  in both regions  $y > 0$  and  $y < 0$ ) we can rewrite this in the defect metric as

$$\vec{r}\Phi = (r, 0, 0)\Phi \longrightarrow \left( \frac{y^2 + b^2}{y}, 0, 0 \right) \Phi. \quad (6.85)$$

Finally, the components  $v_i$  are given by

$$v_y = y \Phi, \quad v_z = 0, \quad v_x = 0. \quad (6.86)$$

Inserting them into Eq. (6.82) gives

$$\begin{cases} (\nabla \wedge v)^y = g^{-1/2} (\partial_z v_x - \partial_x v_z) = 0, \\ (\nabla \wedge v)^z = g^{-1/2} (\partial_x v_y - \partial_y v_x) = g^{-1/2} \partial_x v_y, \\ (\nabla \wedge v)^x = g^{-1/2} (\partial_y v_z - \partial_z v_y) = -g^{-1/2} \partial_z v_y, \end{cases} \quad (6.87)$$

from which we can immediately read the magnetic field solution of type  $E$  and the electric field solution of type  $M$

$$\begin{cases} B_y^E = -E_y^M = 0, \\ B_z^E = -E_z^M = \frac{mk}{\sqrt{y^2 + b^2} \sin z} j_l(k\sqrt{y^2 + b^2}) Y_l^m(z, x), \\ B_x^E = -E_x^M = \frac{ik}{\sqrt{y^2 + b^2} \sin z} j_l(k\sqrt{y^2 + b^2}) \partial_z Y_l^m(z, x). \end{cases} \quad (6.88)$$

For the electric field solution of type  $E$  (and for the magnetic field solution of type  $M$ ), we still have to insert the components (6.87) into Eq. (6.82). For simplicity, we introduce the vector  $u_i = g_{ij}(\nabla \wedge v)^j$ , the components of which are

$$u_y = 0, \quad u_z = \frac{\sqrt{y^2 + b^2}}{y \sin z} \partial_x v_y, \quad u_x = -\frac{\sqrt{y^2 + b^2} \sin z}{y} \partial_z v_y. \quad (6.89)$$

As a result, one obtains

$$\begin{cases} (\nabla \wedge \nabla \wedge v)^y = (\nabla \wedge u)^y = g^{-1/2} (\partial_z u_x - \partial_x u_z), \\ (\nabla \wedge \nabla \wedge v)^z = (\nabla \wedge u)^z = -g^{-1/2} \partial_y u_x, \\ (\nabla \wedge \nabla \wedge v)^x = (\nabla \wedge u)^x = g^{-1/2} \partial_y u_z. \end{cases} \quad (6.90)$$

The electric (magnetic) field solution of type  $E$  ( $M$ ) turns out to be

$$\begin{cases} E_y^E = B_y^M = \frac{l(l+1)}{y} j_l(k\sqrt{y^2 + b^2}) Y_l^m(z, x), \\ E_z^E = B_z^M = \frac{1}{y\sqrt{y^2 + b^2}} \partial_y \left( \sqrt{y^2 + b^2} j_l(k\sqrt{y^2 + b^2}) \right) \partial_z Y_l^m(z, x), \\ E_x^E = B_x^M = \frac{im}{y\sqrt{y^2 + b^2} \sin^2 z} \partial_y \left( \sqrt{y^2 + b^2} j_l(k\sqrt{y^2 + b^2}) \right) Y_l^m(z, x). \end{cases} \quad (6.91)$$

The solutions obtained above correspond to what we called  $(\vec{E}^{(+)}, \vec{B}^{(+)})$  in Eqs. (6.73) and (6.74). A second set of solutions, corresponding to  $(\vec{E}^{(-)}, \vec{B}^{(-)})$ , can be obtained starting from the Debye potential

$$\Phi = j_l(-k\sqrt{y^2 + b^2}) Y_l^m(z, x). \quad (6.92)$$

### 6.3.1.2 From a change of coordinates

The set of electromagnetic solutions of type  $E$  and  $M$  in spherical coordinates in Minkowski spacetime can be calculated easily by following the derivation of the previous subsection. One has to start from the massless Klein-Gordon solution in Minkowski spacetime ( $\Phi = j_l(kr)Y_l^m(\theta, \phi)$ ), and then use the Minkowski metric in spherical coordinates ( $g_{ij} = \text{diag}(1, r^2, r^2 \sin^2 \theta)$ ) in Eq. (6.81). The result is

$$\begin{cases} E_r^E = B_r^M = \frac{l(l+1)}{r} j_l(kr) Y_l^m(\theta, \phi), \\ E_\theta^E = B_\theta^M = \frac{1}{r^2} \partial_r(r j_l(kr)) \partial_\theta Y_l^m(\theta, \phi), \\ E_\phi^E = B_\phi^M = \frac{im}{r^2 \sin^2 \theta} \partial_r(r j_l(kr)) Y_l^m(\theta, \phi), \end{cases} \quad (6.93)$$

and

$$\begin{cases} B_r^E = -E_r^M = 0, \\ B_\theta^E = -E_\theta^M = \frac{mk}{r \sin \theta} j_l(kr) Y_l^m(\theta, \phi), \\ B_\phi^E = -E_\phi^M = \frac{ik}{r \sin \theta} j_l(kr) \partial_\theta Y_l^m(\theta, \phi). \end{cases} \quad (6.94)$$

We observe that these solutions are slightly different from those discussed in Ref. [74], which is due to the different normalizations of the basis vectors (in Ref. [74] the solutions are expressed in an orthonormal frame).

The relations between spherical coordinates and defect coordinates  $\{y, z, x\}$  are

$$\begin{cases} r = \sqrt{y^2 + b^2}, \\ \theta = z, \\ \phi = x, \end{cases} \quad y > 0, \quad \begin{cases} r = \sqrt{y^2 + b^2}, \\ \theta = \pi - z, \\ \phi = x + \pi, \end{cases} \quad y < 0, \quad (6.95)$$

and the components of the electric and magnetic vectors transform in the two regions according to the standard rule:

$$\begin{aligned} \vec{E} = E^i(x) \frac{\partial}{\partial x^i} &= E'^j(y) \frac{\partial}{\partial y^j} = \left( E'^j(y(x)) \frac{\partial x^i}{\partial y^j} \right) \frac{\partial}{\partial x^i} = \left( E^i(x(y)) \frac{\partial y^j}{\partial x^i} \right) \frac{\partial}{\partial y^j} \\ \implies E'^j(y) &= \frac{\partial y^j}{\partial x^i} E^i(x(y)), \quad E^i(x) = \frac{\partial x^i}{\partial y^j} E'^j(y(x)). \end{aligned} \quad (6.96)$$

The change of basis matrix for the transformation (6.95) is

$$\frac{\partial y^j}{\partial x^i} = \text{diag} \left( \frac{\sqrt{y^2 + b^2}}{y}, c, 1 \right), \quad \text{where } c = \begin{cases} +1 & y > 0, \\ -1 & y < 0. \end{cases} \quad (6.97)$$

Explicitly, from the change of coordinates defined in the region  $y > 0$ , one obtains

$$\begin{cases} E_y = \frac{\sqrt{y^2 + b^2}}{y} E_r(\sqrt{y^2 + b^2}, z, x), \\ E_z = E_\theta(\sqrt{y^2 + b^2}, z, x), \\ E_x = E_\phi(\sqrt{y^2 + b^2}, z, x), \end{cases} \quad \begin{cases} B_y = \frac{\sqrt{y^2 + b^2}}{y} B_r(\sqrt{y^2 + b^2}, z, x), \\ B_z = B_\theta(\sqrt{y^2 + b^2}, z, x), \\ B_x = B_\phi(\sqrt{y^2 + b^2}, z, x). \end{cases} \quad (6.98)$$

From Eqs. (6.93) and (6.94), we finally arrive at

$$\begin{cases} E_y^E = B_y^M = \frac{l(l+1)}{y} j_l(k\sqrt{y^2 + b^2}) Y_l^m(z, x), \\ E_z^E = B_z^M = \frac{1}{y\sqrt{y^2 + b^2}} \partial_y \left( \sqrt{y^2 + b^2} j_l(k\sqrt{y^2 + b^2}) \right) \partial_z Y_l^m(z, x), \\ E_x^E = B_x^M = \frac{im}{y\sqrt{y^2 + b^2} \sin^2 z} \partial_y \left( \sqrt{y^2 + b^2} j_l(k\sqrt{y^2 + b^2}) \right) Y_l^m(z, x), \end{cases} \quad (6.99)$$

and

$$\begin{cases} B_y^E = -E_y^M = 0, \\ B_z^E = -E_z^M = \frac{mk}{\sqrt{y^2 + b^2} \sin z} j_l(k\sqrt{y^2 + b^2}) Y_l^m(z, x), \\ B_x^E = -E_x^M = \frac{ik}{\sqrt{y^2 + b^2} \sin z} j_l(k\sqrt{y^2 + b^2}) \partial_z Y_l^m(z, x). \end{cases} \quad (6.100)$$

Note that these solutions are valid across the whole defect manifold ( $y \in (-\infty, +\infty)$ ). Furthermore, they are equivalent to the solutions obtained in the previous subsection (Eqs. (6.88) and (6.91)) and correspond to the set  $(\vec{E}^{(+)}, \vec{B}^{(+)})$ . The solutions that one obtains using the change of coordinates defined for  $y < 0$  are equivalent to the solutions that one obtains starting from the second Debye potential (6.92), and they correspond to the set  $(\vec{E}^{(-)}, \vec{B}^{(-)})$ .

As a last point, we need to derive the form of the electromagnetic tensor (6.75) in the defect metric. We observe that a second-order tensor transform according to

$$F'^{\rho\sigma}(y) = \frac{\partial y^\rho}{\partial x^\mu} \frac{\partial y^\sigma}{\partial x^\nu} F^{\mu\nu}(x(y)), \quad (6.101)$$

where the indices now also run over the time component. In the coordinate system  $\{t, y, z, x\}$ , using the change of coordinates defined in region  $y > 0$ , the electromagnetic tensor takes the form

$$F^{\mu\nu} = \begin{pmatrix} 0 & -E_y & \frac{-E_z}{y} & \frac{-E_x}{y \sin z} \\ E_y & 0 & -B_x \frac{\sqrt{y^2 + b^2}}{y} \sin z & \frac{B_z \sqrt{y^2 + b^2}}{y \sin z} \\ E_z & B_x \frac{\sqrt{y^2 + b^2}}{y} \sin z & 0 & -\frac{B_x y}{(y^2 + b^2)^{3/2} \sin z} \\ E_x & \frac{B_z \sqrt{y^2 + b^2}}{y \sin z} & \frac{B_x y}{(y^2 + b^2)^{3/2} \sin z} & 0 \end{pmatrix}. \quad (6.102)$$

### 6.3.2 Study of Maxwell equations around $y = 0$

We wish to study in more detail the behavior of the solutions  $(\vec{E}^{(\pm)}, \vec{B}^{(\pm)})$  and  $(\vec{E}^{(Min)}, \vec{B}^{(Min)})$  around the origin  $y = 0$ . The Maxwell equations in a general

metric are given by (see Sec. 5.3.1)

$$\partial_\mu(g^{1/2}F^{\mu\nu}) = 0, \quad \partial_\lambda F_{\mu\nu} + \partial_\mu F_{\nu\lambda} + \partial_\nu F_{\lambda\mu} = 0. \quad (6.103)$$

Explicitly, the first set of equations in the defect metric becomes

$$\begin{cases} E_y = -\frac{y(y^2 + b^2)}{2y^2 - b^2} (\cot z E_z + \partial_x E_x + \partial_z E_z + \partial_y E_y), \\ \partial_t E_y = \frac{\sqrt{y^2 + b^2}}{y} (2 \cos z B_x - \csc z \partial_x B_z + \sin z \partial_z B_x), \\ \partial_t E_z = \frac{1}{y(y^2 + b^2)^{3/2}} \left( \frac{y^2 \partial_x B_y}{\sin z} - (y^2 + b^2) \sin z (2y B_x + (y^2 + b^2) \partial_y B_x) \right), \\ \partial_t E_x = \frac{\csc z}{y(y^2 + b^2)^{3/2}} (2y(y^2 + b^2) B_z - y^2 \partial_z B_y + (y^2 + b^2)^2 \partial_y B_z). \end{cases} \quad (6.104)$$

By substituting into these equations the solutions  $(\vec{E}^{(\pm)}, \vec{B}^{(\pm)})$  obtained in the defect metric (see Eqs. (6.73) and (6.74)) and the Minkowski solutions  $(\vec{E}^{(Min)}, \vec{B}^{(Min)})$  given by Eq. (6.77), we can verify that both are suitable solutions in the two separate regions  $y > 0$  and  $y < 0$ . However, only one of the two sets is a solution at  $y = 0$ . When  $b = 0$ , the set which solves Eqs. (6.104) at  $y = 0$  is  $(\vec{E}^{(Min)}, \vec{B}^{(Min)})$ , while  $(\vec{E}^{(\pm)}, \vec{B}^{(\pm)})$  is discontinuous at the origin. When  $b > 0$ , the solution is  $(\vec{E}^{(\pm)}, \vec{B}^{(\pm)})$  and  $(\vec{E}^{(Min)}, \vec{B}^{(Min)})$  is discontinuous at  $y = 0$ . In Figs. 21 and 22 we show this behavior for the first of Eqs. (6.104). We plot each side of the equation for the solutions  $(\vec{E}^{(+)}, \vec{B}^{(+)})$  and  $(\vec{E}^{(Min)}, \vec{B}^{(Min)})$  for  $b = 0$  and for  $b > 0$ . In both cases, only one set of solutions at a time turns out to be continuous at the origin.

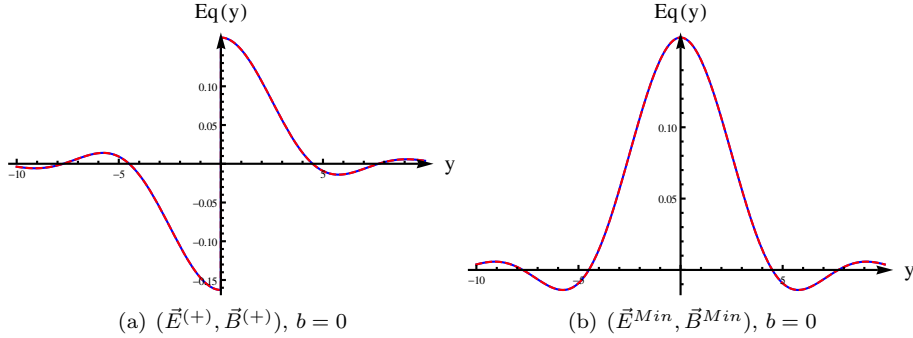


Figure 21: The left-hand side (blue solid line) and right-hand side (red dashed line) of the first of Eqs. (6.104) evaluated for the two sets of solutions  $(\vec{E}^{(+)}, \vec{B}^{(+)})$  and  $(\vec{E}^{Min}, \vec{B}^{Min})$  in standard Minkowski spacetime ( $b = 0$ ). In this case, the equation evaluated for the defect solution is discontinuous at  $y = 0$ , while that evaluated for the Minkowski solution is continuous. We used  $k = 1$ ,  $l = 1$ ,  $m = 0$ , and  $b = 0$ .

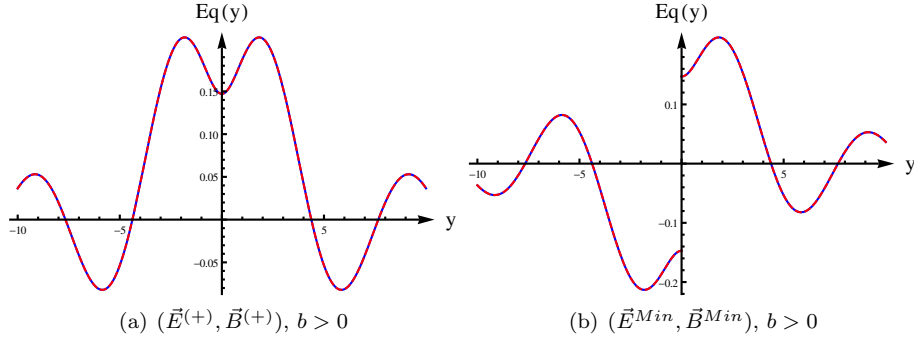


Figure 22: Same as in the previous figure, but for solutions in the defect metric ( $b > 0$ ). In this case, the equation evaluated for the defect solution is continuous at  $y = 0$ , while that evaluated for the Minkowski solution is discontinuous. We used  $k = 1$ ,  $l = 1$ ,  $m = 0$ , and  $b = 1$ . Note that the equation has been multiplied by a factor  $y$ , in order to avoid divergences at the origin.

Analogous behaviors are observed for the other equations.

### 6.3.3 Plane waves

Having obtained the electromagnetic solutions in the defect metric (6.2), we want to study how an electromagnetic plane wave behaves in a spacetime foam model made of defects of this type. Then, we want to compare this behavior with that obtained for defects in Minkowski spacetime (Sec. 5.2).

Since the expansion of plane waves in spherical waves simplifies when the direction of propagation is aligned with the  $x^3 = Z$  Cartesian axis, we would like to use the transformations defined on the chart  $U_3$  to relate spherical and  $\{y, z, x\}$  coordinates. However, from Eqs. (5.11) and (5.12), we see that these transformations are not well-defined. We decide to slightly modify the coordinate system  $\{y, z, x\}$ , to simplify the change of coordinates around the  $Z$  axis. The new coordinate system  $\{y, z', x'\}$  has ranges

$$y \in (-\infty, +\infty), \quad z' \in [0, \pi/2), \quad x' \in [0, 2\pi), \quad (6.105)$$

and is related to standard spherical coordinates by the transformations

$$\begin{cases} y_3 = \sqrt{r^2 - b^2}, \\ z'_3 = \theta, \\ x'_3 = \phi, \end{cases} \quad |\theta| < \frac{\pi}{2}, \quad \begin{cases} y_3 = -\sqrt{r^2 - b^2}, \\ z'_3 = \pi - \theta, \\ x'_3 = \phi - \pi, \end{cases} \quad |\theta| > \frac{\pi}{2}. \quad (6.106)$$

$$\begin{cases} r = \sqrt{y_3^2 + b^2}, \\ \theta = z'_3, \\ \phi = x'_3, \end{cases} \quad y > 0, \quad \begin{cases} r = \sqrt{y_3^2 + b^2}, \\ \theta = \pi - z'_3, \\ \phi = x'_3 + \pi, \end{cases} \quad y < 0. \quad (6.107)$$

Observe that this new set of coordinates does not modify the form of the defect metric or of the electromagnetic solutions.

We can now easily expand a plane electromagnetic wave propagating along the  $Z$  axis in the defect metric in spherical coordinates, analogously to what we did in Sec. 5.2.1. We obtain for the electric field

$$\begin{aligned}
E_r^{(def)} &= E_0 \sum_{l \text{ odd}} i^{l-1} \frac{2l+1}{kr} j_l(kr) P_l^1(\cos \theta) \cos \phi \left\{ \Theta\left(\frac{\pi}{2} - \theta\right) + (-1)^l \Theta\left(\theta - \frac{\pi}{2}\right) \right\}, \\
E_\theta^{(def)} &= E_0 \sum_{l \text{ odd}} i^{l-1} \frac{2l+1}{kr} j_l(kr) P_l^1(\cos \theta) \frac{\cos \phi}{\tan \theta} \left\{ \Theta\left(\frac{\pi}{2} - \theta\right) - (-1)^l \Theta\left(\theta - \frac{\pi}{2}\right) \right\}, \\
E_\phi^{(def)} &= E_0 \sum_{l \text{ odd}} i^{l-1} \frac{2l+1}{kr} j_l(kr) P_l^1(\cos \theta) \frac{\sin \phi}{\sin \theta} \left\{ \Theta\left(\frac{\pi}{2} - \theta\right) + (-1)^l \Theta\left(\theta - \frac{\pi}{2}\right) \right\},
\end{aligned} \tag{6.108}$$

where the results are expressed in standard spherical coordinates. Comparing these expressions with the results that one obtains in standard Minkowski spacetime (see Eq. (6.109) for the radial component), we observe that the two solutions coincide for  $\theta < \pi/2$

$$E_r^{(Min)} = E_0 \sum_{l \text{ odd}} i^{l-1} \frac{2l+1}{kr} j_l(kr) P_l^1(\cos \theta) \cos \phi \left\{ \Theta\left(\frac{\pi}{2} - \theta\right) + \Theta\left(\theta - \frac{\pi}{2}\right) \right\}. \tag{6.109}$$

In principle, it is possible to rewrite the plane wave in the defect metric as the sum of the plane wave in Minkowski spacetime plus a scattered field. However, such a scattered field cannot be expressed as the gradient of a potential of the form (5.38). Hence, we cannot proceed along the line of Ref. [67] to obtain a dispersion relation in this case.

Instead, we use the approach applied in Sec. 6.2.2, where we studied the propagation of scalar plane waves in the defect metric. Consider the incident plane wave ( $\theta < \pi/2$ )

$$\begin{aligned}
\vec{E}_{in} &= E_0 e^{i k r \cos \theta} \hat{X}, \\
\vec{B}_{in} &= E_0 e^{i k r \cos \theta} \hat{Y}.
\end{aligned} \tag{6.110}$$

In spherical coordinates, it takes the form

$$\begin{aligned}
\vec{E}_{in} &= E_0 \sum_l i^{l-1} \frac{2l+1}{kr} j_l(kr) P_l^1(\cos \theta) \left\{ \cos \phi \hat{r} + \frac{\cos \phi}{\tan \theta} \hat{\theta} + \frac{\sin \phi}{\sin \theta} \hat{\phi} \right\}, \\
\vec{B}_{in} &= E_0 \sum_l i^{l-1} \frac{2l+1}{kr} j_l(kr) P_l^1(\cos \theta) \left\{ \sin \phi \hat{r} + \frac{\sin \phi}{\tan \theta} \hat{\theta} + \frac{\cot \phi}{\sin \theta} \hat{\phi} \right\},
\end{aligned} \tag{6.111}$$

and, as we said, it has the same expression in Minkowski spacetime and in the defect metric. Instead, the outgoing wave is different in the two cases. For the electric field, we have

$$\begin{aligned}
\vec{E}_{out}^{(Min)} &= E_0 \sum_l i^{l-1} \frac{2l+1}{kr} j_l(kr) P_l^1(\cos(\pi - \theta)) \left\{ \cos(\phi + \pi) \hat{r} - \right. \\
&\quad \left. - \frac{\cos(\phi + \pi)}{\tan(\pi - \theta)} \hat{\theta} + \frac{\sin(\phi + \pi)}{\sin(\pi - \theta)} \hat{\phi} \right\}, \\
\vec{E}_{out}^{(def)} &= E_0 \sum_l i^{l-1} \frac{2l+1}{kr} j_l(kr) P_l^1(\cos \theta) \left\{ \cos \phi \hat{r} + \frac{\cos \phi}{\tan \theta} \hat{\theta} + \frac{\sin \phi}{\sin \theta} \hat{\phi} \right\},
\end{aligned} \tag{6.112}$$

and similarly for the magnetic field. From these expressions, we obtain

$$\begin{aligned}\vec{E}_{out}^{(def)} &= (-1)^l \vec{E}_{out}^{(Min)}, \\ \vec{B}_{out}^{(def)} &= (-1)^l \vec{B}_{out}^{(Min)}.\end{aligned}\quad (6.113)$$

This result can be expressed in terms of a phase shift  $\delta$  in the outgoing wave. We have  $\delta_{\text{even}} = 0$  and  $\delta_{\text{odd}} = \pi$ , respectively, for even plane waves (when the sum in Eqs. (6.111) and (6.112) is restricted to even values of  $l$ ) and for odd plane wave (when the sum is restricted to odd  $l$ ).

In analogy to the scalar field case, we consider a distribution of defects with centers on the  $Z$  axis at coordinates  $\{Z_i\}$ . Writing the incident electromagnetic plane wave as

$$\begin{aligned}\vec{E}_{in} &= E_0 \cos(kZ + \delta_0) \hat{X}, \\ \vec{B}_{in} &= E_0 \cos(kZ + \delta_0) \hat{Y},\end{aligned}\quad (6.114)$$

where  $\delta_0$  is a generic initial phase, we determine that the phase  $\delta_n$  after  $n$  defects is given by

$$\delta_n = \begin{cases} -\delta_0 + 2k \sum_{i=1}^n (-1)^{i+1} Z_i, & \text{n even,} \\ \pi + \delta_0 - 2k \sum_{i=1}^n (-1)^{i+1} Z_i, & \text{n odd.} \end{cases}\quad (6.115)$$

Given the linear number density of defects  $\rho_l = n/\Delta Z$ , where  $\Delta Z$  is the interval along the  $Z$  axis occupied by  $n$  defects ( $\Delta Z \simeq Z_n - Z_1 + 2b$ ), we find that, for  $\rho_l \ll 1/\Delta Z$ , the approximation (6.59) can be used to calculate the phase  $\delta_n$ , which produces

$$\delta_n \simeq \begin{cases} -\delta_0 - k\Delta Z, & \text{n even,} \\ \pi + \delta_0 - k\Delta Z, & \text{n odd.} \end{cases}\quad (6.116)$$

### 6.3.4 Dispersion relation

We have found that the phase shifts experienced by a plane electromagnetic wave propagating through a distribution of defects (described by the defect metric (6.2)) are equivalent to those experienced by a scalar field. We can therefore repeat the derivation described in Sec. 6.2.3 without any modification. We consider in this case the full 4-dimensional spacetime foam model obtained by a random distribution, in the spatial hypersurface of Minkowski spacetime, of defects (described by the defect metric) with number density  $\rho$ . That is, we now consider defects distributed throughout the 3-dimensional space and not only along the  $Z$  axis. In this case, the presence of the defects produces a shrinking of the effective (spatial) volume perceived by the electromagnetic wave given by

$$\Delta V' = \left(1 - \frac{4}{3}\pi\rho b^3\right) \Delta V, \quad (6.117)$$

which corresponds to an effective distance traveled by the particles given by

$$\Delta L' = (\Delta V')^{1/3} = \left(1 - \frac{4}{3}\pi\rho b^3\right)^{1/3} \Delta L. \quad (6.118)$$

Since the wave can now hit the defect on any point of its surface, the identification of antipodal points introduces an additional “inverting effect” that distorts the shape of the wavefront, and which was not accounted for in the simplified one-dimensional configuration discussed for the scalar field. To keep things simple, we assume that, when  $b$  is much smaller than the wavelength  $\lambda$ , we can neglect this “inverting effect” in the calculation of the dispersion relation. Note also that, even when the wave crosses the defect along a non-radial direction, the phase shift that it experiences is still given by Eq. (6.56). Consequently, even for defects in 4-dimensional spacetime, we can make use of the formula (6.116).

Ultimately, given the incident plane wave

$$\begin{aligned}\vec{E}_{in} &= E_0 \cos(kZ - \omega t + \delta_0) \hat{X}, \\ \vec{B}_{in} &= E_0 \cos(kZ - \omega t + \delta_0) \hat{Y},\end{aligned}\tag{6.119}$$

where we set for simplicity  $\delta_0 = -\pi/2$ , we determine that the dispersion relation for such a wave in the spacetime foam model described herein is given by

$$\omega = \frac{ck}{1 + (1 - \frac{4}{3}\pi\rho b^3)^{1/3}}.\tag{6.120}$$

We emphasize that this result is valid in the limit  $\lambda^3 \gg 1/\rho \gg b^3$ .

Comparing the dispersion relation (6.120) with that for defects in Minkowski spacetime, Eq. (5.46), we observe that the two are completely different. In particular, the result obtained here describes a spacetime foam model that is not dispersive, while Eq. (5.46) describes a dispersive medium.

## Part IV

# Numerical calculations of a lattice spacetime foam model

In this part, we develop a numerical method to study non-perturbatively the effects of a spacetime foam model, made up of extended topological defects, on the propagation of particles. This approach is useful to investigate the effects of a distribution of time-dependent extended defects on particle propagation. We consider a free, massive scalar field in a regular square lattice (of lattice spacing  $a$ ) filled with a random distribution of topological defects. The defects are represented by holes of volume  $v_d$  in the lattice with appropriate boundary conditions (see Fig. 23). In the resulting lattice model, it is useful to introduce dimensionless parameters (defined in terms of the lattice spacing  $a$ ) in place of the dimensionful parameters of the continuous theory. For example, the mass  $m$  is substituted by the dimensionless mass  $m_1 = a m$ , and the number density of defects  $\rho_d$  is substituted by the dimensionless density  $\eta = v_d \rho_d$ , which represents the fraction of lattice sites occupied by the defects.

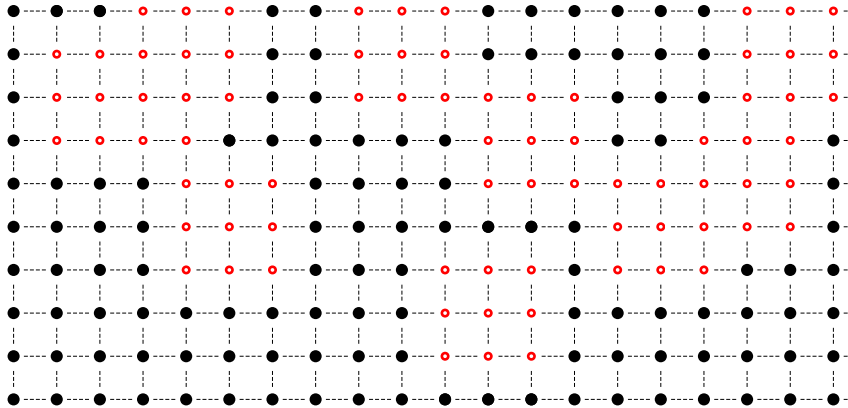


Figure 23: Example of a two-dimensional lattice filled with non-static extended defects. Black disks represent ordinary sites, while small red circles represent sites that have been removed from the lattice (defects). Sites separated by a line or a column of empty sites become nearest neighbors.

For simplicity, we describe the case of a two-dimensional lattice, but the extension to higher dimensions is straightforward, and ultimately we also present results for three- and four-dimensional lattices.

## 7 Lattice action

The lattice scalar field action is obtained by discretizing the continuum action of the free scalar field in Euclidean space. From the standard free scalar field action in two dimensions (see, for example, Ref. [48]), after a Wick rotation, we

obtain

$$\begin{aligned}
S_E &= i \int_V d^2x \frac{1}{2} \{ (\partial_0 \phi(x))^2 + (\partial_1 \phi(x))^2 + m^2 \phi(x)^2 \} \Rightarrow \\
&\Rightarrow i \sum_{i,j}^{N(V)} a^2 \frac{1}{2} \left\{ \left( \frac{\phi(a(i+1), aj) - \phi(ai, aj)}{a} \right)^2 + \right. \\
&\quad \left. + \left( \frac{\phi(ai, a(j+1)) - \phi(ai, aj)}{a} \right)^2 + m^2 \phi(ai, aj)^2 \right\} \Rightarrow \\
&\Rightarrow i \sum_{i,j}^{N(V)} \frac{1}{2} \left\{ (\phi_{i+1,j} - \phi_{i,j})^2 + (\phi_{i,j+1} - \phi_{i,j})^2 + a^2 m^2 \phi_{i,j}^2 \right\},
\end{aligned} \tag{7.1}$$

where  $a$  is the lattice spacing. Finally, we arrive at

$$S_E = i \sum_{i,j}^{N(V)} \left\{ \left( 2 + \frac{a^2 m^2}{2} \right) \phi_{i,j}^2 - (\phi_{i+1,j} + \phi_{i,j+1}) \phi_{i,j} \right\}, \tag{7.2}$$

where the sum over the indices  $i$  and  $j$  runs over all lattice sites. Then, if we consider a lattice filled with a distribution of defects (as shown in Fig. 23), we must obviously restrict the sum to the ordinary sites (black disks) and avoid taking into account the empty sites (red circles).

We wish to investigate how particle motion is modified by the presence of the spacetime defects. As we have seen in the previous parts, the dispersion relation, which can be obtained from the particle propagator, gives useful information in this regard. Consequently, we use a Monte Carlo algorithm to measure the scalar propagator

$$G_\eta(z_0) = \langle \phi(x_0 + z_0, x_1) \phi(x_0, x_1) \rangle = \frac{\int \mathcal{D}\phi \phi(x_0 + z_0, x_1) \phi(x_0, x_1) e^{iS_E}}{\int \mathcal{D}\phi e^{iS_E}}, \tag{7.3}$$

varying the density  $\eta$  of defects. When the density reaches zero, the model reduces to the free theory and the propagator (also called the ‘‘correlator’’) is given by the exact result

$$G_0(z_0) = \int \frac{d^2k}{(2\pi)^2} \frac{1}{k^2 + m^2} e^{-ik_0 z_0} = \frac{1}{2\pi} K_0(m|z_0|), \tag{7.4}$$

where  $K_0$  is the modified Bessel function of the second kind of order zero.

The structure of the defects is that of holes in spacetime of spacetime volume  $v_d$  with opposite points on the boundary identified (we mainly focus on the study of non-static defects). There are two main differences with respect to the spacetime foam model discussed in part II.

The first is that, here, the defects occupy a finite volume in spacetime, while in the model in part II the defects are point-like. This is a problem if we want to build a Lorentz-invariant spacetime foam model (i.e. a distribution of defects that look statistically the same in every reference frame, see Sec. 2.2). In fact, for point-like defects the sprinkling generates such a distribution, but if we assign a finite volume to these sprinkled points, the shape of the defects will change depending on which reference frame we choose.

The second difference is the absence of the charge  $\varepsilon_n$  associated with the defects introduced in part II. Hence, the average effect of the spacetime foam is different from zero in this case and corresponds to a shortening of distances given by

$$L' = (1 - \eta)^{1/d} L. \quad (7.5)$$

The volume of a standard lattice with no defects is given by  $V = N a^d$ , where  $N$  is the total number of sites,  $a$  the lattice spacing, and  $d$  the lattice dimension. The volume occupied by a distribution of defects is  $V_d = \eta N a^d$ , in which case the effective volume of a lattice filled with defects reduces to  $V' = V - V_d = (1 - \eta) N a^d$ , from which follows ( $L = V^{1/d}$ ) Eq. (7.5). The same effect was encountered in the study of static extended defects, see Sec. 6.3.4. Note, however, that for non-static defects the shortening of distances affects both the spatial and temporal directions, while for static defects it only modifies the spatial distances. From this fact, we can infer that the modification of the refractive index produced by a distribution of static defects, Eq. (6.70), does not occur when the defects are non-static (and symmetric in space and time).

Note also that the lattice structure introduced in this model is fundamentally different from the random lattice approach introduced in Ref. [95] (see also Ref. [96] for a numerical calculation of modified dispersion relations in this context). A random lattice is a realization of a sprinkling process, where the position of each lattice site is randomly determined. The only parameter that describes this kind of lattice is the density of sites  $\rho$ , which determines the mean separation between the sites  $\langle a \rangle = 1/\rho$ . Such a lattice is intrinsically Lorentz-invariant; moreover, by taking the continuum limit  $\langle a \rangle \rightarrow 0$  ( $\rho \rightarrow \infty$ ), one obtains continuum euclidean space with no defects. The lattice introduced here is instead characterized by three parameters: the lattice spacing  $a$ , the defect volume  $v_d$ , and the defect density  $\rho_d$ . In this case, only the distribution of defects is obtained by a sprinkling process, thus making it Lorentz-invariant. The lattice itself, being a standard square lattice, is not invariant under Lorentz transformations. By taking the continuum limit, which only affects the lattice spacing  $a \rightarrow 0$ , one obtains a continuum euclidean space filled with a distribution of defects (of density  $\rho_d$  and volume  $v_d$ ).

## 7.1 The algorithm

On the lattice, the structure of the spacetime foam is encoded in the structure of the indices and does not enter into the dynamic of the field, which is still described by the standard free Lagrangian. We have already discretized the scalar action, see Eq. (7.2), and so what remains to be done, in order to compute the propagator  $G(z_0)$ , is to perform the functional integral  $\int \mathcal{D}\phi$  over the field configurations in Eq. (7.3). The algorithm we use for this purpose is the straightforward Metropolis-Hastings algorithm, described by the following steps [94]:

- Create an initial random field configuration, assigning at each lattice site a random value chosen with equal probability in a certain range  $\{-\Delta, \Delta\}$ .
- Selecting the sites one by one, propose a change to the field value,  $\phi_{i,j} \rightarrow \phi'_{i,j} = \phi_{i,j} + \delta$ , where  $\delta$  has been chosen randomly in the range  $\{-\Delta, \Delta\}$ .

- Accept the change with probability  $\min(1, e^{-\delta S(i,j)})$ , where  $\delta S(i,j)$  is the difference between the action evaluated with the new field configuration, where at site  $(i,j)$  the field value is  $\phi'_{i,j}$ , and the action evaluated with the old field configuration, i.e.  $\delta S(i,j) = S\{\phi_{1,1}, \dots, \phi'_{i,j}, \dots, \phi_{n,m}\} - S\{\phi_{1,1}, \dots, \phi_{i,j}, \dots, \phi_{n,m}\}$ .
- When all the sites of the lattice have been visited, measure the quantity  $\phi_{i+L,j} \phi_{i,j}$  (which does not depend on which particular site  $(i,j)$  we choose for the measurement) and repeat the procedure, starting from the second point.
- After a large number  $N$  of iterations, the mean value of the measured quantity  $\langle \phi_{i+L,j} \phi_{i,j} \rangle$  corresponds to the expected value of the propagator  $G(z_0)$ :

$$G(z_0) = G(La) = \lim_{N \rightarrow \infty} \frac{\sum_{n=1}^N (\phi_{i+L,j} \phi_{i,j})_n}{N}, \quad (7.6)$$

where  $(\phi_{i+L,j} \phi_{i,j})_n$  is the result of the measurement obtained in the  $n$ -th iteration.

Some comments and clarifications are necessary:

- In order to optimize the algorithm, the value of  $\Delta$  is chosen so that the acceptance rate at point 3 is roughly 50%.
- Before starting the measurement, a number of Monte Carlo iterations must be performed so that the random initial configuration can reach equilibrium (thermalization).
- The proposed change  $\phi_{i,j} \rightarrow \phi'_{i,j} = \phi_{i,j} + \delta$  at site  $(i,j)$  produces the variation:  $\delta S(i,j) = S\{\phi_{1,1}, \dots, \phi'_{i,j}, \dots, \phi_{n,m}\} - S\{\phi_{1,1}, \dots, \phi_{i,j}, \dots, \phi_{n,m}\}$ . After some manipulations, this can be rewritten as:

$$\delta S(i,j) = \left(2 + \frac{a^2 m^2}{2}\right) (\delta^2 + 2\delta \phi_{i,j}) - \delta (\phi_{i-1,j} + \phi_{i+1,j} + \phi_{i,j-1} + \phi_{i,j+1}). \quad (7.7)$$

- The correlator  $G(L)$  depends only on the distance  $L$  and not on which particular site we choose to make the measurement, in which case we can then select the site  $(i,j)$  randomly while remembering to ensure that the site  $(i+L,j)$  belongs also to the lattice (it could happen that it corresponds to a site that has been removed from the lattice; in fact, the distance  $L$  is measured with respect to the standard lattice devoid of any defects).
- In order to avoid effects caused by a particular configuration of defects, we average the measurements over a number of different lattices (describing different realizations of the distribution of defects).
- The lattice is finite, while the analytic results have been obtained in an infinite continuum space. To serve as a good approximation the lattice must be large enough to resemble an infinite space, i.e. the finite-size effects must be maintained at a negligible level. This can be accomplished by choosing a lattice with edges much larger than the correlation length and with periodic boundary conditions.

## 7.2 Percolation

There are some advantages in employing numerical methods to study spacetime foam models. Consider, for example, the non-static model described in part II. This model is based on the generalization of a result, the CPT anomaly, which has been derived explicitly only for static point-like defects, while the direct study of time-dependent defects is much more complicated. On the lattice, instead, the structure of extended time-dependent defects is very easily implemented. In regard to the study of static defects presented in part III, we observe that the results are based on the dilute gas approximation (the distance between the defects is much greater than their extension). Again, on the lattice, we are not bound by this restriction, and we can therefore investigate the effects of the spacetime foam when the density of defects increases and clusters are formed. On the other hand, it is more difficult to interpret the results of numerical calculations and to give them an unambiguous meaning. This is due to the fact that, in order to be able to implement the defect structure, we are forced to work in configuration space, while we would be more interested in producing results in momentum space (the dispersion relation).

The study of clusters of objects randomly distributed in a lattice or in a continuum space is the goal of percolation theory [61], of which we want to introduce some basic notions herein. We start by describing the simplest model of percolation on a lattice—site percolation—as follows.

Consider an infinitely large lattice whose sites can be either occupied or empty. Sites are occupied randomly with a certain probability  $P$ . Two nearest neighbor sites that are both occupied are said to be linked together, and the connected set of all sites linked together is said to be a cluster (that is, it is possible to move from each site of a cluster to another one following a connected path of nearest neighborhood links, see figure 24). The typical extension of the clusters is related to the probability of occupation  $P$  (larger probabilities lead to larger clusters). Despite its simplicity, this model shows a phase transition at a critical probability  $P_c$ . Below  $P_c$  only clusters with a finite number of elements arise, while for probabilities larger than  $P_c$  clusters with infinite elements appear. At the critical point, the system is scale-invariant and has fractal properties. The critical probability depends on the dimensionality of the space and on the characteristics of the lattice considered. For square ( $2d$ ), cubic ( $3d$ ), and hypercubic ( $4d$ ) lattices, its values are listed in Table 2 [61].

Lattice dimension	$P_c$
$d = 2$	0.5927
$d = 3$	0.3116
$d = 4$	0.197

Table 2: Critical probabilities for regular square lattices in 2, 3, and 4 dimensions.

Consider now a continuous manifold  $M_d$  of dimension  $d$ . It is still possible to define a percolation model in this case (usually indicated as continuum percolation), see also Ref. [64]. Instead of considering occupied lattice sites, one defines extended objects  $P_i$  of volume  $v_d$  which are randomly distributed in  $M_d$  according to a Poisson distribution of density  $\rho$ . Two objects,  $P_i$  and  $P_j$ , are

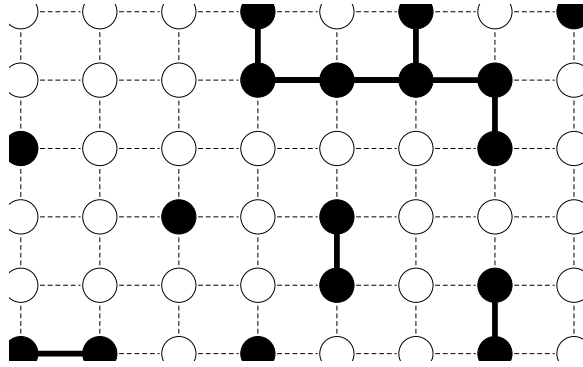


Figure 24: Percolation model on a square lattice. Occupied sites are represented by black disks. Occupied sites connected to each other form clusters.

said to be linked or connected if their intersection is not empty ( $P_i \cap P_j \neq \emptyset$ ). Clusters are defined as the connected sets of all objects  $P_i$  linked together (see Fig. 25). In this case, the dimension of the clusters depends not only on the

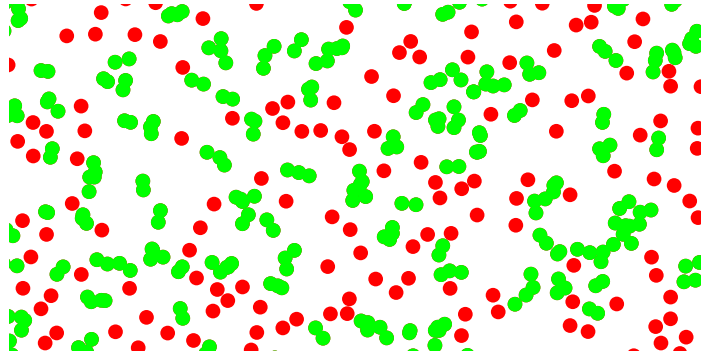


Figure 25: Continuous percolation in two dimensions. Disks are randomly distributed on the plane with density  $\rho$ , when they intersect each other form clusters (colored in green in the figure).

density  $\rho$  of the distribution but also on the volume of the objects  $v_d$  (larger volumes lead to larger clusters). In this instance, it is convenient to introduce, instead of the density, the dimensionless parameter

$$\eta = \rho v_d, \quad (7.8)$$

which is the equivalent of the occupation probability  $P$  on the lattice. Even in this case, the system undergoes phase transition at a critical point  $\eta_c$ . As for the lattice model, below  $\eta_c$  only finite clusters are present, but for  $\eta$  larger than  $\eta_c$  infinitely large clusters appear. The value of  $\eta_c$  depends on the dimension  $d$  and on the specific shape of the objects considered.

Using the algorithm presented in the previous subsection, we want to investigate how clusters of defects modify the propagation of a scalar field and how this modification is related to the occupation probability  $P$ .

## 8 Results

In this section, we present the results obtained from the numerical calculations. As mentioned previously, we use the algorithm described in Sec. 7.1 to calculate the scalar propagator (7.3) on a lattice filled with a distribution of defects varying the probability of occupation  $P$  of the defects. In this work, we mainly focus on the study of time-dependent extended defects in a 2-dimensional lattice. We do provide results regarding 3 and 4-dimensional lattices at the end of this section, and thereafter we present results for static extended defects in 3 and 4-dimensional lattices.

### 8.1 Time-dependent defects

We start by considering the standard case in which no defect is present. For such a case, we know the analytic expression of the correlator (Eq. (7.4)), so we can check if our algorithm works properly. Results are presented in Fig. 26. We repeated the measurement for different values of the mass parameter

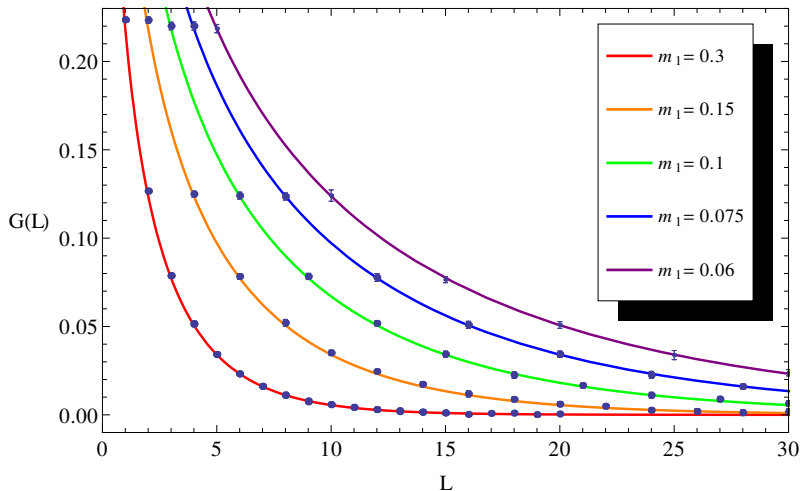


Figure 26: Numerical results for the two-dimensional correlator  $\langle \phi_{i+L,j} \phi_{i,j} \rangle$  in the absence of defects. Different curves correspond to different values of the mass parameter, starting from the bottom:  $m_1 = a m = \{0.3, 0.15, 0.1, 0.075, 0.06\}$ . The interpolating curves represent the analytic result  $G(L) = \frac{1}{2\pi} K_0(m_1 L)$ . Since the correlation length changes in line with the mass parameter, we use lattices of different sizes (from  $80 \times 80$  to  $400 \times 150$ ), in order to maintain negligible finite-size effects. The number of Monte Carlo iterations is  $N = 3 \times 10^6$ .

$m_1 = m a$  (this operation can be interpreted either as a rescaling of the physical mass or as a rescaling of the lattice spacing). As  $m_1$  decreases, the correlation length increases, and it is necessary to increase the size of the lattice in order to maintain negligible finite-size effects.

When we add a certain number of defects to the lattice, we expect a modification of the behavior of the correlator with respect to the standard case. In

Fig. 27, we present the results obtained for a distribution of defects of density  $\eta = \rho v_d = 0.464$  and volume  $v_d = a^2$  (a single site removed from the lattice). We do indeed observe a different behavior of the propagator with respect to the

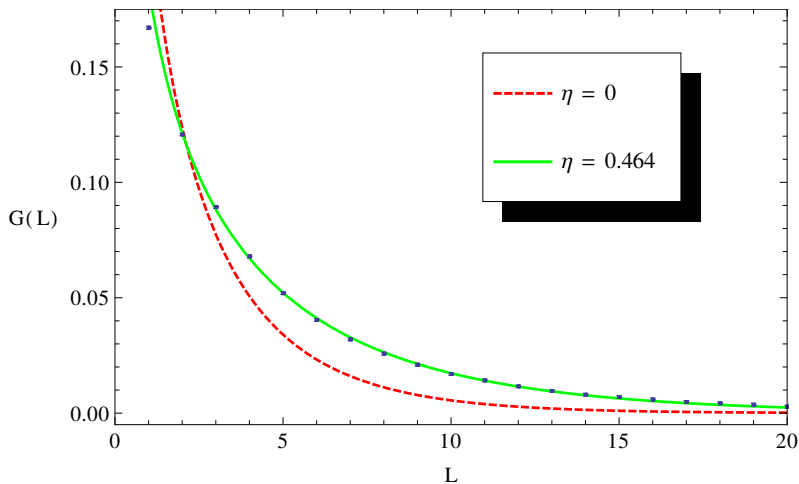


Figure 27: Numerical results for the correlator  $\langle \phi_{i+L,j} \phi_{i,j} \rangle$  in the presence of defects. The density of defects is  $\eta = \rho v_d = 0.464$ , and the scale of the defects is the lattice spacing ( $v_d = a^2$ ). The lattice size is  $80 \times 80$  and the mass parameter is  $m_1 = 0.3$ . The number of iterations is  $N = 10^6$  and the results are averaged over 5 different lattice configurations. The interpolating curve is given by Eq. (8.2).

standard case  $\eta = 0$ . To find an appropriate interpolating curve we follow different approaches. The first is simply to assume a modified dispersion relation given by (in Minkowski space)

$$k_0^2 = m^2 + [1 + a_0(\eta)]k_1^2 + b_0(\eta)k_1^4, \quad (8.1)$$

from which we obtain the modified propagator

$$G_\eta^{(1)}(z_0) = \int \frac{d^2k}{(2\pi)^2} \frac{e^{-ik_0 z_0}}{k_0^2 + [1 + a_0(\eta)]k_1^2 + b_0(\eta)k_1^4 + m^2}. \quad (8.2)$$

We can perform the integral numerically and interpolate the data points with respect to the unknown parameters  $a_0(\eta)$  and  $b_0(\eta)$ . The result of the interpolation is in very good agreement with the data, the reduced  $\chi^2$  has a value of  $\chi^2/\nu = 0.93$  (where  $\nu$  is the number of degrees of freedom).

The second approach involves observing that in statistical mechanics the correlation function of a critical system far from the critical point is given, in general, by the expression [62, 63]

$$G_\eta^{(2)}(z_0) = \frac{A}{z_0^\tau} e^{-z_0/\xi} \quad (8.3)$$

where  $A$  is a normalization factor, while  $\xi$  (the correlation length) and  $\tau$  are two critical exponents (i.e. their value depends only on very general properties

of the model, such as dimensionality and symmetries, but it is unaffected by details such as the lattice structure or the value of the critical point). Again, we can interpolate the data points with respect to the unknown parameters  $A$ ,  $\xi$ , and  $\tau$ . We observe that, in this case, the result is not as good as in the previous case; in fact, we have to exclude the first data point, in order to obtain an acceptable reduced  $\chi^2$  of  $\chi^2/\nu = 1.07$ .

Repeating the same measurement for different densities of defects, we always find good agreement between the interpolating curves (8.2) and (8.3), and the data, see Fig. (28). Note, however, that when the density of defects becomes large, the curve (8.2) no longer provides good interpolation (at least not at short scales). This effect could be related to the percolation of defects. In fact, the discrepancy appears at values of  $\eta$  that correspond to the critical region<sup>4</sup> of the percolation phase transition. It is known that the correlation function of the defects changes from an exponential law to a power law at the critical point. We expect such a behavior to have repercussions for the scalar field propagator, too.

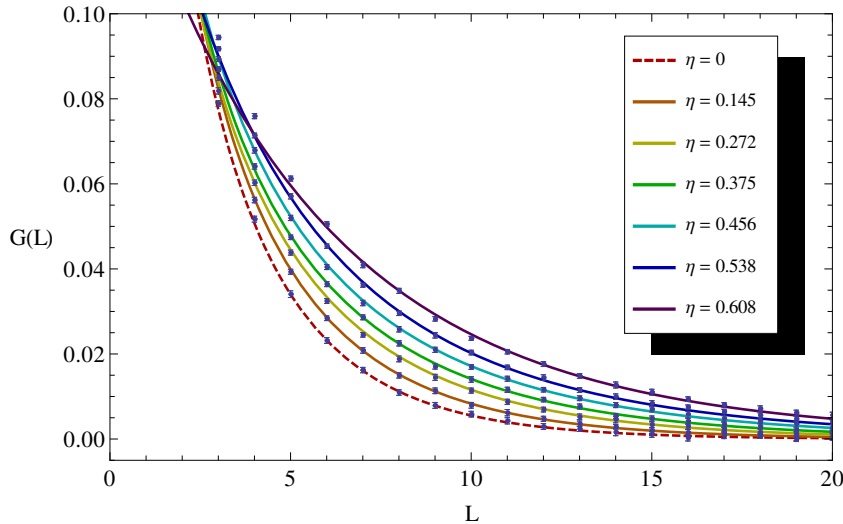


Figure 28: Numerical results for the correlator  $\langle \phi_{i+L,j} \phi_{i,j} \rangle$  in the presence of defects. The density of defects varies from  $\eta = 0$  (bottom line) to  $\eta = 0.608$  (upper line). When the density  $\eta$  reaches the critical region (of the percolation phase transition), Eq. (8.2) no longer provides a good interpolation at short scales.

A third approach to finding the fitting curve to the modified propagator obtained from the numerical calculations is to assume that the only effect of the distribution of defects is the shortening of distances given by Eq. (7.5). In

<sup>4</sup>In a finite lattice, the phase transition does not happen sharply at one critical point, but is smeared over a critical region where there is an increasing probability of observing the transition.

this case, the propagator would be given by Eq. (7.4), with  $z_0$  substituted by  $z'_0 = (1 - \eta)^{1/2} z_0$ . We assume then

$$G_\eta^{(3)}(z_0) = \frac{1}{2\pi(1+c)} K_0 \left( m \sqrt{\frac{1-\eta}{1+c}} |z_0| \right), \quad (8.4)$$

where we have also introduced a free parameter  $c$ . In this way, the propagator in momentum space takes the form

$$\tilde{G}_\eta^{(3)}(k_0, k_1) = \frac{1}{(1+c)(k_0^2 + k_1^2) + (1-\eta)m^2}. \quad (8.5)$$

Comparing this last expression with the Fourier transform of Eq. (8.3), we find good agreement between the two expressions, if we choose  $c \sim \eta\sqrt{2}$ . We can conclude that the propagator (8.4) also provides a good interpolation of the data points. We want to point out that, at this point, this expression is our best candidate, as it depends on just one free parameter and its form is physically motivated by the shortening of distances caused by the distribution of defects.

The coefficients  $a_0(\eta)$  and  $b_0(\eta)$  that appear in Eq. (8.2) have been obtained from the interpolations. Their behavior with respect to the density  $\eta$  is reproduced in Fig. 29. It turns out that they are well-described by power laws:

$$\begin{aligned} a_0(\eta) &= \alpha_a \eta^2, \\ b_0(\eta) &= a^2 \alpha_b \eta^{10}, \end{aligned} \quad (8.6)$$

with  $\alpha_a \simeq 14.07$  and  $\alpha_b \simeq 10.74 \times 10^3$ .

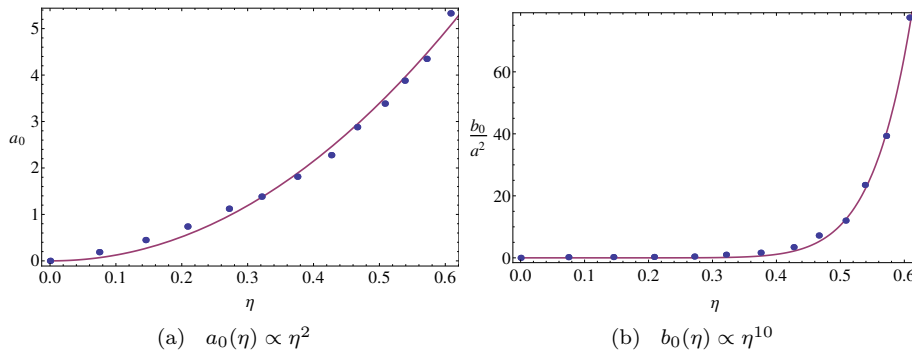


Figure 29: Behavior of the coefficients  $a_0(\eta)$  and  $b_0(\eta)$  in Eq. (8.2) with respect to the defect density  $\eta$ .

In Table 3, we report some explicit values for  $a_0$  and  $b_0$ .

$\eta$	$a_0$	$b_0/a^2$
0.145	0.448	0.25
0.271	1.12	0.434
0.375	1.81	1.66
0.464	2.87	7.21
0.538	3.88	23.5

Table 3: Values of the parameters  $a_0$  and  $b_0$  obtained from the interpolations.

The behaviors of the parameters  $A$ ,  $\tau$  and  $\xi$  in Eq. (8.3) and  $c$  in Eq. (8.4) with respect to the density  $\eta$  are depicted in Fig. 30. They all show linear dependence with respect to  $\eta$

$$A(\eta) = \alpha_A, \quad (8.7a)$$

$$\tau(\eta) = \alpha_\tau + \beta_\tau \eta, \quad (8.7b)$$

$$\xi(\eta) = \alpha_\xi + \beta_\xi \eta, \quad (8.7c)$$

$$c(\eta) = \beta_c \eta, \quad (8.7d)$$

$$(8.7e)$$

where  $\alpha_A \simeq 0.128$ ,  $\alpha_\tau \simeq 0.369$ ,  $\beta_\tau \simeq -0.335$ ,  $\alpha_\xi \simeq 0.302$ ,  $\beta_\xi \simeq 0.412$  and  $\beta_c \simeq 1.41$ .

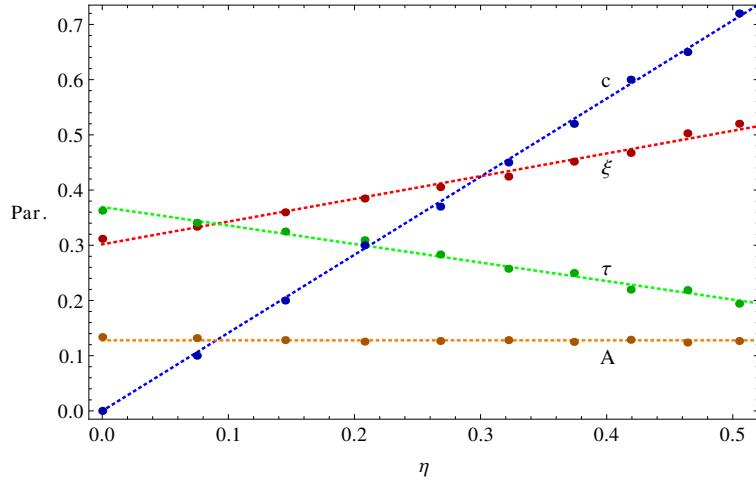


Figure 30: Parameters  $A$ ,  $\tau$ , and  $\xi$  from Eq. (8.3) and  $c$  from Eq. (8.4) as a function of the density of defects  $\eta$ .

In Table 4 we report some of the values obtained for  $A$ ,  $\tau$ , and  $\xi$ .

$\eta$	$A$	$\tau$	$\xi$
0.145	0.128	0.325	0.360
0.268	0.127	0.283	0.405
0.374	0.125	0.250	0.451
0.464	0.124	0.219	0.503
0.505	0.127	0.194	0.520

Table 4: Values of the parameters  $A$ ,  $\tau$ , and  $\xi$  obtained from the interpolations.

### 8.1.1 Continuum limit

The previous results were obtained for a discrete lattice, but the lattice in this context has no physical meaning, as it represents just a cut-off regulator that helps us to compute propagators. Hence, in order to extract physically meaningful results, we have to remove the regulator. This is accomplished by

taking the continuum limit

$$a \rightarrow 0, \quad (8.8)$$

where  $a$  is the lattice spacing.

To achieve this aim, we need to repeat the measurements of the previous section for different lattices, reducing each time the lattice spacing. However, we do not want to modify the other physical parameters of the model defined in terms of  $a$  (the distance  $z_0 = L a$ , the mass  $m = m_1/a$ , and the defect size  $v_d = n a^2$ ).

Therefore, if in the original configuration a defect is represented by  $n$  sites removed from the lattice, when we reduce the lattice spacing ( $a' = \lambda a$ ) it must be represented by  $n' = \lambda^{-2} n$  sites removed from the lattice:

$$\begin{cases} a \rightarrow a' = \lambda a, \\ n \rightarrow n' = \lambda^{-2} n, \end{cases} \implies v'_d = n' a'^2 = n a^2 = v_d. \quad (8.9)$$

In the same way, the physical distance  $z_0 = L a$  at which we perform the measurement stays the same, while the distance  $L$  measured in terms of the lattice spacing increases:

$$\begin{cases} a \rightarrow a' = \lambda a, \\ L \rightarrow L' = \lambda^{-1} L, \end{cases} \implies z'_0 = L' a' = L a = z_0. \quad (8.10)$$

Also, the physical mass  $m$  remains unchanged, while the mass parameter  $m_1$  decreases:

$$\begin{cases} a \rightarrow a' = \lambda a, \\ m_1 \rightarrow m'_1 = \lambda m_1, \end{cases} \implies m' = \frac{m'_1}{a'} = \frac{m_1}{a} = m. \quad (8.11)$$

We have already mentioned that reducing the lattice spacing corresponds to an increase in correlation length and fluctuations, so we also need to increase the size of the lattice, to keep finite-size effects negligible.

In practice, we choose to rerun the algorithm with different lattice spacings given by  $a' = \lambda a$ , with  $\lambda = \{1; 1/2; 1/3; 1/4; 1/5; 1/6\}$ . For these scales, we find (by studying the free theory) that a good choice of lattice sizes is  $\{80 \times 80; 200 \times 100; 250 \times 100; 320 \times 100; 400 \times 150; 450 \times 200\}$ . We repeat the measurement for different densities of defects  $\eta = \{0.074, 0.143, 0.233, 0.385, 0.464, 0.594\}$ .

In the results, we choose to represent distances not in terms of the lattice spacing, but in units of the defect size  $l_d = \sqrt{v_d}$ , i.e.  $z_0 = L l_d$ . With this definition,  $L$  does not depend on  $\lambda$ .

The values of the correlator  $G(L)$ , evaluated at fixed values of  $L$  for different values of the lattice spacing scale  $\lambda$ , are reproduced in the left column of Fig. 31 and Fig. 32 for different values of  $\eta$ . The continuum limit  $\lambda \rightarrow 0$  is obtained from these data through linear interpolation. It is reproduced in the right column compared to the standard propagator (7.4) and to the modified propagator (8.2) (obtained from the interpolations shown in Fig. 28).

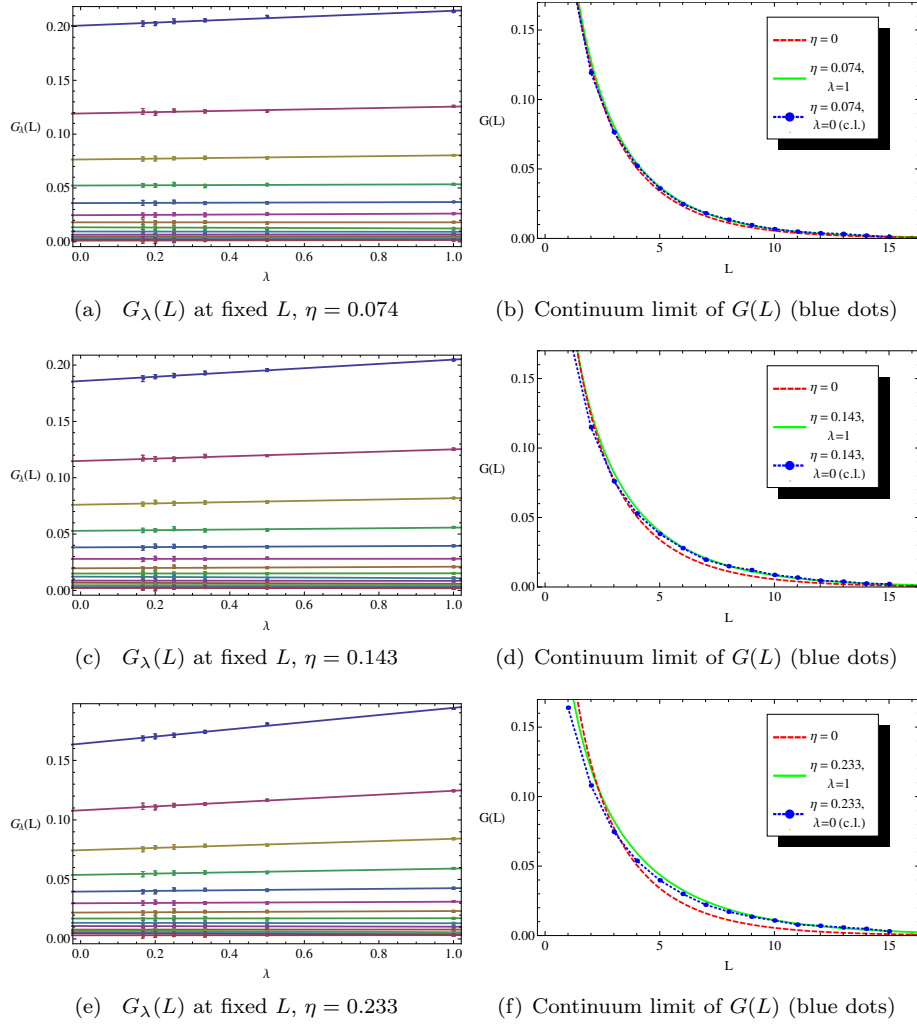


Figure 31: On the left, the correlator  $G_\lambda(L)$  is represented at fixed values of  $L$  as a function of the scale factor  $\lambda$  (the lattice spacing is  $a' = \lambda a$ ), while the distance  $L$  is measured in units of the defect size ( $z_0 = L\sqrt{v_d}$ ). The continuum limit corresponds to  $\lambda = 0$ . On the right, the continuum limit (blue dotted line) is compared to the lattice results from Fig. 28 (green solid line) and to the unmodified propagator from Fig. 26 (red dashed line).

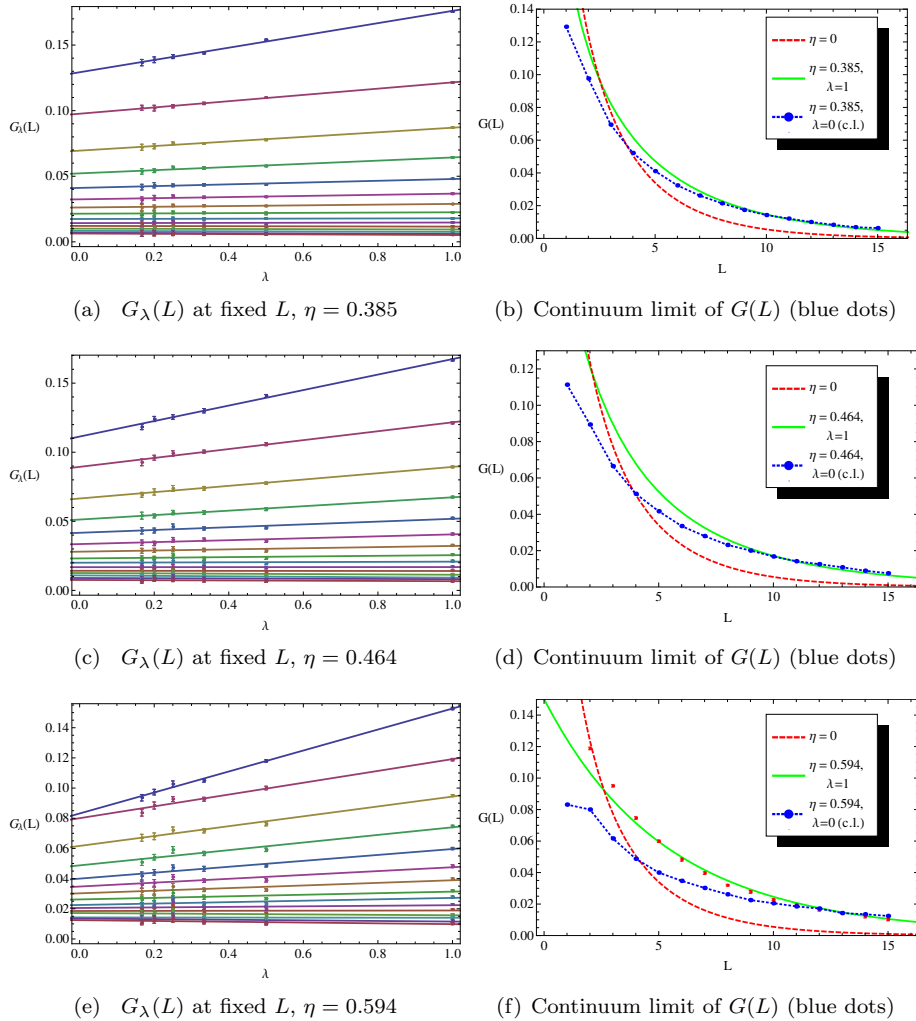


Figure 32: As in the previous Figure 31 for other values of the parameter  $\eta$ . We note that discrepancies between the lattice results from Fig.28 and the corresponding continuum limits increase in line with the density  $\eta$  of defects.

We observe that the continuum limits (Figs. 31 and 32) differ from the results shown in Fig. 28, and in particular they cannot be described by the first proposed propagator Eq. (8.2), at least not at short scales (not even when adding higher powers of  $k_1$  into Eq. (8.1)). On the other hand, it seems that at large scales Eq. (8.2) still provides a good interpolation for the data. In the left side of Figs. 31 and 32, we observe indeed that the slope of the line passing through  $G(L, \lambda = 0)$  and  $G(L, \lambda = 1)$  decreases as  $L$  increases, so that, at large  $L$ , the propagator seems to be almost independent of the lattice spacing scale. Furthermore, we point out that these effects increase in line with the density of defects.

When we consider the second and the third proposed propagators given by, respectively, Eq. (8.3) and Eq. (8.4), we observe that they still provide a good

interpolation of the continuum limit data points. Considering, for example, the case  $\eta = 0.464$ , in Fig. 33 we compare how the first and third proposed propagators interpolate the continuum limit data. We can see that Eq. (8.4)

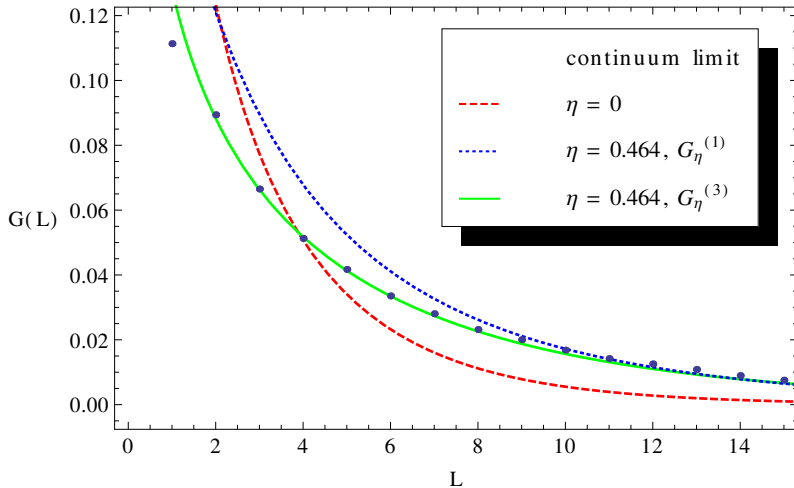


Figure 33: Continuum limit for the correlator  $\langle \phi_{i+L,j} \phi_{i,j} \rangle$  in the presence of a distribution of defects of density  $\eta = 0.464$ . We observe that  $G_\eta^{(3)}$  (Eq. (8.4)), represented by a green solid line, provides an acceptable interpolation of the data in this case, while  $G_\eta^{(1)}$  (Eq. (8.2)), represented by a blue dotted line, provides a good interpolation only at large scales. We omit to plot the second proposed propagator  $G_\eta^{(2)}$  (Eq. (8.3)), which also provides a good interpolation and whose curve overlaps with  $G_\eta^{(3)}$ .

indeed provides a good interpolation of the data, while Eq. (8.2) does not do so. Changing the defect density  $\eta$  we obtain similar results. We observe that the free parameters of Eqs. (8.3), (8.4) ( $A$ ,  $\tau$ ,  $\xi$ ,  $c$ ) are, even in this case, related linearly to  $\eta$  as in Eq. (8.7). The coefficients now take the values  $\alpha_A \simeq 0.112$ ,  $\alpha_\tau \simeq 0.378$ ,  $\beta_\tau \simeq -0.432$ ,  $\alpha_\xi \simeq 0.307$ ,  $\beta_\xi \simeq 0.556$ , and  $\beta_c \simeq 3.27$ , see Fig. 34.

From these considerations, we are led to exclude  $G_\eta^{(1)}$  (Eq. (8.2)) as a valid description of the data in the continuum limit. On the other hand, both  $G_\eta^{(2)}$  and  $G_\eta^{(3)}$  give good interpolation of the data but, for the reasons already discussed, we are inclined to choose the second one. We conclude that, from the measurements we made, the expression (8.4)

$$G_\eta(z_0) = \frac{1}{2\pi(1 + \beta_c\eta)} K_0 \left( m \sqrt{\frac{1-\eta}{1 + \beta_c\eta}} |z_0| \right), \quad \beta_c \simeq 3.27, \quad (8.12)$$

provides a good description of the 2-dimensional scalar propagator in a continuum spacetime foam model made of extended time-dependent defects with density  $\eta$ . From the corresponding expression in momentum space, Eq. (8.5), we can finally extract the dispersion relation (in Minkowski space)

$$k_0^2 - k_1^2 = \frac{1-\eta}{1 + \beta_c\eta} m^2, \quad (8.13)$$

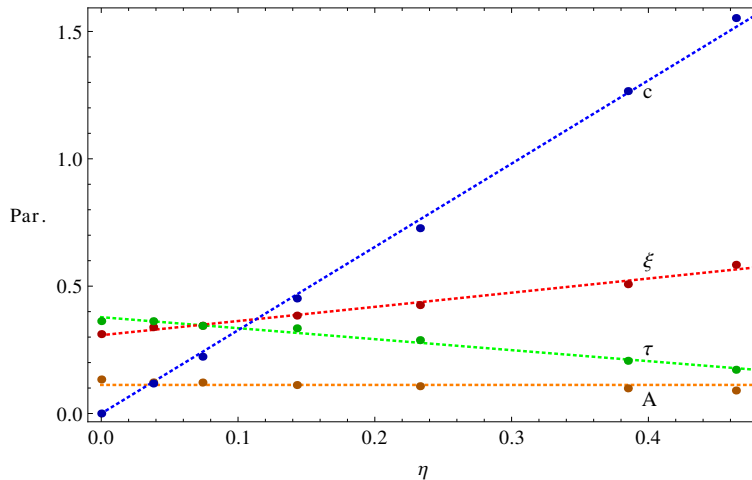


Figure 34: Parameters  $A$ ,  $\tau$ , and  $\xi$  from Eq. (8.3) and  $c$  from Eq. (8.4) as a function of the density of defects  $\eta$  in the continuum limit case.

that describes a non-dispersive medium. The only effect produced by the distribution of defects is a rescaling of the mass of the scalar field. We observe that this is analogous to what has been obtained in part II (see Eq. (3.33)), even if in that case the defects were point-like, while here they have an extension.

### 8.1.2 Results in 3 and 4 dimensions

In this subsection, we want to briefly present our findings for 3- and 4-dimensional lattices. For these cases, we consider only the lattice theory without computing the continuum limit. We observe that, now, the proposed modified propagator  $G_\eta^{(1)}$  (Eq. (8.2) generalized to higher dimensions) does not provide good interpolation of the data, even at the lattice level. This observation provides further confirmation that we must reject it as a possible expression for the numerical modified propagator. On the other hand, we observe that the generalization to higher dimensions of Eq. (8.12) still provides a good interpolation of the data for any value of  $\eta$ , as shown in Figs. 35 and 36 for  $\eta = 0.464$ .

From these observations, we are led to conclude that the modified scalar propagator on a lattice filled with a distribution of defects of density  $\eta$  is well-described in 3 dimensions by the expression

$$G_\eta(z_0) = \frac{1}{4\pi(1-\eta)^{1/3}z_0} e^{-m\left(\frac{1-\eta}{1+\beta_c^{(3)}\eta}\right)^{1/3}z_0}, \quad \beta_c^{(3)} \simeq 1.5, \quad (8.14)$$

and in 4 dimensions by the expression

$$G_\eta(z_0) = \frac{m}{4\pi^2(1-\eta)^{1/4}z_0} K_1\left(m\left(\frac{1-\eta}{1+\beta_c^{(4)}\eta}\right)^{1/4}z_0\right), \quad \beta_c^{(4)} \simeq 25. \quad (8.15)$$

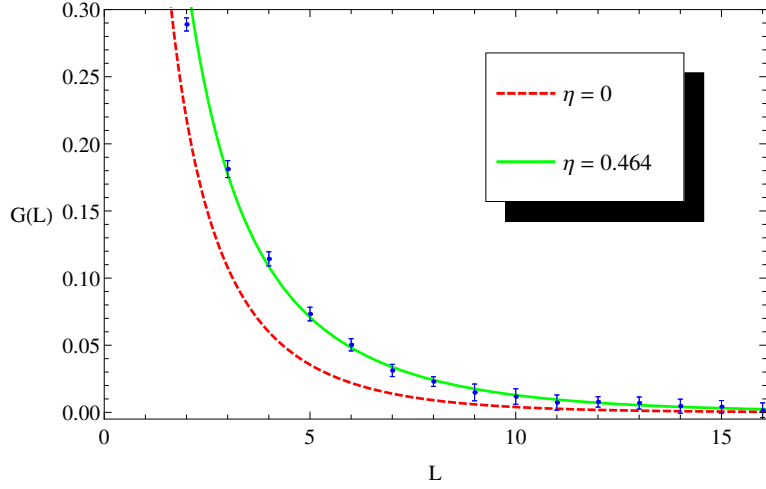


Figure 35: Numerical results for the 3-dimensional correlator  $\langle \phi_{i+L,j,k} \phi_{i,j,k} \rangle$  in the presence of defects. The density of defects is  $\eta = \rho v_d = 0.464$ , while the scale of the defects is the lattice spacing ( $v_d = a^3$ ). The lattice size is  $60 \times 60 \times 60$  and the mass parameter is  $m_1 = 0.3$ . The number of iterations is  $N = 5 \times 10^5$  and the results are averaged over 3 different lattice configurations. The interpolating curve is given by Eq. (8.14).

From these expressions, we can extract the (Minkowskian) dispersion relations

$$k_0^2 - k_1^2 - k_2^2 = \left( \frac{1 - \eta}{1 + \beta_c^{(3)} \eta} \right)^{2/3} m^2, \quad (8.16)$$

in 3 dimensions and

$$k_0^2 - k_1^2 - k_2^2 - k_3^2 = \left( \frac{1 - \eta}{1 + \beta_c^{(4)} \eta} \right)^2 m^2, \quad (8.17)$$

in 4 dimensions, which are analogous to the result obtained in 2 dimensions, see Eq. (8.13).

## 8.2 Static defects

We now consider a lattice spacetime foam model made of static defects. The crucial difference with respect to the previous case is that spacetime is now not isotropic, see Fig. 37. With time-dependent defects, the shortening of lengths affects both the spatial directions and the time direction. Instead, with static defects, the shortening of lengths only affects the spatial directions, while the time direction remains unchanged.

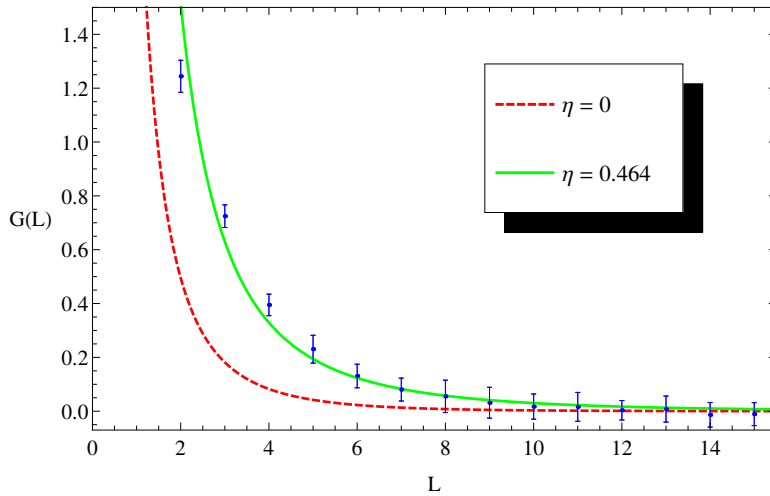


Figure 36: Numerical results for the 4-dimensional correlator  $\langle \phi_{i+L,j,k,l} \phi_{i,j,k,l} \rangle$  in the presence of defects. The density of defects is  $\eta = \rho v_d = 0.464$ , while the scale of the defects is the lattice spacing ( $v_d = a^4$ ). The lattice size is  $72 \times 50 \times 50 \times 50$  and the mass parameter is  $m_1 = 0.3$ . The number of iterations is  $N = 3 \times 10^5$  and the results are averaged over 3 different lattice configurations. The interpolating curve is given by Eq. (8.15).

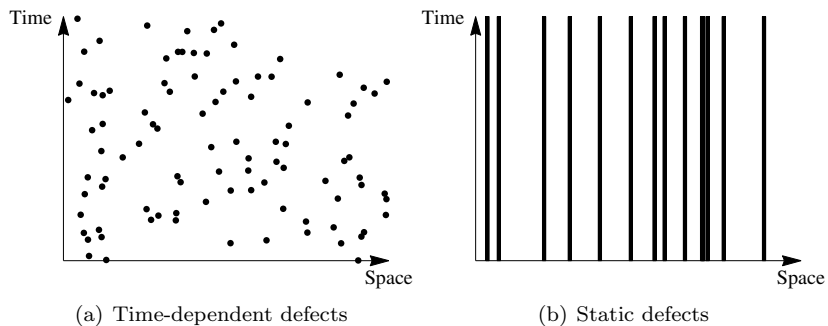


Figure 37: Fig. (a) a distribution of time-dependent defects in a 2-dimensional spacetime is isotropic. Fig. (b) a distribution of static defects is not isotropic.

In Figs. 38 and 39, we show the behavior of the scalar propagator on a lattice filled with static defects in 3 and 4 dimensions.

We observe that the data points, measured in the spatial direction, are well-described by the expressions found in the previous section Eqs. (8.14) and (8.15). Instead, when we measure the correlator along the time direction, we observe a different behavior. Consider the 3-dimensional case, we find that, in

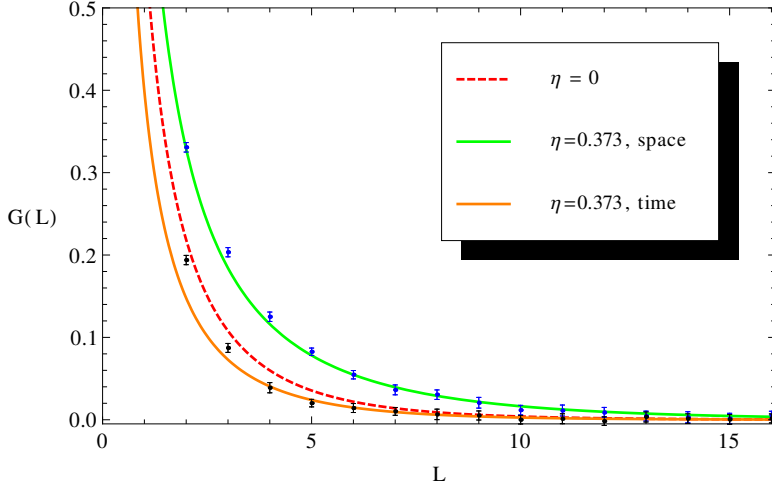


Figure 38: Numerical results for the 3-dimensional correlator  $\langle \phi_{i+L,j,k} \phi_{i,j,k} \rangle$  in the presence of static defects. The density of defects is  $\eta = 0.464$ . The lattice size is  $60 \times 60 \times 60$  and the mass parameter is  $m_1 = 0.3$ . The number of iterations is  $N = 5 \times 10^5$  and the results are averaged over 3 different lattice configurations. We measure the correlator both in the spatial direction (blue data points) and in the time direction (black data points). The interpolating curves are obtained from the correlator (in momentum space) given by Eq. (8.18).

momentum space, the correlator is well-described by the expression

$$\tilde{G}_\eta(k) = \frac{\left(1 + \beta_c^{(3s)} \eta\right)^{1/3}}{(1 - \eta)^{2/3} \left(k_0^2 + \left(\frac{1 + \beta_c^{(3s)} \eta}{1 - \eta}\right)^{2/3} \vec{k}^2 + m^2\right)}. \quad (8.18)$$

In fact, when we evaluate the Fourier transform of this correlator in a spatial direction, we obtain exactly Eq. (8.14). On the other hand, Fourier transforming the above expression along the time direction gives a result proportional to the standard correlator in a space with no defects. From Eq. (8.18), we can extract the 3-dimensional dispersion relation (in Minkowski space)

$$k_0^2 = \left(\frac{1 + \beta_c^{(3s)} \eta}{1 - \eta}\right)^{2/3} \vec{k}^2 + m^2. \quad (8.19)$$

Note that, in this case, the mass of the field is not rescaled. This result is similar to what we found in Sec. 6.2.3, where we showed that a spacetime foam model made of static defects is analogous, for a scalar field, to a non-dispersive medium with a modified index of refraction (see Eq. (6.70)).

Analogous reasoning can be made in 4 dimensions, from which we obtain the 4-dimensional dispersion relation (in Minkowski space)

$$k_0^2 = \left(\frac{1 + \beta_c^{(4s)} \eta}{1 - \eta}\right)^2 \vec{k}^2 + m^2. \quad (8.20)$$

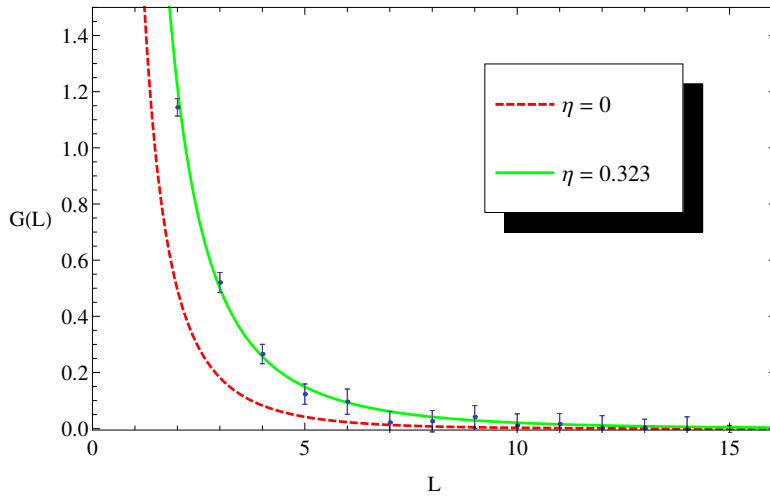


Figure 39: Numerical results for the 4-dimensional correlator  $\langle \phi_{i+L,j,k,l} \phi_{i,j,k,l} \rangle$  in the presence of defects measured along a spatial direction. The density of defects is  $\eta = 0.464$ . The lattice size is  $72 \times 50 \times 50 \times 50$  and the mass parameter is  $m_1 = 0.3$ . The number of iterations is  $N = 3 \times 10^5$  and the results are averaged over 3 different lattice configurations. The interpolating curve is given by Eq. (8.15) for a different value of the parameter  $\beta_c^{4s}$ .

It is important to note that the parameter  $\eta$  describes, even for static defects, the portion of sites removed from the lattice, which is given by

$$\eta = \rho_s v_{d-1} L_0, \quad (8.21)$$

where  $\rho_s$  is the number density of defects in the spatial hypersurface,  $v_{d-1}$  the spatial volume of one defect, and  $L_0$  the dimensionless temporal size of the lattice ( $L_0 = T/a$ ). The correlator (8.18) can be equivalently re-expressed in terms of the fraction of sites removed from the spatial hypersurface,  $\eta_s = \rho_s v_{d-1}$ . In this case, the dispersion relation for static defects in 4-dimensional spacetime, Eq. (8.20), can be rewritten in the form

$$k_0^2 = \left( \frac{1 + \tilde{\beta}_c^{(4s)} \rho_s v_{d-1}}{1 - \rho_s v_{d-1}} \right)^{2/3} \vec{k}^2 + m^2, \quad \text{lattice result}, \quad (8.22)$$

for a different value of the parameter  $\tilde{\beta}_c^{(4s)}$ . This expression is very similar to the result obtained in Sec. 6.2.3. From Eq. (6.70), using the arguments given in Sec. 6.3.4 to generalize the result to higher dimensions, the analytic dispersion relation for a massless scalar field in a 4-dimensional spacetime foam model made of defects obtained from Minkowski spacetime by surgery turns out to be

$$k_0^2 = \left( \frac{1}{1 - \rho_s v_{d-1}} \right)^{2/3} \vec{k}^2, \quad \text{analytic result}. \quad (8.23)$$

## Part V

# Regularized black hole from extended defect metric

In this part, we deviate a little from the general framework of the previous parts. In fact, we consider the defect metric (6.1) not in the context of spacetime foam, as a microscopic fluctuation of spacetime, but rather as a possible regularization of the Schwarzschild black hole. Such an idea was proposed and discussed in Refs. [85, 86, 87].

Consider the case where the defect radius  $b$  is smaller than the Schwarzschild radius  $\ell$ . In the exterior region  $r > \ell$ , the defect metric is equivalent to the Schwarzschild metric (from the results of Sec. 6, we know that the two metrics are diffeomorphic for  $r > b$ ). Instead, in the interior region  $r < \ell$ , while the Schwarzschild metric is singular at  $r = 0$ , the defect metric turns out to be regular everywhere, since the defect of radius  $b$  removes the singular point  $r = 0$  from spacetime. Take, for example, the Kretschmann curvature scalar given in Eq. (6.10), which in spherical coordinates becomes  $K = 12\ell^2/r^3$  both for the Schwarzschild metric and for the defect metric. We see immediately that this quantity is singular in the Schwarzschild metric at  $r = 0$ . Instead, in the defect metric, the radius is constrained to be  $r \geq b > 0$ , and consequently  $K$  is regular everywhere. We remember also that both metrics are perfectly acceptable solutions of the vacuum Einstein field equations.

We have argued that the defect metric (6.2) can provide a simple regularization of the Schwarzschild metric, but we also have to take into account that, while the Schwarzschild topology is simply  $\mathbb{R}^2 \times S^2$ , the defect exhibits a non-trivial topology  $\mathbb{R} \times (\mathbb{R}P^3 - \{0\})$ . So, on the one hand, we are able to solve the singularity problem of the Schwarzschild metric by replacing it with the defect metric. But, on the other hand, we have to explain the emergence of the nontrivial topology of the defect, and we remember that classical general relativity cannot account for topology changes (but they may possibly occur in a quantum theory of gravity).

In the following, we investigate geodesics in the defect metric and establish that closed time-like curves can appear in the regularized version of an eternal black hole. However, these causally violating paths disappear if we consider a non-eternal model of black hole described, for example, as the result of a star collapse.

## 9 Geodesics

### 9.1 Metric and geodesic equations

For convenience, we restate here the defect metric (6.1)

$$ds^2 = - \left( 1 - \frac{\ell}{\sqrt{y^2 + b^2}} \right) dt^2 + \frac{\frac{y^2}{y^2 + b^2}}{1 - \frac{\ell}{\sqrt{y^2 + b^2}}} dy^2 + (y^2 + b^2)(dz^2 + \sin^2 z dx^2). \quad (9.1)$$

To obtain the geodesic equations, we follow the Lagrangian approach (see, for example, Ref. [88]). We rewrite the metric (9.1) in the more general form

$$ds^2 = g_{\mu\nu} dx^\mu dx^\nu = -A(y)dt^2 + B(y)dy^2 + W(y)(dz^2 + \sin^2 z dx^2), \quad (9.2)$$

where

$$A(y) = 1 - \frac{\ell}{\sqrt{y^2 + b^2}}, \quad B(y) = \frac{\frac{y^2}{y^2 + b^2}}{1 - \frac{\ell}{\sqrt{y^2 + b^2}}}, \quad W(y) = y^2 + b^2. \quad (9.3)$$

Then, we can define the Lagrangian

$$\mathcal{L} = -g_{\mu\nu} \frac{dx^\mu}{d\tau} \frac{dx^\nu}{d\tau}, \quad (9.4)$$

whose Euler-Lagrange equations, it can be shown, are equivalent to the standard geodesic equations

$$\frac{d}{d\tau} \frac{\partial \mathcal{L}}{\partial \dot{x}^\mu} - \frac{\partial \mathcal{L}}{\partial x^\mu} = 0 \quad \Longleftrightarrow \quad \frac{d^2 x^\mu}{d\tau^2} + \Gamma_{\nu\lambda}^\mu \frac{dx^\nu}{d\tau} \frac{dx^\lambda}{d\tau} = 0. \quad (9.5)$$

Moreover, evaluating the Lagrangian along a geodesic, we obtain the constraint

$$\mathcal{L} = \epsilon, \quad (9.6)$$

where  $\epsilon = +1, 0, -1$ , respectively, for time-like, null-like, and space-like geodesics.

For the metric (9.2), the Lagrangian (9.4) turns out to be

$$\mathcal{L} = A(y)\dot{t}^2 - B(y)\dot{y}^2 - W(y)(\dot{z}^2 + \sin^2 z \dot{x}^2), \quad (9.7)$$

where  $\dot{x}^\mu = dx^\mu/d\tau$ .

We start by considering the Euler-Lagrange equation of  $z(\tau)$

$$\frac{d}{d\tau}(W(y)\dot{z}) - W(y)\sin z \cos z \dot{x}^2 = 0. \quad (9.8)$$

We note that a solution is given simply by

$$z(\tau) = \text{const} = \frac{\pi}{2}. \quad (9.9)$$

Next, we observe that  $t(\tau)$  and  $x(\tau)$  are cyclic coordinates (that is, only their derivatives appear in the Lagrangian) and therefore are associated with conserved quantities. Their equations are

$$\frac{d}{d\tau}(A(y)\dot{t}) = 0, \quad \frac{d}{d\tau}(W(y)\dot{x}) = 0, \quad (9.10)$$

which give

$$\dot{t} = \frac{E}{A(y)}, \quad \dot{x} = \frac{L}{W(y)}, \quad (9.11)$$

where  $E$  and  $L$  are constants. The results obtained so far are a consequence of the fact that the metric is time-independent and spherically symmetric.

For the radial component  $y(\tau)$ , we do not need to write the Euler-Lagrange equation, it is simpler to substitute the solutions for  $\dot{t}$ ,  $\dot{z}$  and  $\dot{x}$  in the Lagrangian and impose the constraint (9.6). We obtain

$$\frac{E^2}{A(y)} - B(y)\dot{y}^2 - \frac{L^2}{W(y)} = \epsilon, \quad (9.12)$$

which can be rewritten as

$$\dot{y}^2 + \frac{\epsilon}{B(y)} + \frac{L^2}{B(y)W(y)} - \frac{E^2}{B(y)A(y)} = 0. \quad (9.13)$$

Substituting the explicit expressions of  $A(y)$ ,  $B(y)$ , and  $W(y)$  from Eq. (9.1), we get

$$\dot{y}^2 + \frac{\epsilon \left(1 - \frac{\ell}{\sqrt{y^2 + b^2}}\right)}{1 - \frac{b^2}{y^2 + b^2}} + \left(1 - \frac{\ell}{\sqrt{y^2 + b^2}}\right) \frac{L^2}{y^2} - \frac{E^2}{1 - \frac{b^2}{y^2 + b^2}} = 0, \quad (9.14)$$

which, as expected, reduces to the radial geodesic equation for the Schwarzschild metric in the limit  $b \rightarrow 0$

$$b \rightarrow 0 \implies \dot{y}^2 + \epsilon \left(1 - \frac{\ell}{y}\right) + \left(1 - \frac{\ell}{y}\right) \frac{L^2}{y^2} - E^2 = 0. \quad (9.15)$$

We can simplify Eq. (9.14) by rewriting it in terms of the variable  $w = W(y) = y^2 + b^2$ ,

$$\dot{y} = \frac{1}{2y} \frac{d}{d\tau}(y^2 + b^2) = \frac{1}{2y} \dot{w}. \quad (9.16)$$

Inserting this result into Eq. (9.14), we arrive at

$$\dot{w}^2 + 4 \left(1 - \frac{\ell}{\sqrt{w}}\right) (\epsilon w + L^2) - 4E^2 w = 0. \quad (9.17)$$

## 9.2 Massless case

If we consider the case  $\ell = 0$  (defect of zero mass), Eq. (9.17) simplifies and a general analytic solution for the geodesics can be found easily. We have

$$\ell = 0 \implies \dot{w}^2 + 4w(\epsilon - E^2) + 4L^2 = 0, \quad (9.18)$$

whose solutions are

$$w(\tau) = (E^2 - \epsilon)(\tau \pm c)^2 + \frac{L^2}{E^2 - \epsilon}. \quad (9.19)$$

Since  $y = \pm\sqrt{w - b^2}$ , we arrive at

$$y(\tau) = \begin{cases} y^{(+)}(\tau) = +\sqrt{(E^2 - \epsilon)(\tau + c)^2 + \frac{L^2}{E^2 - \epsilon} - b^2}, & \tau \geq 0, \\ y^{(-)}(\tau) = -\sqrt{(E^2 - \epsilon)(\tau - c)^2 + \frac{L^2}{E^2 - \epsilon} - b^2}, & \tau < 0, \end{cases} \quad (9.20)$$

where the integration constant  $c$  is determined by the condition  $y(0) = 0$ :

$$c = \sqrt{\frac{b^2}{E^2 - \epsilon} - \frac{L^2}{(E^2 - \epsilon)^2}}. \quad (9.21)$$

Substituting the result (9.20) into the equation for the angular coordinate  $x$  (Eq. (9.11)), we obtain

$$x(\tau) = \begin{cases} x^{(+)}(\tau) = x_0 + \arctan\left(\frac{E^2 - \epsilon}{L}(\tau + c)\right), & \tau \geq 0, \\ x^{(-)}(\tau) = -x_0 + \arctan\left(\frac{E^2 - \epsilon}{L}(\tau - c)\right), & \tau < 0. \end{cases} \quad (9.22)$$

The equation for the time coordinate is trivial when  $\ell = 0$  and gives

$$t(\tau) = t_0 + E\tau. \quad (9.23)$$

We recall that the other angular coordinate has been fixed to  $z(\tau) = \pi/2$ , so we have completely solved the geodesic equations.

In order to represent graphically this solution, we have to change variables from the set  $(t, y, z, x)$  to the standard spherical coordinates  $(t, r, \theta, \phi)$ . We recall that these two systems of coordinates are related by the transformations (see Eq. (6.7))

$$r = \begin{cases} \sqrt{y^2 + b^2}, & y > 0, \\ \sqrt{y^2 + b^2}, & y < 0. \end{cases} \quad \theta = \begin{cases} z, \\ \pi - z, \end{cases} \quad \phi = \begin{cases} x, \\ x + \pi, \end{cases} \quad (9.24)$$

The geodesic solution in the spherical coordinate system turns out to be

$$\begin{cases} t(\tau) = t_0 + E\tau, \\ r(\tau) = \Theta(\tau)\sqrt{(y^{(+)}(\tau))^2 + b^2} + \Theta(-\tau)\sqrt{(y^{(-)}(\tau))^2 + b^2}, \\ \theta(\tau) = \frac{\pi}{2}, \\ \phi(\tau) = \Theta(\tau)x^{(+)}(\tau) - \Theta(-\tau)\left(x^{(-)}(\tau) + \pi\right), \end{cases} \quad (9.25)$$

where  $\Theta(\tau)$  is the Heaviside step function. The result is plotted in Fig. 40. We observe that, when  $b$  goes to zero, these equations describe geodesics in Minkowski spacetime.

### 9.3 Massive case

In the case of a massive defect,  $\ell > 0$ , the geodesic equations become much more complicated and cannot be solved in the general case. Therefore, in the following, we consider separately the special cases of a null-like particle ( $\epsilon = 0$ ) and a time-like particle ( $\epsilon = +1$ ), both restricted to the simplest situation of radial motion ( $L = 0$ ) for which analytic solutions can be found. The case in which the motion of the particle also has an angular component could be studied numerically but, since it is not possible to obtain an analytic solution, we will not consider it in this instance.

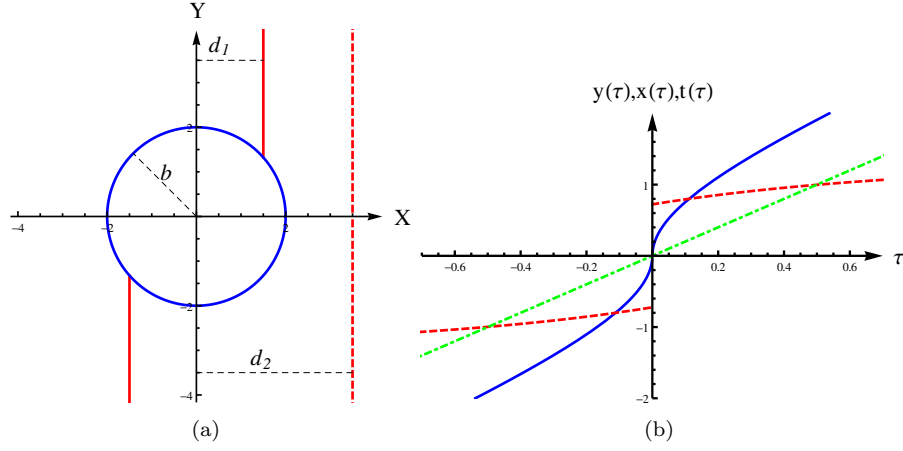


Figure 40: Fig. (a), geodesics from Eq. (9.25) in the plane  $\theta = \pi/2$  for  $b = 2$ ,  $\epsilon = 0$ ,  $E = 2$ ,  $x_0 = 0$  and impact parameters  $d_1 = 3/2 < b$  and  $d_2 = 7/2 > b$  (the impact parameter is given by  $d = \sqrt{L^2/(E^2 - \epsilon)}$ ). Fig. (b), radial geodesic (Eq. (9.20)), blue solid line, angular geodesic (Eq. (9.22)), red dashed line, and time geodesic (Eq. (9.23)), green dot-dashed line, evaluated for the same set of parameters ( $d_1 < b$ ).

### 9.3.1 Null-like geodesics

In order to study the case  $\ell \neq 0$ , we begin by considering the simplest possibility of a massless particle ( $\epsilon = 0$ ) moving in the radial direction ( $L = 0$ ). Then, the radial equation (9.14) reduces to

$$\dot{y}^2 - \frac{y^2 + b^2}{y^2} E^2 = 0, \quad (9.26)$$

whose solution is

$$y(\tau) = \begin{cases} y^{(+)}(\tau) = \sqrt{E^2 (\tau + b/E)^2 - b^2}, & \tau > 0, \\ y^{(-)}(\tau) = -\sqrt{E^2 (\tau - b/E)^2 - b^2}, & \tau < 0, \end{cases} \quad (9.27)$$

where again the integration constant has been chosen so that  $y(0) = 0$ .

Since  $L = 0$ , the equation for the angular coordinate  $x$  reduces to  $\dot{x} = 0$ , which gives the solution  $x = \text{const.}$  The only other equation we need to solve is that for the time coordinate:

$$\dot{t} = \frac{E}{1 - \frac{\ell}{\sqrt{y(\tau)^2 + b^2}}}. \quad (9.28)$$

Because of the simplified situation we are studying, this is the only equation in which the mass  $\ell$  appears, which means that all differences with respect to the

flat case  $\ell = 0$  are contained in this equation. Solving it yields the solution

$$t(\tau) = \begin{cases} t^{(+)}(\tau) = t_0 + E\tau + \ell \log \left| \frac{E\sqrt{(\tau + b/E)^2/\ell - 1}}{b/\ell - 1} \right|, & \tau > 0, \\ t^{(-)}(\tau) = t_0 + E\tau - \ell \log \left| \frac{E\sqrt{(\tau - b/E)^2/\ell - 1}}{b/\ell - 1} \right|, & \tau < 0. \end{cases} \quad (9.29)$$

In Fig. 41, we show the behavior of the two solutions  $y(\tau)$  and  $t(\tau)$  for the two cases  $b > \ell$  and  $b < \ell$ . In the first case, the particle approaching the defect behaves almost as in the flat case  $\ell = 0$ , the only difference being that the velocity decreases in proximity to the defect. In the second case, the particle behaves almost as in the Schwarzschild metric. It takes an infinite amount of time to reach the event horizon, but once crossed, instead of falling into singularity (which is shielded by the defect), the particle can proceed toward the horizon on the other side (reaching it again in an infinite amount of time).

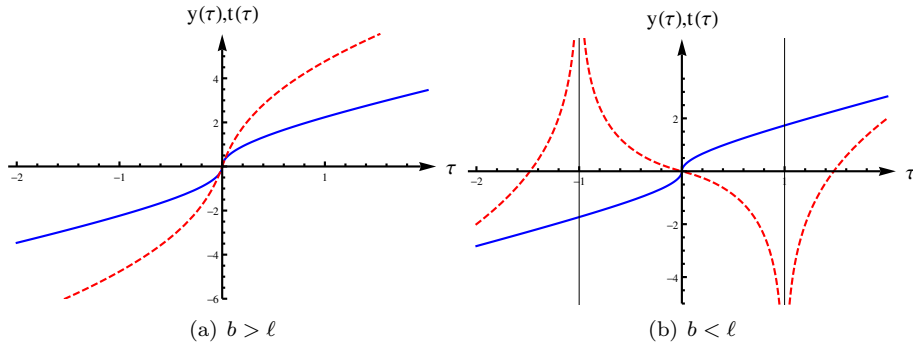


Figure 41: Radial null geodesic for  $b > \ell$  (a) and  $b < \ell$  (b). The radial component  $y(\tau)$  (Eq. (9.27)) is represented by a blue solid line, while the time component  $t(\tau)$  (Eq. (9.29)) is represented by a red dashed line.

We wish to point out that the coordinates used here describe the behavior of the particle as seen by an observer located far away from the event horizon. However, the particle itself, in its own reference frame, has no problem in reaching and crossing the horizon in a finite amount of time.

### 9.3.2 Painlevé-Gullstrand extension

With regard to the last point of the previous subsection, it can be more enlightening to rewrite the solution in terms of Painlevé-Gullstrand (PG) coordinates [97, 98]. PG coordinates describe the point of view of an observer which start with zero velocity at infinity and free-fall radially into the black hole (or defect). They are obtained by the transformation

$$T_+^* = t + 2\ell \left( \sqrt{r/\ell} + \frac{1}{2} \log \left| \frac{\sqrt{r/\ell} - 1}{\sqrt{r/\ell} + 1} \right| \right), \quad (9.30)$$

where we use the relation  $r = \sqrt{y^2 + b^2}$ . Under this change of coordinates, the metric (9.1) becomes

$$ds^2 = -dT_+^{*2} + \left(dr + \sqrt{\ell/r} dT_+^*\right)^2 + r^2 d\Omega^2, \quad (9.31)$$

where  $d\Omega^2 = dz^2 + \sin^2 z dx^2$ . We consider the case  $b < \ell$  (size of the defect smaller than the event horizon) and note that the metric (9.31) is now regular at the horizon, i.e. it provides a future extension of the defect metric. Another interesting feature is that slices of constant time are described by the flat metric

$$ds^2|_{T_+^*=\text{const}} = dr^2 + r^2 d\Omega^2. \quad (9.32)$$

Nonetheless, we must emphasize that such a coordinate system, in the region inside the horizon, is only valid for describing ingoing geodesics ( $\tau < 0$  in Eqs. (9.27), (9.29)) but not outgoing geodesics. This can be seen by calculating the radial velocity

$$r' = \frac{dr}{dT_+^*} = \pm 1 - \sqrt{\frac{\ell}{r}}, \quad (9.33)$$

from which we read that, when  $r < \ell$ , the velocity is always negative. If we use these coordinates to represent outgoing geodesics in the interior region, we find particles moving backward in time, and that the time coordinate  $T_+^*$  is singular at the horizon (see Fig. 42).

To circumvent this problem, it is possible to introduce another set of PG coordinates which corresponds to outgoing radial geodesics (and provides a past extension of the defect metric) by defining

$$T_-^* = t - 2\ell \left( \sqrt{r/\ell} + \frac{1}{2} \log \left| \frac{\sqrt{r/\ell} - 1}{\sqrt{r/\ell} + 1} \right| \right), \quad (9.34)$$

which leads to the metric

$$ds^2 = -dT_-^{*2} + \left(dr^2 - \sqrt{\ell/r} dT_-^*\right)^2 + r^2 d\Omega^2. \quad (9.35)$$

This new set of coordinates, in the region  $r < \ell$ , can only describe outgoing geodesics ( $\tau > 0$ ) but not ingoing geodesics (see Fig. 42).

To summarize, when  $b < \ell$ , the radial null geodesic given by Eqs. (9.27) and (9.29) in its ingoing phase ( $\tau < 0$ ) can be described in the coordinate system  $(T_+^*, r)$  (which provides a future extension of the defect metric), while in its outgoing phase ( $\tau > 0$ ) can be described in the coordinate system  $(T_-^*, r)$  (which provides a past extension to the defect metric). However, it is not possible to visualize the full geodesic in a single coordinate system. To achieve this aim (so that we can better understand the causal structure of the defect metric) we must turn to Kruskal coordinates or Penrose diagrams.

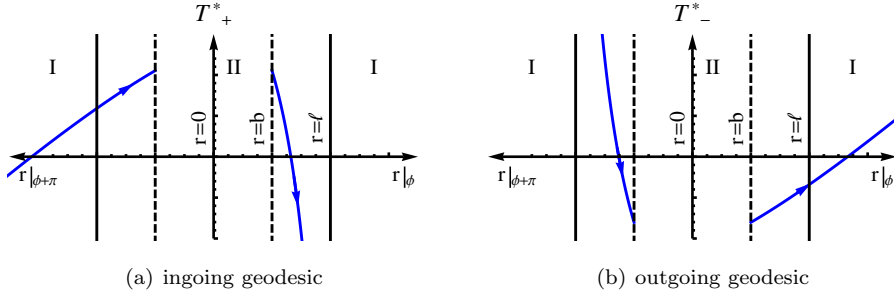


Figure 42: Section of a defect with  $b < \ell$  in PG coordinates (the radial coordinate is positive on both sides of the  $T^*$  axis, while the angular coordinate  $\phi$  changes by  $\pi$ ). Fig. (a) ingoing radial null geodesic described by coordinates  $(T_+, r)$ . Here, region II is a future extension of Schwarzschild spacetime (region I). Fig. (b) outgoing geodesic described by coordinates  $(T_-, r)$ . Region II is now a past extension of Schwarzschild spacetime. The arrows represent the direction of increasing proper time  $\tau$ .

### 9.3.3 Kruskal extension

We now introduce Kruskal coordinates that provide a maximal extension to the defect metric [99]:

$$\begin{cases} T = T_I(t, y) = e^{\frac{\sqrt{y^2+b^2}}{2\ell}} \left| \frac{1}{\ell} \sqrt{y^2+b^2} - 1 \right|^{\frac{1}{2}} \sinh\left(\frac{t}{2\ell}\right), \\ R = R_I(t, y) = e^{\frac{\sqrt{y^2+b^2}}{2\ell}} \left| \frac{1}{\ell} \sqrt{y^2+b^2} - 1 \right|^{\frac{1}{2}} \cosh\left(\frac{t}{2\ell}\right). \end{cases} \quad (9.36)$$

In these coordinates, the defect metric (9.1) becomes

$$ds^2 = \frac{4\ell^3 e^{-\frac{\sqrt{y^2+b^2}}{\ell}}}{\sqrt{y^2+b^2}} (-dT^2 + dR^2) + (y^2+b^2)d\Omega^2, \quad (9.37)$$

where  $y$  must be considered as a function of  $R$  and  $T$ , explicitly

$$r = \sqrt{y^2+b^2} = \ell \left( 1 + W_0 \left( \frac{|R^2 - T^2|}{e} \right) \right), \quad (9.38)$$

where  $W_0(x)$  is the Lambert  $W$  function and  $e$  is the base of the natural logarithm. We observe that the metric (9.37) is regular everywhere.

In Fig. 43, using Kruskal coordinates, we show the behavior of the radial null geodesic (Eqs. (9.27), (9.29)) for  $b > \ell$  and  $b < \ell$  compared to the behavior of the radial null geodesic in the standard Schwarzschild metric ( $b = 0$ ).

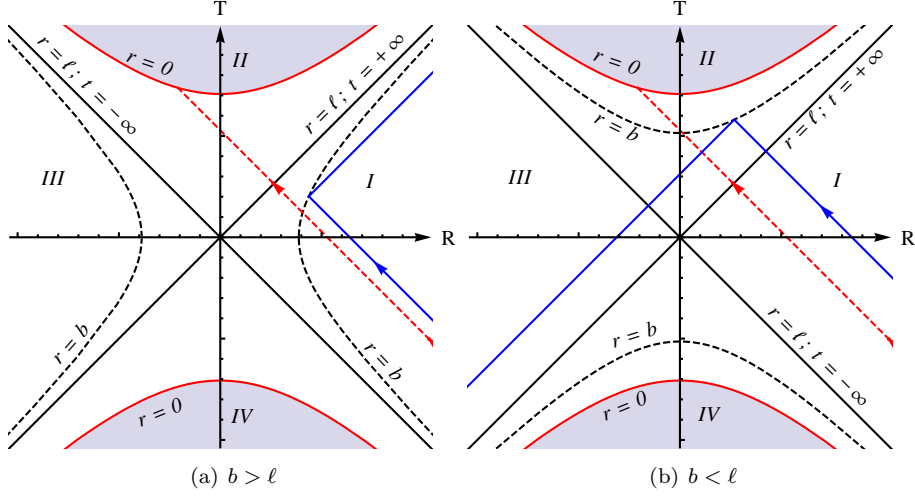


Figure 43: Radial null geodesic in Kruskal coordinates for  $b > \ell$  (a) and  $b < \ell$  (b). The standard Schwarzschild geodesic is represented by a red dashed line (that ends on the singularity at  $r = 0$ ), while the geodesic in the defect metric is represented by a blue solid line (that changes direction hitting the defect at  $r = b$ ). Again, the arrows indicate the direction of increasing proper time. The event horizon is represented by the curve  $T = \pm R$ .

First, we observe that the event horizon divides spacetime into four distinct regions (labeled I, II, III, and IV in Fig. 43). We must point out that Eq. (9.36) provides the correct transformation between defect coordinates  $\{t, y\}$  and Kruskal coordinates  $\{T, R\}$  only in region I (which is why we introduced the subscript I in Eq. (9.36)). In the other regions the correct transformations are

$$\begin{cases} T_{II}(t, y) = R_I(t, y), \\ R_{II}(t, y) = T_I(t, y), \end{cases} \quad \begin{cases} T_{III}(t, y) = -T_I(t, y), \\ R_{III}(t, y) = -R_I(t, y), \end{cases} \quad \begin{cases} T_{IV}(t, y) = -R_I(t, y), \\ R_{IV}(t, y) = -T_I(t, y). \end{cases} \quad (9.39)$$

In Schwarzschild spacetime, regions I and III are both asymptotically flat regions describing the exterior of the black hole, but they are causally disconnected (i.e. there is no null-like or time-like curve that can lead from I to III). In the defect metric, this is no longer the case (when  $b < \ell$ ), and in fact, we can see from Fig. 43(b) that a null particle falling into the black hole in region I is prevented from reaching the singularity by the presence of the defect. Instead, the particle passes through the defect and continues to propagate, eventually crossing the event horizon on the other side. It is interesting that it does not emerge in region I (as happens in the case  $b > \ell$ ), but instead it emerges in region III. In this case, the two regions are not causally disconnected. It is also important to note that, while the null particle in region I crosses the horizon located at  $t = +\infty$ , it emerges in region III from the horizon located at  $t = -\infty$  (which represents a white hole).

In relation to the previous subsection 9.3.2, we observe that ingoing PG coordinates  $(T_+^*, y)$  cover only regions I and II (or alternatively their equivalent counterparts, regions III and IV). Instead, outgoing PG coordinates  $(T_-^*, y)$

cover only regions IV and I (or alternatively II and III). However, we have seen (Fig. 43(b)) that the maximally extended defect metric (9.37) admits geodesics that move, for example, from region I to region III (passing through region II). As a result of these considerations, we conclude that the defect metric in ingoing PG coordinates Eq. (9.31) (or outgoing PG coordinates Eq. (9.35)) is not geodesically complete (i.e. it contains geodesics that cannot be extended indefinitely).

### 9.3.3.1 Kruskal topology

We wish to discuss the topology of the defect metric (9.1) and of its maximal extension (9.37). We start by considering the simpler Schwarzschild metric.

The Schwarzschild metric in spherical coordinates is singular at  $r = 0$  and  $r = \ell$ , and so we can divide the manifold into an internal region ( $r < \ell$ ) and an external region ( $r > \ell$ ). The topology of the two region is

$$\begin{cases} \mathcal{M}_S^I = P^I \times S^2, & P^I = \{(t, r) \in \mathbb{R}^2 \mid 0 < r < \ell\}, \\ \mathcal{M}_S^E = P^E \times S^2, & P^E = \{(t, r) \in \mathbb{R}^2 \mid r > \ell\}. \end{cases} \quad (9.40)$$

Instead, the topology of the Schwarzschild metric in Kruskal coordinates is [100]

$$\mathcal{M}_{SK} = \mathbb{R}^2 \times S^2. \quad (9.41)$$

In this coordinate system, the horizon surface  $r = \ell$  is not singular.

In the defect metric we have a similar situation whereby, in spherical coordinates, we need to divide the manifold into two regions. Using the diffeomorphism  $r \rightarrow \rho = b/r$ , we deduce that the topology is

$$\begin{cases} \mathcal{M}_d^I = \mathbb{R} \times (\mathbb{R}P^3 - D), & D = \{(\rho, \theta, \phi) \in \mathbb{R}^3 \mid \rho \leq b/\ell\}, \\ \mathcal{M}_d^E = \mathbb{R} \times D^E, & D^E = \{(\rho, \theta, \phi) \in \mathbb{R}^3 \mid 0 < \rho < b/\ell\}. \end{cases} \quad (9.42)$$

In order to obtain the topology of the defect in Kruskal coordinates, we make a couple of considerations. First, we observe that the transformation law from spherical to Kruskal coordinates Eqs. (9.36) and (9.39) is a diffeomorphism (and hence a homeomorphism) in each separate region I, II, III, and IV. Second, the defect metric is diffeomorphic to the Schwarzschild metric for  $r > b$ . We can use this information to obtain the topology of the defect metric in Kruskal coordinates. To do so, we introduce a new length  $b < a < \ell$  so that we can rewrite the defect manifold as

$$\begin{cases} \mathcal{M}_d^{I1} = \mathbb{R} \times (\mathbb{R}P^3 - D'), & D' = \{(\rho, \theta, \phi) \in \mathbb{R}^3 \mid \rho < b/a\}, \\ \mathcal{M}_d^{I2} = P^{I2} \times S^2, & P^{I2} = \{(t, r) \in \mathbb{R}^2 \mid a < r < \ell\}, \\ \mathcal{M}_d^E = P^E \times S^2, & P^E = \{(t, r) \in \mathbb{R}^2 \mid r > \ell\}. \end{cases} \quad (9.43)$$

We observe that  $\mathcal{M}_d^{I2} \cup \mathcal{M}_d^E$  is homeomorphic to the Schwarzschild manifold, and therefore its topology in Kruskal coordinates is again  $\mathbb{R}^2 \times S^2$ . Conversely, the topology of  $\mathcal{M}_d^{I1}$  is unchanged when moving to Kruskal coordinates. We can use the transformation  $r \rightarrow \rho = b/r$  again to map  $\mathcal{M}_d^{I2} \cup \mathcal{M}_d^E$  into the ball  $D'$  removed from  $\mathcal{M}_d^{I1}$ . In doing so, we finally find that the topology of the defect metric in Kruskal coordinates is

$$\mathcal{M}_{dK} = \mathbb{R} \times (\mathbb{R}P^3 - \{\text{point}\}). \quad (9.44)$$

### 9.3.4 Penrose diagram

With a further conformal transformation [101]

$$\begin{cases} \psi = \arctan(T + R) + \arctan(T - R), \\ \xi = \arctan(T + R) - \arctan(T - R), \end{cases} \quad (9.45)$$

we can map the infinite-range Kruskal coordinates to a new set of finite-range coordinates, from which in turn we obtain the Penrose diagram of the defect metric (9.1) shown in Fig. 44.

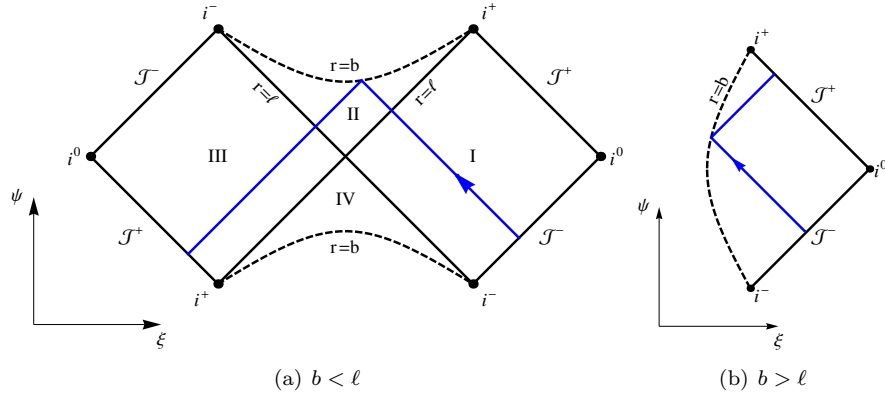


Figure 44: Penrose diagram of the defect metric (9.1) for  $b < \ell$  (a) and  $b > \ell$  (b).  $i^-$  and  $i^+$  indicate, respectively, past and future time-like infinities,  $\mathcal{I}^-$  and  $\mathcal{I}^+$  indicate past and future null-like infinities, and  $i^0$  indicates space-like infinity. The behavior of a radial null geodesic is shown in both cases (blue solid line).

As we observed in the previous subsection 9.3.3, when the radius of defect  $b$  is smaller than its Schwarzschild radius  $\ell$ , the two asymptotically flat regions I and III become causally connected. Here, we want to show that this feature can be used to build a “time machine” with all the causal paradoxes involved. As a simple example, we can consider an emitter/receiver of electromagnetic radiation placed at a fixed distance from the defect in region I (we consider a spherical apparatus enclosing the defect). The apparatus is programmed to emit a signal radially directed toward the defect at a certain time,  $t_0$ , if it does not receive any signal from the defect before  $t_0$ . Similarly, in region III, someone has placed a mirror at a fixed distance from the defect (a spherical mirror enclosing the defect) so that the signal emerging from the defect is reflected back radially. Thus, the reflected signal emerges back in region I and, in certain circumstances, can reach the surface of the emitter before it has been emitted, hence preventing its own emission. This configuration is illustrated in Fig. 45.

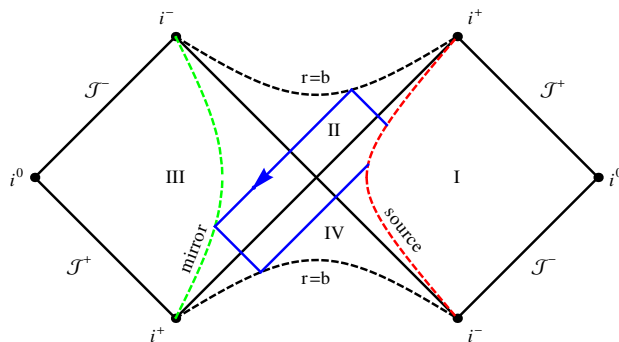


Figure 45: Penrose diagram showing a paradoxical closed time loop: A signal (blue solid line) reaches its source before it has been emitted, hence preventing its own emission.

### 9.3.5 Time-like geodesics

We turn now to the study of radial time-like geodesics ( $\epsilon = 1$ ,  $L = 0$ ). The geodesic equation for the radial coordinate, Eq. (9.14), when  $L = 0$ , is

$$\dot{y}^2 + \frac{y^2 + b^2}{y^2} \left( 1 - \frac{\ell}{\sqrt{y^2 + b^2}} - E^2 \right) = 0, \quad (9.46)$$

which, using the change of variables  $r = \sqrt{y^2 + b^2}$ , becomes

$$\dot{r}^2 = E^2 - V(r), \quad V(r) = 1 - \frac{\ell}{r}. \quad (9.47)$$

We can distinguish between three cases:

- $E > 1$ , where the energy of the particle is larger than the gravitational potential at infinity ( $V(\infty) = 1$ ). The orbit is unbounded, the particle directed toward the defect passes through it and continues to propagate, reaching infinity with non-zero velocity.
- $E = 1$ , where the energy of the particle is equal to the gravitational potential at infinity. The particle reaches infinity with zero velocity.
- $E < 1$ , where the energy of the particle is smaller than the gravitational potential at infinity. The orbit is bounded, and so the particle cannot reach infinity but oscillates between two turning points passing through the defect.

### 9.3.6 $E > 1$

We start by studying the first case,  $E > 1$ . The solution of Eq. (9.47), in this case, has a simple form expressed parametrically in (hyperbolic) cycloidal form:

$$\begin{cases} r(\eta) = \frac{R}{2} (\cosh(\eta + \eta_0) - 1), \\ \tau(\eta) = \frac{R}{2} \sqrt{\frac{R}{\ell}} (\sinh(\eta + \eta_0) - \eta + C), \end{cases} \quad R = \frac{\ell}{E^2 - 1}. \quad (9.48)$$

That this is a solution of Eq. (9.47) can be verified by direct insertion:

$$\left(\frac{dr}{d\tau}\right)^2 = \left(\frac{dr}{d\eta} \frac{d\eta}{d\tau}\right)^2 = \frac{\ell(\cosh(\eta + \eta_0)^2 - 1)}{R(\cosh(\eta + \eta_0) - 1)^2} = \frac{R\ell}{4r^2} \left(\frac{4r^2}{R^2} + \frac{4r}{R}\right) = \frac{\ell}{r} + \frac{\ell}{R}. \quad (9.49)$$

Transforming back to the coordinate  $y$ , and imposing the conditions  $y(0) = 0$  and  $\tau(0) = 0$ , we obtain

$$\begin{cases} y^{(+)}(\eta) = +\sqrt{\frac{R^2}{4}(\cosh(\eta + \eta_0) - 1)^2 - b^2}, & \eta > 0, \\ y^{(-)}(\eta) = -\sqrt{\frac{R^2}{4}(\cosh(\eta - \eta_0) - 1)^2 - b^2}, & \eta < 0, \end{cases} \quad (9.50)$$

and

$$\begin{cases} \tau(\eta) = \frac{R}{2} \sqrt{\frac{R}{\ell}} (\sinh(\eta + \eta_0) - \eta - \sinh \eta_0), & \eta > 0, \\ \tau(\eta) = \frac{R}{2} \sqrt{\frac{R}{\ell}} (\sinh(\eta - \eta_0) - \eta + \sinh \eta_0), & \eta < 0, \end{cases} \quad (9.51)$$

where

$$\eta_0 = \operatorname{arccosh}\left(\frac{2b}{R} + 1\right). \quad (9.52)$$

Integrating the equation for the time coordinate (9.28) is rather complicated in this instance. Fortunately, the result has been obtained for the Schwarzschild metric and we can transform it appropriately for the defect metric. We therefore obtain

$$\begin{aligned} t^{(\pm)}(\tau) = & t_0^{(\pm)} - \frac{R}{2} \left(\frac{R}{\ell} + 1\right)^{1/2} \left[ \left(1 - \frac{2\ell}{R}\right) \eta - \sinh(\eta \pm \eta_0) \right] + \\ & + \ell \log \left| \frac{(R/\ell + 1)^{1/2} - \coth((\eta \pm \eta_0)/2)}{(R/\ell + 1)^{1/2} + \coth((\eta \pm \eta_0)/2)} \right|, \end{aligned} \quad (9.53)$$

where the “+” sign corresponds to  $\tau > 0$ , while the “−” sign has to be picked when  $\tau < 0$ . The constant  $t_0^{(\pm)}$  has been chosen so that  $t(0) = 0$ :

$$t_0^{(\pm)} = \pm \frac{R}{2} \left(\frac{R}{\ell} + 1\right)^{1/2} \sinh \eta_0 + \ell \log \left| \frac{(R/\ell + 1)^{1/2} \mp \coth(\eta_0/2)}{(R/\ell + 1)^{1/2} \pm \coth(\eta_0/2)} \right|. \quad (9.54)$$

Results are shown in Fig. 46 in coordinates  $(r, \tau)$  and in Fig. 47 in Penrose coordinates.

### 9.3.7 $E = 1$

The second case is the simplest to be solved. In fact, when  $E = 1$ , Eq. (9.47) simplifies further and one gets

$$r(\tau) = \left(\frac{9\ell}{4}(\tau \pm \tau_0)^2\right)^{1/3}, \quad (9.55)$$

which, rewritten in terms of the coordinate  $y$  (and imposing  $y(0) = 0$ ), becomes

$$\begin{cases} y^{(+)}(\tau) = +\sqrt{\left(\frac{9\ell}{4}(\tau + \tau_0)^2\right)^{2/3} - b^2}, & \tau > 0, \\ y^{(-)}(\tau) = -\sqrt{\left(\frac{9\ell}{4}(\tau - \tau_0)^2\right)^{2/3} - b^2}, & \tau < 0. \end{cases} \quad \tau_0 = \frac{2}{3}\sqrt{\frac{b^3}{\ell}}. \quad (9.56)$$

Inserting this result into the equation for the time coordinate (9.28), we obtain

$$\begin{cases} t^{(+)}(\tau) = \tau + t_0 + [3(2\ell)^2(\tau_0 + \tau)]^{1/3} - \ell \log \left| \frac{1 + (3/(2\ell)(\tau_0 + \tau))^{1/3}}{1 - (3/(2\ell)(\tau_0 + \tau))^{1/3}} \right|, & \tau > 0, \\ t^{(-)}(\tau) = \tau - t_0 - [3(2\ell)^2(\tau_0 - \tau)]^{1/3} + \ell \log \left| \frac{1 + (3/(2\ell)(\tau_0 - \tau))^{1/3}}{1 - (3/(2\ell)(\tau_0 - \tau))^{1/3}} \right|, & \tau < 0, \end{cases} \quad (9.57)$$

where again  $t_0$  has been chosen so that  $t(0) = 0$ :

$$t_0 = - [3(2\ell)^2\tau_0]^{1/3} + \ell \log \left| \frac{1 + (3\tau_0/(2\ell))^{1/3}}{1 - (3\tau_0/(2\ell))^{1/3}} \right|. \quad (9.58)$$

Results are shown in Figs. 46 and 47.

### 9.3.8 $E < 1$

The case  $E < 1$  is complicated by the fact that the geodesics pass through the defect more than once. For the rest, the study of this case is similar to the first one ( $E > 1$ ). The solution of Eq. (9.47) can again be expressed parametrically in (standard) cycloidal form, to produce

$$\begin{cases} r_n(\eta) = \frac{R}{2}(1 + \cos(\eta - \eta_n)), \\ \tau_n(\eta) = \frac{R}{2}\sqrt{\frac{R}{\ell}}(\eta + \sin(\eta - \eta_n) + C_n), \end{cases} \quad R = \frac{\ell}{1 - E^2}, \quad (9.59)$$

where the subscript  $n$  indicates that we are considering only the  $n$ th cycle. Transforming back to the coordinate  $y$  and imposing the conditions  $y(0) = 0$  and  $\tau(0) = 0$ , we obtain

$$\begin{cases} y_0^{(+)}(\eta) = +\sqrt{\frac{R^2}{4}(1 + \cos(\eta + \eta_0^{(+)})^2 - b^2}, & 0 \leq \eta \leq 2\eta_*, \\ y_0^{(-)}(\eta) = -\sqrt{\frac{R^2}{4}(1 + \cos(\eta + \eta_0^{(-)})^2 - b^2}, & -2\eta_* \leq \eta \leq 0, \end{cases} \quad (9.60)$$

and

$$\begin{cases} \tau_0^{(+)}(\eta) = \frac{R}{2}\sqrt{\frac{R}{\ell}}(\eta + \sin(\eta + \eta_0^{(+)}) + C_0^{(+)}, & 0 \leq \eta \leq 2\eta_*, \\ \tau_0^{(-)}(\eta) = \frac{R}{2}\sqrt{\frac{R}{\ell}}(\eta + \sin(\eta + \eta_0^{(-)}) - C_0^{(-)}, & -2\eta_* \leq \eta \leq 0, \end{cases} \quad (9.61)$$

where  $\eta_0^{(\pm)} = \mp \eta_*$ ,  $C_0^{(\pm)} = \pm \sin \eta_*$ , and  $\eta_*$  is given by

$$\eta_* = \arccos\left(\frac{2b}{R} - 1\right). \quad (9.62)$$

This solution is only valid for the 0th cycle around the origin,  $\eta \in (-2\eta_*, 2\eta_*)$ .

When the geodesic returns to hit the defect surface ( $y = 0$ ) at  $\eta = 2\eta_*$  (or  $\eta = -2\eta_*$ , if we consider the past direction), we have to update the integration constants for the next cycle ( $\eta_1^{(\pm)}$ ,  $C_1^{(\pm)}$ ) so that the solution will satisfy the conditions  $y_1(2\eta_*) = y_0(2\eta_*) = 0$  and  $\tau_1(2\eta_*) = \tau_0(2\eta_*)$ . This operation has to be applied to each cycle, and we obtain the result

$$\begin{aligned} \eta_n^{(+)} &= -(4n+1)\eta_*, & C_n^{(+)} &= (4n+1)\sin\eta_*, \\ \eta_n^{(-)} &= -(4n-1)\eta_*, & C_n^{(-)} &= (4n-1)\sin\eta_*. \end{aligned} \quad (9.63)$$

At this point, it is easy to construct solutions  $y(\eta)$ ,  $\tau(\eta)$  that are valid everywhere by replacing the constant  $n$  in  $\eta_n^{(\pm)}$  and  $C_n^{(\pm)}$  with an  $\eta$  dependent function  $n(\eta)$  defined as

$$n(\eta) = \left\lfloor \frac{\eta}{4\eta_*} \right\rfloor - \Theta(-\eta), \quad (9.64)$$

where  $\lfloor x \rfloor$  is the integer part of  $x$  and  $\Theta(x)$  is the Heaviside step function. Introducing also the function

$$n'(\eta) = \left\lfloor \frac{\eta}{2\eta_*} \right\rfloor - \Theta(-\eta), \quad (9.65)$$

we can finally determine the general solutions  $y(\eta)$  and  $\tau(\eta)$ :

$$y(\eta) = y^{(+)}(\eta) \frac{1 + (-1)^{n'(\eta)}}{2} + y^{(-)}(\eta) \frac{1 - (-1)^{n'(\eta)}}{2}, \quad (9.66a)$$

$$\tau(\eta) = \tau^{(+)}(\eta) \frac{1 + (-1)^{n'(\eta)}}{2} + \tau^{(-)}(\eta) \frac{1 - (-1)^{n'(\eta)}}{2}, \quad (9.66b)$$

where  $y^{(\pm)}(\eta)$ ,  $\tau^{(\pm)}(\eta)$  are

$$y^{(\pm)}(\eta) = \pm \sqrt{\frac{R^2}{4}(1 + \cos(\eta + \eta_{n(\eta)}^{(\pm)}))^2 - b^2}, \quad (9.67a)$$

$$\tau_0^{(\pm)}(\eta) = \frac{R}{2} \sqrt{\frac{R}{\ell}} (\eta + \sin(\eta + \eta_{n(\eta)}^{(\pm)}) + C_{n(\eta)}^{(\pm)}). \quad (9.67b)$$

Again, we can obtain the time coordinate (Eq. (9.28)) by transforming appropriately the result for the Schwarzschild metric. In this respect we find

$$\begin{aligned} t^{(\pm)}(\eta) = & t_0^{(\pm)}(\eta) + \frac{R}{2} \left(\frac{R}{\ell} - 1\right)^{1/2} \left[ \left(1 + \frac{2\ell}{R}\right) \eta + \sin(\eta + \eta_{n(\eta)}^{(\pm)}) \right] + \\ & + \ell \log \left| \frac{(R/\ell - 1)^{1/2} + \tan((\eta + \eta_{n(\eta)}^{(\pm)})/2)}{(R/\ell - 1)^{1/2} - \tan((\eta + \eta_{n(\eta)}^{(\pm)})/2)} \right|, \end{aligned} \quad (9.68)$$

where  $t_0^{(\pm)}(\eta)$  is given by

$$t_0^{(\pm)}(\eta) = C_{n(\eta)}^{(\pm)} \left\{ \frac{R}{2} \left( \frac{R}{\ell} - 1 \right)^{1/2} + \frac{\ell}{\sin \eta_*} \log \left| \frac{(R/\ell - 1)^{1/2} + \tan(\eta_*/2)}{(R/\ell - 1)^{1/2} - \tan(\eta_*/2)} \right| \right\}. \quad (9.69)$$

Results are shown in Figs. 46 and 47.

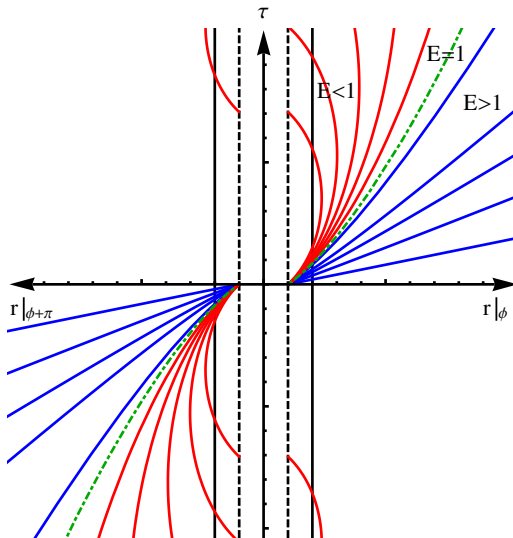


Figure 46: Time-like radial geodesics expressed in coordinates  $(r, \tau)$  for different energies. Note that we depict a section of the defect (the coordinate  $r$  is positive both on the right and on the left of the  $\tau$  axis, while the angular coordinate  $\phi$  changes by  $\pi$ ). Also shown are the horizon  $r = \ell$  (black solid line) and the defect  $r = b$  (black dashed line)

Referring to Fig. 47, we observe that time-like geodesics with  $E < 1$  are causality-violating curves. That is, they cross the horizon in region I at  $t = +\infty$  and emerge (again in region I) from the horizon at  $t = -\infty$ , i.e. before they cross it in the first place. As a result, the paradoxical time machine described at the end of Sec. 9.3.4 for null geodesics can be simplified for  $E < 1$  time-like geodesics, because we do not need to place a mirror in region III.

Since we would like to avoid paradoxes, we will study, in Sec. 10, a more realistic model of defect described as the result of a star collapse, where it is shown that closed time-like curves do not arise.

### 9.3.9 Closed time-like curves in a Skyrme exact solution

We now wish to discuss in this subsection geodesics in the defect solution obtained in Ref. [69] in the presence of matter. The framework introduced in that work describes a Skyrme scalar field  $\Omega \in SO(3)$  that lives in a spacetime manifold with metric  $g_{\mu\nu}$ . The scalar field is governed by the standard Skyrme Lagrangian [102] plus another contribution [103], while the metric is governed by the standard Einstein Hilbert action [75]. Explicitly, the total action of the

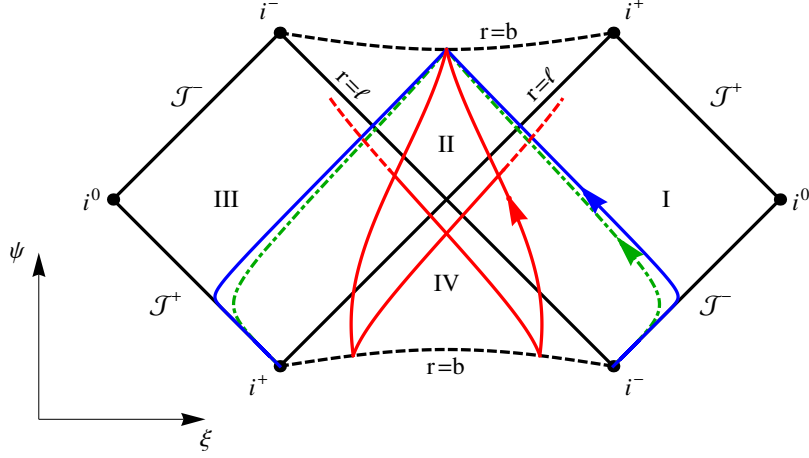


Figure 47: Time-like radial geodesics in Penrose coordinates for  $E > 1$  (blue solid line),  $E = 1$  (green dot-dashed line), and  $E < 1$  (red solid line); the arrows indicate the direction of increasing proper time. The first two curves start at  $i^-$  in region I and terminate at  $i^+$  in region III, while the last curve oscillates between the two regions (along a causality-violating path).

model is

$$S = \int d^4x \sqrt{-g} (\mathcal{L}_{\text{grav,EH}} + \mathcal{L}_{\text{mat,kin}} + \mathcal{L}_{\text{mat,Skyrme}} + \mathcal{L}_{\text{mat,metastab}}), \quad (9.70)$$

where the Lagrangian densities are given by

$$\mathcal{L}_{\text{grav,EH}} = \frac{1}{16\pi G_N} R, \quad (9.71)$$

$$\mathcal{L}_{\text{mat,kin}} = \frac{f^2}{4} \text{tr}(\omega_\mu \omega^\mu), \quad (9.72)$$

$$\mathcal{L}_{\text{mat,Skyrme}} = \frac{1}{16e^2} \text{tr}([\omega_\mu, \omega_\nu][\omega^\mu, \omega^\nu]), \quad (9.73)$$

$$\mathcal{L}_{\text{mat,metastab}} = \frac{\gamma}{48e^2} (\text{tr}(\omega_\mu \omega^\mu))^2, \quad (9.74)$$

$$(9.75)$$

and  $\omega_\mu = \Omega^{-1} \partial_\mu \Omega$ . Moreover, the metric is constrained by the spherically symmetric *Ansatz*

$$ds^2 = -e^{2\bar{\nu}(b^2+y^2)} dt^2 + e^{2\bar{\lambda}(b^2+y^2)} dy^2 + (y^2 + b^2)(dz^2 + \sin^2 z dx^2), \quad (9.76)$$

and the scalar field is given by the *Ansatz*

$$\Omega = \cos(\tilde{F}(r^2)) \mathbf{1} - \sin(\tilde{F}(r^2)) \hat{x} \cdot \vec{S} + (1 - \cos(\tilde{F}(r^2))) \hat{x} \otimes \hat{x}, \quad (9.77)$$

where  $\vec{S} = (S_1, S_2, S_3)$  is the vector of the  $SO(3)$  generators and  $r^2 = y^2 + b^2$ .

Observe that, in setting  $\tilde{F}(r^2) = 0$ , the matter Lagrangians evaluate to zero, meaning that the action (9.70) describes a vacuum spacetime from which one

can derive the vacuum solution (9.1). Another exact solution can be obtained by setting  $\tilde{F}(r^2) = \pi$ , which corresponds to a non-vanishing matter sector. It is precisely this metric whose geodesics we want to study. Explicitly, this solution, in the form of Eq. (9.2), is

$$ds^2 = -A(y)dt^2 + B(y)dy^2 + W(y)(dz^2 + \sin^2 z dx^2), \quad (9.78)$$

with

$$A(y) = 3C_2^2 \left( 1 + \frac{C_1}{\sqrt{y^2 + b^2}} + 4\tilde{\eta} \left( \frac{1 - \frac{4}{3}\gamma}{y^2 + b^2} - 1 \right) \right), \quad (9.79a)$$

$$B(y) = \frac{\frac{y^2}{y^2 + b^2}}{1 + \frac{C_1}{\sqrt{y^2 + b^2}} + 4\tilde{\eta} \left( \frac{1 - \frac{4}{3}\gamma}{y^2 + b^2} - 1 \right)}, \quad (9.79b)$$

$$W(y) = y^2 + b^2, \quad (9.79c)$$

where  $\tilde{\eta} = 8\pi G_N f^2$  and  $C_1, C_2$  are two integration constants. Note that, by setting  $\tilde{\eta} = 0$  and  $C_2 = 1/\sqrt{3}$ , this solution reduces to the vacuum solution with the identification  $C_1 = \ell$ .

Another interesting case is obtained by choosing for the coupling constant the value  $\gamma = 3/4$ . By setting  $C_2 = 1/(\sqrt{3}(1 - \tilde{\eta}))$ , defining  $\tilde{\ell} = -C_1/(1 - 4\tilde{\eta})^{3/2}$ , and rescaling the coordinates to  $t = \sqrt{1 - 4\tilde{\eta}} t$  and  $y = \sqrt{1 - 4\tilde{\eta}} \tilde{y}$ , the metric takes the form

$$ds^2 = - \left( 1 - \frac{\tilde{\ell}}{\sqrt{\tilde{y}^2 + \tilde{b}^2}} \right) d\tilde{t}^2 + \frac{\frac{\tilde{y}^2}{\tilde{y}^2 + \tilde{b}^2}}{1 - \frac{\tilde{\ell}}{\sqrt{\tilde{y}^2 + \tilde{b}^2}}} d\tilde{y}^2 + (1 - 4\tilde{\eta})(\tilde{y}^2 + \tilde{b}^2) d\Omega^2, \quad (9.80)$$

which is equivalent, in the radial and temporal coordinates, to the vacuum solution (9.1). From this fact, we can see immediately that all the results derived in the previous sections for the vacuum massive solution (since they concern only the radial motion) are also valid for the solution with matter for the particular choice  $\gamma = 3/4$ . In particular, the appearance of closed time-like curves, discussed at the end of Sec. 9.3.4 for null-like radial geodesics and at the end of Sec. 9.3.8 for time-like geodesics, affects also the metric (9.80) obtained in the presence of matter.

To obtain the geodesics for a generic value of  $\gamma$ , we need to insert the expressions (9.79) into the equations (9.11) and (9.13). Explicitly, for a massless particle ( $\epsilon = 0$ ) moving along a radial trajectory ( $L = 0$ ), these equations become

$$\dot{t} = \frac{E}{3C_2^2 \left( 1 + \frac{C_1}{\sqrt{y^2 + b^2}} + 4\tilde{\eta} \left( \frac{1 - \frac{4}{3}\gamma}{y^2 + b^2} - 1 \right) \right)}, \quad (9.81a)$$

$$\dot{y}^2 = \frac{y^2 + b^2}{y^2} E^2, \quad (9.81b)$$

where the radial equation is equal to that in the vacuum (9.26) whose solution, we recall, is (9.27)

$$y(\tau) = \begin{cases} y^{(+)}(\tau) = \sqrt{E^2 (\tau + b/E)^2 - b^2}, & \tau > 0, \\ y^{(-)}(\tau) = -\sqrt{E^2 (\tau - b/E)^2 - b^2}, & \tau < 0. \end{cases} \quad (9.82)$$

Substituting this result into the equation for the time variable, we obtain

$$t(\tau) = \begin{cases} t^{(+)}(\tau), & \tau > 0, \\ t^{(-)}(\tau), & \tau < 0, \end{cases} \quad (9.83)$$

where

$$\begin{aligned} t^{(+)}(\tau) &= t_0 + E\tau + \frac{\ell}{2} \log \left[ 3(1-4\eta)\ell(E\tau + b) \left( 1 - \frac{4(1-4/3\gamma)\eta}{\ell(E\tau + b)(1-4\eta)} - \frac{E\tau + b}{\ell} \right) \right] + \frac{\ell^2 - \frac{8(1-4/3\gamma)\eta}{1-4\eta}}{\sqrt{\ell^2 - 16\eta\frac{1-4/3\gamma}{1-4\eta}}} \operatorname{arctanh} \left( \frac{\ell - 2(E\tau + b)}{\sqrt{\ell^2 - 16\eta\frac{1-4/3\gamma}{1-4\eta}}} \right), \\ t^{(-)}(\tau) &= t_0 + E\tau - \frac{\ell}{2} \log \left[ 3(1-4\eta)\ell(b - E\tau) \left( 1 - \frac{4(1-4/3\gamma)\eta}{\ell(b - E\tau)(1-4\eta)} - \frac{b - E\tau}{\ell} \right) \right] + \frac{\ell^2 - \frac{8(1-4/3\gamma)\eta}{1-4\eta}}{\sqrt{\ell^2 - 16\eta\frac{1-4/3\gamma}{1-4\eta}}} \operatorname{arctanh} \left( \frac{\ell - 2(E\tau + b)}{\sqrt{\ell^2 - 16\eta\frac{1-4/3\gamma}{1-4\eta}}} \right), \end{aligned} \quad (9.84)$$

where we have set, for simplicity,  $C_1 = -\ell(1-4\eta)$  and  $C_2 = 1/(\sqrt{3}(1-4\eta))$ , and  $t_0$  has been chosen so that  $t(0) = 0$ . This solution is compared with the vacuum solution (9.29) in Fig. 48.

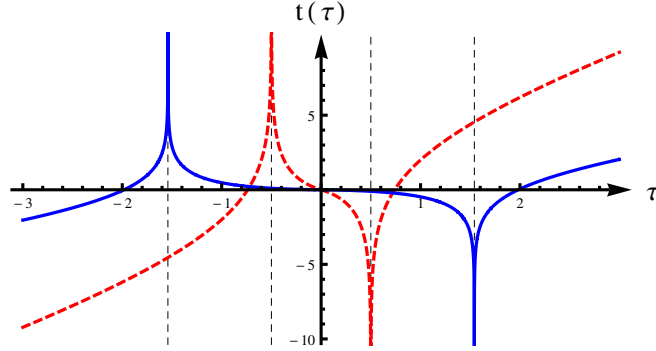


Figure 48: Time component of the null-like radial geodesic with matter, Eq. (9.84), (blue solid line) compared with the same component obtained in vacuum, Eq. (9.29), (red dashed line). For this particular plot we used  $\eta = 0.15$  and  $\gamma = 5$ , but analogous results are obtained for other values of  $\eta$  and  $\gamma$ , and in particular for  $\eta = 0$  the two curves coincide.

From Fig. 48, we see that, even for a generic value of  $\eta$  and  $\gamma$ , the radial null geodesics with matter are qualitatively equivalent to the radial null geodesics in the vacuum, apart for a shift in the event horizon given by

$$r_h = \sqrt{y_h^2 + b^2} = \frac{1}{2} \left( \ell + \sqrt{\ell^2 - 16\eta\frac{1-4/3\gamma}{1-4\eta}} \right). \quad (9.85)$$

We see that this expression reduces to the standard result ( $r_h = \ell$ ) for  $\eta = 0$  or  $\gamma = 3/4$ . From this fact, we can immediately conclude that the same features

that characterize the vacuum's radial geodesics, in particular the appearance of closed time-like curves (due to the causally connectedness of the two asymptotically flat regions that appear in the maximal extension of the metric), must also affect the radial geodesics of the defect metric in the presence of matter.

## 10 Star collapse

In the previous section, we saw that the maximally extended defect metric (9.1) contains causality-violating geodesics. However, as pointed out also for the standard Schwarzschild metric [104], it could be that this metric is not a realistic description of a physical object such as a black hole. In fact, it describes a static eternal geometry, though one might expect that a black hole can originate only as the result of some physical process such as the collapse of a star. Here, we want to study this process in order to verify that, in this more realistic scenario, causality-violating paths are not possible.

In the simplest model of collapse [105, 75], the star is represented by a ball of dust with uniform density and zero pressure. The interior of the star is described by the FLRW (closed) metric

$$ds_I^2 = -d\tau^2 + a^2(\tau) (d\chi^2 + \sin^2 \chi d\Omega^2) , \quad (10.1)$$

where the radial coordinate is given by  $r = a(\tau) \sin \chi$ . The (vacuum) region outside the star is described by the Schwarzschild metric

$$ds_E^2 = - \left( 1 - \frac{\ell}{r} \right) dt^2 + \frac{dr^2}{1 - \ell/r} + r^2 d\Omega^2 . \quad (10.2)$$

The evolution of the star's interior geometry is determined by the Friedmann equations, and one obtains in cycloidal form

$$\begin{aligned} a(\eta) &= \frac{a_0}{2} (1 + \cos \eta) , \\ \tau(\eta) &= \frac{a_0}{2} (\eta + \sin \eta) , \end{aligned} \quad (10.3)$$

and for the density

$$\rho(\eta) = \frac{3}{\pi a_0^2} (1 + \cos \eta)^{-3} . \quad (10.4)$$

The evolution of particles on the star's surface  $R_*(\tau)$  is described by radial time-like geodesics in the Schwarzschild metric (Eq. (9.59)):

$$\begin{aligned} R_*(\eta) &= \frac{R_0}{2} (1 + \cos \eta) , \\ \tau(\eta) &= \frac{R_0}{2} \sqrt{\frac{R_0}{\ell}} (\eta + \sin \eta) . \end{aligned} \quad (10.5)$$

Note that, since the pressure is zero, the motion of particles inside the star (at an initial position  $r_0$ ) is also described by radial time-like geodesics in a Schwarzschild metric (determined this time by the mass contained in the sphere of radius  $r_0$ ).

By matching the internal and external solutions at the star's surface, one obtains the identifications

$$R_0 = a_0 \sin \chi_0, \quad \ell = a_0 \sin^3 \chi_0. \quad (10.6)$$

From these equations, we see that the star collapses from its initial radius  $R_* = R_0$  at  $\eta = 0$ , to the singularity  $R_* = 0$  at  $\eta = \pi$ , where the density  $\rho$  becomes infinite.

We want to modify this model by adding a transition at some critical density  $\rho_c$ , where the topology of spacetime changes and the defect appears. Furthermore, we assume that the defect size  $b$  is equal to the size of the region whose density has reached  $\rho_c$ . Since the density of the star is uniform in this model, the entire star reaches the critical density at the same proper time  $\tau_c$ . Consequently, the entire star is transformed simultaneously to a defect whose size is given by

$$b = R_*(\tau_c). \quad (10.7)$$

After this transition, spacetime is described by the defect metric (9.1). This scenario is illustrated in Fig. 49.

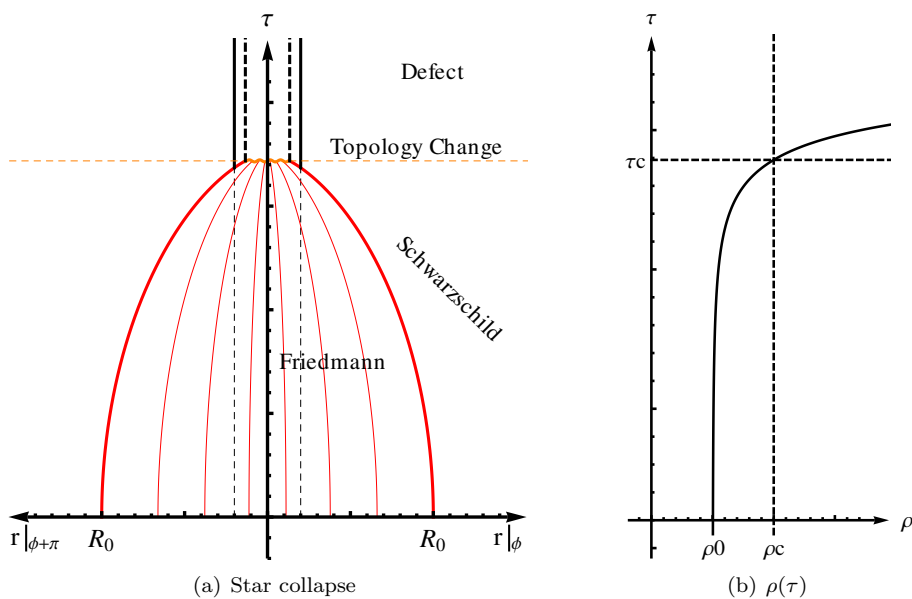


Figure 49: Fig. (a) section of a star collapsing into a defect in coordinates  $(r, \tau)$ . The horizon  $r = \ell$  is represented by a black solid line, the defect  $r = b$  is represented by a black dashed line, and the region of critical density is represented by an orange wavy line. Note that the entire star experiences a topology change at the same proper time  $\tau_c$ . Fig. (b) density evolution  $\rho(\tau)$  from Eq. (10.4).

It is important to note that topology changes in classical general relativity are not allowed [12, 106], but they can possibly occur in a quantum theory of gravity. Consequently, we can infer that the critical density  $\rho_c$  may be related to the Planck density  $\rho_P = m_P/l_P^3 \simeq 5.1 \times 10^{96} \text{ kg/m}^3$ .

We can now turn to analyze the behavior of a null particle moving toward the defect along a radial geodesic. Since both the star's surface and the approaching null particle are moving toward the defect, we can represent both of them in PG coordinates (Sec. 9.3.2). This is shown in Fig. 50.

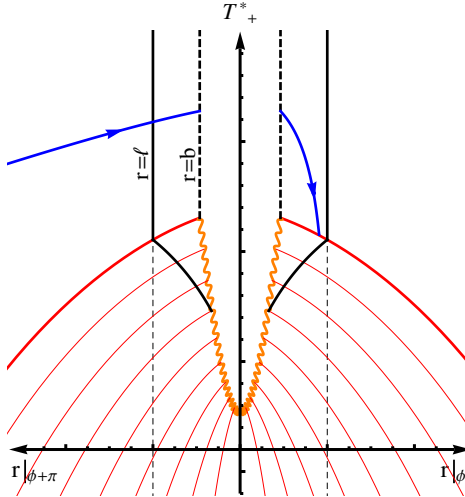
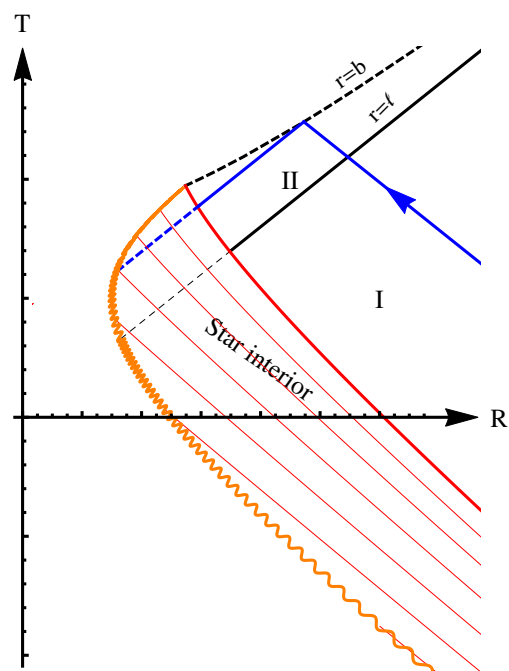


Figure 50: Section of the collapsing star in PG coordinates; note that the topology change (orange wavy line) is not simultaneous in this frame. Also depicted is a null radial geodesic and the shrinking of the horizon (black solid line) perceived by the null particle inside the star.

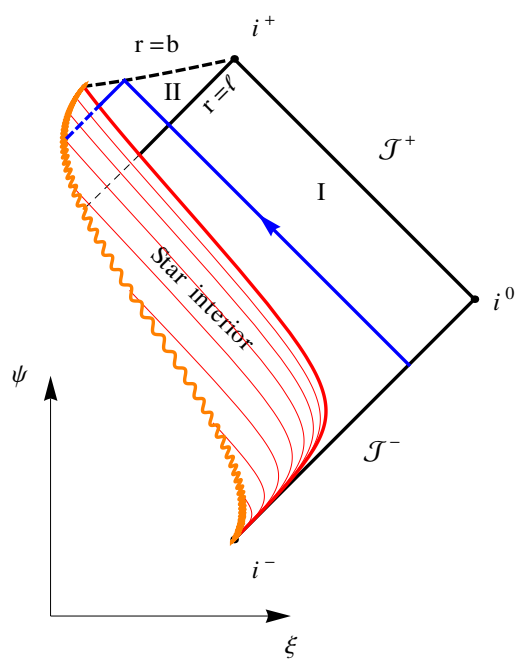
One can observe that, in this reference frame, the topology change does not occur at the same time. Moreover, the radial null geodesic, which after crossing the defect  $r = b$  is moving backward in time, ends its path on the star's surface. If the null particle is not interacting (or weakly interacting) with the star, it can continue to propagate inside the star. In this case, its path will end in the region of critical density at which the topology change occurs. In fact, inside the star, the particle is still propagating in a Schwarzschild metric, where the only mass which contributes to the gravitational field is that contained in a sphere of radius equal to the particle's position (as happens for the star's internal layers). This produces a shrinking of the horizon, as shown in Fig. 50. Since, in this reference frame, the particle cannot cross the horizon in a finite amount of time, it must fall into the critical region  $\rho_c$ .

One could argue that this phenomenon is due to the particular choice of PG coordinates, which are not good for representing outgoing geodesics. Therefore, in Fig. 51, we illustrate the same process in Kruskal and Penrose coordinates. We observe that in these coordinates the behavior of the null geodesics is the same as described for the PG coordinates. The particle that has entered the horizon can either stop at the star's surface (and be dragged into the  $\rho_c$  region), or propagate inside the star until, once again, it reaches the surface of topology change.

From these diagrams, we see also that only one asymptotically flat region (I) appears, and there is no anti-horizon. In this case, the outside of the black hole is safe from causality-violating paths.



(a)



(b)

Figure 51: Kruskal (a) and Penrose (b) diagrams of the defect originating by a collapsing star. In this case spacetime does not contain causality-violating paths (at least in the outside region I).

## Part VI

# Conclusions

In this thesis, we have studied different classical models of spacetime foam in different frameworks. The differences between these models reside mainly in the particular representation of spacetime fluctuations, which we have modeled using different types of topological defects. In particular, we were interested in investigating how these models affect the propagation of particles, which was achieved by calculating the particles' modified dispersion relations. As we discussed in part I, there is in fact a realistic chance to observe the effects of spacetime fluctuations experimentally, or at least to use the experimental results to place constraints on the parameters of the models. Here, we summarize the results taken from these studies.

## 11 Summary of the results

In part II, we investigated how to construct a Lorentz-invariant spacetime foam model. We observed that this is feasible, provided one uses point-like topological defects and distributes them in spacetime according to a sprinkling process. Then, we calculated the dispersion relations of scalar and vector particles in this spacetime foam model, observing that Lorentz invariance is maintained in the results as well. In particular, the only effect of the distribution of defects on the scalar field is a rescaling of the mass of the field observed in the modified dispersion relation (3.33). For the photon field we found instead that the presence of defects does not produce any modification in the dispersion relation, see Eq. (4.102). However, in a  $PT$  symmetric extension of the model considered, the photon dispersion relation is modified as well and is given by Eq. (4.115), from which we find that, in certain circumstances, the photon can become massive.

In part III, we considered different types of static extended topological defects with the same topological structure but different differential structures. In Sec. 5, we studied a type of defect obtained by removing a ball from the spatial hypersurface of Minkowski spacetime and identifying antipodal points on its boundary. Such a defect was used in Ref. [67] to build a spacetime foam model where the propagation of electromagnetic waves was modified according to the modified dispersion relation (5.46), which describes a dispersive medium. We generalized this result to the case of a massive defect obtaining, for electromagnetic waves, the dispersion relation (5.114). We note that this dispersion relation predicts that spacetime should become opaque to low-energy photons. Since no such effect is observed in nature, we are led to rule out this model as a realistic description of spacetime foam.

In Sec. 6, we introduced a second type of defect obtained in Ref. [69] as a vacuum solution of general relativity. This new defect is homeomorphic but not diffeomorphic to the previous one, and we showed that, consequently, the scalar solutions of the Klein-Gordon equation in the two cases are different (see Eqs. (6.32), (6.34)). In particular, the two solutions exhibit different behaviors under parity (see Fig. 14). Then, we calculated the dispersion relations for

scalar waves in the two cases (i.e. considering two spacetime foam models with the same characteristics but based on different types of defects), showing that these results are different, too. We also observed that, for the scalar field, both spacetime foam models describe a non-dispersive medium with a modified refractive index (see Eqs. (6.70)).

From the scalar solution for the second type of defect, we were able to obtain the corresponding electromagnetic solutions and calculate the modified dispersion relation for photons (see Eq. (6.120)). We observed that, also in this case and differently from what happens with the first type of defects, the spacetime foam model describes a non-dispersive medium with a modified index of refraction.

In part IV, we created a numerical program to study the propagation of a scalar field in a regular lattice filled with a distribution of extended topological defects (obtained by removing sites from the lattice and identifying opposite points on the boundary). The program is based on a simple Metropolis algorithm employed to calculate the modified propagator of the scalar field. First, we examined the case of a distribution of extended time-dependent defects, obtaining a result analogous to that of part II, i.e. that the only modification to the dispersion relation is a rescaling of the mass of the scalar field. See Eq. (8.13) for the dispersion relation obtained in 2 dimensions, and Eqs. (8.16) and (8.17) for the dispersion relations in 3 and 4 dimensions. Next, we considered the case of static extended defects, for which we obtained a result analogous to that obtained in part III for scalar particles. In other words, the static spacetime foam model describes a non-dispersive medium with a modified index of refraction. In particular, we obtained the modified dispersion relations in 3 and 4 dimensions given by, respectively, Eqs. (8.19) and (8.22). Observe that the latter expression resembles the analytic result given by Eq. (8.23).

In part V, we investigated the subject from a different perspective. In fact, instead of regarding the topological defects as representations of the microscopic fluctuations of spacetime, we considered one of these defects in the context of black hole physics. As previously mentioned, the second type of defect discussed in part III (which is a vacuum solution of general relativity) has been suggested to provide a regularization to the Schwarzschild black hole. Here, we considered a black hole described by this type of defect, and studied the geodesics of this solution. We found that the main difference with respect to the standard Schwarzschild black hole is that, in this case, the two asymptotically flat regions that appear in the maximal extension of the solution are causally connected (in the Schwarzschild case they are not). A consequence of this fact is that closed time-like curves are allowed to appear, as shown in Figs. 45 and 47. We also showed that an analogous situation arises in the case where matter is present.

Lastly, we studied the case in which the black hole is not eternal but has been originated by the collapse of a star. We observed that, in this case, closed time-like curves are forbidden and the model is safe from causal paradoxes (see Figs. 50 and 51). This result seems to indicate that the defect solution can provide a consistent description of black holes that avoids the problem of singularity, provided that the black hole is not eternal but is the result of a star collapse. Note, however, that this scenario is based on the assumption that a mechanism of topology change occurs at some point, and this can only be accounted for in

a quantum theory of gravity. It must also be pointed out that this regularized solution requires the relaxation of the elementary flatness condition [87].

## 12 Discussion

The scope of this thesis was to study the topological structures of spacetime and to investigate how these structures can influence the propagation of particles. This idea is motivated by the search for experimental evidence of quantum gravity. Nontrivial topological structures of spacetime are expected to be the result at the microscopic scale of quantum gravitational fluctuations. Gaining an understanding of how these structures modify the propagation of particles can lead to predictions, which, constrained by experimental observations, in turn can help to understand quantum gravitational interactions.

This study can be viewed as part of a more general investigation into the effects of topological structures of spacetime; see, for example, Refs. [39, 107, 40, 109, 108, 67, 68, 69]. The approaches that we adopted (in particular in parts II and III) are based on the works of Ref. [40] and Ref. [67], and represent an extension of these studies. We observe that the approaches of these two works are completely different and that, as pointed out in the latter article (Ref. [67]), the first is less general than the second. As we have seen in part II, the framework of Ref. [40] is valid only for chiral gauge theories, while the framework of Ref. [67], which studies the direct interaction between photons and defects, does not depend on the chirality of the theory. However, both approaches have important characteristics that make them useful.

In the framework of Ref. [40] it is manageable to study time-dependent defects, and so we used it in part II to formulate a Lorentz-invariant model of spacetime foam. In the framework of Ref. [67], instead, the investigation of time-dependent defects is much more complicated, which is one of the motivations that led us to develop a lattice model of spacetime foam in part IV, where the study of time-dependent extended defects presents no difficulties. On the other hand, the approach of Ref. [67] is more suitable to investigating the particular structure of the defects, and so we used it in part III to compare the effects of different types of static topological defects (described in Refs. [67, 68] and in Ref. [69]). From this comparison, we find the most interesting result of this thesis, i.e. the implications of spacetime defects on particle propagation do not depend solely on the topological structure of the defects but also on their differential structure.

We observed that the analytic results of parts II and III for scalar fields are in agreement with the numerical results of part IV. This is interesting, especially for the case of time-dependent defects. In fact, the analytic results of part II are obtained for point-like defects (which are Lorentz-invariant), while the numerical results of part IV concern extended defects (which are not Lorentz-invariant). An analytic investigation into extended time-dependent defects is necessary, in order to better understand this point.

One must bear in mind that, lacking any direct experimental evidence of spacetime foam, it is very difficult to draw definitive conclusions on the topic, so all experimental results must be considered model-dependent. Spacetime foam is usually expected to cause Lorentz violations which imply the vacuum must be depicted as a dispersive medium. Particles in such a context display

modified dispersion relations of the form found in Eq. (1.20). Most of the current experiments are based on this assumption, a typical example of which is the measurement of the time of flight of photons, which Eq. (1.20) predicts to be energy-dependent. However, the assumption of a dispersive spacetime is not a general result, and in many cases, as in those studied in this thesis, spacetime foam turns out to describe a non-dispersive medium for which these kinds of experiments are irrelevant (the velocity of propagation does not depend on the photon energy in this case).

When the distribution of topological defects is explicitly Lorentz-invariant, we saw in part II that no modifications in the dispersion relation of photons appear (at most, in certain circumstances, the photon can become massive). For a distribution of extended static defects, which explicitly breaks Lorentz invariance, we would expect to obtain modified dispersion relations corresponding to a dispersive medium. Nevertheless, we observed in part III that, for electromagnetic waves, this is the case only when the defects are not solutions of general relativity. When the defect manifold is a vacuum solution of general relativity, the corresponding spacetime foam model describes a non-dispersive medium.

In this latter case the defect manifold, whose geodesics we studied in part V, can also serve to regularize the Schwarzschild black hole. We observed that the regularization can be used consistently (without the appearance of paradoxical time-machines), albeit only for non-eternal black holes and under the condition of allowing for mechanisms of topology change.

## References

- [1] D. M. Gingrich, “Practical Quantum Electrodynamics,” Boca Raton, USA: Taylor & Francis Group (2006) 341 p. (p. 5)
- [2] M. Nicholas, “Higgs force: The symmetry-breaking force that makes the world an interesting place,” Cambridge: James Clarke & Co. (2012) 328 p. (p. 5)
- [3] C. M. Will, “The Confrontation between general relativity and experiment,” Living Rev. Rel. **9** (2006) 3 [gr-qc/0510072]. (p. 5)
- [4] D. J. Bird *et al.* [HIRES Collaboration], “The Cosmic ray energy spectrum observed by the Fly’s Eye,” *Astrophys. J.* **424** (1994) 491. (p. 5), (p. 11)
- [5] J. A. Wheeler, “Geons,” *Phys. Rev.* **97** (1955) 511. (p. 7), (p. 12)
- [6] J. A. Wheeler, “On the nature of quantum geometrodynamics,” *Annals Phys.* **2**, 604 (1957). (p. 7), (p. 17)
- [7] T. A. Welton, “Some Observable Effects of the Quantum-Mechanical Fluctuations of the Electromagnetic Field,” *Phys. Rev.* **74** (1948) 1157. (p. 7)
- [8] K. A. Milton, “The Casimir effect: Recent controversies and progress,” *J. Phys. A* **37** (2004) R209 [hep-th/0406024]. (p. 7)
- [9] A. Connes, M. Heller, S. Majid, R. Penrose, J. Polkinghorne, A. Taylor, “On Space and Time,” Cambridge University Press, Cambridge, (2012). (p. 8)
- [10] R. M. Wald, “General Relativity,” Chicago, USA: Univ. Pr. (1984) 491p. (p. 8)
- [11] <http://universe-review.ca/I01-16-quantumfoam.jpg>. (p. 9)
- [12] M. Visser, “Lorentzian wormholes: From Einstein to Hawking,” Woodbury, USA: AIP (1995) 412 p. (p. 9), (p. 10), (p. 54), (p. 137)
- [13] M. Visser, “Sakharov’s induced gravity: A Modern perspective,” *Mod. Phys. Lett. A* **17** (2002) 977 [gr-qc/0204062]. (p. 10)
- [14] S. Liberati, F. Girelli and L. Sindoni, “Analogue Models for Emergent Gravity,” arXiv:0909.3834 [gr-qc]. (p. 10)
- [15] S. W. Hawking, “Space-Time Foam,” *Nucl. Phys. B* **144** (1978) 349. (p. 10)
- [16] S. W. Hawking, “Wormholes in Space-Time,” *Phys. Rev. D* **37** (1988) 904. (p. 10)
- [17] S. W. Hawking, “Virtual black holes,” *Phys. Rev. D* **53** (1996) 3099 [hep-th/9510029]. (p. 10)
- [18] I. Raptis and R. R. Zapatrin, “Algebraic description of space-time foam,” *Class. Quant. Grav.* **18** (2001) 4187 [gr-qc/0102048]. (p. 10)

- [19] J. R. Ellis, N. E. Mavromatos and D. V. Nanopoulos, “Space-time foam effects on particle interactions and the GZK cutoff,” *Phys. Rev. D* **63** (2001) 124025 [hep-th/0012216]. (p. 10)
- [20] A. Iqbal, N. Nekrasov, A. Okounkov and C. Vafa, “Quantum foam and topological strings,” *JHEP* **0804** (2008) 011 [hep-th/0312022]. (p. 10)
- [21] N. E. Mavromatos, “Stringy Space-Time Foam and High-Energy Cosmic Photons,” *J. Phys. Conf. Ser.* **283** (2011) 012022 [arXiv:1010.5399 [gr-qc]]. (p. 10)
- [22] R. Gambini and J. Pullin, “Nonstandard optics from quantum space-time,” *Phys. Rev. D* **59** (1999) 124021 [gr-qc/9809038]. (p. 10)
- [23] G. Preparata, S. Rovelli, S. S. Xue, “Review: Gas of Wormholes: A Possible Ground State of Quantum Gravity,” *Gen. Rel. and Grav.* **32** (2000) 9. (p. 10)
- [24] R. Garattini, “Large N wormhole approach to space-time foam,” *Phys. Lett. B* **446** (1999) 135 [hep-th/9811187]. (p. 10)
- [25] G. Amelino-Camelia, “Are we at the dawn of quantum gravity phenomenology?,” *Lect. Notes Phys.* **541** (2000) 1 [gr-qc/9910089]. (p. 10), (p. 15)
- [26] Y. J. Ng, “Quantum foam and quantum gravity phenomenology,” *Lect. Notes Phys.* **669** (2005) 321 [gr-qc/0405078]. (p. 10)
- [27] Y. J. Ng, “Holographic foam, dark energy and infinite statistics,” *Phys. Lett. B* **657** (2007) 10 [gr-qc/0703096 [GR-QC]]. (p. 10)
- [28] M. Kramer and F. J. P. Soler, “Large hadron collider phenomenology,” CRC Press, (2004). (p. 11)
- [29] G. Amelino-Camelia, J. R. Ellis, N. E. Mavromatos, D. V. Nanopoulos and S. Sarkar, “Tests of quantum gravity from observations of gamma-ray bursts,” *Nature* **393** (1998) 763 [astro-ph/9712103]. (p. 11)
- [30] G. Amelino-Camelia, “Quantum-Spacetime Phenomenology,” *Living Rev. Rel.* **16** (2013) 5 [arXiv:0806.0339 [gr-qc]]. (p. 11)
- [31] J. Collins, A. Perez, D. Sudarsky, L. Urrutia and H. Vucetich, “Lorentz invariance and quantum gravity: an additional fine-tuning problem?,” *Phys. Rev. Lett.* **93** (2004) 191301 [gr-qc/0403053]. (p. 11)
- [32] R. Gambini, S. Rastgoo and J. Pullin, “Small Lorentz violations in quantum gravity: do they lead to unacceptably large effects?,” *Class. Quant. Grav.* **28** (2011) 155005 [arXiv:1106.1417 [gr-qc]]. (p. 11)
- [33] J. Polchinski, “Comment on [arXiv:1106.1417] ‘Small Lorentz violations in quantum gravity: do they lead to unacceptably large effects?’,” *Class. Quant. Grav.* **29** (2012) 088001 [arXiv:1106.6346 [gr-qc]]. (p. 11)
- [34] A. Vilenkin, E. P. S. Shellard, “Cosmic Strings And Other Topological Defects,” Cambridge University Press, Cambridge, (1994). (p. 12)

- [35] V. A. Kostelecky and S. Samuel, “Spontaneous Breaking of Lorentz Symmetry in String Theory,” *Phys. Rev. D* **39** (1989) 683. (p. 13)
- [36] D. Colladay and V. A. Kostelecky, “Lorentz-violating extension of the standard model,” *Phys. Rev. D* **58** (1998) 116002 [hep-ph/9809521]. (p. 14)
- [37] S. Liberati, “Tests of Lorentz invariance: a 2013 update,” *Class. Quant. Grav.* **30** (2013) 133001 [arXiv:1304.5795 [gr-qc]]. (p. 15), (p. 16)
- [38] F. R. Klinkhamer, *Nucl. Phys. B* **535** (1998) 233 [hep-th/9805095]. (p. 18)
- [39] F. R. Klinkhamer, “A CPT anomaly,” *Nucl. Phys. B* **578** (2000) 277 [hep-th/9912169]. (p. 18), (p. 142)
- [40] F. R. Klinkhamer and C. Rupp, “Space-time foam, CPT anomaly, and photon propagation,” *Phys. Rev. D* **70**, 045020 (2004), hep-th/0312032. (p. 18), (p. 24), (p. 26), (p. 142)
- [41] O. W. Greenberg, “CPT violation implies violation of Lorentz invariance,” *Phys. Rev. Lett.* **89** (2002) 231602 [hep-ph/0201258]. (p. 18)
- [42] S. -S. Chern and J. Simons, “Characteristic forms and geometric invariants,” *Annals Math.* **99** (1974) 48. (p. 18)
- [43] L. Alvarez-Gaume, S. Della Pietra and G. W. Moore, “Anomalies and Odd Dimensions,” *Annals Phys.* **163** (1985) 288. (p. 18)
- [44] L. Bombelli, J. Lee, D. Meyer and R. Sorkin, “Space-Time as a Causal Set,” *Phys. Rev. Lett.* **59** (1987) 521. (p. 20)
- [45] J. Henson, “The Causal set approach to quantum gravity,” In \*Oriti, D. (ed.): Approaches to quantum gravity\* 393-413 [gr-qc/0601121]. (p. 20)
- [46] F. Dowker, J. Henson, and R. D. Sorkin, “Quantum gravity phenomenology, Lorentz invariance and discreteness,” *Mod. Phys. Lett. A* **19**, 1829 (2004), gr-qc/0311055. (p. 20), (p. 21)
- [47] L. Bombelli, J. Henson, and R. D. Sorkin, “Discreteness without symmetry breaking: A Theorem,” *Mod. Phys. Lett. A* **24**, 2579 (2009), gr-qc/0605006. (p. 20), (p. 21)
- [48] M. E. Peskin and D. V. Schroeder, “An Introduction to quantum field theory,” Reading, USA: Addison-Wesley (1995) 842 p. (p. 26), (p. 33), (p. 34), (p. 35), (p. 38), (p. 97)
- [49] K. Huang, “Quantum field theory: From operators to path integrals,” John Wiley & Sons (2010). (p. 26)
- [50] G. Passarino and M. J. G. Veltman, “One Loop Corrections for  $e^+ e^-$  Annihilation Into  $\mu^+ \mu^-$  in the Weinberg Model,” *Nucl. Phys. B* **160** (1979) 151. (p. 29)
- [51] F. R. Klinkhamer, private communication. (p. 30)
- [52] D. B. Melrose, “Quantum Plasmadynamics,” New York: Springer (2008). (p. 31)

- [53] M. Schreck, F. Sorba and S. Thambiyahpillai, “A simple model of point-like spacetime defects and implications for photon propagation,” *Phys. Rev. D* **88** (2013) 125011 [arXiv:1211.0084 [hep-th]]. (p. 31)
- [54] C. M. Bender and S. Boettcher, “Real spectra in non-Hermitian Hamiltonians having  $PT$  symmetry,” *Phys. Rev. Lett.* **80**, 5243 (1998), physics/9712001. (p. 48)
- [55] C. M. Bender, S. Boettcher and P. Meisinger, *J. Math. Phys.* **40** (1999) 2201 [quant-ph/9809072]. (p. 48)
- [56] S. Bittner, B. Dietz, U. Günther, H. L. Harney, M. Miski-Oglu, A. Richter, and F. Schäfer, “ $PT$  symmetry and spontaneous symmetry breaking in a microwave billiard,” *Phys. Rev. Lett.* **108**, 024101 (2012). (p. 48)
- [57] Z. Lin, H. Ramezani, T. Eichelkraut, T. Kottos, H. Cao, and D. N. Christodoulides, “Unidirectional invisibility induced by  $PT$ -symmetric periodic structures,” *Phys. Rev. Lett.* **106**, 213901 (2011). (p. 48)
- [58] J. Rubinstein, P. Sternberg, and Q. Ma, “Bifurcation diagram and pattern formation of phase slip centers in superconducting wires driven with electric currents,” *Phys. Rev. Lett.* **99**, 167003 (2007). (p. 48)
- [59] C. M. Bender, D. C. Brody, and H. F. Jones, “Extension of  $PT$  symmetric quantum mechanics to quantum field theory with cubic interaction,” *Phys. Rev. D* **70**, 025001 (2004), Erratum-ibid. *D* **71**, 049901 (2005), hep-th/0402183. (p. 48)
- [60] C. M. Bender, V. Branchina and E. Messina, *Phys. Rev. D* **85** (2012) 085001 [arXiv:1201.1244 [hep-th]]. (p. 48)
- [61] D. Stauffer, A. Aharony “Introduction to Percolation Theory,” Taylor & Francis, London, (2003). (p. 49), (p. 50), (p. 101)
- [62] K. Huang, “Statistical Mechanics,” John Wiley & Sons (1987). (p. 50), (p. 104)
- [63] J. M. Yeomans, “Statistical Mechanics of Phase Transitions,” Oxford University Press (1992). (p. 50), (p. 104)
- [64] P. Blanchard, G. F. Dell’Antonio, D. Gandolfo, M. Sirugue-Collin, “Continuous percolation: Tree approximation and most probable clusters,” in “Mathematical Physics and Stochastic Analysis: Essays in Honour of Ludwig Streit,” edited by S. Albeverio, P. Blanchard, L. Ferreira, T. Hida, Y. Kondratiev, and R. V. Mendes, World Scientific, Singapore, (2000), pp. 84–98. (p. 50), (p. 101)
- [65] S. Hossenfelder, “Phenomenology of Space-time Imperfection I: Nonlocal Defects,” *Phys. Rev. D* **88** (2013) 124030 [arXiv:1309.0311 [hep-ph]]. (p. 50)
- [66] S. Hossenfelder, “Phenomenology of Space-time Imperfection II: Local Defects,” *Phys. Rev. D* **88** (2013) 124031 [arXiv:1309.0314 [hep-ph]]. (p. 50)

- [67] S. Bernadotte and F. R. Klinkhamer, “Bounds on length-scales of classical spacetime foam models,” *Phys. Rev. D* **75** (2007) 024028 [hep-ph/0610216]. (p. 13), (p. 51), (p. 55), (p. 58), (p. 62), (p. 94), (p. 140), (p. 142)
- [68] M. Schwarz, “Nontrivial Spacetime Topology, Modified Dispersion Relations, and an  $SO(3)$ -Skyrme Model,” PhD Thesis, KIT, July 2010. (p. 51), (p. 52), (p. 54), (p. 55), (p. 142)
- [69] F. R. Klinkhamer and C. Rahmede, “A nonsingular spacetime defect,” *Phys. Rev. D* **89** (2014) 084064 [arXiv:1303.7219 [gr-qc]]. (p. 51), (p. 69), (p. 132), (p. 140), (p. 142)
- [70] A. Einstein and N. Rosen, “The Particle Problem in the General Theory of Relativity,” *Phys. Rev.* **48** (1935) 73. (p. 54)
- [71] M. Nakahara, “Geometry, topology and physics,” Boca Raton, USA: Taylor & Francis (2003) 573 p. (p. 55)
- [72] J. D. Jackson, “Classical electrodynamics,” Wiley, (1999). (p. 56)
- [73] J. D. Jackson, “Mathematics for quantum mechanics: an introductory survey of operators, eigenvalues, and linear vector spaces,” Courier Dover Publications, (2012). (p. 56)
- [74] W. K. H. Panofsky and M. Phillips, “Classical Electricity And Magnetism,” Courier Dover Publications, (2012). (p. 57), (p. 58), (p. 60), (p. 62), (p. 88), (p. 90)
- [75] C. W. Misner, K. S. Thorne and J. A. Wheeler, “Gravitation,” San Francisco (1973), 1279p. (p. 59), (p. 132), (p. 136)
- [76] M. Gasperini, “Theory of Gravitational Interactions,” Springer (2013). (p. 59)
- [77] V. P. Nair, “Quantum field theory: A modern perspective,” Springer (2005). (p. 60)
- [78] H. Stephani, “Debye potentials in Riemannian spaces,” *J. Math. Phys.* **15**, 14 (1974). (p. 60)
- [79] E. Herlt and H. Stephani, “Diffraction of a Plane Electromagnetic Wave at a Schwarzschild Black Hole,” *Int. J. Theor. Phys.* **12** (1975), No. 2, pp. 81-93. (p. 60)
- [80] J. M. Cohen and L. S. Kegeles, “Electromagnetic fields in curved spaces - a constructive procedure,” *Phys. Rev. D* **10** (1974) 1070. (p. 60)
- [81] R. Fabbri, “Scattering and absorption of electromagnetic waves by a Schwarzschild black hole,” *Phys. Rev. D* **12** (1974) 933. (p. 60)
- [82] N. G. Sanchez, “Absorption and Emission Spectra of a Schwarzschild Black Hole,” *Phys. Rev. D* **18** (1978) 1030. (p. 60)

- [83] M. W. Kearney, L. S. Kegeles, J. M. Cohen, "SCHWARZSCHILD ELECTRODYNAMICS: BLACK HOLES, NEUTRON STARS," *Astrophysics and Space Science* **56** (1978) 129-190. (p. 60), (p. 61), (p. 62), (p. 63), (p. 65)
- [84] P. G. Molnar, "Electrostatic boundary value problems in the Schwarzschild background," *Class. Quant. Grav.* **18** (2001) 1853 [gr-qc/0105004]. (p. 63)
- [85] F. R. Klinkhamer, "Black-hole solution without curvature singularity," *Mod. Phys. Lett. A* **28** (2013) 1350136 [arXiv:1304.2305 [gr-qc]]. (p. 69), (p. 117)
- [86] F. R. Klinkhamer, "Black-hole solution without curvature singularity and closed time-like curves," *Acta Phys. Polon. B* **45** (2014) 1, 5 [arXiv:1305.2875 [gr-qc]]. (p. 69), (p. 117)
- [87] F. R. Klinkhamer, "A new type of nonsingular black-hole solution in general relativity," arXiv:1309.7011 [gr-qc]. (p. 69), (p. 117), (p. 142)
- [88] S. M. Carroll, "Spacetime and geometry: An introduction to general relativity," San Francisco, USA: Addison-Wesley (2004) 513 p. (p. 71), (p. 118)
- [89] N. D. Birrell and P. C. W. Davies, "Quantum Fields in Curved Space," Cambridge University Press, Cambridge, (1984). (p. 72)
- [90] F. V. Atkinson, "LXI. On Sommerfeld's "radiation condition.", " *Philosophical Magazine* **45** (1949) 305, 645, Taylor & Francis. (p. 75)
- [91] M. Tenenbaum, H. Pollard, "Ordinary differential equations," New York: Harper&Row (1963). (p. 77), (p. 80)
- [92] F. R. Klinkhamer and F. Sorba, "Comparison of spacetime defects which are homeomorphic but not diffeomorphic," arXiv:1404.2901 [hep-th]. (p. 80)
- [93] R. P. Feynman, R. B. Leighton, M. Sands, "The Feynman Lectures on Physics, Volume I," New York: Basic Books (2013). (p. 84)
- [94] C. Morningstar, "The Monte Carlo method in quantum field theory," hep-lat/0702020. (p. 99)
- [95] N. H. Christ, R. Friedberg and T. D. Lee, "Random Lattice Field Theory: General Formulation," *Nucl. Phys. B* **202** (1982) 89. (p. 99)
- [96] H. Sahlmann, "Wave propagation on a random lattice," *Phys. Rev. D* **82** (2010) 064018 [arXiv:0911.4180 [gr-qc]]. (p. 99)
- [97] P. Painlevé, "La mécanique classique et la théorie de la relativité," *C. R. Acad. Sci. (Paris)* **173**, 677 (1921). (p. 122)
- [98] A. Gullstrand, "Allgemeine Lösung des statischen Einkörperproblems in der Einsteinschen Gravitationstheorie," *Arkiv. Mat. Astron. Fys.* **16**, 1 (1922). (p. 122)

- [99] M. D. Kruskal, “Maximal extension of Schwarzschild metric,” *Phys. Rev.* **119** (1960) 1743. (p. 124)
- [100] E. M. Monte, “What is the topology of a Schwarzschild black hole?,” *Int. J. Mod. Phys. Conf. Ser.* **18** (2012) 125 [arXiv:1111.5790 [gr-qc]]. (p. 126)
- [101] R. Penrose, “Conformal treatment of infinity,” *Gen. Rel. Grav.* **43** (2011) 901. (p. 127)
- [102] T. H. R. Skyrme, “A Nonlinear field theory,” *Proc. Roy. Soc. Lond. A* **260** (1961) 127. (p. 132)
- [103] D. E. L. Pottinger and E. Rathske, “Metastability of Solitons in a Generalized Skyrme Model,” *Phys. Rev. D* **33** (1986) 2448. (p. 132)
- [104] G. W. Gibbons, S. W. Hawking “Euclidean quantum gravity,” *World Scientific* (1993). (p. 136)
- [105] J. R. Oppenheimer and H. Snyder, “On Continued gravitational contraction,” *Phys. Rev.* **56** (1939) 455. (p. 136)
- [106] F. J. Tipler, “Singularities and Causality Violation,” *Annals Phys.* **108** (1977) 1. (p. 137)
- [107] F. R. Klinkhamer, “Fundamental time asymmetry from nontrivial space topology,” *Phys. Rev. D* **66** (2002) 047701 [gr-qc/0111090]. (p. 142)
- [108] F. R. Klinkhamer, “Nontrivial spacetime topology, CPT violation, and photons,” hep-ph/0511030. (p. 142)
- [109] F. R. Klinkhamer and C. Rupp, “Spacetime foam and high-energy photons,” *New Astron. Rev.* **54** (2010) 211 [astro-ph/0511267]. (p. 142)